# ANALYSIS AND CONTROL OF STAND ALONE GENERATOR

**A THESIS**

*Submitted in partial fulfilment of the requirements for the award of the degree of*

DOCTOR OF PHILOSOPHY

*in*

ELECTRICAL ENGINEERING

*by*

**DHEERAJ KUMAR PALWALIA**




DEPARTMENT OF ELECTRICAL ENGINEERING
INDIAN INSTITUTE OF TECHNOLOGY ROORKEE
ROORKEE - 247 667 (INDIA)

OCTOBER, 2009

# NDIAN INSTITUTE OF TECHNOLOGY ROORKEE
# ROORKEE

## CANDIDATE'S DECLARATION

I hereby certify that the work which is being presented in this thesis entitled **ANALYSIS AND CONTROL OF STAND ALONE GENERATOR** in partial fulfilment of the requirements for the award of *the Degree of Doctor of Philosophy* and submitted in the Department of Electrical Engineering of Indian Institute of Technology Roorkee, Roorkee is an authentic record of my own work carried out during a period from July 2006 to October 2009 under the supervision of Dr. S. P. Singh, Professor, Department of Electrical Engineering, Indian Institute of Technology Roorkee, Roorkee.

The matter presented in this thesis has not been submitted by me for the award of any other degree of this or any other Institution.

**(DHEERAJ KUMAR PALWALIA)**

This is to certify that the above statement made by the candidate is correct to the best of my knowledge.

(S. P Singh)

Supervisor

Date: October 12, 2009

The Ph.D. Viva-Voce Examination of ***Mr. Dheeraj Kumar Palwalia***, QIP Research Scholar, has been held on..29/5 March, 10

Signature of Supervisor

Signature of External Examiner

# ABSTRACT

Electrification of un-electrified remote rural areas not connected to national grid is an important task for the sustainable development of country. Low electric load demand, economical and technical difficulties in extension of grid is main constraint for electrification of such areas. The un-electrified remote and far-flung areas have potential of sustainable renewable energy resources such as mini/ micro hydro, wind, bio-mass etc., which can be used to produce and supply electricity. The objective of the harnessing of such non-conventional energy sources could be achieved in a big way by the development of the suitable low cost generating systems. The electric power generation from these sources will not only supply the energy to the remote and isolated areas, but can also supplement the power requirements of the inter-connected systems. However, these systems could become more viable if their cost is reduced to the minimum.

The self excited induction generator (SEIG) is a suitable power generation source utilizing renewable energy sources due to its advantages like simplicity, low cost, ruggedness, little maintenance, brushless construction, self-protection capability, ability to generate power while driven at variable speed etc. as compared to conventional synchronous generator. These advantages facilitate induction generator operation in stand-alone/ isolated mode or in parallel with synchronous generator for supplying local load and in grid mode. The self excited induction generator has a major drawback of poor voltage regulation. The inherent poor voltage and frequency regulation of the SEIG is due to the difference between the reactive power supplied by the excitation capacitors and that demanded by the load and the machine. This is a major bottleneck for its application in isolated mode.

The generated voltage of the SEIG depends upon the speed, excitation capacitance, load current and power factor of the load. Among various renewable energy based power systems, mini/micro hydro power scheme employs an uncontrolled turbine which maintains the constant input of hydro power. The use of governor for input control is not an economical option due to its cost and operational maintenance. One way to regulate the voltage and frequency of the SEIG is to maintain a constant load at its terminals. Under

such operation, SEIG requires fixed capacitance for excitation resulting in a fixed-point of operation. For this purpose, a suitable control scheme is to be developed such that the load on the SEIG remains constant despite the change in the consumer load. Also, such control scheme should be simple, economical, rugged and reliable.

The power output is kept constant by connecting a dump load in parallel with the consumer load such that the total generated power is held constant in order to regulate voltage and frequency of SEIG. The analog controllers are in use, need sensing, control and protection circuit which need too many electronic components. In event of failure of any component it becomes tedious and time consuming job to find the fault, repair and then put the system in order. However, a single chip like DSPs which gives cost effective solution and can eliminate the use of complicated control circuit. A single chip provides flexible solution, multiple features fast processing to implement advanced and complex algorithm. Accordingly, a DSP based load controller has been designed, developed and implemented through a new sample based controller. The proposed sample based controller is simple as compared to traditional PI controller as it requires only one parameter to be tuned for optimal operation. Experiments are carried out on developed prototype of DSP based load controller for SEIG system. The transient behavior of DSP TMS320F2812 based load controller for SEIG system at different operating conditions such as application and removal of static (resistive and reactive) and dynamic load is investigated to demonstrate the capabilities of the proposed load controller. The MATLAB based digital simulation results of the transient analysis have been compared with the experimental results to validate the developed model.

Remote and isolated areas are characterized by sparsely distributed population with electric loads of single-phase. The single phase power supply is preferred over three phase in order to render the distribution system simple and cost effective. It is possible to use a three-phase induction motor as a single-phase SEIG. Beyond 5 kW load, the three phase induction machine, being inexpensive, readily available in the market with higher efficiency than equivalent rating of single phase induction machine, thus has become attractive proposition for supplying single phase power up to 20 kW. Three phase SEIG supplying single phase load is the case of unbalanced operation, it is required to operate the machine at de-rated power so that the temperature rise in the machine is restricted within permissible limits. A detailed study supported with MATLAB based digital

simulation and application of load controller to regulate the voltage and frequency of single phase SEIG using three phase induction machine have been examined. A DSP based load controller is designed, developed and implemented for single phase SEIG using three phase induction motor. Further, different excitation capacitor configuration for delta and star connected machine as single phase SEIG have been analyzed.

Single-phase induction motors can be used as single phase self excited induction generators for single phase power generation for the purpose of supplying smaller loads of less than 5kW. Single phase induction machine is an unsymmetrical machine having two phase windings. These two windings are normally unbalanced and classified as the main and auxiliary windings. When it is used as the SEIG, it has the flexibility of using the main and/or the auxiliary windings both for excitation and main winding for loading. The analysis of two winding SEIG for improved performance has been performed. Further, the same DSP based control algorithm as load controller has been tested and implemented with single phase induction motor working as single phase SEIG for its voltage and frequency regulation.

The economical implementation of digital systems from a hardware complexity standpoint, with the goal of minimizing the computational work load have always been appealing research topic. The electrical load is maintained constant at SEIG terminals through a mark space ratio controlled load controller. The load controller keeps the total electrical power constant at variable consumer load though a dump load. The power dissipated in dump load is governed by the difference of generated power to consumer load. The load controller with uncontrolled rectifier and series connected chopper switch with mark space ratio chopper control gives unity power factor operation and it requires only one dump load. Such a load controller is nonlinear in nature and injects harmonics in the system. The harmonic generated are random in nature. The SEIG performance is severely affected with these harmonics. A dip in voltage is also observed as the harmonic content increases.

An effort has been made to improve performance of load controller which injects minimum harmonics and work as a linear dump load. The AC chopper control gives wide control range. The harmonic pattern is symmetrical and only odd harmonics are present. The low order harmonics are eliminated and the order of dominant voltage harmonics can be controlled by adjusting the chopper frequency. It gives the linear control of the

fundamental component of the output voltage. Two different kind of AC chopper have been analyzed based on equal time ratio control (ETRC) AC chopper and sinusoidal PWM AC chopper control. The digital design and implementation of DSP based SEIG-load controller based on ETRC AC chopper controllable load controller for three phase SEIG and based on sinusoidal PWM AC chopper controllable load controller for single phase two winding SEIG has been examined.

The developed sample based controller is simple as compared to traditional PI controller based application. The PI controller is to be tuned for proportional ($K_p$) and integral gain ($K_i$) for dynamic responses, where as in the developed sample based controller only gain (A) is to be adjusted for a given system to regulate overshoot. Further, a fuzzy logic based load controller have also been analyzed and implemented. A fuzzy logic based load controller gives nonlinear control with fast response and virtually no overshoot. The ETRC AC chopper load controller regulates the dump load as linear load with minimum harmonics and excellent dynamic response. A prototype SEIG-load controller system through fuzzy logic based controller with TMS320F2812 DSP has been developed, implemented and its transient behavior is investigated at different operating conditions such as application and removal of static (resistive and reactive) and dynamic loads.

The application of load controller to SEIG system is a simple and cost effective approach to regulate the voltage and frequency but the load controller does not compensate for variable reactive power demand. The performance of SEIG is largely affected by power factor of the load as it draws a reactive current. Then, a part of the excitation capacitance is used to compensate for this reactive load current, so less leading VARs are available for the SEIG itself. On the other hand the load controller injects harmonics in SEIG system. The AC chopper based load controller reduces the harmonics in the system up to satisfactory level. In practice, with the increased used of electronic equipment, a large number of consumer loads are nonlinear in nature and therefore, they inject harmonics in the system. The SEIG's performance is also affected by these harmonics. Hence there is a need to develop a control scheme to regulate the voltage and frequency of SEIG with variable reactive power compensation and harmonic elimination.

The static compensator (STATCOM) compensates for reactive power with increase in load current. STATCOM comprises of a current controlled voltage source inverter with

self sustained DC bus capacitor and coupling inductor. The DC bus capacitor along with coupling inductor together works as a second order filter and eliminates harmonics in the system. STATCOM balances the phase current and thus works as a load balancer. A digital control algorithm for STATCOM based SEIG system has been developed. The control algorithm has been first co-simulated with processor in the loop (PIL) using TMS320F2812 fixed point DSP and then experimentally validated. The Processor-in-the-loop (PIL) provides one verification capability in development process. It is a co-simulation technique which helps to evaluate as how well a control algorithm operates on the fixed point digital signal processor selected for the application. The transient behaviour of SEIG-STATCOM system at different operating conditions such as application and removal of balanced/unbalanced, nonlinear and dynamic load have been investigated. The MATLAB based digital simulation of the transient response has been compared with the experimental results to validate the developed model.

The stand alone operation of SEIG based fixed pitch wind energy conversion system (WECS) with regulated voltage and frequency has also been designed and simulated. The wind turbine is connected to the rotor of the SEIG through a step up gear box which gives a variable torque input with varying wind speed. The proposed controller consists of IGBT based voltage source converter (VSC) and a battery bank in parallel with DC link capacitor. The proposed controller is having bidirectional flow capability of active and reactive power by which it controls the system voltage and frequency with variation of consumer load and the speed of the wind. The VSC functions as a voltage regulator, harmonic eliminator, load balancer for varying consumer load and varying wind speed. The feasibility of the proposed system is verified by simulations.

# ACKNOWLEDGEMENTS

In writing acknowledgements for my Ph. D. thesis, both words and space fall short to express gratitude for a number of individuals/organizations. I would like to pen down some of them through this opportunity. This research work is an out come of moral support from many individuals/organizations directly or indirectly involved with me during my research work at Indian Institute of Technology, Roorkee.

From the deep of my heart, the acknowledgements with warm regards and gratitude goes to my thesis supervisor Dr. S. P. Singh, Professor, Department of Electrical Engineering, Indian Institute of Technology, Roorkee for his proficient and enthusiastic guidance, useful criticism, encouragement and immense support throughout the research work for Ph.D. degree and shape out this thesis in the present form. I sincerely appreciate their pronounced individualities, humanistic and warm personal approach, which has given me strength and inspiration to carry out this research work smoothly. Working under them has been a wonderful experience, which has provided me with a deep insight in the world of research. I humbly acknowledge a lifetime's gratitude to them.

I am thankful with humble submission to Dr. S. P. Shrivastava, Chairman, Dr. J. D. Sharma and Dr. R. P. Saini, Members of my 'Students Research Committee' for inspiring and approving this research work.

My heartily gratitude to Dr. Vinod Kumar, Head, Electrical Engineering Department for his humanistic, encouraging and warm personal approach and for the necessary facilities provided to me to carryout my research work. My full honor goes to Dr. J. D. Sharma, Professor, EED for their co-operations and motivations. I am grateful to the whole administrative and technical staff of EED for their co-operations and help.

I take this opportunity to express my sincere thanks to Vice-Chancellor, Rajasthan Technical University, Kota for sponsoring me to pursue the Ph.D. programme under QIP scheme of MHRD, Govt. of India. My heartfelt gratitude goes to Dr. Y. P. Mathur, Dr. D. Birla, Dr. R. Maheswari, Dr. A. Bindlesh, Mr. A. Khunteta, Mr. Manoj Kumar, Mr. R. S. Sharma, Mr. A. K. Sharma, Mr. S. C. Mittal, Dr. Sunil Jain and R. P. Tripathy of UCE, RTU, Kota for their encouragement and support, which has been constant source of inspiration to me. My special thanks to my colleague and friend Mr. S. R. Kapoor for his

help in different aspects. Thanks are also due to other faculty and staff members of Electrical Engineering Department of my parent Institute for their good wishes and moral supports.

My sincere thanks to the family of my supervisor, Dr. S. P. Singh who have rendered immense support to him so that he can devote enough of his time to research scholars. His affectionate patronage, inexhaustible enthusiasm, kind enough to encourage, sympathetic ear on numerous occasions, positive discussions on research work are deeply recognized. I am thankful to Mrs. Meena Singh and Mr. Rohit Singh for the sign of love and affection towards me.

I am thankful to Dr. Vinod Kumar, Coordinator, QIP Centre, IIT Roorkee for their valuable suggestions and encouragements. I express my thanks to the staff of QIP Centre for their co-operation to carryout the official matters during my stay at IIT Roorkee. The financial support provided by MHRD, Govt. of India through AICTE is sincerely and honestly acknowledged.

My special thanks to Shri Shiv Lal Yadav and Shri Ravindra of Junior Machine Laboratory, Department of Electrical Engineering who generously extended their help and co-operation during my experimental work.

I will never forget my good friends Mr. Sandeep Sood, Mr. S. K. Tomar, Mr. R. Bhakar, Mr. A. Goswami, Mr. J. Upendar, Mr. C. Kotwal, Mr. J. J. Patel, Mr. Subhash, Mr. Nitin Gupta, Mr. R. D. Patidar for their invaluable technical discussion. I am also thankful to friendly hands from Mr. Kranti Kumar, Mr. Harmeet Singh, Mr. Kulbhushan and Mr. Rakesh Sharma, Research Scholars for keeping me always in good sense by their caring words and wholehearted supports and help during the research work.

I wish to thank everybody who has directly or indirectly helped me throughout my research work.

I acknowledge the blessings of my parent Mr. Matadeen and Mrs. Gomti Devi for encouragement and moral support rendered to me throughout my life. I sincerely acknowledge the moral support and encouragement from my brother, Mr. N. K. Palwalia along with his family for the sign of love and affection towards me.

I also acknowledge the kind blessing and support from my sister Mrs. Annu Govind and her husband Mr. Omendra Govind along with their parents Mr. and Mrs. Murari Lal.

I am especially indebted to my wife Mrs. Anjana Palwalia. Her contribution to this work is unexplainable in words. Cheerfulness and tolerance capacity of my daughter Nunmun, who missed many precious moments of fatherly love and care, is really admirable.

Above all, I express my deepest regards and gratitude to "All Mighty: God" whose Divine light and warmth showered upon me the perseverance, inspiration, faith and enough strength to keep the momentum of work high even at tough moments of research work.

I dedicate this research work to my parents, wife and my loving daughter.

**(DHEERAJ KUMAR PALWALIA)**

# CONTENTS

# LIST OF FIGURES

# LIST OF TABLES

# NOMENCLATURE

The symbols used in the text have been defined at appropriate places, however, for easy reference, the important nomenclatures are given below:

| | |
|---|---|
| $a$ | unit complex operator |
| $A$ | gain |
| $C_{dc}$ | DC capacitor |
| $C_f$ | filtering capacitor |
| $C_p$, $C_s$ | capacitances in $C_p$-$C_s$ scheme |
| $V_g$ | air-gap voltage |
| $F$, $\gamma$ | per unit frequency and per unit rotor speed |
| $F_l$, $F_u$ | lower and upper limits of per unit frequency |
| $f$ | frequency |
| $f_b$ | base frequency |
| $i_{ds}$ , $i_{qs}$ | d-axis and q-axis components of stator currents of the SEIG |
| $i_{dr}$ , $i_{qr}$ | d-axis and q-axis components of rotor currents referred to stator of the SEIG |
| $I_{AC}$, $I_{AC,peak}$ | AC line current and Peak AC line current |
| $I_s$ | per phase stator current |
| $I_r$ | per phase rotor current |
| $I_L$ | load current |
| $I_m$ | magnetizing currents of the SEIG |
| $I_{ab}$, $I_{bc}$, $I_{ca}$ | AC line current of SEIG |
| $J$ | moment of inertia of the SEIG including the prime-mover |
| $k_1$, $k_2$ | coefficients of prime-mover characteristics |
| $K_P$, $K_I$ | proportional and integral gain constants of the PI controller |
| $L_m$ | magnetizing inductance of the SEIG |
| $L_f$ | source inductance |
| $L_s$, $L_r$ | per phase stator and rotor (referred to stator) inductance of the SEIG |
| $L_{ls}$, $L_{lr}$ | per phase stator and rotor (referred to stator) leakage inductance of the SEIG |

| | |
|---|---|
| $M$ | time ratio or modulation index |
| $p$ | number of pulse per half cycle |
| $P$ | number of poles of the SEIG |
| $P_c$ | consumer load power |
| $P_d$ | dump load power |
| $P_{out}$ | output power |
| p.u. | per unit |
| pf | power factor |
| $R_L$ | load resistance |
| $R_D$ | Dump load resistance |
| $R_s$ , $R_r$ | per phase stator and rotor (referred to stator) resistances of the SEIG |
| $R_f$ | source resistance |
| $\Psi_m$ | magnetic flux linkage |
| $T_e$ | electromagnetic torque of the SEIG |
| $T_{shaft}$ | shaft torque |
| $T_L$ | load torque |
| $\mu F$ | micro-farad |
| $V_{DC}$, $V_{DC,peak}$ | DC voltage and peak DC voltage |
| $V_P$ | peak amplitude of AC voltage |
| $V_{LL}$ | line to line AC voltage |
| $V_t$ | terminal voltage of SEIG |
| $V_{abc}$ | terminal voltage |
| $v_{ds}$ , $v_{qs}$ | d-axis and q-axis components of stator voltages of the SEIG |
| $v_p$, $v_n$, $v_o$ | positive, negative and zero sequence components of generator voltage |
| $v_a$ , $v_b$ , $v_c$ | stator voltages of a, b, c phases of the SEIG |
| $v_{ab}$ , $v_{bc}$ , $v_{ca}$ | AC line voltages |
| $\omega$ | angular frequency |
| $\omega_r$ | rotor speed of the SEIG |
| $X_{ls}$ , $X_{lr}$ | per phase stator and rotor (referred to stator) leakage reactances of the SEIG |
| $X_m$ | magnetizing reactance |
| $X_{ml}$, $X_{mu}$ | lower and upper limits of magnetizing reactance |

| | |
|---|---|
| $Y_p$, $Y_n$, $Y_0$ | positive, negative and zero sequence components of generator admittances |
| $Z$ | impedance |
| $Z_L$ | load impedance |

# ABBREVIATIONS

| | |
|---|---|
| AC | Alternating current |
| DC | Direct current |
| DSP | Digital signal processor |
| ELC | Electronic load controller |
| ETRC | Equal time ratio control |
| GIC | Generalized impedance controller |
| HP | Horse power |
| IG | Induction generator |
| IGBT | Insulated Gate Bipolar Transistor |
| IM | Induction motor |
| MMF | Magneto motive force |
| PI | Proportional and integral |
| PM | Prime-mover |
| PWM | Pulse width modulated |
| RF | Ripple factor |
| SEIG | Self-excited induction generator |
| STATCOM | Static synchronous compensator |
| SUMT | Sequential unconstrained minimization technique |
| SVC | Static VAR compensator |
| TCR | Thyristor-controlled reactor |
| THD | Total harmonic distortion |
| TSC | Thyristor switched capacitor |
| VAR | Volt-ampere reactive |
| VSI | Voltage source inverter |
| VSC | Voltage source converter |
| WECS | Wind energy conversion system |

# CHAPTER-1

# INTRODUCTION AND LITERATURE REVIEW

## 1.1 INTRODUCTION

The excessive use of conventional sources of energy has increased the fast depletion of the fuel reserves. This has resulted in the subsequent increase in energy cost, the environmental pollution and above all the global warming. Many studies have been conducted to rationalize the use of the conventional sources of the energy and to explore the use of other forms of the energy. This has motivated the world wide interest in reducing the pollution and conservation of the limited conventional fuels by encouraging more and more use of the energy available from the non-conventional/renewable sources such as the wind, the biogas, the tidal waves and the small hydro power stations on the running canals and rivulets etc. The potential of the energy available from the small hydro and the wind sources seems to be quite promising to meet the future energy demands, especially in the remote and isolated areas. The objective of the harnessing of such non-conventional energy sources could be achieved in a big way by the development of the suitable low cost generating systems. The electric power generation from these sources will not only supply the energy to the remote and isolated areas, but can also supplement the power requirements of the inter-connected systems. However, these systems will become more viable if their cost is reduced to the minimum. Therefore, the squirrel cage rotor induction generators are receiving much attention for such applications due to its low cost and robust construction.

An induction machine can be used as an induction generator in two ways, namely, in the externally excited mode and in the self excited mode. The externally excited induction generator draws its excitation in terms of lagging magnetizing current from power source to which it is connected, to produce its rotating magnetic field. The frequency and voltage of the externally excited induction generator is governed by the frequency and voltage of the power source with which it is excited. However, if an appropriate capacitor bank is connected across the terminals of rotating induction machine, a voltage is developed across the machine terminals. The residual magnetism in

the magnetic circuit of the machine sets up small voltage in its stator winding. This voltage is applied to the capacitor and causes the flow of lagging current in the stator winding which produces rotating flux in its air gap. This rotating field produces the voltage across the machine terminals. Such generators are called as the "Self Excited Induction Generators (SEIG)" and can be used to generate the power from constant as well as variable speed prime movers. Figure 1.1 shows a schematic diagram of self excited induction generator.

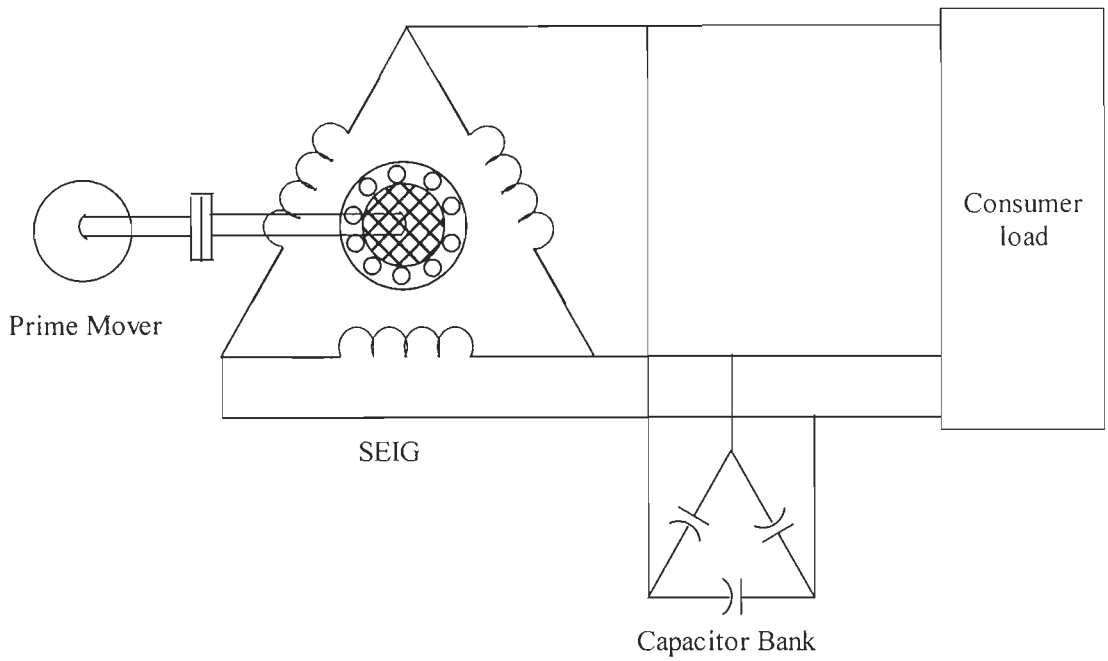


**Figure 1.1: Schematic diagram of self-excited induction generator.**

Harnessing the renewable energy sources for electric power generation is an area of research interest and nowadays the emphasis is being laid on the cost effective utilization of theses resources for quality and reliable power supply. Traditionally, synchronous generators have been used for power generation, but induction generators are increasingly being used these days to harness renewable energy resources because of their relative advantageous features. These features include maintenance and operational simplicity, brushless and rugged construction, lower unit cost, good dynamic response, self protection against faults and ability to generate power at varying speed. Also, the induction generator does not require separate DC exciter and its related equipment like field breaker, rheostat and automatic voltage regulator and therefore requires less

maintenance. These advantages facilitate induction generator operation in stand-alone/ isolated mode or in parallel with synchronous generator for supplying local load and in grid mode. In remote locations or hilly areas, a micro-hydro system with unregulated low head turbines, which maintain almost constant input power due to fixed head and discharge coupled with self excited induction generator may be one of the most suitable option for supplying local loads. Figure 1.2 shows a typical schematic of micro hydro power system.

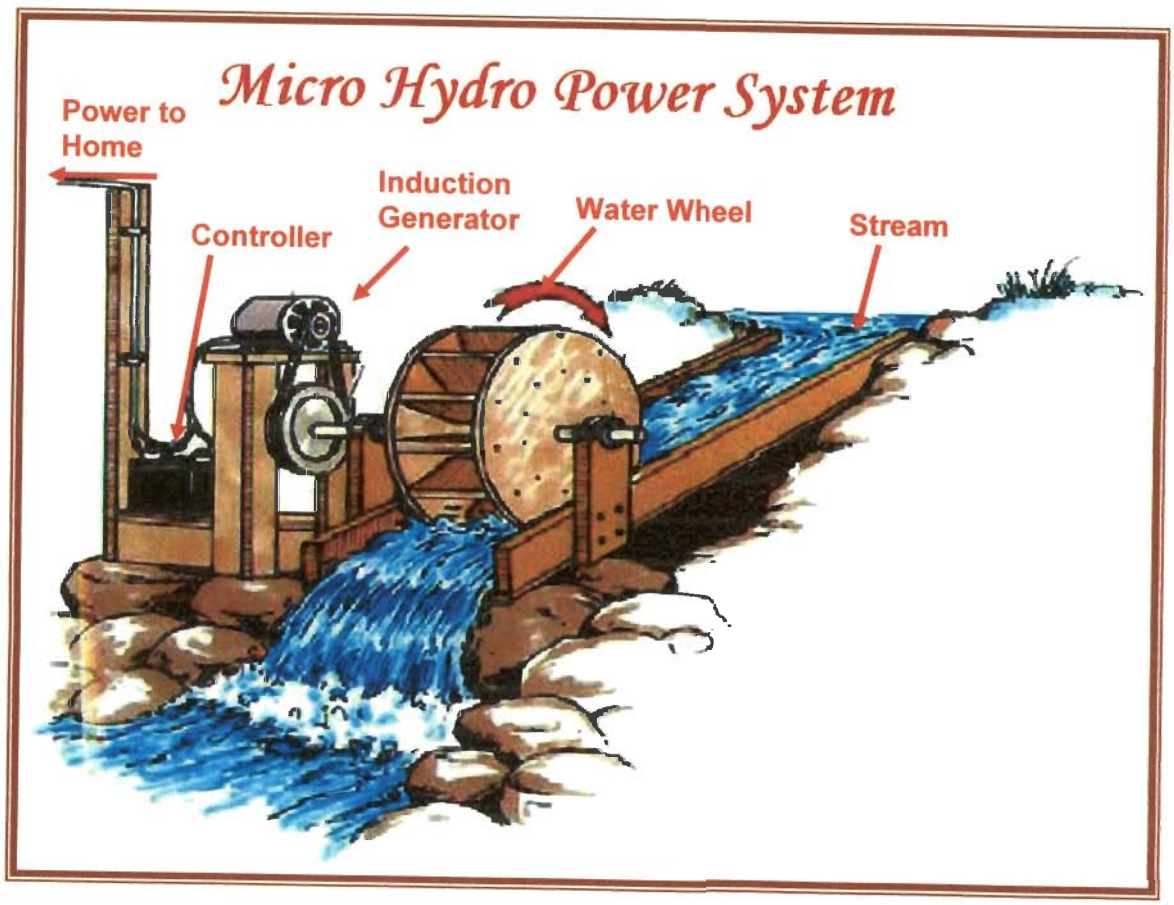


**Figure 1.2: Typical schematic of micro hydro power system.**

In spite of a number of advantages, the SEIG suffers form inherent poor voltage and frequency regulation. The generated voltage depends upon the speed, excitation capacitance, load current and power factor of the load. Hence, a suitable control scheme is to be developed to regulate the voltage and frequency of SEIG. Also, such control scheme should be simple, economical, rugged and reliable. The importance of induction generator in small scale power generation systems utilizing the renewable energy resources to

enhance the rural electrification justifies the selection of the topic of research on stand-alone induction generator systems.

## 1.2 LITERATURE REVIEW

The concept of self-excitation of induction machine emerged for the first time in 1935, when Basset and Potter [26] reported that the induction machine can be operated as an induction generator in isolated mode by using external capacitor. Authors concluded that the induction machine with capacitive excitation would build up its voltage exactly as does a dc shunt generator, the final value being determined by the saturation curve of the machine and by the value of reactance of the excitation capacitance. The induction generator can be made to handle almost any type of load. The performance characteristics of the three phase SEIG at no load and on load has been given by Wanger [221]. The terminal voltage and slip are obtained for given load, excitation capacitance and prime mover speed by separating real and imaginary parts of the equivalent circuit.

Barkle et al. [25] have described the theory and application of an induction generator. Authors have given the equivalent circuit and phasor diagram of an induction generator. Authors further reported that equivalent circuit contains two variables: the slip (s) which is a function of speed and magnetizing reactance ($X_m$) that is determined by saturation and is a function of the air-gap voltage ($E_g$). After knowing the values of variables, performance characteristics of SEIG can be achieved. Authors have reported that behavior of induction generator depends on the terminal voltage to establish the magnetizing current hence under short circuit condition terminal voltage collapses. Authors have mentioned that generated frequency of SEIG increases with speed. Due to increase in frequency, VAR output of capacitor increases directly and consequently maximum voltage resulting from self-excitation also increases. The application of SEIG for aircraft systems [54, 68] has been reported. In late seventies Novotny et al. [141] investigated the self-excitation in the inverter driven induction machine when the inverter switching frequency is below the machine speed. During self excitation, the generator found capable of supplying load via slip control. In this mode, the inverter acts as controllable means of energy circulation for the reactive kVA of the machine and load. In early eighties Murthy et al. [133] reported a procedure to analyze the SEIG using the fixed and variable parameters of the machine. Following this, many researchers has undertaken the steady state analysis of SEIG and documented in the literature.

The analysis of SEIG is more complicated compared to grid connected induction generator due to magnetic nonlinearity. The steady state analysis of SEIG involves computation of magnetizing reactance and frequency for specified speed, load, excitation capacitance and magnetizing characteristic. Broadly, the methods to obtain magnetizing reactance and frequency can be classified in two categories namely loop impedance method or nodal admittance method. Murthy et al. [133] suggested the analytical technique in which the equivalent loop impedance was resolved into two polynomials by separating real and imaginary parts. These polynomials are solved to obtain magnetizing reactance and frequency by Newton-Raphson method. The accurate physical interpretation of self excitation phenomenon, the importance of residual magnetism for self excitation, possible causes for loss of residual magnetism and correspondingly, the measures for its revival are described by Elder et al. [66]. Quazene and McPherson [153] have reported the nodal admittance method considering the admittance across the nodes defining air gap voltage. The frequency is computed by solving polynomials for real power balance across air gap and the magnetizing reactance is obtained by equating imaginary part of the admittance to zero. Tandon et al. [207] have given a complex frequency approach with operation equivalent circuit and its characteristic polynomial is formed which is of fourth degree with complex coefficients and solved by numerical method to obtain the frequency of operation. Further, authors [208] have introduced another simplified method assuming per unit speed equal to per unit frequency and forming a quadratic equation. The quadratic equation is solved to obtain magnetizing reactance and per unit generated frequency.

The analysis presented in papers [133,153] is carried out neglecting the core loss, which is considered by Malik and Haque [121] for computing the performance of the SEIG. Murthy et al. [138] have observed that the induction motor with restriction on stator thermal limit can be used as SEIG. Bailey [23] has recommended different protection systems for the induction generator connected to a grid system. Author has recommended the switching device to start or stop the unit during abnormal conditions, short circuit protection device, over load protective device, ground fault protection device, rotor overheating protection, bearing over temperature device, vibration protection device, over speed protective device, reverse power protective device, over voltage and over excitation protection and utility interface protection. Al-Jabri and Alolah [19] have reported the upper and lower limiting values of capacitance and speed for SEIG to maintain self

excitation and observed that there is an optimal choice for the speed, terminal capacitor and load that gives maximum output power. Al-Jabri [21] has developed closed form of expression for both unit frequency and the magnetizing reactance based on approximate method.

Singh et al. [194] has developed an analytical technique to obtain the performance characteristics of a cage induction machine operating as SEIG in stand-alone mode. The developed technique has been extended and single-variable optimization is carried out for the selection of optimum voltage corresponding to maximum output power at a given speed and specified stator current. Chan [45] has proposed two techniques of the steady-state analysis of the SEIG. The first technique employs a parameter elimination procedure to yield a seventh degree polynomial in the per unit frequency. The numerical solution of the polynomial then enables the prediction of performance of the SEIG. The second technique is based on the nodal admittance method where the symbolic programming method is employed for the derivation and solution of the higher degree polynomial. Later on, author [44] proposed an iterative technique to include core loss effect and the series capacitance compensation in the performance analysis of the SEIG. Singh et al. [195] have used the simplified equivalent circuit to compute the per unit frequency and magnetizing reactance. A single variable optimization is applied for the computation of the excitation requirement for a given terminal voltage. Subsequently, authors extended the technique [193] to the case of three-variable optimization. The papers [17, 46,158] describe the methods to analyze the steady-state performance of SEIG driven by regulated and unregulated prime-mover.

Appropriate choice of excitation capacitance is required to initiate voltage build up and to maintain a given terminal voltage with variation in load. Different techniques for determination of capacitance requirement for excitation of the SEIG have been reported in literature [20, 35, 41, 67, 80, 117, 118, 119, 122, 123, 134, 201, 204, 205, 218, 219, 228]. Murthy et al. [134] have presented the steady state analysis to determine the reactive power requirement of SEIG with constant speed and variable speed prime mover. Malik and Mazi[123] have given a trial and error method to compute the capacitance requirement of the SEIG. Authors have shown that the minimum capacitance requirement of the SEIG varies inversely to the square of the speed and inversely proportional to the maximum saturated magnetizing reactance. Al-Jabri and Alolah [20] gave a direct method for

computing the minimum capacitance for excitation of stand alone SEIG. Malik and Al-Bharani [122] have shown the influence of excitation capacitor on the steady state performance characteristic of stand alone SEIG feeding a balanced load and gave the value of excitation capacitance range to sustain self excitation. The method for calculating minimum capacitance required for the initiation of the voltage build up has been explored [41, 204, 205] and has also been extended for maintaining a given terminal voltage under load. Shridhar et al. [201] have examined the self regulating feature of the SEIG by connecting additional capacitors in series with the load in long shunt and short shunt configuration. Authors have further explained a methodology to choose appropriate set of values of these capacitors for desired voltage regulation.

Wang and Lee [218] proposed a direct and simple method, based on eigen value and eigen value sensitivity analysis to predict the minimum value of capacitance required for self-excitation of an induction generator. The method has been extended by Mahato et al. [117, 118, 119] for computing the optimal value of capacitor for maximum efficiency for three phase induction machine used as a single phase SEIG. Authors further gave a methodology to determine the minimum and maximum value of capacitance for single phase SEIG using three phase induction machine. A new simple approach for computing the minimum value of capacitance necessary to initiate the self-excitation process in three-phase isolated induction generators has been presented by Harrington and Bassiouny [80]. It is based on the analysis of the complex impedance matrix of the induction generator when inductive load is connected. Chakraborty et al. [35] have given direct methods derived from loop and nodal analysis to find different criteria for maintaining self-excitation. Wang and Su [219] have presented a simple approach based on a linearized d-q axes dynamic model using first-order eigenvalue sensitivity to determine both minimum and maximum values of capacitance for a isolated SEIG. Zidani and Naciri [228] have reported a numerical approach for the optimal capacitor used for the SEIG. A new simple formula to determine minimum capacitance required for SEIG has been presented by Eltamaly [67]. By using this formula, there is no need to use iterative technique and it can be used to obtain the minimum capacitance required on-line.

In remote locations or hilly areas, electrical energy can be obtained from local resources at cheaper cost compared to grid connection. Such areas are characterized by sparsely distributed population with electric loads of single-phase. The single phase power

supply is preferred over three phase in order to render the distribution system simple and cost effective. It is possible to use a three-phase induction motor as a single-phase generator with suitable excitation capacitor connection. Three phase SEIG supplying single phase load is the case of unbalanced operation; hence it is required to operate the machine at de-rated power so that the temperature rise, vibration in shaft and stress on insulation of the machine is restricted within permissible limits. The appropriate choice of excitation capacitance and connection scheme is necessary in order to initiate voltage build up, maintain given terminal voltage and optimized operation of the three phase induction machine working as single phase SEIG. Study state performance analysis of three phase SEIG for single phase power generation is given in literature [14, 22, 27, 38, 39, 40, 42, 47, 48, 49, 50, 73, 74, 75, 94, 112, 113, 114, 115, 116, 155, 166, 168, 197, 212, 213,]. Smith [197] has suggested the balanced operation of a three phase induction generator connected to a single phase line using two phase-shifting capacitors. This method requires the use of unit ratio transformer, which makes the system costly. Rahim [155] has given the performance analysis of a three phase induction generator when a single excitation capacitor is connected across one phase or between two lines and loads are connected to the other phases or lines. Alolah and Alkanhal[22] have given an optimization method to determine the excitation requirements of three-phase delta connected SEIG under single phase mode operation using two excitation capacitors. A novel scheme based on eigen value method [212, 213] has been proposed to determine the minimum and maximum value of excitation capacitance required for an autonomous three phase SEIG feeding a single phase load. Chang and Lai [40] have given a method for computing the minimum capacitance needed to initiate voltage build up in a three phase SEIG with a single capacitor and supplying a single phase load.

A two capacitor excitation scheme in '*C-2C*' configuration [27] of three phase SEIG for supplying single phase load offers almost balanced operation of three phase delta connected SEIG at partial power output. Further, for a purely resistive load, if the current of '*C*' valued capacitor is equal to square root of three times of current in resistive load then '*C-2C*' connected generator behaves as a balanced three phase machine. Shilpakar et al. [166] have given the transient performance of the three phase SEIG supplying single phase load with '*C-2C*' configuration. Authors have developed a dynamic model in stationary reference frame along d-q axes and found that the balanced operation is

maintained at fixed load depending on the value of excitation capacitance. Fukami et al. [73, 74, 75] have proposed a new single phase induction generator consisting of the three phase induction machine with three excitation capacitors and have shown that in addition to improved voltage regulation, the inherent vibration and noise in the generator can be significantly reduced. A novel and simple approach [112, 113, 115] has been given based on eigen value and also sequential unconstrained minimization technique for determination of both the minimum and maximum values of capacitance required for self excitation of an isolated single phase induction generator using a three phase machine with three excitation capacitor in '$C_p$-$C_s$' connection.

Chan[42] has analyzed the performance of a three phase induction generator connected to a single phase power system and found that significant improvement in machine performance in terms of phase imbalance, efficiency and power factor is obtained by using a single static phase converter. Chang and Lai [39, 47] proposed a novel scheme for single phase power generation using a three phase induction machine with each shunt and series excitation capacitor. Single phase operation of a three phase induction generator using a novel line current injection method is reported in [49, 50], which shows that capacitances that result in perfect phase balance depends on the generator admittance, power factor angles and the turn ratio of the current injection transformer. Kumaresan [94] has given a genetic algorithm based approach for analysis of single phase operation of three phase SEIG.

Single phase two winding induction motor can be used as single phase SEIG. Their use is limited to relatively small power outputs up to 5kW. The available literature [11, 36, 43, 86, 132, 135, 136, 142, 143, 145, 146, 147, 148, 149, 150, 156, 171, 173, 184, 187] divulge the use of two winding single phase induction motor as single phase self excited induction generator. The steady state analysis [43, 132, 135, 136, 156, 171] helps to find appropriate choice of excitation capacitance necessary in order to initiate voltage build-up and to maintain a given terminal voltage, when the SEIG is loaded. Singh et al. [173, 187] has analyzed the steady state performance of single phase self excited induction generator and experimental investigation for lighting loads has been reported. Murthy et al. [132, 135] reported the self regulating feature of single phase SEIG by connecting a capacitor in series with the load. The mathematical model used for the analysis, however, is based on the simplification that the current in the magnetization reactance referred to the backward

field is neglected. Since, the forward rotating field is associated with the generator action and the backward rotating field is associated with the plug-braking action, the predicted power output of the generator based on these assumptions yields the optimistic result.

Rahim et al. [156] have shown that power can be extracted from the main winding when the machine is excited through the auxiliary winding. Chan [43] reported the analysis of single phase SEIG in which the excitation capacitors and load are connected across the terminals of the same winding and per unit frequency independent of the magnetization reactance is determined with assumption that the magnetization reactance referred to backward field is neglected. Ojo [145] has explored the dependency of load impedance on generator self excitation using large signal and dynamic models of a single phase two winding SEIG. Further, author has concluded that for self excitation, minimum amount of air gap flux linkage is required and also, maximum load impedance for specified rotor speed and excitation capacitors when load is connected in series with main winding. In another work [146] authors demonstrated the influence of three capacitor excitation topologies of shunt, short shunt and long shunt on the steady state and dynamic performance of a single phase SEIG. The steady-state and dynamic performance characteristics of a novel, stand-alone single-phase induction generator scheme in which the load voltage and frequency are regulated using a full-bridge PWM DC/AC inverter has been reported by Ojo and Gonoh [143]. The operation, performance and the expansion of the operating range of a single-phase self excited induction generator with a PWM inverter have been presented by Ojo et al. [86, 147, 148, 149, 150]. The basis for design, analysis and quantifications of the conditions for self-excitation in a source less PWM inverter excited and controlled single-phase induction generator are established and demonstrated in [86]. The enhancement of the operating range of a stand-alone single-phase induction generator scheme with an inverter battery system connected to the auxiliary winding is discussed in [148]. Singh and Shilpakar [171] have presented the steady-state analysis of a single-phase SEIG and verified with experimental results for fixed shunt capacitor excitation, fixed and variable shunt capacitor excitation and shunt-series capacitor excitation.

The over voltage, current surge, torque etc. resulting from various transient conditions such as sudden change in load, capacitance and input power, short circuit, open circuit and various unbalanced conditions can be accurately estimated by using appropriate

dynamic model. These parameters help in finding the suitability of winding, insulation level, capacitor rating and drawing the guidelines for control and protection. The park transformation, which refers stator variables to the variables associated with fictitious winding rotating with rotor, has revolutionized the dynamic analysis of synchronous generator eliminating all time varying inductances [152]. Krause and Thomas [92] have suggested that referring both stator and rotor variables to a reference frame rotating at arbitrary speed eliminates all time varying inductances of induction machine. In the literature transient analysis of induction machine is carried out in a, b, c phase reference frame or d-q reference frame [16, 53, 55, 61, 104] with either the currents or the fluxes as state variables. Based on models listed above, some other models have been worked out such as small signal model [127], reduced order model [222], hybrid model [130]. For most of the analysis, the d-q model with currents as state variables is found suitable and the analysis can be carried out in stationary, synchronous, rotor or arbitrary reference frames. However, the accuracy of the model depends on appropriate treatment of saturation.

The transient/dynamic analysis of self excited induction generator is well documented in literature [26, 69, 78, 79, 83, 105, 106, 107, 108, 109, 120, 127, 128, 144, 159, 161, 200, 211, 214, 217, 218, 220]. The assumption made in classical theory that the magnetizing characteristic of machine can be approximated by straight line through origin is found unsatisfactory for many transient conditions such as switching off and reclosing transients of induction motor. The need to model the saturation is experienced for the simulation of these conditions, however, the development in converter fed induction motor drives and induction motor application for generation has increased considerable interest in including main flux saturation in dynamic model. Even, the self excitation process can not be modeled unless main flux saturation is included in model. Melkebeek [127, 128] gave an improved method for incorporating the main flux saturation in small signal model of saturated induction machine and examined the stability limit of self excited induction generator. The saturation of leakage path [109] is found important during start up and reverse transients of induction motor, however its effect is small. Vas et al. [211] have explained that in quadrature phase smooth air-gap machine, saturation in one axis affects the saturation in the other and vice versa, and the effect of coupling terms between the two axes are introduced. This phenomenon is known as cross saturation. Grantham et al. [78]

modeled the transient process of voltage and current, both during self excitation and load perturbations of the SEIG excluding the effect of cross saturation. Hallenius et al. [79] have stressed the importance of cross saturation in self excited induction generators. The transient performance of SEIG and short shunt SEIG under balanced conditions is presented by Shridhar et al. [200].

A complex current state space model is developed by Levi and Rauski [211] to predict the transient process of saturated deep bar and double cage SEIG for wind power generation. Levi [106] has given a generalized method of main flux saturation modeling in orthogonal axis models of induction machines. Ojo [144] has given that a minimum air gap flux linkage is required for the self excitation and the stable operation of SEIG. The minimum air gap flux linkage is the value at which the derivative of the magnetizing inductance with respect to the air gap flux linkage is zero. Liu and Chang [108] have reported a digital simulation technique to study the operations of self excited generator systems with arbitrary external switching network configuration and to analyze the system transient responses under various system conditions. This technique has the ability to investigate the detailed on-off operation of switching elements in the self excited generator system. Also, the total numbers of system equation are greatly reduced by this technique.

Wang et al. [214, 218] have presented the transient performance of stand alone SEIG under the voltage build up process, sudden switching off one excitation capacitor and sudden switching off of two excitation capacitor. It has been observed that one of the three balanced excitation capacitor is switched off from the machine terminal, still SEIG can maintain self excitation and generates adequate voltage on other two phases. When two out of the three balanced excitation capacitors are switched off from the machine, the SEIG generated voltage collapse and gradually reduces to zero. Slama and Holmes [161] have carried out transient and steady state load performance of a stand alone SEIG. An optimization technique has developed to compute the minimum value of capacitance. Jain et al. [83] carried out the transient performance of three-phase SEIG during balanced and unbalanced faults considering the effect of main and cross flux saturation. Kuo and Wang [96] have studied both the transient and steady-state performances of an isolated SEIG supplying a rectifier load considering a hybrid model based on a-b-c and q-d induction machine models to improve the simulation results. Mahato et al. [120] has presented the transient behavior of a three-phase star connected SEIG using three capacitors connected

in series and parallel with a single-phase load. Authors developed steady state and dynamic model based on stationary reference frame *d*–*q*-axes theory incorporating the effect of cross-saturation.

The dynamic loads, particularly induction motors, constitute a large percentage of the practical loads. These machines when put into operation, causes voltage dip, large inrush current and their power factor does not remain constant throughout the loading range. The analysis of SEIG supplying induction motor load (SEIG-IM) configuration is important for the wider applicability of SEIG. Shridhar et al. [202] have given a method for evaluating the steady state performance analysis of SEIG feeding induction motor load and discussed the capacitance required for the startup of motor and for the steady state operation of the configuration. Subsequently Singh et al. [191] have presented the transient performance analysis and Alghuwainem [18] have also given the steady state analysis of SEIG feeding dynamic/induction motor load. Kuo and Wang [95, 97] have proposed an eigen value analysis based on synchronous reference frame to determine the critical operating conditions and dynamic stability of a SEIG feeding a loaded induction motor. Later, they investigated and compared the validity of dynamic eigen value analysis of the studied SEIG on stationary reference frame and synchronously rotating reference frames. Wang and Lee [215] have presented a comparative study of long shunt and short shunt configurations on dynamic performance of SEIG feeding induction motor load. Singh et al. [192] have identified the unstable behavior of short-shunt SEIG feeding induction motor during the starting of the induction motor load and proposed the use of damping resistors across series capacitors to obtain the stable operation during the starting and loading.

The increasing load demand in stand alone system can be fulfilled by operating a number of SEIG in parallel [13, 15, 37, 71, 72, 103, 151, 160, 165, 216, 223]. Shilpakar et al. [165] have reported the transient behavior of SEIGs operating in parallel. Chakraborty et al. [37] have analyzed the effect of parameter variations on the performance of parallel-operated SEIGs. Farret et al. [71, 72] have developed an automatic procedure to build-up a matrix model for steady-state and transient analysis, valid for any number of SEIGs operating in parallel. Dynamic simulation and analysis of parallel SEIGs for isolated wind farm systems have been carried out by Palle et al. [151]. Watson and Milner [223] have examined the parallel operation of single-phase SEIGs. Al-Bahrani and Malik [13] have

proposed two general methods of analysis to control the terminal voltage of any number of parallel SEIGs.

The dynamic performance of SEIG operating in parallel and feeding induction motor load is presented by Wand and Lee [216] and the minimum value of shunt capacitance required for excitation is obtained. Shunt capacitors which are being employed with induction motor for reactive power compensation during start up and steady state[160], are found effective in regulating terminal voltage during small load changes. However, series capacitors are found effective for voltage control during large load changes. The compensated SEIG-IM configuration may involve sub synchronous resonance (SSR). The SSR phenomenon is observed even with negligible series compensation during starting and large transients and the use of damping resistors across series capacitors. To supply widely varying reactive load, induction and synchronous generator can be operated in parallel. The synchronous and induction generators operating in parallel with adequate capacitors may provide robust and cost-effective operation [174].

The self excited induction generator has a major drawback of poor voltage regulation. The inherent poor voltage regulation of the SEIG is due to the difference between the reactive power supplied by the excitation capacitors and that demanded by the load and the machine. This is a major bottleneck of its application in isolated mode. The generated voltage of the SEIG depends upon the speed, excitation capacitance, load current and power factor of the load. Effort have been made by researcher to overcome this problem [1, 2, 3, 4, 5, 6, 7, 8, 9, 10, 11, 12, 28, 29, 30, 33, 51, 52, 53, 62, 63, 64, 78, 84, 85, 87, 89, 90, 91, 96, 99, 100, 110, 124, 125, 126, 129, 131, 137, 146, 154, 162, 164, 172, 176, 177, 178, 179, 180, 181, 182, 183, 185, 186, 188, 189, 192, 198, 199, 201, 203, 204, 215, 226]. The voltage regulation schemes are based on to compensate for variable reactive power demand of SEIG under varying consumer load. The voltage regulation with saturable core reactor [64, 129, 176] is costly, not only due to the cost of the inductor required, but also because they must be matched to particular machine used. The poor voltage regulation can be improved by using the voltage regulator based on six pulse naturally commutated converter [215], AC-DC converter [64], PWM inverter [131, 225], switched capacitor [63, 64] but these are not cost effective solutions. Voltage regulation based on shunt and series capacitor excitation [28, 192, 201, 215] gives a cost effective solution but they are not suitable for dynamic load and series capacitor produces sub

synchronous resonance. The configuration requires different value of capacitances for optimum voltage regulation. Marra and Pomilio [126] have proposed a constant frequency operation mode to isolated induction generator systems. The control strategies for both voltage and frequency regulation of SEIG are presented on the basis of variable structure control theory with sliding mode control [203] that can offer good dynamic response and robust behavior upon changes in load and generator parameters.

A considerable work has been reported on the voltage regulation using SVC [1, 2, 3, 4, 5, 6, 7, 8, 9, 10, 11, 33]. Experimental work on the voltage regulation of SEIG driven by a constant speed prime mover (CSPM) using SVC composed of thyristor-controlled reactor (TCR) with a fixed capacitor has been presented [33]. Ahmed et al. [10] have proposed the static VAR compensator (SVC) composed of the fixed excitation capacitor bank in parallel with the thyristor phase controlled reactor (TCR) and thyristor switched capacitor (TSC) for the voltage regulation of the three-phase SEIG driven by variable speed prime-mover and described an algorithm for evaluating the minimum excitation capacitance required for the three-phase SEIG. An algorithm [7, 8, 9] has been presented for evaluating the steady-state performance analysis of three-phase SEIG and designed a PI controller based feedback closed loop voltage regulation of the three-phase SEIG using SVC. The single-phase SVC composed of TCR, TSC and the fixed excitation capacitor [2, 4, 11] is applied for smooth regulation of generated output voltage of the single-phase SEIG system. Ahmed et al. [6] proposed SVC and AC load voltage regulation scheme for DC outputted three-phase induction generator. The dynamic performance responses of the three-phase SEIG, directly connected to the full bridge diode rectifier circuit for a DC load, have been demonstrated [3, 5].

A cost effective voltage and frequency regulation can be obtained by using a load controller. The load controller controls the load at SEIG terminal by connecting a dump load in parallel with consumer load and keeps the load at generator terminal constant. Under this mode of operation, SEIG requires constant value of exaction capacitance. A number of load controller schemes for both induction and synchronous generators are reported in literature [29, 30, 53, 63, 91, 99, 137, 179, 180, 181, 182, 183, 188, 189]. A four-step binary weighted load controller (BWLC) using integral cycle method was reported by Elder et al. [63]. Henderson [78] proposed the BWLC with current balancing feature for the synchronous generator. A load controller consisting of a thyristor bridge

with phase angle control and a chopper with pulse width control has been described in [29, 30]. Transient analysis of SEIG with ELC has been performed by Singh et. al [181]. Authors have also reported an improved ELC for micro-hydel applications [179], and designed and developed electronic load controller for SEIG [180, 183]. A new control scheme consisting of a STATCOM with chopper and dump load is proposed in [189], for voltage and frequency regulation of the uncontrolled small-hydro power turbine driven SEIG. The combination of chopper with dump load at DC bus of STATCOM keeps the load constant on the SEIG. Chatterjee et al. [53] have presented the performance analysis of a stand-alone SEIG with generalized impedance controller (GIC) (voltage source pulse width-modulated bi-directional inverter with DC link battery), from the point of view of the SEIG terminal voltage and frequency. The GIC is found to be capable of maintaining the frequency of the SEIG constant under open-loop condition, following the speed and load perturbations. Singh and Kasal [188] have given the voltage and frequency controller for isolated asynchronous generator feeding 3-phase 4-wire loads for constant power applications such as pico-hydro with uncontrolled turbines.

The load controller is a simple and cost effective solution for voltage and frequency regulation of SEIG but it doesn't provide reactive power compensation. The consumer load of reactive nature affects the performance of SEIG. A static synchronous compensator (STATCOM) can provide continuous variable reactive power to the SEIG with varying load. The STATCOM consists of IGBT based current controlled inverter with DC bus capacitor and AC filtering inductor. A STATCOM based voltage regulation has been reported in literature [12, 89, 90, 96, 100, 124, 125, 126, 131, 162, 164, 172, 177, 178, 179, 185, 186, 226]. Alan and Lipo [12] have proposed a new generating system consisting of poly-phase induction generator/motor that is completely isolated from the utility. Margato and Santana [124] have presented the modeling and behavior of the induction generator excited by current source inverter and supplying a diode bridge at constant output voltage. Larsen et al. [100] have given the benefits of STATCOM over the SVC system and showed that the steady state as well as transient performance can be improved with STATCOM. Singh and Shilpakar [172] have reported a solid-state voltage regulator for SEIG with static load. Marra and Pomilio [125] have explored the SEIG controlled by variable speed PWM bi-directional converter to provide high quality AC sinusoidal regulated voltage with constant frequency for rural application. A controller to

regulate three-phase AC output voltage of the SEIG with varying rotor speed, transient load conditions and reactive loads have been proposed by Wekhande and Agrawal [226]. A method of voltage control of SEIG under unbalanced/non-linear load using current controlled voltage source inverter has been described by Kuo and Wang [96]. Modeling, analysis and control of a current-source inverter (CSI) based STATCOM is reported by Shen and Lehn [164] who presented d-q frame model of the CSI-STATCOM and derived its steady-state characteristics. Singh et al. [178, 185] described the STATCOM based voltage regulator for SEIG feeding unbalanced / non-linear loads. Analysis and design of STATCOM based voltage regulator for SEIGs has been reported in [186].

The continuous research on power generation from wind through different schemes using solid state converters has resulted in significant progress in wind energy electric systems for supplying isolated load with SEIG [56, 57, 58, 70, 111, 163, 169, 175, 224, 225, 226]. Daly et al. [56] have explored water storage heating system by wind-driven induction generator. The paper is mainly concerned with design of the controller to operate the wind turbine at its optimum tip-speed ratio and maximize the generator efficiency. Wekhande and Agarwal [224, 225, 226] have proposed a new PWM controller to regulate the terminal voltage of the SEIG with varying rotor speed, transient load conditions and reactive load. The controller does not require any mechanical sensor thereby reducing complexity and cost of the system. Lopes et al. [111] and Singh et al. [175] have discussed the voltage and frequency regulation of wind driven self excited induction generator through current controlled voltage source inverter.

## 1.3 AUTHOR'S INFERENCE

On the basis of literature reported in the preceding section, it is found that there is a strong need to develop a simple and cost effective power supply system for rural areas. A suitable mechanism may be given for their trouble free operation with quality power supply in isolated mode using SEIG addressing the issue of voltage and frequency regulation. The scope of the proposed research is outlined as follows:

The economical implementation of digital systems from a hardware complexity standpoint, with the goal of minimizing the computational work load has always been an appealing research topic. As of now, analog controllers are in use and need sensing and control circuit which needs too many circuit element. In event of failure of any component

it becomes tedious and time consuming job to find the fault and repair and put the system in order. However, a single chip solution is cost effective and can eliminate the use of complicated control circuit. A control algorithm can be loaded in the chip. A single chip provides flexible solution, multiple features implementation on single processor and fast processing to implement advanced and complex algorithm.

The load controllers for SEIG system developed by different researchers are based on analog circuits with conventional PI controller. The digital controller design and single chip integration can reduce the hardware complexity and increase the reliability of the system. The use of fixed point DSP is cost effective. Load controllers based on mark space ratio control are non-linear in nature which injects harmonics in the system. Hence there is a need to improve the control technique. An AC chopper control based on equal time ratio control (ERTC) and sinusoidal PWM makes the load controller system linear and harmonic injected in the system are less.

The fuzzy logic control has advantage of coping with larger parameter variation of the system and it provides improved performances in terms of overshoot limitation and sensitivity to parameter variation. The use of DSP gives flexibility to implement such soft computing algorithm. A control algorithm for load controller can be designed using fuzzy logic and be implemented with DSPs.

The poor voltage and frequency regulation of SEIG is due to the variable reactive power demand with variable consumer load. The use of static compensator (STATCOM) can provide the variable reactive power demand as the change in consumer load occurs. A suitable control algorithm can be designed for STATCOM to regulate varying reactive VAR demand. The STATCOM eliminates the harmonics, provides load balancing and supplies the reactive power to the load and generator under variable consumer load. Therefore, keeps the terminal voltage and frequency constant with variable load.

The application of SEIG employing squirrel cage induction motor in stand alone mode for wind energy conversion system (WECS) has been limitedly explored. The WECS with variable wind speed gives variable torque. Researchers have used slip ring induction machine as double power output induction generator by employing slip power control. Some other researchers have proposed a PWM controller to regulate the terminal voltage of the SEIG with varying rotor speed. With the varying wind speed the power output, voltage and frequency of the SEIG is variable. A control mechanism may be proposed to regulate the voltage and frequency of the SEIG employing cage machine.

## 1.4 AUTHOR'S CONTRIBUTION

The work done for the thesis is being briefly summarized as below:

1. A digital load controller has been designed, developed and implemented to regulate voltage and frequency of the SEIG using TMS320F2812 fixed point digital signal processor. The proposed sample based controller is easy to tune as compared to traditional PI controller and control the power dissipated across the dump load using mark space ratio DC chopper control.
2. The performance characteristics of three phase star and delta connected machine as a single phase SEIG has been analyzed. A single phase load controller based on proposed sample based controller has been designed, developed and implemented for voltage and frequency regulation of single phase SEIG based on mark space ratio DC chopper control.
3. Analysis of single phase two winding induction motor as a single phase SEIG has been examined and implementation of single phase load controller for voltage and frequency regulation has been carried out with DSP based controller.
4. The mark space ratio control based load controller is a non linear system and injects harmonics in the system. A new load controller based on ETRC and based on sinusoidal PWM AC chopper has been designed, developed and implemented which results as a linear dump load and injects minimum harmonics in the system. The load controller based on AC chopper controller is linear in nature. The harmonics appear as the side band and minimum order of harmonics are very high. Only odd harmonics are present. The THD appearing in SEIG with AC chopper controlled load controller system are less as compared to mark space ratio control despite of it doesn't involve any filter.
5. A fuzzy logic based load controller with ETRC AC chopper control has been analyzed and implemented through a fixed point digital signal processor. A fuzzy logic based load controller gives nonlinear control with fast response and virtually no overshoot. The terminal voltage remains constant on application and removal loads. The fuzzy logic control has the advantage of coping with larger parameter variation of the system and it provides improved performances in terms of overshoot limitation and sensitivity to parameter variation.

6. The load controller doesn't compensate for variable reactive power demand of SEIG system, hence a STATCOM based voltage and frequency controller has been designed and developed. The developed digital design of STATCOM based controller regulates the terminal voltage and frequency of the SEIG under application of resistive, reactive, unbalanced, nonlinear loads. The STATCOM controller compensates the additional VAR required when reactive load is connected. The STATCOM controller balances the SEIG currents and voltage under unbalanced load and acts as load balancer. The harmonics generated by nonlinear load are eliminated by proposed STACOM based controller. The control algorithm has been first co-simulated with processor in the loop (PIL) and then validated experimentally.
7. The application of SEIG for wind energy conversion system has been designed and analyzed under varying load and wind speed. A VSC based voltage and frequency regulation through a function of frequency control using a battery storage system have been designed and validated with simulation for stand alone WECS with SEIG. The proposed controller has bidirectional power flow capability of active and reactive power by which it regulates the system voltage and frequency with variation of consumer load and the speed of the wind. The VSC also acts as harmonic eliminator and load balancer for non linear unbalanced consumer load.

## 1.5 ORGANIZATION OF THE THESIS

The present thesis embodies detailed investigation on the specific contributions made by the author listed in previous section. The thesis is organized into nine chapters and the work included in each chapter is briefly outlined as follows:

The present **Chapter-1** describes an overview of self excited induction generator, its advantages, shortcoming and possible areas of application. Brief literature review on analysis, operation and control of induction generator operating in isolated mode has been presented. The scope of the work has been highlighted and author's contribution in the research area has been summarized.

The **Chapter-2** deals with modeling of three phase SEIG. The development of a digital sample based controller design has been given. The application of developed controller for SEIG load controller system has been simulated. The performance of SEIG-load controller system has been experimentally validated through DSP.

The **Chapter-3** presents the analysis of three phase induction motor as a single phase SEIG with star and delta connection. The application of single phase DSP load controller has also been examined. The transient analysis of single phase SEIG-load controller system has been presented.

The **Chapter-4** presents the use of single phase two winding induction motor as a single phase induction generator. The performance analysis of single phase SEIG has been given and implementation of single phase mark space ratio control based load controller for voltage and frequency regulation have been carried out with DSP based controller.

The **Chapter-5** presents a new load controller based on AC chopper control. Design analysis and implementation of equal ratio time control (ERTC) AC chopper control load controller with three phase SEIG has been presented. The transient and harmonic analysis has been given. Further a single phase SEIG with sinusoidal PWM AC chopper controlled load controller has been analyzed.

The **Chapter-6** describes the application of fuzzy logic based load controller to SEIG. The fuzzy logic design and its implementation with fixed point processor for SEIG-load controller system have been presented.

The **Chapter-7** presents the STATCOM based SEIG system. A digital design for STATCOM based voltage and frequency regulation under application of balanced/unbalanced and nonlinear load has been given. The control algorithm has been first co-simulated with processor in loop application for fixed point DSP and then validated experimentally.

The **Chapter-8** presents the application of SEIG using cage machine for wind energy conversion system with energy storage system. A voltage source converter with bidirectional active and reactive power control capability for voltage and frequency regulation of SEIG under varying wind speed and consumer load has been given.

The **Chapter-9** highlights the main conclusions and significant contribution of the thesis and states the scope for further research in this area.

## 1.6 CONCLUSION

In this chapter, brief review of the literature on the research topic has been carried out and the scope of the research work has been outlined. The author's contributions in the research area are summarized and the organization of the thesis has been outlined.

# CHAPTER-2

# ANALYSIS AND DESIGN OF A THREE PHASE SEIG WITH LOAD CONTROLLER

## 2.1 INTRODUCTION

Literature review presented in preceding chapter reveals that induction motor can be used as a self excited induction generator when enough excitation is provided and its rotor is driven to a speed higher than that of the stator magnetic field. The induced voltage and its frequency in the winding will increase up to a level governed by magnetic saturation in the machine. The required excitation for self excited induction generator (SEIG) is given by connecting appropriate capacitors across the terminals. Appropriate choice of excitation capacitance is necessary in order to initiate voltage build-up and to maintain a given terminal voltage, when the SEIG is loaded. The per phase equivalent circuit model using loop impedance method [133] and nodal admittance method [41] are basic approach employed for calculating minimum capacitance necessary for self excitation of the SEIG. An analytical method [123] to compute the minimum capacitance requirement for self excitation under no-load conditions show that minimum capacitance requirement for SEIG varies inversely proportional to the square of the speed and inversely proportional to the maximum saturated magnetizing reactance. A novel approach [218] based on eigen value sensitivity is reported to predict both minimum and maximum values of capacitance required for SEIG. Eltanmaly [67] developed a new formula that can be used for on-line computation of the minimum capacitance required for SEIG.

The SEIG has relative advantages over conventional synchronous generators like low cost, self-protection capacity, rugged, least maintenance and ability to generate power while driven at variable speed. These advantages facilitate induction generator operation in stand-alone/ isolated mode or in parallel with synchronous generator for supplying local load and in grid mode. The self excited induction generator has a major drawback of poor voltage regulation. The inherent poor voltage regulation of the SEIG is due to the difference between the reactive power supplied by the excitation capacitors and that demanded by the load and the machine. This is a major bottleneck of its application in isolated mode.

The generated voltage of the SEIG depends upon the speed, excitation capacitance, load current and power factor of the load. Among various renewable energy based power systems, mini/micro hydro power scheme employs an uncontrolled turbine which maintains the input hydro power constant. The SEIG can be used to generate constant voltage and frequency if the load is maintained constant at its terminals. Under such operation, SEIG requires constant capacitance for excitation resulting in a fixed-point operation. For this purpose, a suitable control scheme is required to develop such that the load on the SEIG remains constant despite the change in the consumer load. Also, such control scheme should be simple, economical, rugged and reliable. Several load controller scheme have been reported in literature [29, 30, 63, 81, 137, 180, 181, 182, 183, 189, 190, 196] The load governing through binary weighted control load control [63, 81] exhibits a stepped characteristic and switching operation occurs during the transient period only. The major drawback of this scheme is that in three phase system, large numbers of resistances are required which becomes bulky, prone to failure and require large number of switches. Also, the voltage regulation would be stepped. A load controller using phase controlled thyristors [29] and chopper [30] connected to a single resistive load eliminate the repeated switching. The firing angle of the power electronic switching devices is adjusted for regulating the power dissipated by ballast load. The controlled thyristor need reactive power resulting in increased reactive burden on the generator and their operations also injects harmonics in the system which leads to the de-rating of generator. The load controller with uncontrolled rectifier and series connected chopper switch [180, 181, 182, 183, 189] with mark space ratio chopper control gives unity power factor operation. It generates low harmonics and only one dump load is required. The control scheme involves a PI controller to maintain constant load on the SEIG. The PI controller needs to tune for its proportional and integral gain. The control scheme is based on analog system. The literature review reveals that for mini/micro hydro power generation where input power is constant, a control scheme should be simple, economical, rugged and reliable. In this chapter a load controller with sample based controller have been designed and implemented. The developed prototype model of DSP based load controller for SEIG system is simple, cost effective, flexible and capable of network based application for remote operation with TCP/IP stack. The transient behavior of DSP TMS320F2812 based load controller for SEIG system at different operating conditions such as application and

removal of static (resistive and reactive) and dynamic load is investigated to demonstrate the capabilities of the proposed load controller.

## 2.2 SYSTEM DESCRIPTION

A schematic diagram of the proposed DSP based load controller for SEIG system is shown in Figure 2.1. It consist of a three phase SEIG driven by a constant power prime mover. The excitation capacitors are connected at the terminals of the SEIG, which have a fixed value to result in rated terminal voltage at rated load. Consumer load and load controller are connected in parallel at generator terminals. The load controller consist an uncontrolled rectifier, a filtering capacitor, IGBT based chopper and a series resistive (dump) load. The uncontrolled rectifier converts the SEIG AC terminal voltage to DC. The output ripples are filtered by filter capacitor ($C_f$). An IGBT is used as a chopper switch. When gate pulse to chopper switch is high, the current flows through the dump load and the power is consumed. The pulse width or duty cycle of chopper is decided by the difference of power generation to consumer load. A TMS320F2812 (32-bit, 150 MIPS fixed point digital signal processor) DSP is used for generation of suitable pulse width in accordance with consumer load. The DSP reads the terminal voltage through a voltage transducer as a feedback signal from its ADC input and gives the suitable pulse from its PWM output to IGBT chopper.

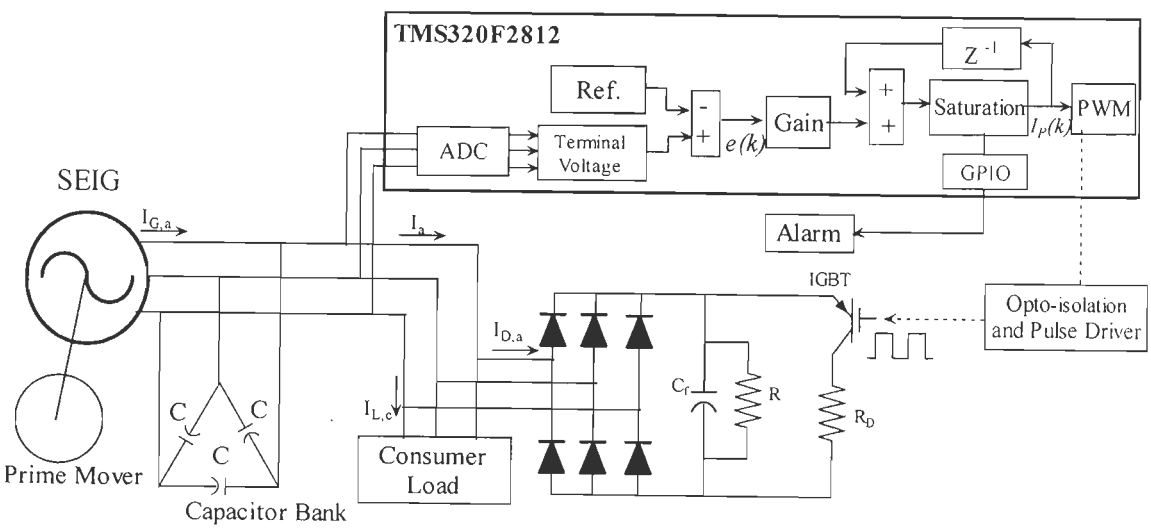


**Figure 2.1: Schematic diagram of three phase SEIG with load controller**

The SEIG feeds two loads in parallel such that the total power is constant, that is

$$P_{out} = P_c + P_d \tag{2.1}$$

where, $P_{out}$ is the generated power of the generator (which must be kept constant), $P_c$ is the consumer load power, and $P_d$ is the dump load power. This dump load power ($P_d$) may be used for non priority load such as heating, battery charging, cooking etc. The amount of dump load power is controlled by IGBT chopper. The duty cycle of gate pulse of IGBT gives the average conduction period of chopper and hence the amount of power dissipated in dump load. A variable mark-space ratio chopping approach has been adopted for the IGBT chopper because it produces a variable unity power factor load with just a single ballast or dump load.

## 2.3 MODELING AND SIMULATION

### 2.3.1 Mathematical Model of SEIG

The voltage and current equations of induction generator in stationary dq reference frame are given as:

$$pi_{ds} = K_1'[v_{ds} - R_s i_{ds} + (L_m/L_r)R_r i_{dr} + w_r(L_m^2/L_r)i_{qs} + w_r L_m i_{qr}] \tag{2.2}$$

$$pi_{qs} = K_1'[v_{qs} - R_s i_{qs} + (L_m/L_r)R_r i_{qr} - w_r(L_m^2/L_r)i_{ds} - w_r L_m i_{dr}] \tag{2.3}$$

$$pi_{dr} = K_2'[-(R_r/L_r)i_{dr} - (L_m/L_s L_r)v_{ds} + (L_m/L_s L_r)R_s i_{ds} - w_r(L_m/L_r)i_{qs} - w_r i_{qr}] \tag{2.4}$$

$$pi_{qr} = K_2'[-(R_r/L_r)i_{qr} - (L_m/L_s L_r)v_{qs} + (L_m/L_s L_r)R_s i_{qs} + w_r(L_m/L_r)i_{ds} + w_r i_{dr}] \tag{2.5}$$

where '$p$' represents the derivative with respect to time and

$$L_s = L_{ls} + L_m;\quad L_r = L_{lr} + L_m;\quad K_1' = [1/(L_s - (L_m^2/L_r)];\quad K_2' = [1/(1 - L_m^2/L_s L_r)]$$

The SEIG operates in saturation region and its magnetizing current can be calculated in terms of stator and rotor currents as

$$I_m = \sqrt{((i_{ds} + i_{dr})^2 + (i_{qs} + i_{qr})^2} \tag{2.6}$$

The magnetizing inductance ($L_m$) is function of magnetizing current ($I_m$) .and is given as

$$L_m = |\psi_m| / |I_m| \tag{2.7}$$

where $\Psi_m$ is magnetic flux linkage. Figure 2.2 shows the relation between applied voltage and magnetizing current ($I_m$) while induction motor under study is driven at synchronous speed.

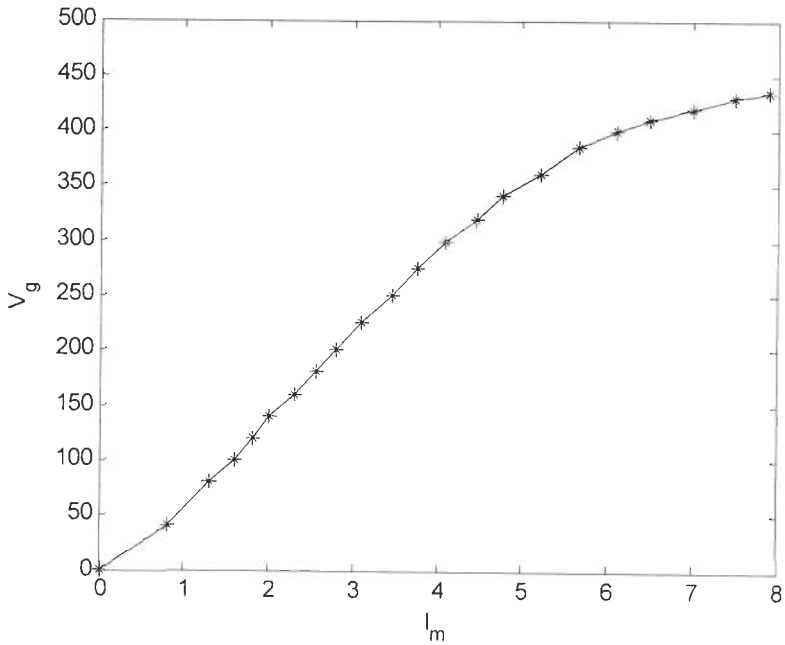


**Figure 2.2: The applied voltage and magnetizing current at synchronous speed.**

From the synchronous speed test data and active power absorbed by the machine, a polynomial function of fourth order curve fitting relation is established as shown in Figure 2.3 which describes the nonlinear relation between magnetizing inductance and current given as

$$L_m = A_1 + A_2 I_m + A_3 I_m^{\,2} + A_4 I_m^{\,3} \tag{2.8}$$

where $A_1$, $A_2$, $A_3$, $A_4$ are constants summarized in Appendix-A.

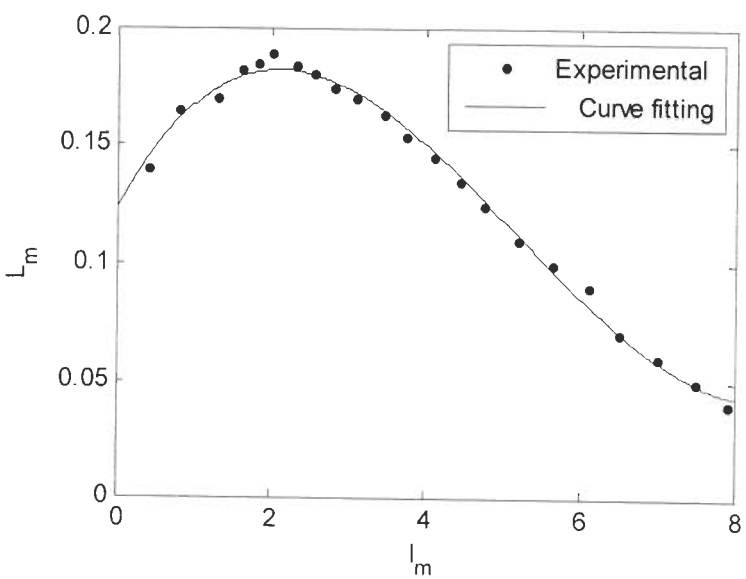


**Figure 2.3: Nonlinear relation between $L_m$ and $I_m$**

The shaft torque of the prime mover is considered as a function of speed and given as:

$$T_{shaft} = (K_1 - K_2 w_r) \tag{2.9}$$

where, $K_1$ and $K_2$ are the prime mover coefficients given in Appendix-A.

### 2.3.2 Determination of Excitation Capacitor

Figure 2.4 shows the per phase equivalent circuit of three phase SEIG with load where $R_s$, $X_{ls}$, $R_r$, $X_{lr}$ are per phase stator and rotor resistances and reactance; $X_m$ and $X_C$ are per phase magnetizing and capacitive reactance; $I_s$, $I_r$, $I_L$ are per phase stator, rotor and load currents; $V_g$ is air gap voltage and F, v are per unit frequency and speed. Rotor parameters are referred to stator and all reactance are at base frequency.

applying Kirchhoff's voltage law we have:

$$(Z + Z_L) I_L = 0 \tag{2.10}$$

where, $Z = Z_C \parallel (Z_S + (Z_M \parallel Z_r))$

and $Z_c = -jX_c/F$, $Z_s = R_s + jFX_{ls}$, $Z_r = R_rF/(F-v) + jFX_{lr}$, $Z_M = jFX_m \| R_m$.

Under steady state condition, $I_L$ can not be equal to zero, hence,

$$(Z + Z_L) = 0 \tag{2.11}$$

which can be define as the function of capacitive reactance ($X_c$) and per unit frequency (F) as:

$$f(X_c, F) = | Z + Z_L | \tag{2.12}$$

For solving equation (2.12) to determine the variables $X_c$ and F by minimization technique, the function $f(X_{csh}, F)$ is taken as an objective function and the optimization problem is stated as:

Minimize $f(X_c, F)$

such that, $X_{c,l} \le X_c \le X_{c,u}$ and $F_l \le F \le F_u$ ;

where subscripts 'l' and 'u' denote lower and upper limits of the variables respectively. This is minimized by sequential unconstrained minimization technique (SUMT) in conjunction with Rosenbrock's method of rotating coordinates. The function must converge to zero and the value of tolerance to check the convergence is taken quite small, say equal to 0.0001. The required capacitance is then calculated from the $X_c$ as:

$$C = 1/(2\pi f_b X_c) \tag{2.13}$$

Figure 2.5 shows the variation of terminal voltage with power output at different value of excitation capacitor and constant speed for a 3.73 kW machine. The parameters of machine are summarized in Appendix-A. The machine delivers 3kW output power with the 25μF per phase delta connected excitation capacitor. The Figure 2.6 shows the simulated and experimental voltage buildup at 25 μF capacitor connected at SEIG terminal in delta connection.

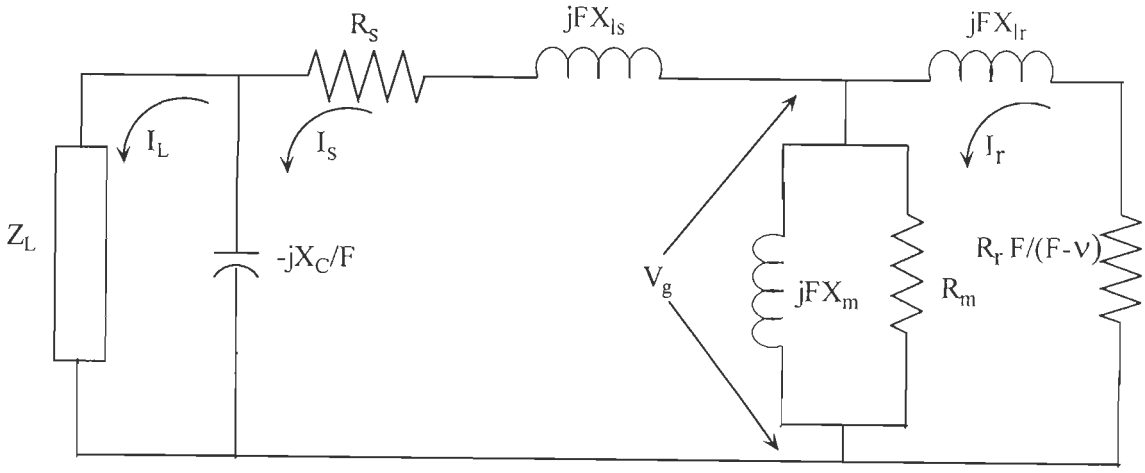


**Figure 2.4: Steady state equivalent circuit of SEIG with a balanced load**

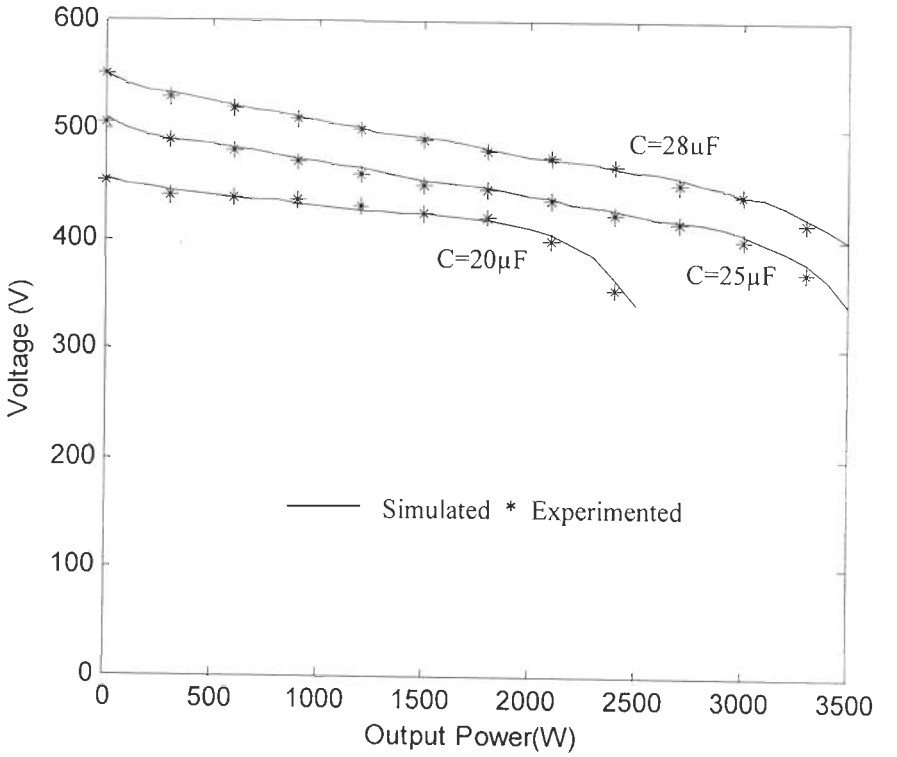


**Figure 2.5: Variation of terminal voltage with output power at constant speed**

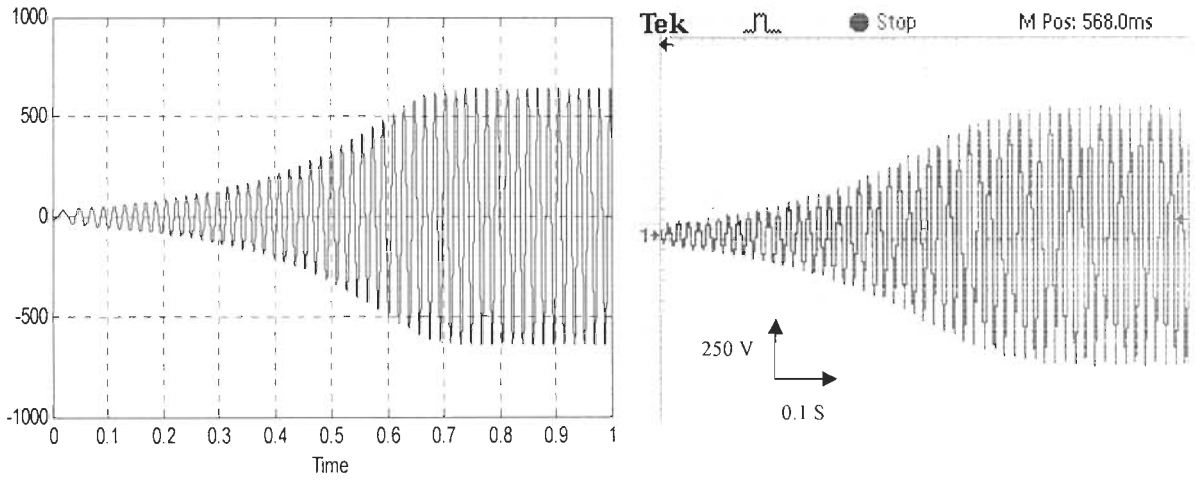


(a) (b)

**Figure 2.6: (a) Simulated (b) experimented voltage build up of SEIG with 25 μF capacitor per phase**

### 2.3.3 Controller Design

The schematic diagram of controller is shown in Figure 2.7. To maintain the terminal voltage of the SEIG constant, the terminal voltage error e($k$) at $k^{th}$ sampling instant is computed as:

$$e(k) = V_P(k) - V_{ref} \tag{2.14}$$

where, $V_P(k)$ is the peak amplitude of SEIG terminal voltage and $V_{ref}(k)$ is the reference voltage at $k^{th}$ sampling instant.

The terminal voltage error is processed through a load controller. The output of the load controller at $k^{th}$ sampling instant is given as:

$$I_P(k) = A\,e(k) + I_P(k-1) \tag{2.15}$$

where, A is the gain of the controller to adjust overshoot, $I_P$ $(k\text{-}1)$ is the load controller reference at $(k\text{-}1)^{th}$ sampling instant.

Taking z transform:

$$I_P(z) = AE(z) + z^{-1}I_P(z) \tag{2.16}$$

$$\frac{I_P(z)}{E(z)} = A\frac{1}{1-Z^{-1}} \tag{2.17}$$

The developed controller is applied with a second order system having pole at -1 and -2 on s-plane. A ZOH is cascaded with the second order system to obtain discrete step response. The step response of uncompensated system and compensated with controller is

shown is Figure 2.8. The application of developed controller improves the steady state error and transient response of the system.

The Fig 2.1 shows the schematic diagram of DSP based load controller for SEIG system where the proposed controller is used. It receives the input from ADC of DSP and compares it with preset reference. The error is scaled (gain, $A$) to control the overshoot. The output is algebraically added to previous sample level of PWM reference. Thus obtained PWM reference is processed through the DSP PWM block which have inbuilt symmetrical triangular carrier wave. The DC PWM reference compared with inbuilt symmetrical triangular wave gives the require pulse width for IGBT switch.

In order to tune the SEIG for satisfactory dynamic performance, the SEIG may be approximated as a first-order system with the following transfer function:

$$G(s)=\frac{K.e^{-st_0}}{st+1} \tag{2.18}$$

where, $K$ is the gain of the system, $t$ is the time constant of the system and $t_o$ is the time delay of the system. The parameters of the transfer function are determined using the open-loop step response method. With the transfer function identified, the gain of the controller can be determined using open-loop tuning method. For the prototype experimental system, the controller parameters are determined as follows:

$K = 1.04$; $t = 0.6$s; $t_o = 0.312$; $A = 0.85$;

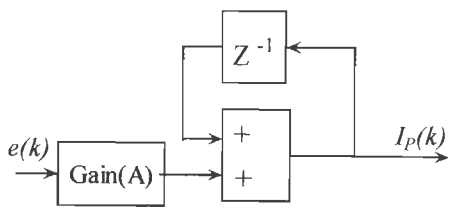


**Figure 2.7: Schematic diagram of proposed controller**

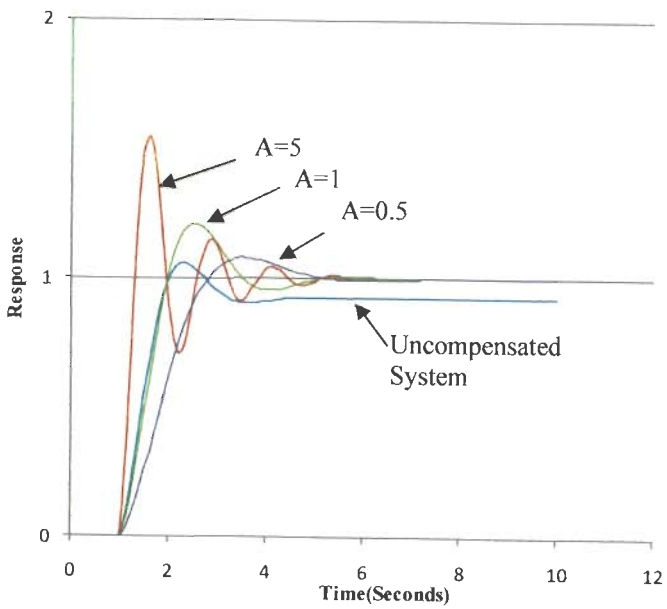


**Figure 2.8: Step response of second order system with and without controller**

### 2.3.4 Preliminary Design of Dump Load

The DC output voltage of rectifier is given by:

$$V_{DC} = \frac{3\sqrt{2}\,V_{LL}}{\pi} = (1.3505)V_{LL} = (1.3505) \times 400 = 540.20 \text{ V} \quad (2.19)$$

where, $V_{LL}$ is the rms value of the output voltage of the SEIG and the input voltage of the diode bridge rectifier.

Taking an over voltage 10% of rated ac voltage for transient condition, the peak DC voltage is given as:

$$V_{DC,\,peak} = \sqrt{2} \times 400 \times 1.10 = 622.25 \text{ V} \quad (2.20)$$

The AC input current is calculated as:

$$I_{AC} = \frac{P}{V_{LL}} = \frac{3000}{400} = 7.5 \text{ A} \quad (2.21)$$

where, P is the rated power output for SEIG.

Taking distortion factor of 0.9 and crest factor of 1.8, then AC peak input current to diode rectifier is:

$$I_{AC,peak} = 1.8 \times I_{AC} / 0.9 = 15 \text{ A} \quad (2.22)$$

The maximum voltage and current ratings are 622.25 V and 8 A respectively. Commercially available rating of diodes for single phase rectifier and IGBT chopper switches are selected of 900 V and 15 A.

The dump load resistance is given by:

$$R_D = (V_{DC})^2 / P = (540.20)^2 / 3000 = 97.27\ \Omega \quad (2.23)$$

The value of filtering capacitor ($C_f$) is selected on the basis of ripple factor (RF) and given by the relations as:

$$C_f = \{1/(4 \times f \times R_D)\}[1 + \{1/(\sqrt{2} \times RF)\}] \quad (2.24)$$

for 15 % ripple factor, filtering capacitor is:

$$C_f = \{1/(4 \times 50 \times 97.27)\}[1 + \{1/\sqrt{2} \times 0.15)\}] = 293.73\ \mu F \quad (2.25)$$

A nearest commercially available value of 470 μF is taken as filtering capacitor

### 2.3.5 Simulation

Digital simulation of proposed load controller with SEIG system has been carried out with MATLAB Version 7.2 on Simulink Version 6.4. This Power System Blockset facilitates to simulate saturation in asynchronous machines. A 3.73 kW, 400 V 50 Hz Delta connected asynchronous machine is used as an SEIG including the machine saturation characteristics

which is determined by conducting synchronous speed test. The synchronous speed test specifies the no load saturation curve for induction machine. The voltage and current of synchronous speed test is given in a 2-by-n matrix, where n is the number of points taken from the saturation curve to simulate saturation on MATLAB. Figure 2.9 shows the schematic MATLAB model of the SEIG-load controller system. The block rotor test and no load test give the machine parameters which are summarized in Appendix-A.

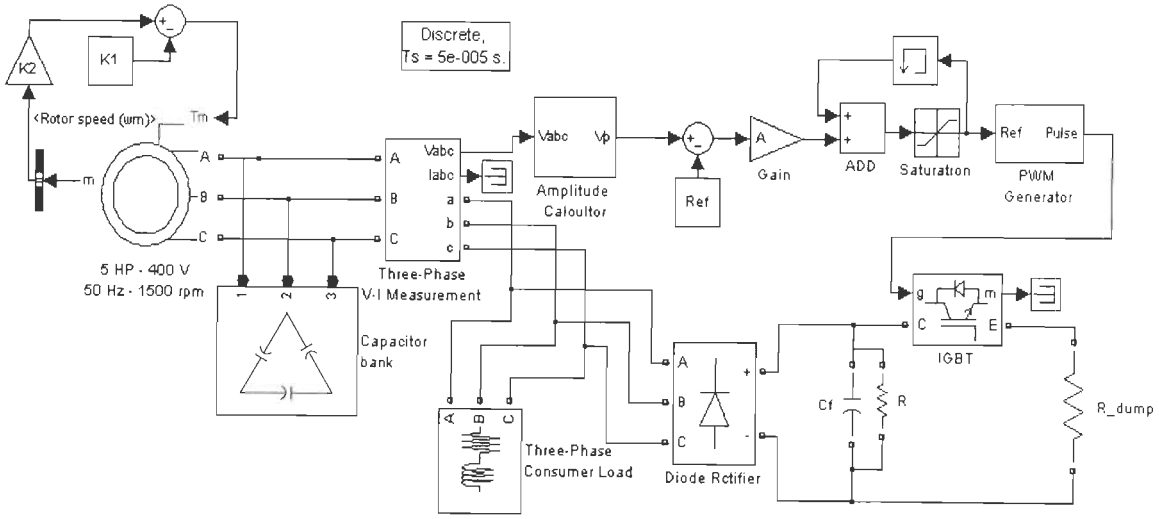


**Figure 2.9: Schematic diagram of MATLAB based model of three phase SEIG with load controller**

The dropping torque-speed characteristics of prime mover is given as $T_{shaft} = (K_1 - K_2 w_r)$ where, $K_1$ and $K_2$ are the prime mover constants given in Appendix-A. The terminals of the machines are connected with delta connected capacitor bank of 25 μF each phase. The output is connected with a consumer load of resistive and reactive nature and load controller in parallel. The voltage amplitude is calculated as $V_p = \{2/3(V_{ab}^2 + V_{bc}^2 + V_{ca}^2)\}^{1/2}$, where $V_{ab}$, $V_{bc}$, $V_{ca}$ are the line voltage and $V_p$ is the peak amplitude. The peak amplitude is compared with the reference and processed through the controller. The output of the controller is compared with symmetrical triangular wave and through a relational operator to obtain a pulse of suitable duration (width). This pulse is given to gate of the IGBT chopper switch. A universal bridge is used for diode rectifier and filtering capacitor is added for smoothening and filtering. The dump load resistance and filtering capacitance values are selected as per calculation. Figure 2.10 shows the voltage build up and steady state voltages ($V_{abc}$), load current ($I_{L,abc}$).

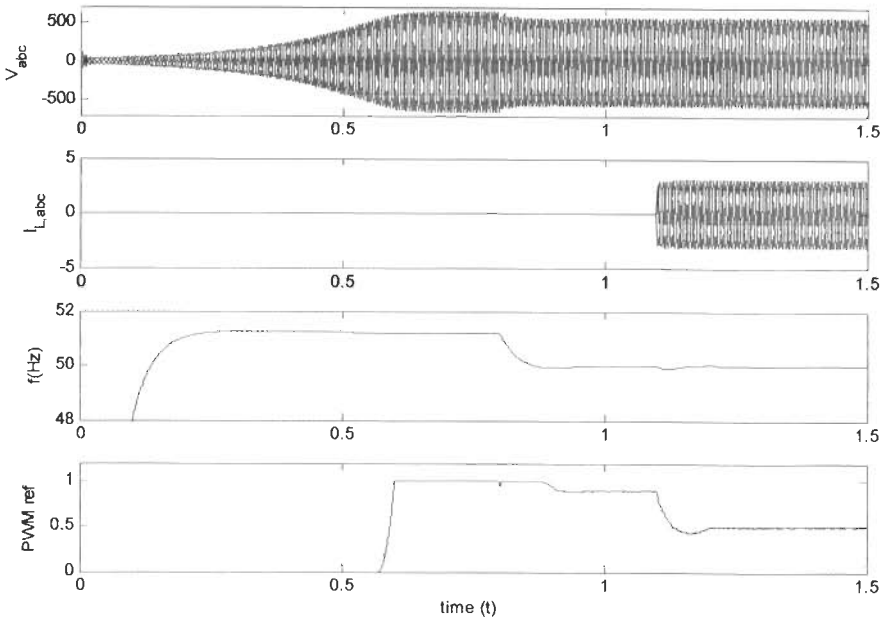


**Figure 2.10: SEIG-load controller system supplying resistive loads**

## 2.4 IMPLEMENTATION

The output power of the SEIG is kept constant by load controller under varying consumer load. The terminal voltage for feedback is sensed with voltage transducer. The voltage transducer converts and linearizes the input AC terminal voltage to output DC voltage.

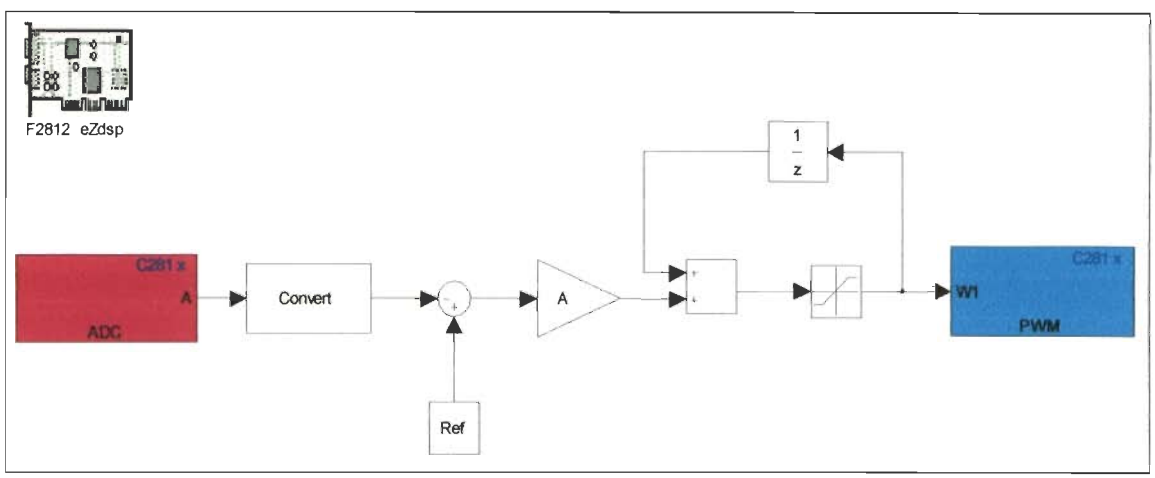


**Figure 2.11: MATLAB CCS project for automatic code generation.**

A single voltage transducer is used as the three phase system is balanced. This voltage is given to ADC input of the DSP TMS320F2812. The TMS320F2812 DSP has 16 ADC input channels with an input range of 0- 3 Volt. The output values are in the range of 0 to 4095 as TMS320F2812 DSP ADC is 12- bit converter. It reads the input with a sample

rate of 0.001 seconds (maximum 0.0004 seconds). The DC output of voltage transducer has peak to peak ripples. A running mean is taken in software to overcome this problem. The sensed voltage is compared with a reference voltage signal, which is taken as proportional to the rated terminal voltage of the SEIG and may be altered as and when required. The error signal is scaled (gain) to limit the overshoot and algebraically added to previous sample PWM reference level. This PWM reference is processed through the PWM of DSP. The TMS320F2812 DSP has 6x2 high resolution PWM outputs which have inbuilt symmetrical/unsymmetrical triangular carrier wave. The PWM reference is in the range of 0-64000 as the waveform period, for 75 MHz clock operation with prescaler set to 2 for a PWM carrier to 1.08 kHz [210]. The PWM reference compared with inbuilt symmetrical triangular wave that gives the require pulse width for IGBT switch. The out pulse are configure for active low control logic. The pulse from DSP is processed through opto-isolation and gate driver circuit. A photocoupler TLP250 is used as gate driver circuit. It includes an opto-isolator, NPN and PNP transistor and the necessary logic to control them, all within an integrated package. Only the addition of two resistors is required to complete the gate driver circuit. If the PWM reference is at extreme of 0 or 64000 and desired terminal voltage level is not achieved then either generator is overloaded or dump load need to be adjusted. To signal this, the PWM reference is processed through a saturator which gives the output on both extremes. It can be processed through a general purpose digital output (GPIO) of DSP which may be used to alarm or trip the circuit.

## 2.5 RESULTS

Experiments are carried out on the developed prototype of DSP based load controller for SEIG system. A three phase 3.73 kW, 400 V, 7.5 A, 50 Hz, 1500 rpm delta connected squirrel cage induction machine is used as a self-excited induction generator. The SEIG is driven by 220 V, 20 A, 5 HP, 1500 rpm shunt wound DC machine is used as a prime mover. To generate 3 kW at 400 V and rated speed, 25 μF capacitor of 400 V is connected in delta across the SEIG terminals. The test results are recorded with three phase balanced resistive load, 0.8 lagging power factor reactive load and three phase induction motor as a dynamic load. Figure 2.12 shows the simulated and experimented transient responses of DSP based load controller for SEIG system on application of 1.5 kW three

phase balanced resistive load. The simulated waveforms from top to bottom are terminal voltage ($V_{abc}$) of SEIG, stator current of SEIG ($I_{G,abc}$), Load current ($I_{L,abc}$) and dump load current ( $I_{D,a}$), line current ($I_a$) and frequency(f) respectively. The experimental waveforms from top to bottom are terminal voltage of the SEIG ($V_{ab}$), Load current ($I_{L,a}$), Dump load current ($I_{D,a}$) and line current ($I_a$) respectively. On application of resistive load, load current increases and dump load current decreases so that power transfers from dump load to consumer load and SEIG experiences constant load on it.

Figure 2.13 shows the simulated and experimented transient responses of SEIG system on application and removal of 1kW, 0.8 lagging power factor load. On application and removal of load the terminal voltage remains constant. When an inductive load is connected to the SEIG, it draws a reactive current. Then a part of the excitation capacitance is used to compensate for this reactive current, so less capacitance is available for the SEIG itself. It react to this with an increase in frequency, causing the capacitors to produce some more magnetizing current while the SEIG needs less, thus the two balance again and frequency varies as well. The frequency variation caused by reactive load is under acceptable. With a SEIG running at a normal degree of saturation, frequency variation would be less. As modern induction machines tend to be highly saturated, the frequency regulation with variation in load power factor is quite small. A small increase in frequency results in a significant reduction in magnetizing current. In addition, extra VARs are produced by the excitation capacitors due to reduced impedance. Figure 2.14 shows the simulated and experimental transient response for dynamic load. A three phase induction motor of 1 HP is used as dynamic load for experiment. At the time of starting, the power factor of motor is poor and it draws more reactive VARs. Under steady state, it draws a constant current under no load. Simulated transient response shows that terminal voltage remains constant on application and removal of dynamic load. Experimental results verify the simulated results. On application of induction motor on no load as dynamic load, there is around 15% dip in terminal voltage which recovers after few cycles. Figure 2.15 shows the measured and simulated frequency under resistive and 0.8 lagging power factor reactive load application respectively. The frequency remains constant with the application of resistive load. A slight increment in frequency is observed for loads of lagging power factor which is under acceptable limits.

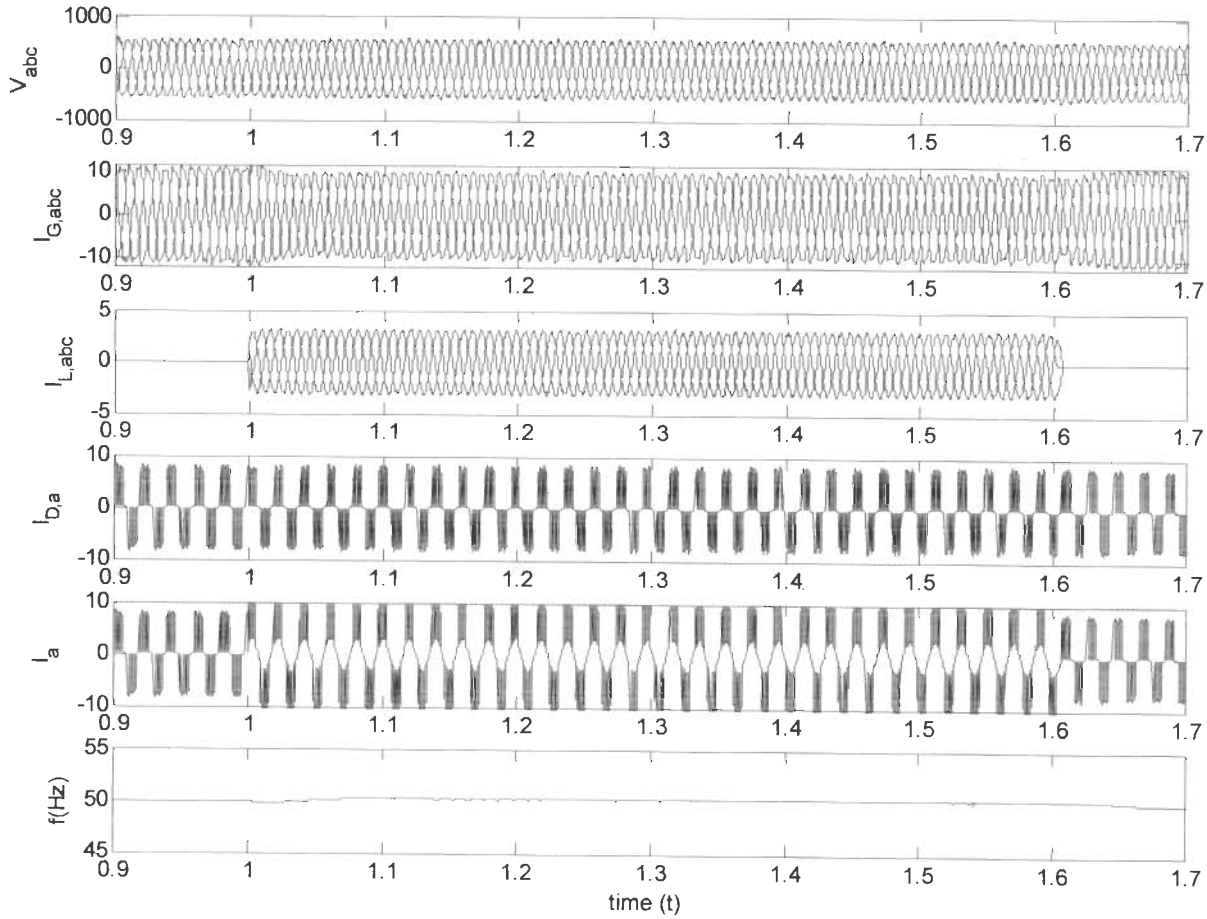


**(a) Simulated**

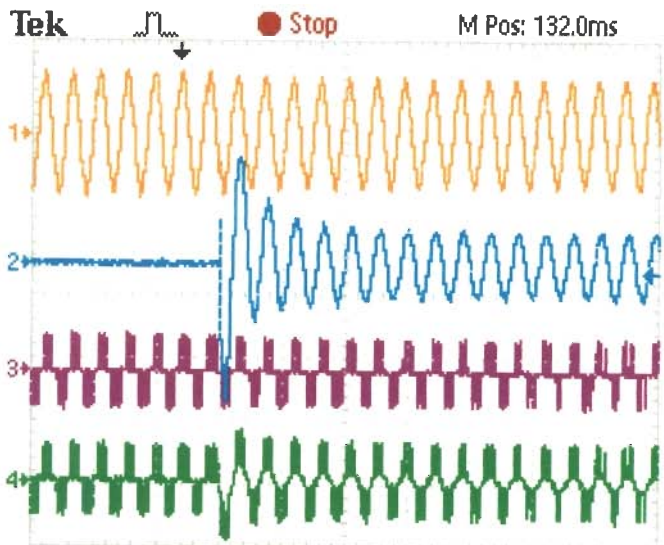


Horizontal scale:-Time 50msec/Div, Vertical Scale ch1 to ch 4:-
$V_{ab}$ (600V/Div) $I_{L,a}$ (4A/Div), $I_{D,a}$(8A/Div), $I_a$(8A/Div)

**(b) Experimented**

**Figure 2.12: Transient waveform on application of balanced three phase resistive load**

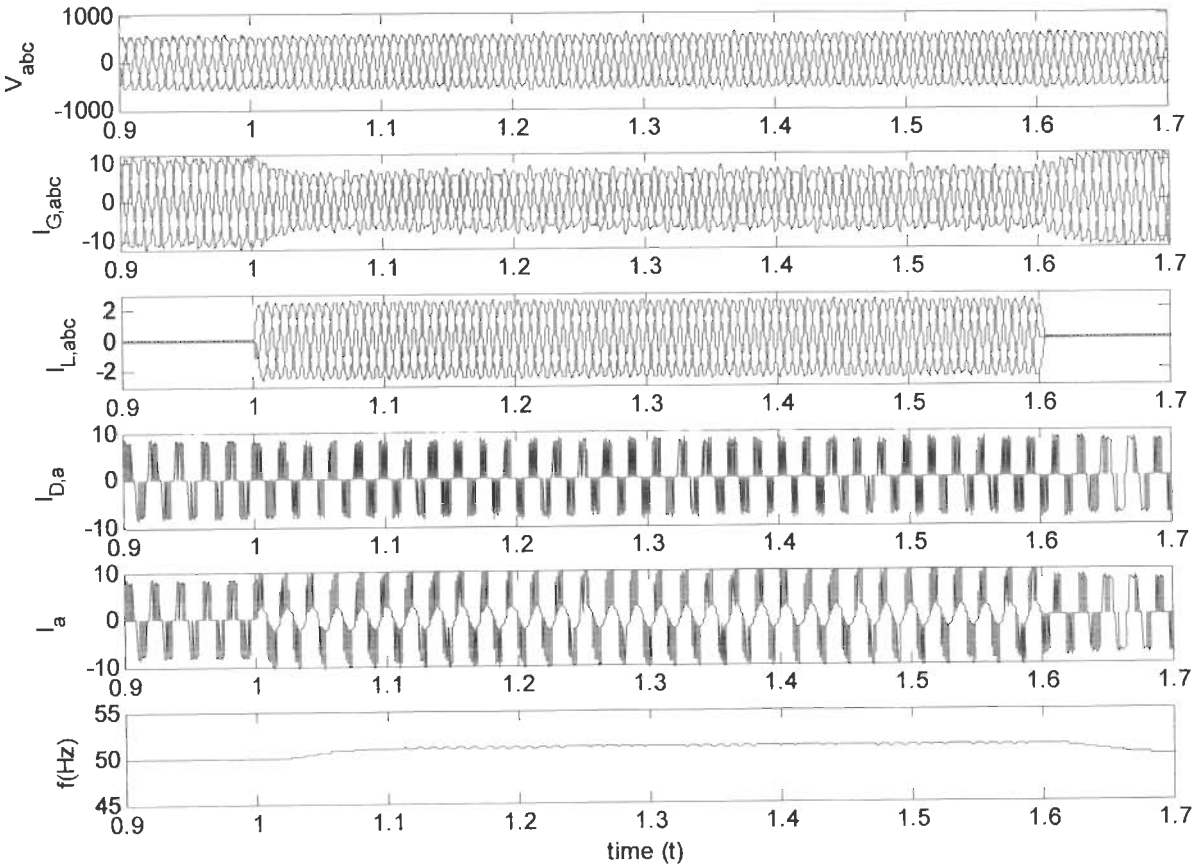


**(a) Simulated**

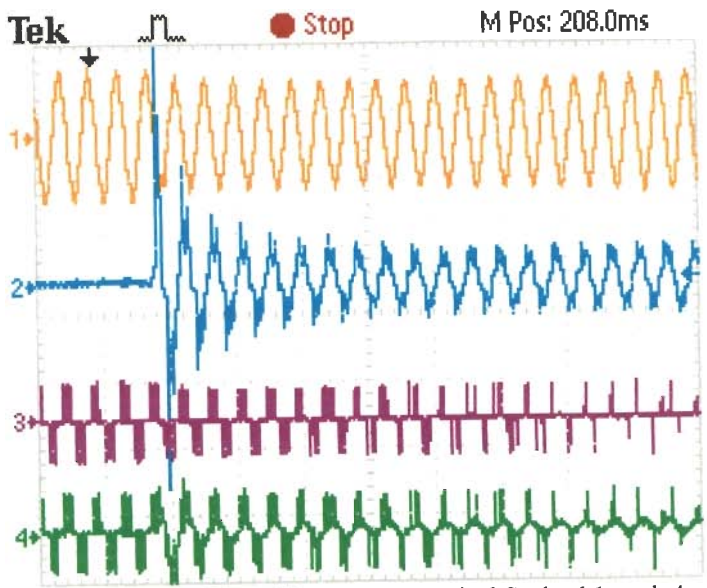


Horizontal scale:-Time 50msec/Div, Vertical Scale ch1 to ch 4:-
$V_{ab}$ (600V/Div) $I_{L,a}$ (8A/Div), $I_{D,a}$(8A/Div), $I_a$(8A/Div)

**(b) Experimented**

**Figure 2.13: Transient waveform on application of balanced three phase reactive load**

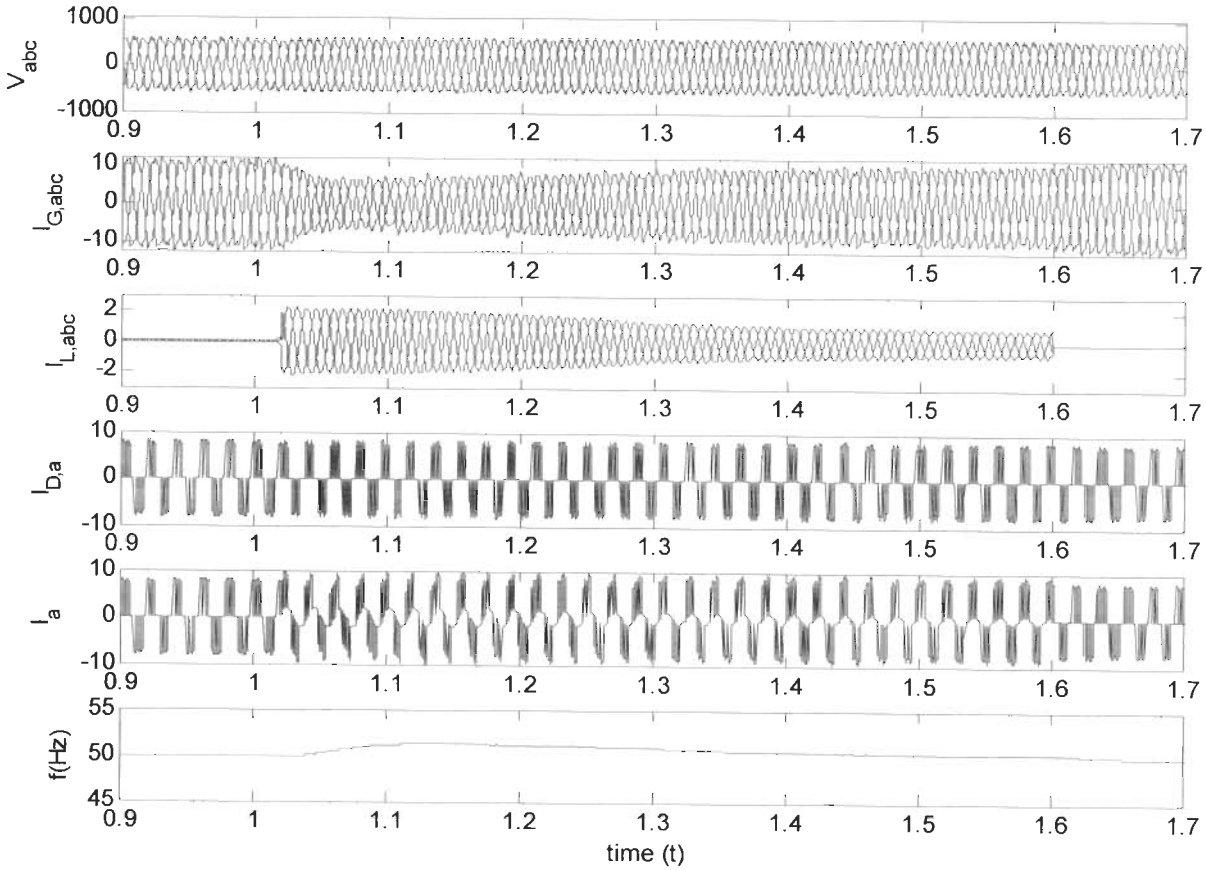


**(a) Simulated**

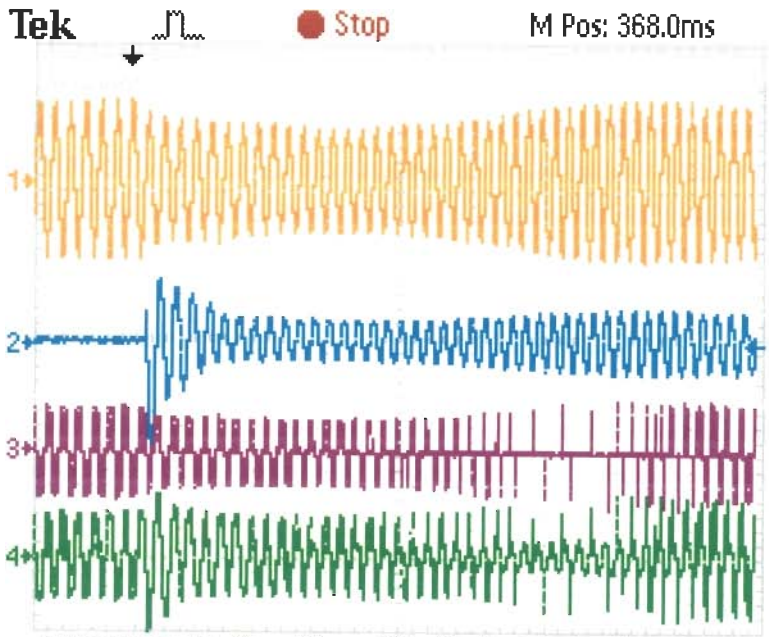


Horizontal scale:-Time 50msec/Div, Vertical Scale ch1 to ch 4:-
$V_{ab}$ (600V/Div) $I_{L,a}$ (8A/Div), $I_{D,a}$(8A/Div), $I_a$(8A/Div)

**(b) Experimented**

**Figure 2.14: Transient waveform on application of dynamic load**

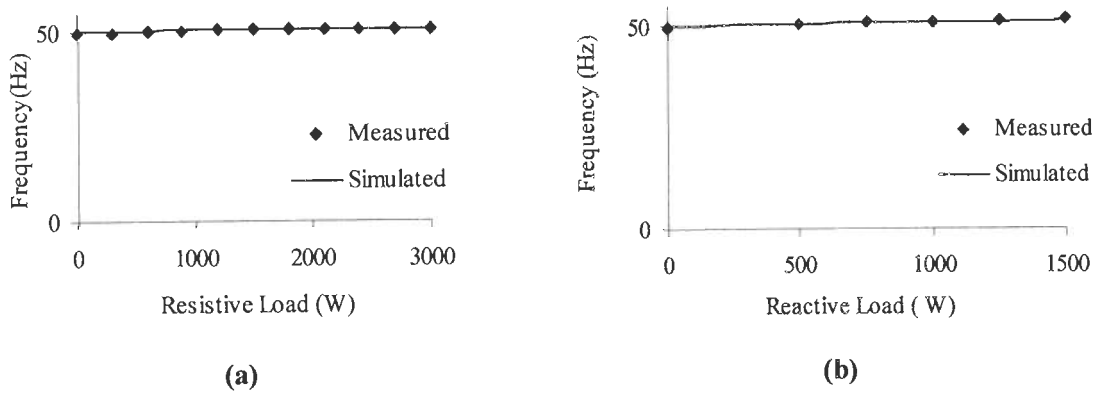


**Figure 2.15: Frequency characteristic of SEIG-load controller system with (a) resistive and (b) reactive loads**

The load controller is a non-linear system and feeds harmonics in the SEIG. With application of resistive main load, power dissipating in dump load reduces therefore less harmonics are generated and SEIG voltages and currents are close to sinusoidal. Capacitive current also decreases due to less reactive burden. Table2.1summarizes the main load, terminal voltage, voltage THD and current THD of main load, dump load and generator at different steps of resistive, reactive load application. The good voltage regulation is observed. There is a slight increase in terminal voltage as the voltage THD in the system increases. An increase in voltage and current THD is observed for reactive loads on SEIG.

**Table 2.1 Terminal voltage, voltage and current THD at different main load**

| S. No. | Main Load (W) | Terminal Voltage | | Voltage THD (%) | | Current THD (%) | | | | | |
|---|---|---|---|---|---|---|---|---|---|---|---|
| | | | | | | Main Load | | Dump Load | | Generator | |
| | | Sim. | Meas. | Sim. | Meas | Sim. | Meas | Sim. | Meas | Sim. | Meas |
| 1 | 0 | 401.8 | 399.8 | 5.79 | 8.7 | - | - | 30.16 | 37.0 | 10.07 | 14.30 |
| 2 | 1000 | 401.7 | 397.2 | 3.91 | 5.8 | 2.94 | 7.4 | 35.01 | 44.7 | 7.86 | 12.98 |
| 3 | 2000 | 399.1 | 397.3 | 3.17 | 3.5 | 2.35 | 4.4 | 43.66 | 58.4 | 5.98 | 10.70 |
| 4 | 3000 | 398.7 | 396.4 | 1.81 | 2.3 | 2.07 | 3.6 | 59.74 | 63.3 | 3.86 | 8.37 |
| 5 | 500 0.8pf lag | 397.2 | 396.3 | 4.32 | 4.7 | 2.24 | 9.6 | 31.17 | 37.4 | 14.55 | 16.90 |
| 6 | 1000 0.8pf lag | 395.6 | 394.5 | 7.66 | 9.6 | 3.44 | 11.0 | 33.41 | 42.2 | 8.90 | 13.10 |
| 7 | 1 HP IM at no load | 395.4 | 395.1 | 4.11 | 5.1 | 2.60 | 7.4 | 33.54 | 37.4 | 8.91 | 10.4 |

Sim. :- Simulated Meas. :- Measured

## 2.6 CONCLUSION

A DSP based load controller has been designed, developed and implemented for three phase induction motor working as a self excited induction generator. The developed load controller acts as the voltage and frequency regulator for the SEIG. The transient analysis of the SEIG with load controller system has been carried out for resistive, reactive and dynamic load.

From the analysis and experimentation; the following conclusions are drawn.

(i) The terminal voltage remains constant on application and removal of resistive and reactive load. A voltage dip of 15% for few cycles is observed for dynamic load. After few cycle it recovers to rated value.

(ii) The frequency remains constant on application of resistive load application. There is a slight increase in frequency on application of reactive load. The variation in frequency is found under satisfactory limits.

(iii) The developed sample based controller is simple as compared to conventional PI controller. The PI controller is need to be tuned for proportional gain ($K_p$) and integral gain ($K_I$) for its dynamic responses while proposed sample based controller need to be tuned for gain(A) only.

(iv) The load controller is a non-linear system and feeds harmonics in the SEIG system. The increase in main load reduces the power to be dissipated in dump load and hence duty cycle of chopper switch decreases which increases the THD in dump load system. The THD of dump load system after passing through filtering capacitor, affect very little to main load. The total harmonic distortion is within satisfactory limits.

(v) The simulated and the experimental results are in close agreement indicating the effectiveness and accuracy of the developed model.

# CHAPTER-3

# THREE-PHASE IM AS A SINGLE PHASE SEIG WITH LOAD CONTROLLER

## 3.1 INTRODUCTION

The use of three phase induction motor as a three phase self excited induction generator and its voltage and frequency regulation with a load controller has been discussed in previous chapter. From this work, it is observed that terminal voltage of the SEIG drops with increase of the load. A three phase induction machine can be used to generate three phase supply at constant voltage and frequency if the electrical load is maintained constant at its terminals. Under such operation SEIG would require constant excitation through fixed capacitors and this is called single point operation where all parameters of the system are fixed.

In remote locations or hilly areas, electrical energy can be obtained from local resources at cheaper cost as compared to grid connection. A micro-hydro system with unregulated low head turbines, which maintains almost constant input power due to fixed head and discharge coupled with self excited induction generator may be one of the most suitable option. Such areas are characterized by sparsely distributed population with electric loads of single-phase. The single phase power supply is preferred over three phase in order to render the distribution system simple and cost effective.

It is possible to use a three-phase induction motor as a single-phase generator with only 20 to 25% power de-rating, and thus become the preferred approach for providing a single-phase supply. Beyond 5 kW load, the three phase induction machine, being inexpensive and readily available in the market with higher efficiency than equivalent rating single phase induction machine has become attractive proposition for supplying single phase power up to 20 kW. Three phase SEIG, supplying single phase load is the case of unbalanced operation and it is required to operate the machine at de-rated power so that the temperature rise of the machine is restricted within permissible limits.

From the literature review it is revealed that the appropriate choice of excitation capacitance and connection scheme is necessary in order to initiate voltage build up,

maintain given terminal voltage and optimized operation of the three phase induction machine working as single phase SEIG. Steady state performance analysis of three phase SEIG for single phase power generation is given in literature [14, 22, 27, 38, 39, 40, 42, 73, 74, 75, 94, 112, 113, 114, 115, 116, 155, 168, 197, 212, 213]. Alolah and Alkanhal [22] have used an optimization technique to determine the excitation requirements of three-phase delta connected SEIG under single phase mode operation using two excitation capacitors. A novel scheme based on eigenvalue method [213] has been proposed to determine the minimum and maximum value of excitation capacitance required for an autonomous three phase SEIG feeding a single phase load. Chang and Lai [40] have given a method for computing the minimum capacitance needed to initiate voltage build up in a three phase SEIG with a single capacitor and supplying a single phase load.

A two capacitor excitation scheme in '*C-2C*' configuration [27] of three phase SEIG for supplying single phase load offer almost balanced operation of three phase delta connected SEIG at partial power output. Further, for a purely resistive load, if the current of '*C*' valued capacitor is equal to root three times of current in resistive load then '*C-2C*' connected generator behaves as a balanced three phase machine. Shilpakar et al. [166] have presented the transient analysis of the three phase SEIG supplying single phase load with '*C-2C*' configuration. Fukami et al. [73, 74, 75] have proposed a new single phase induction generator consisting of the three phase induction machine with three excitation capacitors and shown that in addition to improved voltage regulation, the inherent vibration and noise in the generator can be significantly reduced. A novel and simple approach based on eigen value methods and sequential unconstrained minimization technique has been presented [112, 113, 115] for determination of both the minimum and maximum values of capacitance required for self excitation of an isolated single phase induction generator using a three phase machine with three excitation capacitor in '$C_p$-$C_s$' connection.

Based on the above discussions, this chapter is an attempt to analyze the three phase induction machine as a single phase SEIG and its voltage and frequency regulation with DSP based load controller. The two type of excitation scheme have been considered for study. Two capacitor excitation of three phase delta connected induction motor to work as single phase SEIG, known as the *'C-2C'* connection, is commonly used due to its simplicity. This connection gives optimum output at 415 V phase voltage for 415 V delta connected induction machine. The three capacitor excitation scheme for three phase star

connected induction machine working as single phase SEIG known as '$C_p$-$C_s$' is also been analyzed. This connection gives 220V single phase voltage output for 415 V star connected three phase induction machine. In order to regulate voltage and frequency of the SEIG, the power output is kept constant by connecting a dump load in parallel with the consumer load such that the total generated power is held constant. A DSP based load controller regulates the amount of power to be dissipated in dump load in accordance to change in consumer load. The use of DSPs gives flexibility of generating multiple high frequency and high resolution PWM waveforms, fast processing to implement the advance algorithms. Multiple features can also be implemented using the same controller. It makes the complete implementation simple and emulates a flexible solution. The future modifications can be realized by appropriate modifications in software instead of redesigning a separate hardware platform.

## 3.2 DELTA CONNECTED THREE PHASE IM AS SINGLE PHASE SEIG

### 3.2.1 Mathematical Modeling

Referring to Figure 3.1, the following equations can be written:

$$V_a + V_b + V_c = 0 \tag{3.1}$$

$$V_L = V_a \tag{3.2}$$

$$I_L + I_{ca} + I_{ga} - I_{gc} = 0 \tag{3.3}$$

$$I_{cb} + I_{gb} - I_{gc} = 0 \tag{3.4}$$

$$I_{ca} = Y_{ca} V_a = V_a / j\omega C_a \quad \text{and} \quad I_{cb} = Y_{cb} V_b = V_b / j\omega C_b \tag{3.5}$$

Using the symmetrical components transformation, we have the stator phase voltage and stator phase current as:

$$\begin{bmatrix} V_a \\ V_b \\ V_c \end{bmatrix} = \begin{bmatrix} 1 & 1 & 1 \\ 1 & a^2 & a \\ 1 & a & a^2 \end{bmatrix} \begin{bmatrix} V_o \\ V_p \\ V_n \end{bmatrix} \tag{3.6}$$

$$\begin{bmatrix} I_{ga} \\ I_{gb} \\ I_{gc} \end{bmatrix} = \begin{bmatrix} 1 & 1 & 1 \\ 1 & a^2 & a \\ 1 & a & a^2 \end{bmatrix} \begin{bmatrix} V_o Y_o \\ V_p Y_p \\ V_n Y_n \end{bmatrix} \tag{3.7}$$

where, 'a' is the unit complex operator given by $e^{j\frac{2\pi}{3}}$.

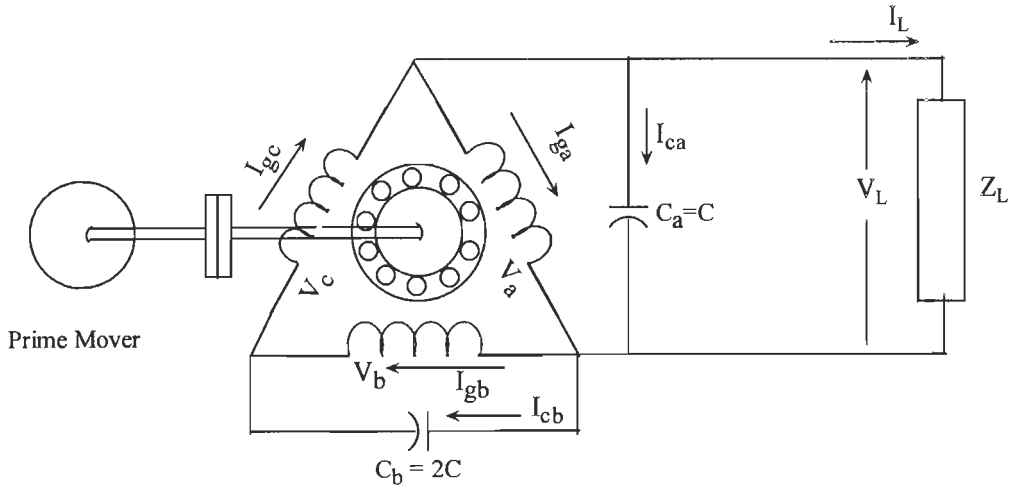


**Figure 3.1: C-2C Scheme of three phase SEIG for single phase power generation.**

For delta connected SEIG,

$$V_o = \frac{V_a + V_b + V_c}{3} \tag{3.8}$$

From equation (3.2),(3.6) and (3.8)

$$V_L = V_p + V_n, \quad \text{since } V_0=0; \tag{3.9}$$

From equation (3.4) , (3.5) and (3.6),(3.7) :

$$K_1 V_p = K_2 V_n \tag{3.10}$$

where, $K_1 = a^2 Y_{cb} + (a^2 - a) Y_p$ and $K_2 = -aY_{cb} - (a - a^2) Y_n$

Substituting $V_n$, from equation (3.10) to (3.9):

$$V_L = \{(K_1 + K_2) / K_2\} V_p \tag{3.11}$$

From equation (3.3) , (3.5) and (3.6),(3.7) :

$$I_L = -K_3 V_p - K_4 V_n \tag{3.12}$$

where, $K_3 = Y_a + (a-1)Y_p$ and $K_4 = Y_a + (a^2 - 1)Y_n$

Substituting $V_n$, from equation (3.10) to (3.12):

$$I_L = -\{(K_1 K_3 + K_2 K_4)/K_2\} V_p \tag{3.13}$$

Dividing equation (3.11) and (3.13):

$$\frac{V_L}{I_L} = -Z \tag{3.14}$$

where, $Z = \dfrac{K_1 + K_2}{K_1 K_3 + K_2 K_4}$

Hence, the single phase SEIG using three phase machine viewed from the load terminals can be represented by a single-phase circuit shown in Figure 3.2.

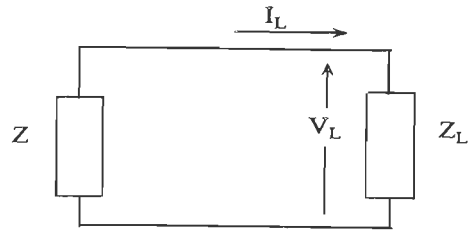


**Figure 3.2:- Equivalent circuit of SEIG feeding single phase load**

Applying Kirchhoff's voltage law we have:

$$(Z + Z_L) I_L = 0 \tag{3.15}$$

where, $Z_L = R_L$ is the load resistance.

Under steady state condition, $I_L$ can not be equal to zero and hence,

$$(Z + Z_L) = 0 \tag{3.16}$$

The output power can be calculated as:

$$P_o = |I_L|^2 R_L$$

***Determination of Minimum Capacitance from Steady-State Model:***

For steady-state condition, the air-gap voltage $E_g$ and the magnetizing reactance $X_m$ are taken as constant. For determination of minimum capacitance, the value of $X_m$ should be equal to the maximum saturated magnetizing reactance, which is constant. To calculate realistic values of the variables, upper and lower limits are imposed on them. Impedance $(Z + Z_L)$ can be represented in functional form as:

$$f(X_a, F) = |(Z + Z_L)| \tag{3.17}$$

For solving the equation (3.16) to determine the variables $X_a$ and F by minimization technique, the function $f(X_a, F)$ is taken as an objective function and the optimization problem is stated as:

Minimize $f(X_a, F)$

such that,

$$X_{al} \leq X_a \leq X_{ah} \quad \text{and} \quad F_l \leq F \leq F_u$$

where subscripts 'l' and 'u' denote lower and upper limits of the variables respectively. This is minimized by sequential unconstrained minimization technique (SUMT) in conjunction with Rosenbrock's method of rotating coordinates. The function must converge to zero and the value of tolerance to check the convergence is taken quite small, say equal to 0.0001. The required capacitance is then calculated from the $X_{csh}$ as:

$$C_a = \frac{1}{(2\pi f_b X_a)} \tag{3.18}$$

and $C_b = 2C_a$

***Modeling for Performance Analysis from Steady-State Model:***

For performance analysis at steady-state with fixed values of capacitances, $X_m$ and F are the two unknowns in equation (3.16) and $(Z + Z_L)$ can be represented in functional form as:

$$f(X_m, F) = |(Z + Z_L)| \tag{3.19}$$

For solving the equation (2.23) to determine the variables $X_m$ and F by minimization technique, the function $f(X_m, F)$ is taken as an objective function and the optimization problem is stated as:

Minimize $f(X_m, F)$

such that, $X_{ml} \leq X_m \leq X_{mu}$ and $F_l \leq F \leq F_u$

where subscripts 'l' and 'u' denote lower and upper limits of the variables respectively.

### 3.2.2 Performance analysis

The study has been carried out for 3.7 kW, 3-phase, 400 V delta connected induction machine. The single phase operation of three phase induction motor as the SEIG is extreme case of unbalanced operation but at certain combination of excitation capacitance and load the voltage and current converge to balanced condition. Figure 3.3 and Figure 3.4 shows the load characteristic of the SEIG for $C_a$=20 μF and $C_b$ = 40 μF. It can be observed that phase voltage and phase current converge to a common point at the power output of 1000 W. This shows that the system is operating at balanced condition at this power output. Figure 3.5 and Figure 3.6 shows the load characteristics for $C_a$=25 μF and $C_b$ = 50

μF. It can be observed that phase voltage and phase current converge to a common point at the power output of 2000 W. Figure 3.7 shows the simulated phase voltage and current waveform for a load application of 2 kW. It can be observed that at no load phase voltage and phase current are unbalanced and on application of load at time t=0.55 seconds, both voltages and currents converge to balanced condition. The power output at which balanced operation is obtained depends on the values of the excitation capacitance. The generator can operate at balanced condition at higher power output with higher excitation capacitance but it causes the phase voltage and phase current imbalance at high value on no load which is not suitable for practical applications. The maximum power output capability of the SEIG decreased to lower value in the backward direction of rotation as the unbalance in the phase quantities grow more due to opposite phase sequence.

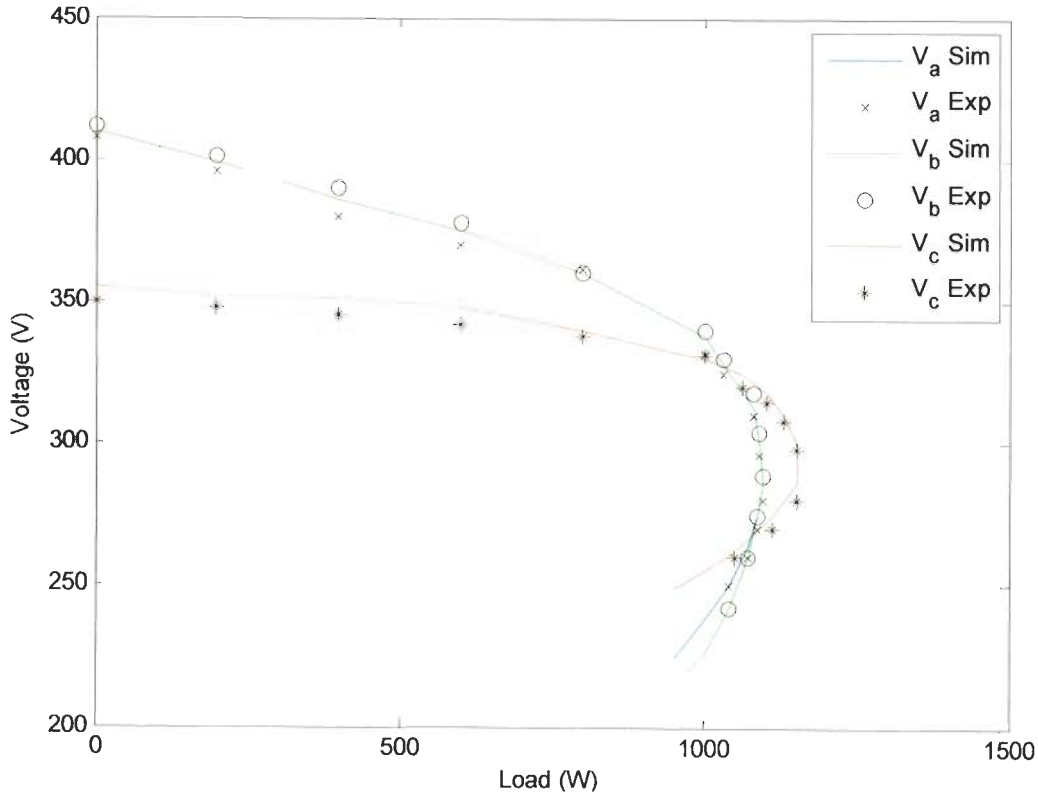


**Figure 3.3: Phase voltage variation with load for $C_a$=20 μF and $C_b$= 40 μF**

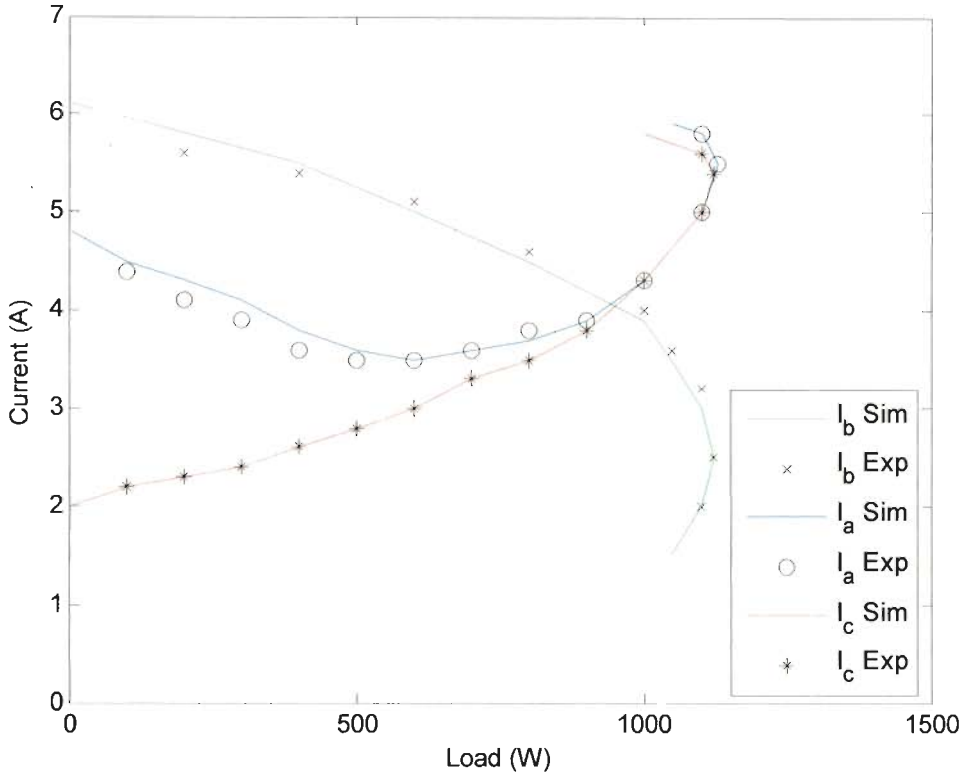


**Figure 3.4: Phase current variation with load for $C_a$=20 μF and $C_b$= 40 μF**

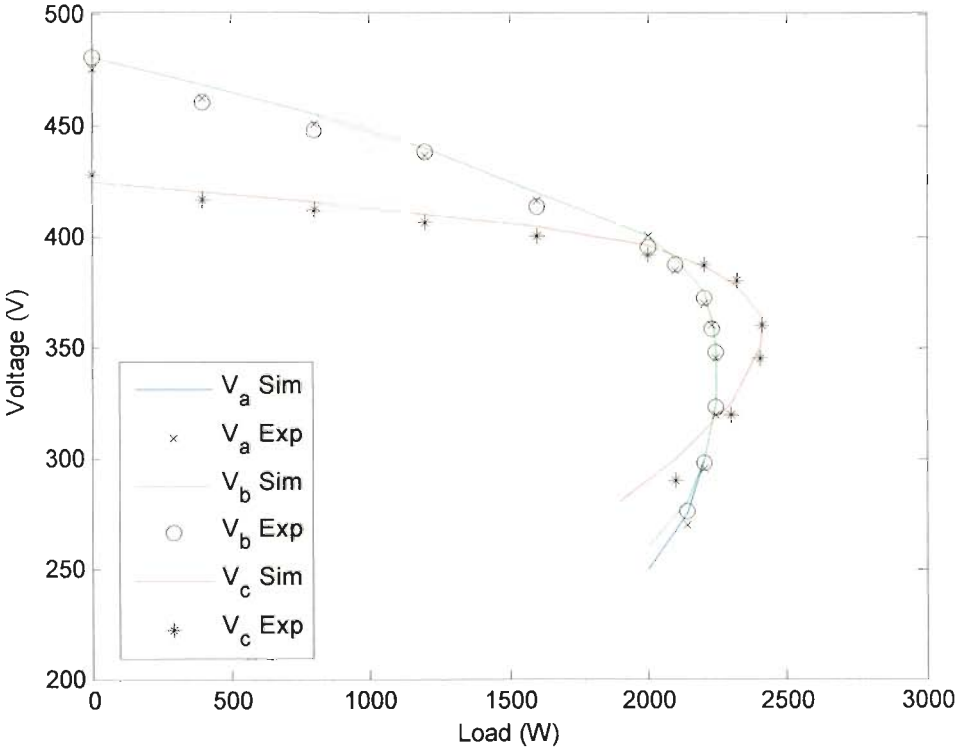


**Figure 3.5: Phase voltage variation with load for $C_a$=25 μF and $C_b$= 50 μF**

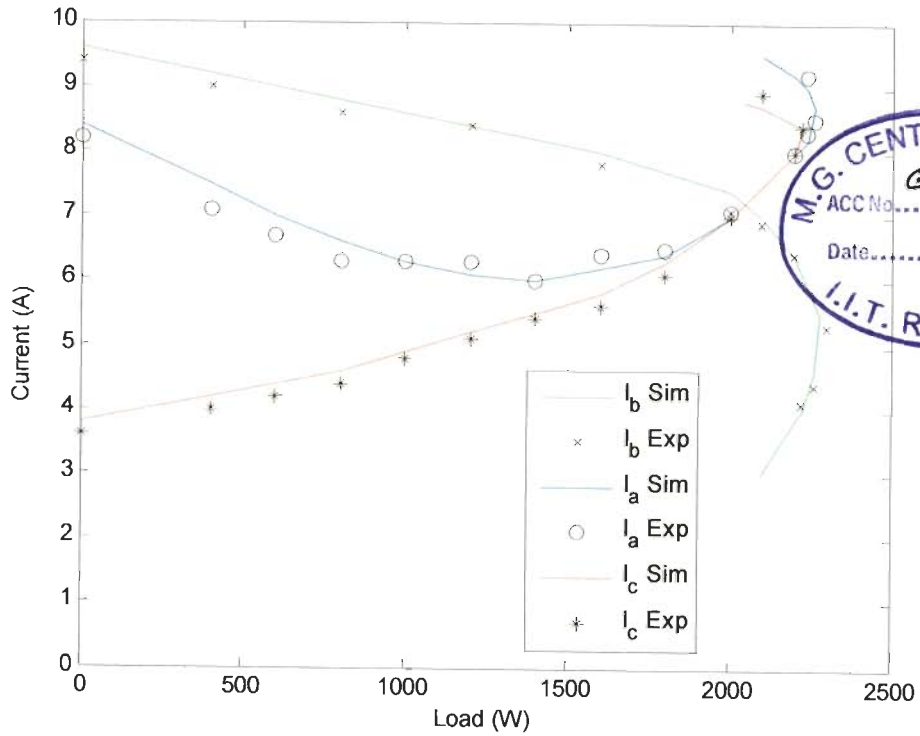




**Figure 3.6: Phase current variation with load for $C_a$=25 μF and $C_b$= 50 μF**

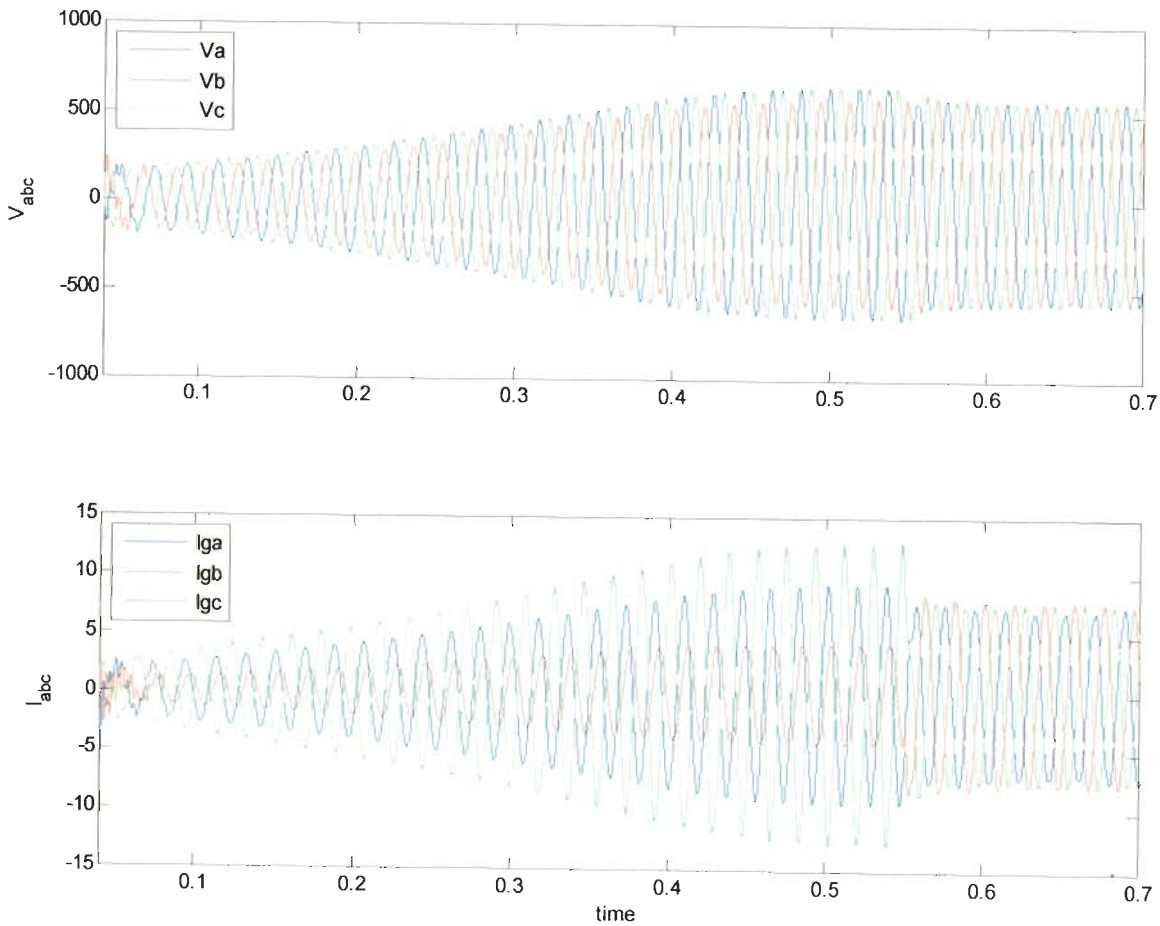


**Figure 3.7: Voltage and current build up and variation on application of resistive load**

### 3.2.3 Voltage and frequency regulation with load controller

A schematic diagram of the developed DSP based SEIG-load controller system is shown in Figure 3.8. It consists of a three phase delta connected squirrel cage induction motor (working as SEIG) driven by a constant power prime mover (typically, an un-regulated micro-hydro turbine). The excitation capacitors are connected at the terminals of the SEIG in C-2C configuration as shown in Figure 3.8, which have a fixed value to result in rated terminal voltage at rated load. Consumer load and load controller are connected in parallel at generator terminals.

The load controller consists of an uncontrolled rectifier, a filtering capacitor ($C_f$), IGBT based chopper and a series resistive dump load ($R_D$). The uncontrolled rectifier converts the SEIG AC terminal voltage to DC. The output ripples are filtered by filter capacitor. An IGBT is used as a chopper switch. When gate pulse to IGBT is high, the current flows through the dump load and the power is consumed. The pulse width or duty cycle of chopper is decided by the difference of power generation to consumer load. A TMS320F2812 (32-bit, 150 MIPS fixed point digital signal processor) DSP is used for generation of suitable pulse width in accordance with consumer load. The DSP reads the terminal voltage through a voltage transducer as a feedback signal from its ADC input and gives the suitable pulse from its PWM output to IGBT chopper through a pulse driver circuit.

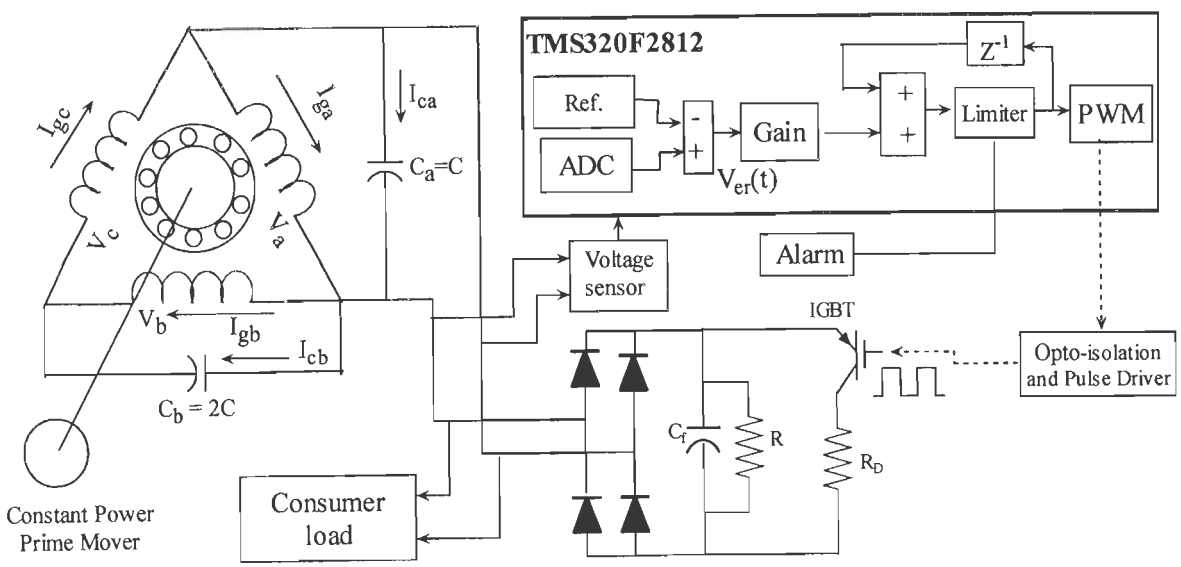


**Figure 3.8: Schematic diagram of three-phase SEIG with DSP based load controller**

### 3.2.4 Implementation

A three phase squirrel cage induction motor is connected in delta connection and excitation capacitors are connected in '*C-2C*' configuration. Excitation capacitance has to provide required voltage on load at the operating speed for the given induction machine operating as SEIG. The amount of capacitor excitation at no load and rated load may be determined iteratively. The equivalent circuit parameters may be obtained from open circuit and blocked-rotor test. Performance of SEIG depends on its magnetizing characteristics. The magnetizing characteristics of these machines are obtained from the synchronous speed test.

The SEIG feeds two loads in parallel such that the total power is constant, that is

$$P_{out} = P_c + P_d \tag{3.20}$$

where, $P_{out}$ is the generated power of the generator (which must be kept constant), $P_c$ is the consumer load power, and $P_d$ is the dump load power. The amount of dump load power is controlled by IGBT chopper. The duty cycle of gate pulse of IGBT gives the average conduction period of chopper and hence the average power dissipating in dump load. A variable mark-space ratio chopping approach has been adopted for the IGBT chopper because it produces a variable unity power factor load with just a single ballast or dump load.

The output power of the SEIG is kept constant by load controller. The terminal voltage for feedback is sensed with voltage transducer to achieve a DC value proportional to SEIG output voltage. The voltage transducer converts and linearizes the input AC terminal voltage to output DC voltage. This voltage is given to ADC input of the DSP TMS320F2812. The inputs of the ADC of the DSP controller (TMS320F2812) is limited to 0-3 Volt. The output values are in the range of 0 to 4095 because the TMS320F2812 DSP ADC is 12- bit converter. It reads the input with a sample rate of 0.001 seconds (maximum 0.0004 seconds). The DC output of voltage transducer has peak to peak ripples. A running mean is taken in software to overcome this problem. The sensed voltage is compared with a reference voltage signal, which is taken as proportional to the rated terminal voltage of the SEIG and may be altered as and when required. The error output decides the increase or decrease of pulse width. The error is scaled (gain) and subtracted to pulse width. The process is repeated till the desired terminal voltage is achieved. If the pulse width is 0% or 100% and terminal voltage is not up to desired level then generator is overloaded or dump load required to be adjusted respectively. To signal this, the general purpose digital output (GPIO) pulse is made high. This may be used for

alarming or tripping the circuit. The pulse width references are fed to PWM of DSP. The TMS320F2812 DSP has 6x2 high resolution PWM outputs. The PWM output is then given to IGBT chopper through an opto isolation and pulse driver circuit.

### 3.2.5 Results and Discussion

Digital simulation has been carried out on MATLAB Simulink environment. The simulation results are shown in Figure 3.9 and Figure 3.10 for resistive and reactive load application and removal. Waveform from top to bottom are terminal voltage ($V_t$), load current ($I_L$), SEIG phase voltage ($V_{abc}$), SEIG phase current ($I_{abc}$), dump load current ($I_{Dump}$) and frequency (f). On application of resistive load in steps of 500x3=1500 W, the terminal voltage and frequency remains constant. The phase voltage and current of the SEIG does also remain balanced. Figure 3.10 shows the waveforms for application and removal of 500 W, 0.8 lagging power factor load. On application of reactive load, the terminal voltage remains constant. There is a slight increase in frequency to compensate for reactive power demanded by the load. The SEIG phase voltage remains balanced but there is unbalance in the SEIG phase currents.

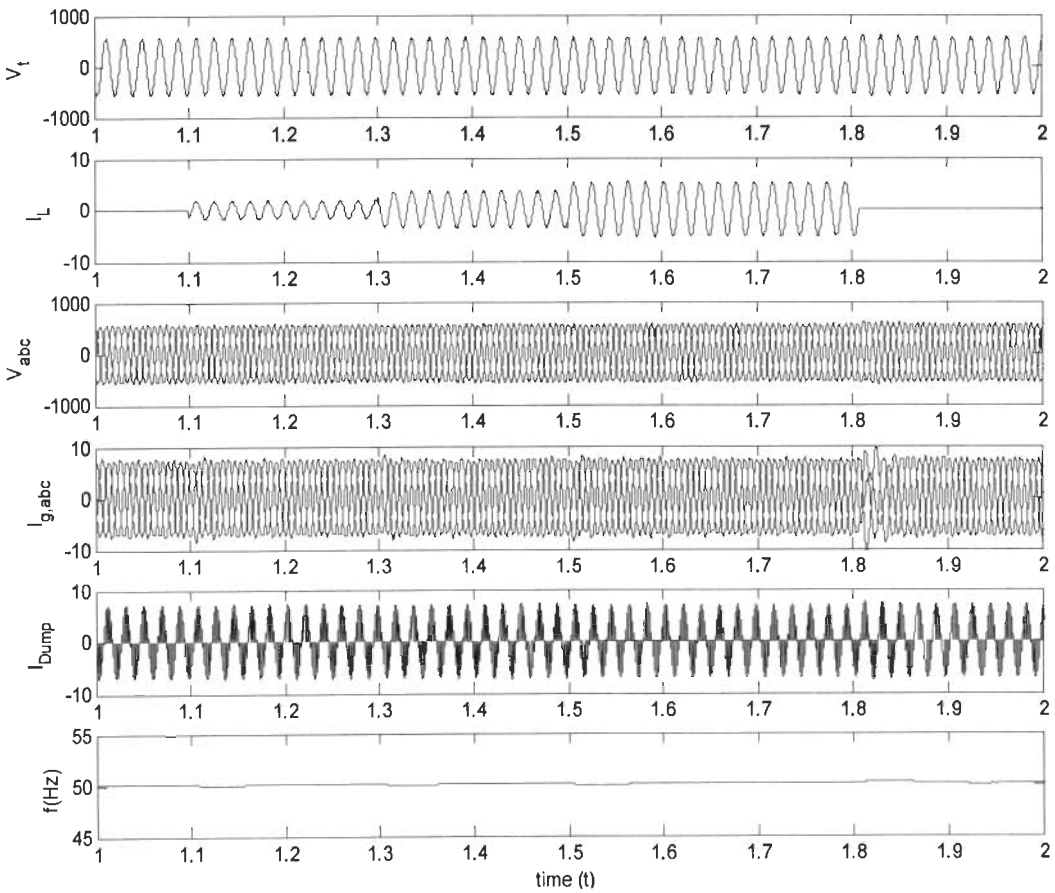


**Figure 3.9: Transient waveform of SEIG load controller system on application of resistive load**

Experiments are carried out on developed prototype of DSP based SEIG-load controller system. A three phase 3.73 kW, 400 V, 7.5 A 50Hz, 1440 rpm delta connected squirrel cage induction machine is used as a single phase self-excited induction generator. The SEIG is driven by 220 V, 20 A, 5 HP, 1500 rpm shunt wound DC machine used as a prime mover. To generate 2 kW at 400 V and rated speed, 25 μF and 50μF capacitors of 400 V are connected as C and 2C across the SEIG terminals. The test results are carried out with resistive load, 0.8 pf reactive load and 750 W, 220/230 V, 5.2 A, 50 Hz, 1425 rpm single phase induction motor with start capacitor of 125 μF, 275 V and run capacitor of 10μF, 400 V as dynamic load at developed SEIG-load controller system. A resistive load of 60 Ω is connected as dump load [refer dump load design, sec 2.3.4].

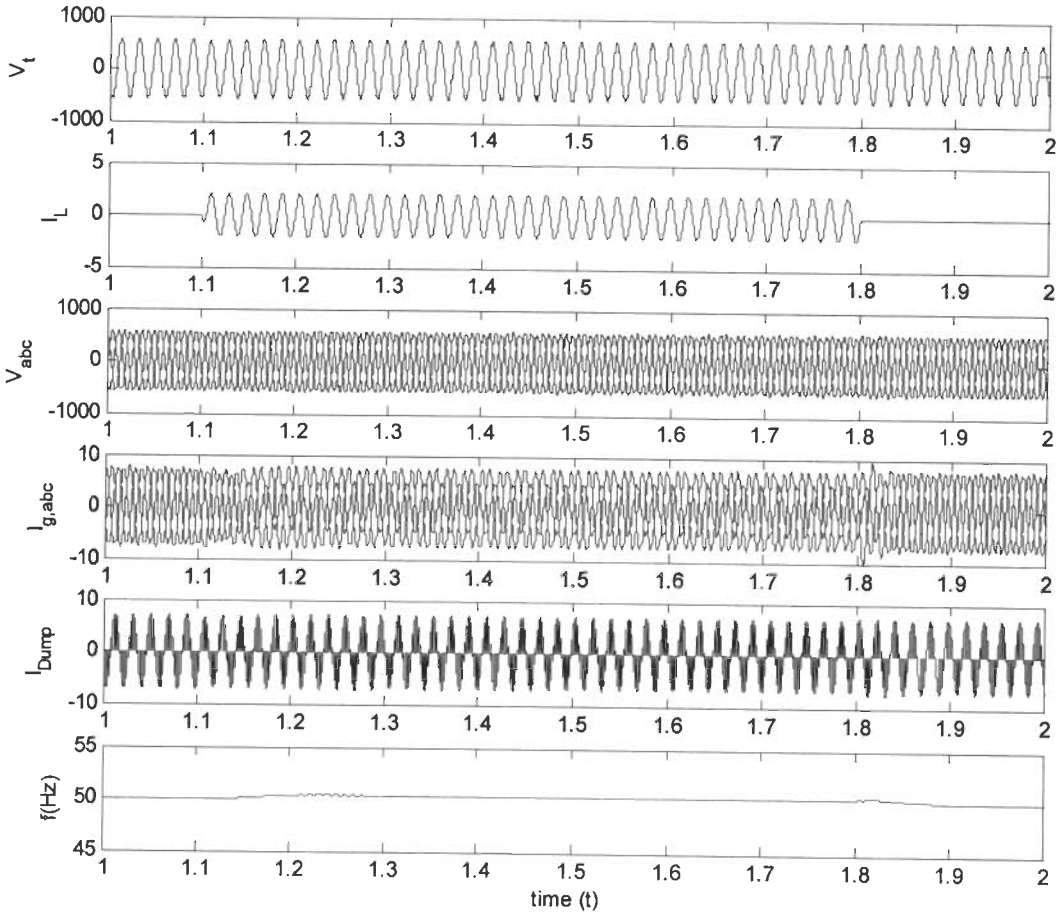


**Figure 3.10: Transient waveform of SEIG load controller system on application of reactive load**

Figure 3.11(a) shows the terminal voltage and load current transient waveforms of DSP based SEIG-load controller system on application of 1000 W resistive loads. In Figure 3.11(b), the steady state terminal voltage and load current trends are shown on

successive application and removal of 1000 W resistive load in steps of 250 W. On application and removal of load, the terminal voltage remains constant. On application of resistive load, main load current increases and dump load current decreases so that power transfers from dump load to consumer load and SEIG experiences constant load on it. The load controller is a non-linear system and feeds the harmonics in the SEIG. With application of resistive main load, power dissipating in dump load reduces therefore less harmonics are generated and SEIG voltages and currents are close to sinusoidal. Capacitive current also decreases due to less reactive burden.

Figure 3.12(a) shows the terminal voltage and load current transient waveforms on application of 500 W, 0.8 pf load. Figure 3.12(b) shows the steady state terminal voltage and load current trends on application and removal of 500 W 0.8 pf load. On application and removal of load the terminal voltage remains constant. When an inductive load is connected to the SEIG, it draws a reactive current. Then a part of the excitation capacitance is used to compensate for this reactive current, so less capacitance is available for the SEIG itself. It react to this with an increase in frequency, causing the capacitors to produce some more magnetizing current while the SEIG needs less so the two balance again and frequency varies as well with the reactive load. The frequency variation caused by reactive load is under acceptable. With a SEIG running at a normal degree of saturation, frequency variation would be less. As modern induction machines tend to be highly saturated, therefore the frequency regulation with variation in load power factor is quite small. A small increase in frequency results in a significant reduction in magnetizing current. In addition, extra VARs are produced by the excitation capacitors due to reduced impedance.

Figure 3.13(a) shows the transient terminal voltage and load current waveforms of DSP based SEIG-load controller system at starting and running of single phase 1 HP induction motor at no load. A step down transformer is used to step down the voltage level appropriate for single phase motor. An approximate 10% change in voltage observed for a few cycles and then it recovers very near to rated value. Simultaneously, there is a small increase in frequency to compensate for lagging power factor load and decrease in generator current. Figure 3.13(b) shows the steady state terminal voltage and load current trends on starting and running of single phase induction motor.

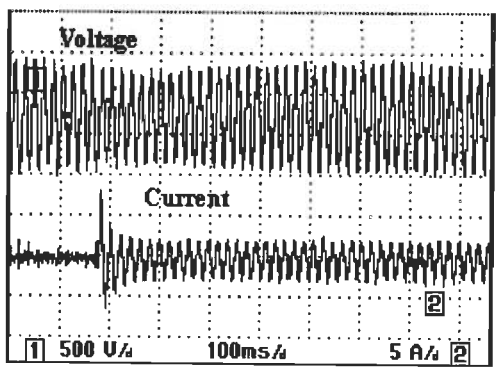


(a)

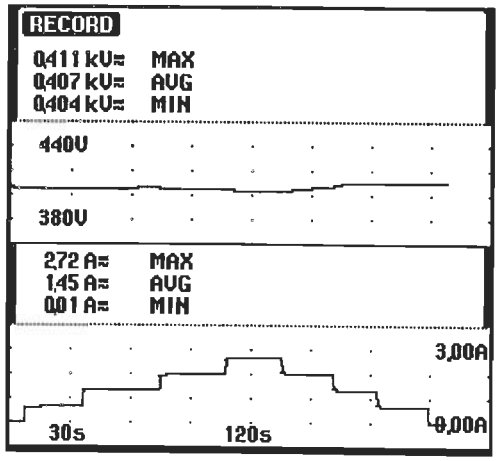


(b)

**Figure 3.11: (a) Transient response of terminal voltage and load current at application of 1000 W resistive load (b)Steady state terminal Voltage and load current trends at application and removal of 1000 W resistive load in 250 W steps**

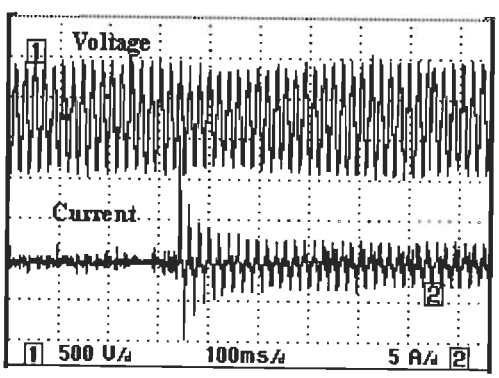


(a)

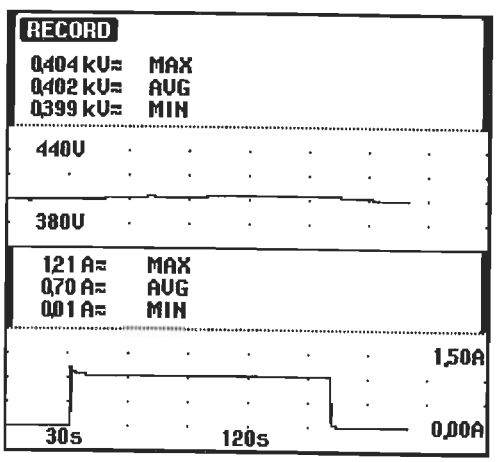


(b)

**Figure 3.12: (a) Transient response of terminal voltage and load current at application of 500W 0.8 pf load (b) Steady state terminal Voltage and load current trends at application and removal of 500W 0.8 pf load.**

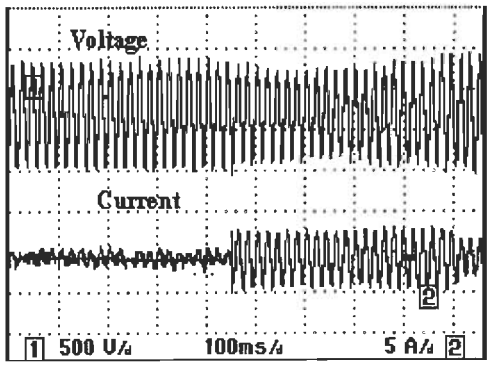


(a)

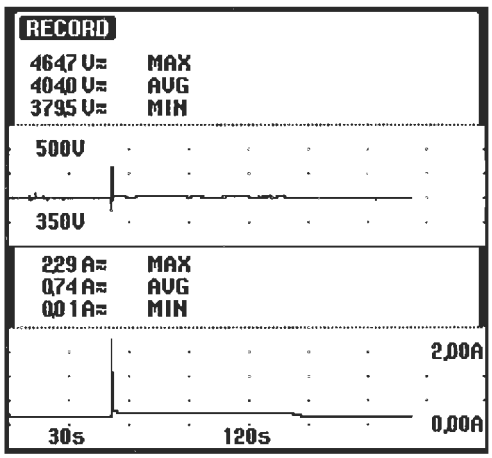


(b)

**Figure 3.13 (a) Transient response of terminal voltage and load current at starting of single phase 1HP induction motor (b) Steady state terminal voltage and load current trends at starting, running and removal of single phase 1HP induction motor**

The load controller is a non-linear system and feeds harmonics in the SEIG. Table 3.1 summarizes the main load, dump load, terminal voltage, frequency variations, voltage THD and current THD of main load, dump load and generator at different steps of resistive, reactive and dynamic load application.

**Table 3.1 Terminal voltage and frequency regulation, voltage and current THD at different load applications**

| Main load (W) | Terminal Voltage(V) | | Frequency (Hz) | | Voltage THD (%) | | Current THD (%) | | | | | |
|---|---|---|---|---|---|---|---|---|---|---|---|---|
| | | | | | | | Main load | | Dump load | | Generator | |
| | Sim | Meas | Sim | Meas | Sim | Meas | Sim | Meas | Sim | Meas | Sim | Meas |
| 0 | 400.3 | 400.3 | 50.01 | 50.33 | 3.0 | 4.0 | - | - | 5.3 | 8.6 | 4.1 | 7.1 |
| 300 | 400.4 | 402.6 | 50.15 | 50.65 | 4.1 | 5.3 | 4.1 | 6.2 | 10.3 | 30.9 | 4.7 | 7.7 |
| 600 | 400.4 | 403.4 | 50.13 | 50.52 | 4.3 | 7.5 | 4.4 | 7.0 | 28.3 | 58.5 | 5.1 | 7.7 |
| 900 | 400.6 | 403.0 | 50.12 | 50.43 | 4.3 | 6.6 | 5.2 | 6.8 | 43.4 | 73.1 | 5.4 | 7.4 |
| 1200 | 400.4 | 402.1 | 50.11 | 50.40 | 4.5 | 5.6 | 5.1 | 5.8 | 58.2 | 78.5 | 5.5 | 7.6 |
| 1500 | 400.1 | 401.6 | 50.09 | 50.35 | 4.2 | 4.8 | 4.1 | 4.8 | 63.4 | 80.6 | 5.2 | 7.9 |
| 1800 | 400.1 | 400.1 | 50.03 | 50.15 | 4.1 | 4.9 | 4.1 | 4.9 | 76.2 | 84.3 | 4.2 | 7.2 |
| 200W 0.8pf lagging | 401.6 | 404.2 | 50.26 | 50.51 | 5.1 | 6.5 | 24.2 | 44.5 | 22.7 | 42.5 | 6.1 | 9.2 |
| 400W 0.8pf lagging | 402.4 | 406.1 | 50.65 | 50.89 | 6.7 | 8.9 | 30.1 | 43.4 | 43.3 | 66.4 | 8.5 | 20.2 |
| 600W 0.8pf lagging | 404.6 | 408.3 | 50.85 | 51.23 | 7.1 | 9.4 | 16.3 | 22.4 | 35.6 | 37.8 | 9.6 | 18.3 |
| Single phase 1 HP motor running on no load | 402.1 | 403.4 | 50.45 | 50.84 | 4.2 | 4.9 | 12.1 | 16.4 | 31.2 | 41.4 | 4.9 | 5.6 |

The good voltage and frequency regulation is observed. There is a slight increase in terminal voltage as the voltage THD in the system increases. A slight increment in frequency is observed for loads of lagging power factor. Three phase induction motor working as a single phase induction generator in C-2C configuration principally behaves as unbalanced generator for reactive loads. An increase in voltage and current THD is observed for reactive loads on SEIG.

## 3.3 STAR CONNECTED THREE PHASE IM AS SINGLE PHASE SEIG

### 3.3.1 Mathematical Modeling

The steady-state equivalent circuit of the induction generator feeding inductive load is shown in Fig. 3.14.

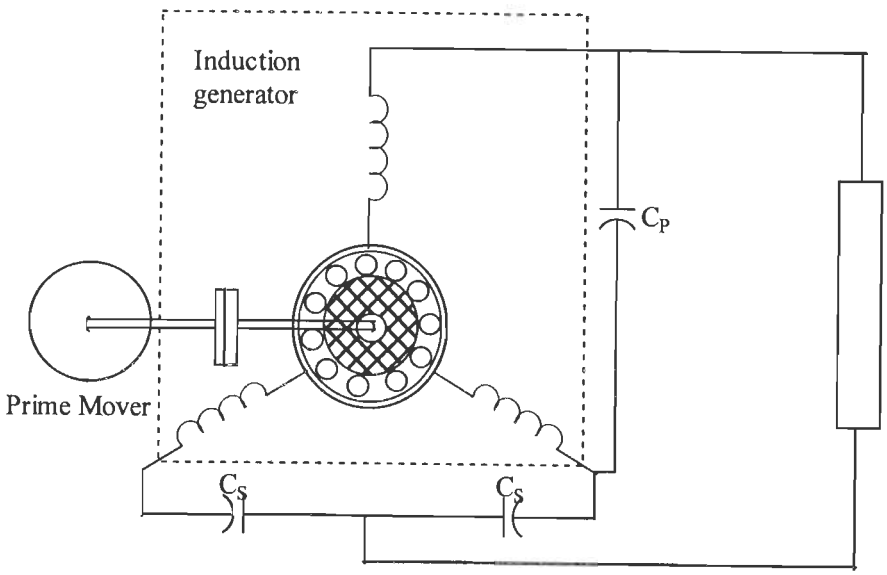


**Figure 3.14 : $C_p$-$C_s$ scheme of three phase SEIG for single phase power generation.**

Detail formulation of the equations for determination of the equivalent circuit can be found in [74]. The steady state equivalent of three phase star connected induction motor working as a SEIG is given in Figure 3.15.

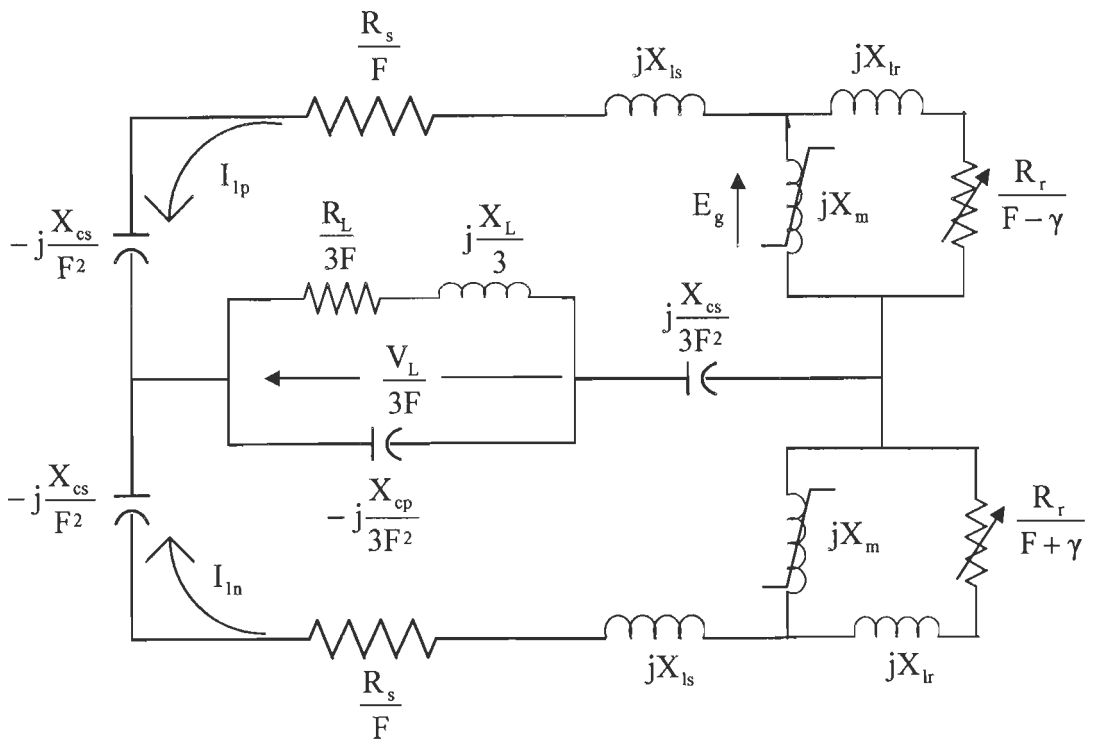


**Figure 3.15: Steady state equivalent circuit of the single-phase induction generator**

From the Fig. 3.15, the loop equation for the positive sequence component of stator current $I_{1p}$ can be written as:

$$Z\, I_{1p} = 0 \tag{3.21}$$

where Z is the total loop impedance seen by $I_{1p}$ and is given by:

$$Z = \frac{Z_{gp}}{F} - j\frac{X_{cs}}{F^2} + \frac{\left(\frac{Z_{gn}}{F} - j\frac{X_{cs}}{F^2}\right)\left(\frac{Z_e}{3F} + j\frac{X_{cs}}{3F^2}\right)}{\frac{Z_e}{3F} + j\frac{X_{cs}}{3F^2} + \frac{Z_{gn}}{F} - j\frac{X_{cs}}{F^2}} \tag{3.22}$$

where, $Z_{gp}$, $Z_{gn}$ are positive and negative sequence components of generator impedance,

$Z_e$ is the equivalent impedance of load and capacitor $C_p$,

$X_{cs}$ is the reactance of the capacitor $C_s$

and F is the per unit frequency.

The expressions of $\frac{Z_{gp}}{F}$, $\frac{Z_{gn}}{F}$ and $\frac{Z_e}{3F}$ are given as follows:

$$\frac{Z_{gp}}{F} = A_1 + A_2, \qquad \frac{Z_{gn}}{F} = A_1 + A_3,$$

where, $A_1 = \frac{R_s}{F} + jX_{ls}$, $A_2 = \frac{(jX_m)(\frac{R_r}{F-\gamma} + jX_{lr})}{\frac{R_r}{F-\gamma} + j(X_m + X_{lr})}$, $A_3 = \frac{(jX_m)(\frac{R_r}{F+\gamma} + jX_{lr})}{\frac{R_r}{F+\gamma} + j(X_m + X_{lr})}$

and $\frac{Z_e}{3F} = \frac{\left(\frac{R_L}{3F}\right)\left(-j\frac{X_{cp}}{3F^2}\right)}{\frac{R_L}{3F} - j\frac{X_{cp}}{3F^2}}$ for resistive load

$= \frac{\left(\frac{R_L}{3F} + j\frac{X_L}{3}\right)\left(-j\frac{X_{cp}}{3F^2}\right)}{\frac{R_L}{3F} + j\left(\frac{X_L}{3} - \frac{X_{cp}}{3F^2}\right)}$ for inductive load.

For the sake of simplicity in analysis, it is assumed that both $C_p$ and $C_s$ are equal to C and $X_{cp} = X_{cs} = X_c$. Under the steady-state self-excited condition, $I_{1p}$ in equation (3.21) can not be zero. Hence,

$$Z = 0 \tag{3.23}$$

***Determination of Minimum Capacitance from Steady-State Model:***

At steady-state condition, the air-gap voltage $E_g$ and the magnetizing reactance $X_m$ are taken as constant. For minimum capacitance required for self-excitation, the value of $X_m$ should be equal to the maximum saturated magnetizing reactance, which is constant. Hence in equation (3.23), $X_c$ and F are the two unknowns. To calculate realistic values of the variables, upper and lower limits are imposed on them. Impedance Z can be represented in functional form as:

$$f(X_c, F) = \left| \frac{Z_{gp}}{F} - j\frac{X_{cs}}{F^2} + \frac{\left(\frac{Z_{gn}}{F} - j\frac{X_{cs}}{F^2}\right)\left(\frac{Z_e}{3F} + j\frac{X_{cs}}{3F^2}\right)}{\frac{Z_e}{3F} + j\frac{X_{cs}}{3F^2} + \frac{Z_{gn}}{F} - j\frac{X_{cs}}{F^2}} \right| \tag{3.24}$$

For solving (3.23) in which $X_c$ and F are the two unknowns by minimization technique, the function $f(X_c, F)$ is taken as an objective function and the optimization problem is stated as:

Minimize $f(X_c, F)$

such that, $X_{cl} \le X_c \le X_{cu}$ and $F_l \le F \le F_u$

where subscripts 'l' and 'u' denote lower and upper limits of the variables. The minimization of this function is carried out by sequential unconstrained minimization technique (SUMT) in conjunction with Rosenbrock's method of rotating coordinates. The function must converge to zero and the value of tolerance to check the convergence is taken quite small, say equal to 0.0001. The required capacitance is then calculated from $X_c$ as:

$$C_p = C_s = C = \frac{1}{(2\pi f_b X_c)}. \tag{3.25}$$

***Performance Analysis from Steady-State Equivalent Circuit:***

For performance analysis at steady-state with fixed values of capacitances, $X_m$ and F are the two unknowns in equation (3.23). Hence, the impedance Z can be represented in functional form as:

$$f(X_m, F) = \left| \frac{\frac{Z_{gp}}{F} - j\frac{X_{cs}}{F^2} + \frac{\left(\frac{Z_{gn}}{F} - j\frac{X_{cs}}{F^2}\right)\left(\frac{Z_e}{3F} + j\frac{X_{cs}}{3F^2}\right)}{\frac{Z_e}{3F} + j\frac{X_{cs}}{3F^2} + \frac{Z_{gn}}{F} - j\frac{X_{cs}}{F^2}}}{} \right| \tag{3.26}$$

For solving (3.23) in which $X_m$ and F are the two unknowns by minimization technique, the function $f(X_m, F)$ is taken as an objective function and the optimization problem is stated as:

Minimize $f(X_m, F)$

such that, $X_{ml} \le X_m \le X_{mu}$ and $F_l \le F \le F_u$

where subscripts 'l' and 'u' denote lower and upper limits of the variables. This equation is solved by SUMT in conjunction with Rosenbrock's method of rotating coordinates. The next step is to estimate the air-gap voltage $E_g$ corresponding to the variation of $X_m$ during power generation. For this, the magnetization characteristic of the machine has been used. After calculating $E_g$ from $X_m$, the following relations can be used for the computation of the machine performance:

$$I_{1p} = \frac{E_g}{\frac{R_s}{F} + jX_{ls} - j\frac{X_{cs}}{F^2} + \frac{\left(\frac{Z_{gn}}{F} - j\frac{X_{cs}}{F^2}\right)\left(\frac{Z_e}{3F} + j\frac{X_{cs}}{3F^2}\right)}{\frac{Z_e}{3F} + \frac{Z_{gn}}{F} - j\frac{2X_{cs}}{3F^2}}} \tag{3.27}$$

$$I_{ln} = -\frac{\frac{Z_e}{3F} + j\frac{X_{cs}}{3F^2}}{\frac{Z_e}{3F} + \frac{Z_{gn}}{F} - j\frac{2X_{cs}}{3F^2}} I_{lp} \tag{3.28}$$

For resistive load, the load current and load voltage may be written as:

$$I_L = \frac{-j\frac{X_{cp}}{F^2}}{\frac{R_L}{F} - j\frac{X_{cp}}{F^2}} \left(I_{lp} + I_{ln}\right) \tag{3.29}$$

$$V_L = R_L I_L \tag{3.30}$$

Similarly, for inductive load, the expressions for load current and load are given as:

$$I_L = \frac{-j\frac{X_{cp}}{F^2}}{\frac{R_L}{F} + jX_L - j\frac{X_{cp}}{F^2}} \left(I_{lp} + I_{ln}\right) \tag{3.31}$$

$$V_L = (R_L + jX_L)\, I_L \tag{3.32}$$

The output power is expressed as:

$$P_0 = |I_L|^2 R_L \tag{3.33}$$

### 3.3.2 Performance analysis

The study has been carried out for 3.7 kW, 3-phase, 400 V star connected induction machine. The parameters of induction machine are obtained by conducting DC resistance test, blocked rotor test and magnetization characteristic obtained by synchronous speed test. The parameters and the magnetization characteristics are of the induction machine are summarized in Appendix A. From the steady state model of the generator, it has been found that to obtain a voltage of 220 V at load of 2000 W, the capacitance required is $C_p = C_s = 47\ \mu F$.

The output voltage with increase in output power is shown in Figure 3.16. Experimental and simulation result shows that as the output power increases the terminal voltage decreases. Figure 3.17 shows the variation of stator phase currents with output power. Figure 3.18 shows the simulated voltage build up. The Figure 3.19 shows that on application of 2 kW resistive load, the stator phase current becomes unbalanced but it is below the current rating and does not cause to rise in temperature

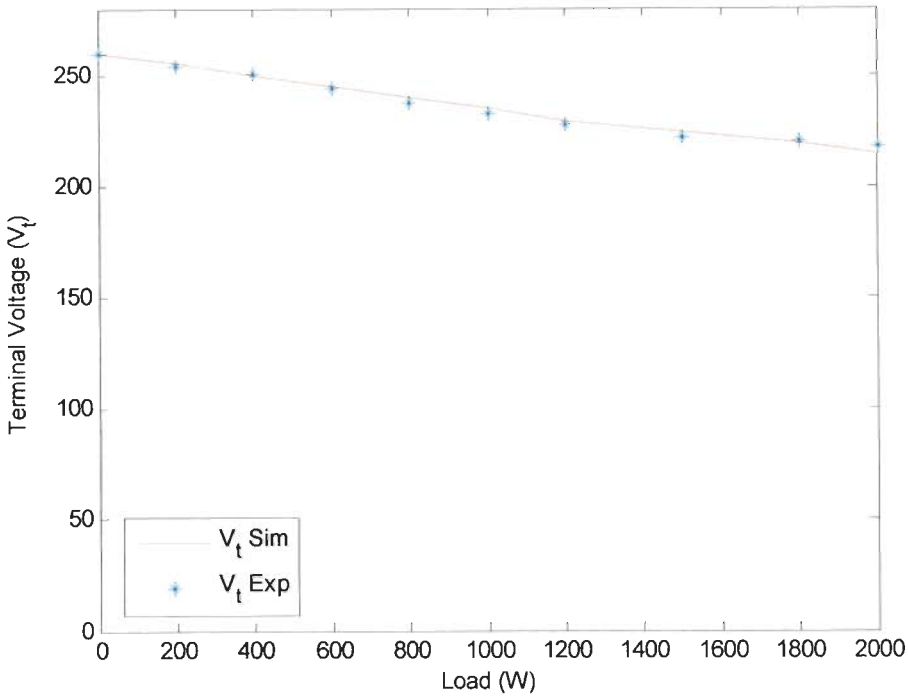


**Figure 3.16: Variation of terminal voltage with resistive load.**

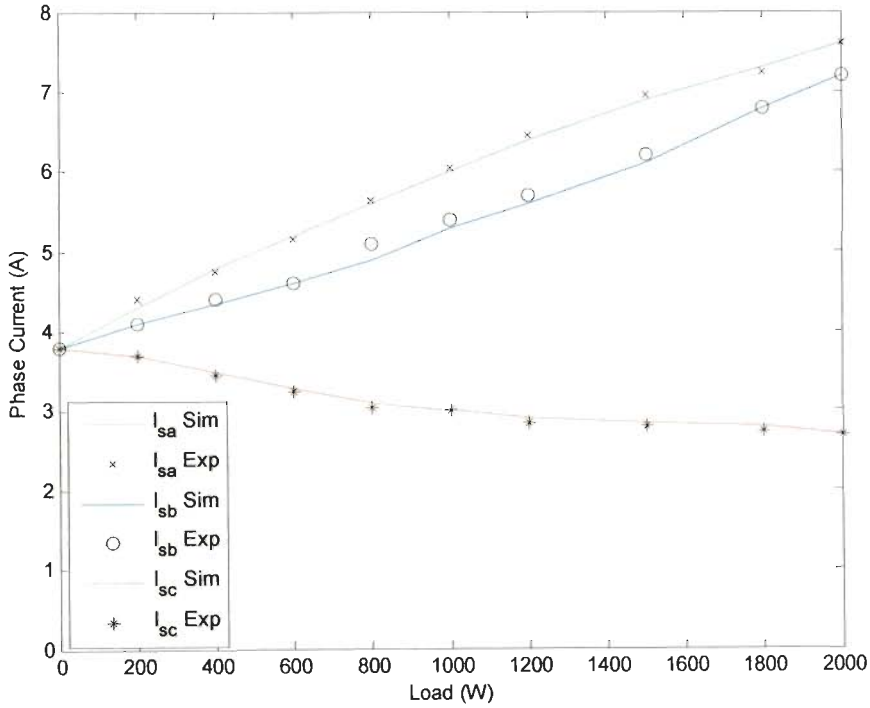


**Figure 3.17: Variation of phase current with load**

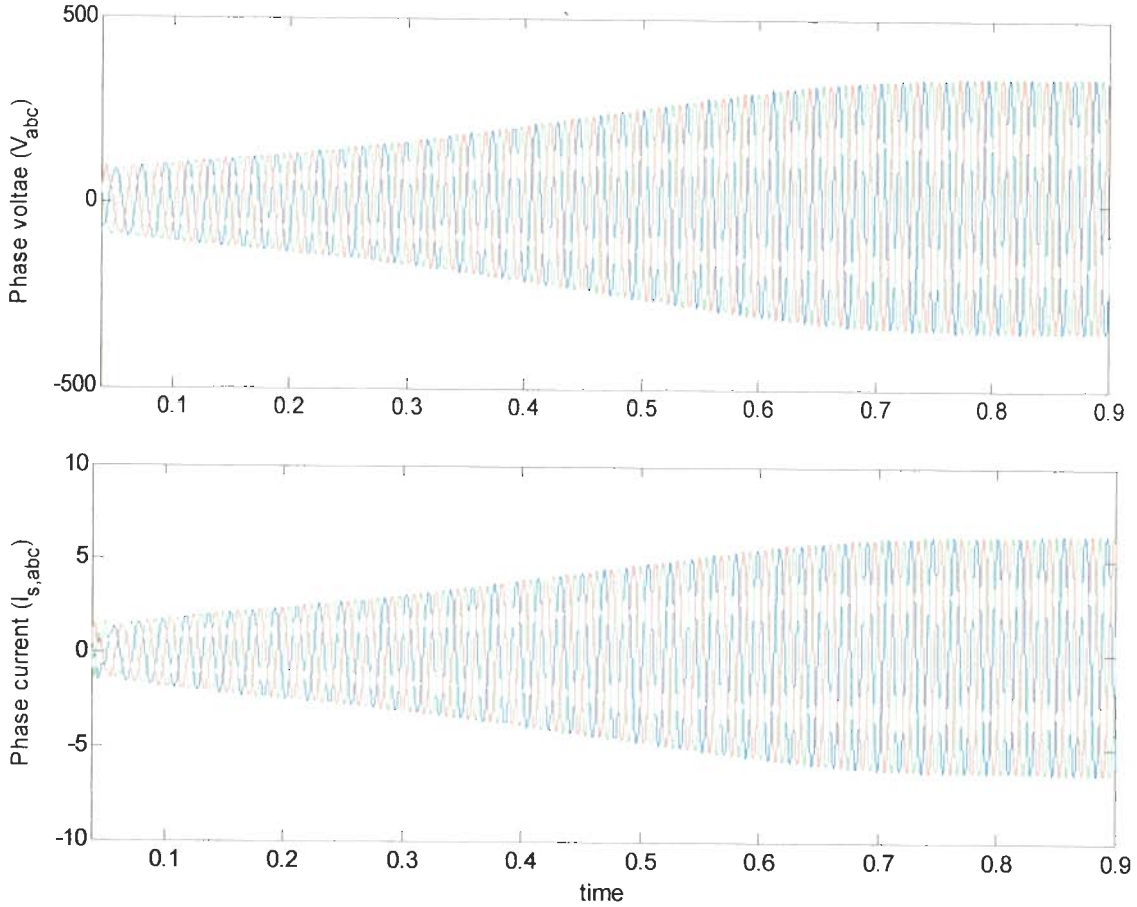


**Figure 3.18: Voltage build up and phase current at no load.**

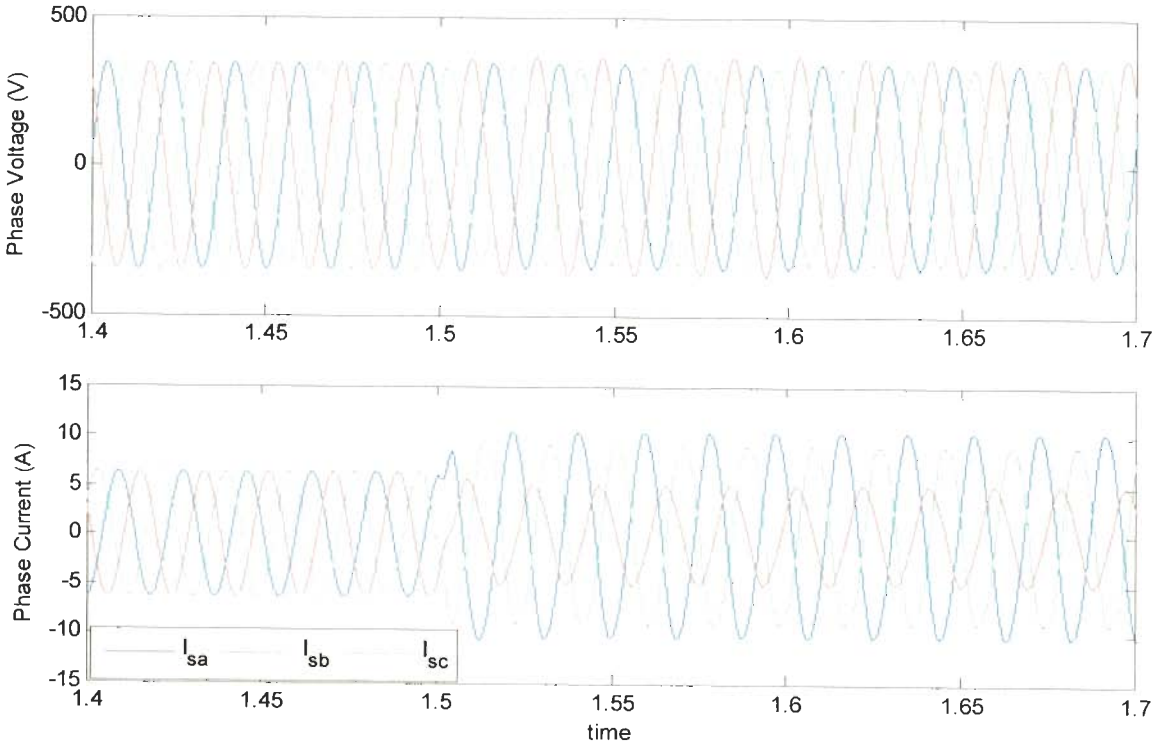


**Figure 3.19: Three phase voltage and current on no load and after application of rated load.**

### 3.3.3 Voltage and frequency regulation with load controller

A schematic diagram of the developed DSP based SEIG-load controller system is shown in Figure 3.20(a) and 3.20(b). It consists of a three phase star connected squirrel cage induction motor (working as SEIG) driven by a constant power prime mover (typically, an un-regulated micro-hydro turbine). The excitation capacitors are connected at the terminals of the SEIG in $C_p$-$C_s$ configuration as shown in Figure 3.20, which have a fixed value to result in rated terminal voltage at rated load. Consumer load and load controller are connected in parallel at generator terminals.

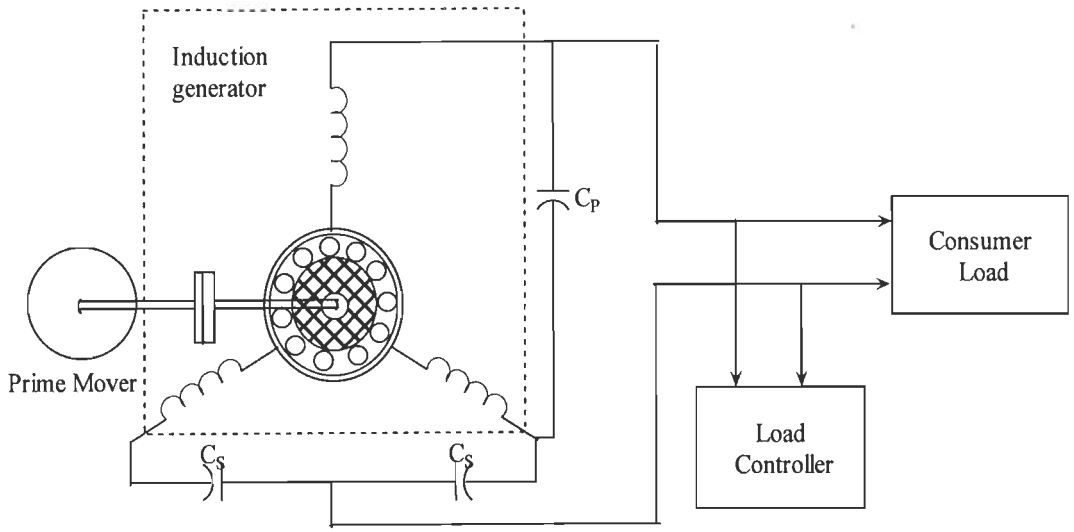


**Figure 3.20(a): Schematic diagram of Single-phase SEIG**

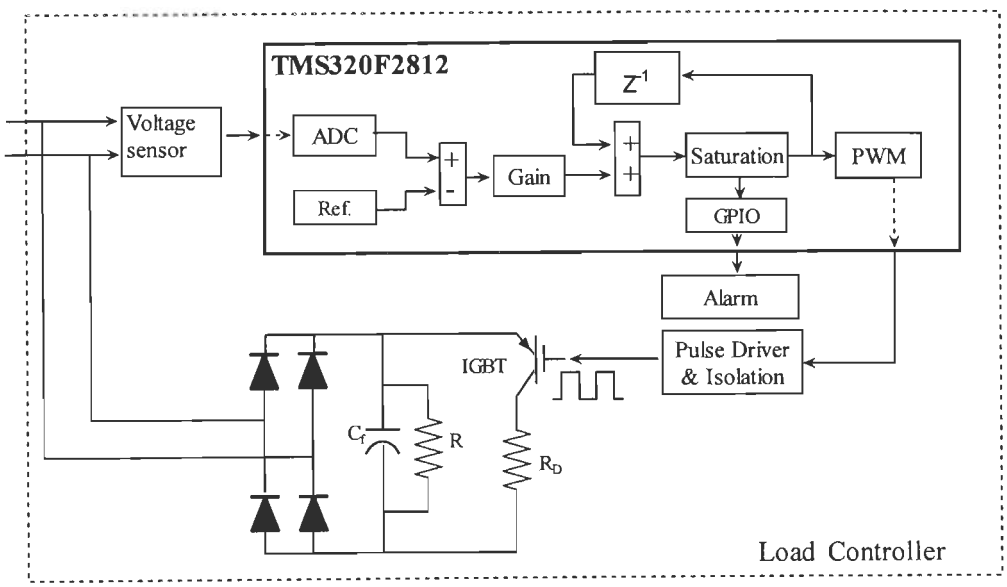


**Figure 3.20(b): Schematic diagram DSP based load controller for SEIG**

The load controller consist of an uncontrolled rectifier, a filtering capacitor ($C_f$), IGBT based chopper and a series resistive dump load ($R_D$). The uncontrolled rectifier converts the SEIG AC terminal voltage to DC. The output ripples are filtered by filter capacitor. An IGBT is used as a chopper switch. When gate pulse to IGBT is high, the current flows through the dump load and the power is consumed. The pulse width or duty cycle of chopper is decided by the difference of power generation to consumer load. A TMS320F2812 (32-bit, 150 MIPS fixed point digital signal processor) DSP is used for generation of suitable pulse width in accordance with consumer load. The DSP reads the terminal voltage through a voltage transducer as a feedback signal from its ADC input and gives the suitable pulse from its PWM output to IGBT chopper through a pulse driver circuit.

### 3.3.4 Implementation

The performance analysis shows that the as the load increases on the SEIG, there is a decrease in terminal voltage. In order to regulate voltage and frequency of the SEIG, it is operated at constant load. To regulate the load a parallel dump load is connected at the SEIG terminals. The SEIG feeds two loads in parallel such that the total power $P_{out}=P_c+P_d$ is constant, Where, $P_{out}$ is the generated power of the generator (which must be kept constant), $P_c$ is the consumer load power, and $P_d$ is the dump load power. This dump load power ($P_d$) may be used for non priority load such as heating, battery charging, cooking etc. Excitation capacitance has to provide required leading VAR to maintain rated voltage on load at the operating speed for the given induction machine operating as SEIG. The amount of capacitor excitation at no load and rated load may be determined iteratively.

The output power of the SEIG is kept constant by load controller. Figure 3.20(b) shows the control scheme for voltage regulation of the SEIG. The terminal voltage for feedback is sensed with voltage transducer to achieve a DC value proportional to SEIG output voltage. The voltage transducer converts and linearizes the input AC terminal voltage to equivalent output DC voltage. This voltage is given to ADC input of the DSP TMS320F2812. The output values are in the range of 0 to 4095 as the TMS320F2812 DSP ADC is 12- bit converter. It reads the input with a sample rate of 0.001 seconds. The sensed voltage is compared with a reference, which is taken as proportional to the rated

terminal voltage of the SEIG and may be altered as and when required. The error is scaled (gain) and algebraically added to previous sample time PWM reference level. As the desired terminal voltage is achieved the error signal becomes zero and PWM reference holds its level. The pulse width references are fed to PWM of DSP. The PWM block have self carrier triangular wave. The carrier frequency is selected according to static switching device. The TMS320F2812 DSP has 6x2 high resolution PWM outputs. The PWM output is then given to IGBT chopper through an opto isolation and pulse driver circuit.

### 3.3.5 Results and Discussion

Digital simulation has been carried out on MATLAB Simulink environment. The simulation results are shown in Figure 3.21 and Figure 3.22 for resistive and reactive load application and removal. Waveform from top to bottom are terminal voltage ($V_t$), load current ($I_L$), SEIG phase voltage ($V_{abc}$), SEIG phase currents ($I_{s,abc}$), dump load current ($I_{Dump}$) and frequency (f) respectively. On application of resistive load of 1000 W, the terminal voltage and frequency remains constant. The phase voltage and current of the SEIG does also remain balance. Figure 3.22 shows the waveforms for application and removal of 500 W, 0.8 lagging power factor load. On application of reactive load, the terminal voltage remains constant. There is a slight increase in frequency to compensate for reactive power demanded by the load. The SEIG phase voltage remains balanced but there is a unbalance in the SEIG phase current.

Experiments are carried out on developed prototype of DSP based SEIG-load controller system. A three phase 3.73 kW, 400 V, 7.5 A 50Hz, 1440 rpm star connected squirrel cage induction machine is used as a single phase self-excited induction generator. The SEIG is driven by 220 V, 20 A, 5 HP, 1500 rpm shunt wound DC machine used as a prime mover. To generate 2 kW at 220 V and rated speed, 47 μF capacitors of 400 V are connected as $C_p$ and $C_s$ across the SEIG terminals. The test results are carried out with resistive load, 0.8 pf reactive loads.

Figure 3.23(a) and Figure 3.23(b) shows the voltage and current transient waveforms of DSP based SEIG-load controller system on application of 500 W resistive loads. In Figure 3.23(c), voltage and current trends are shown on successive application and removal of 800 W resistive load in step of 200 W.

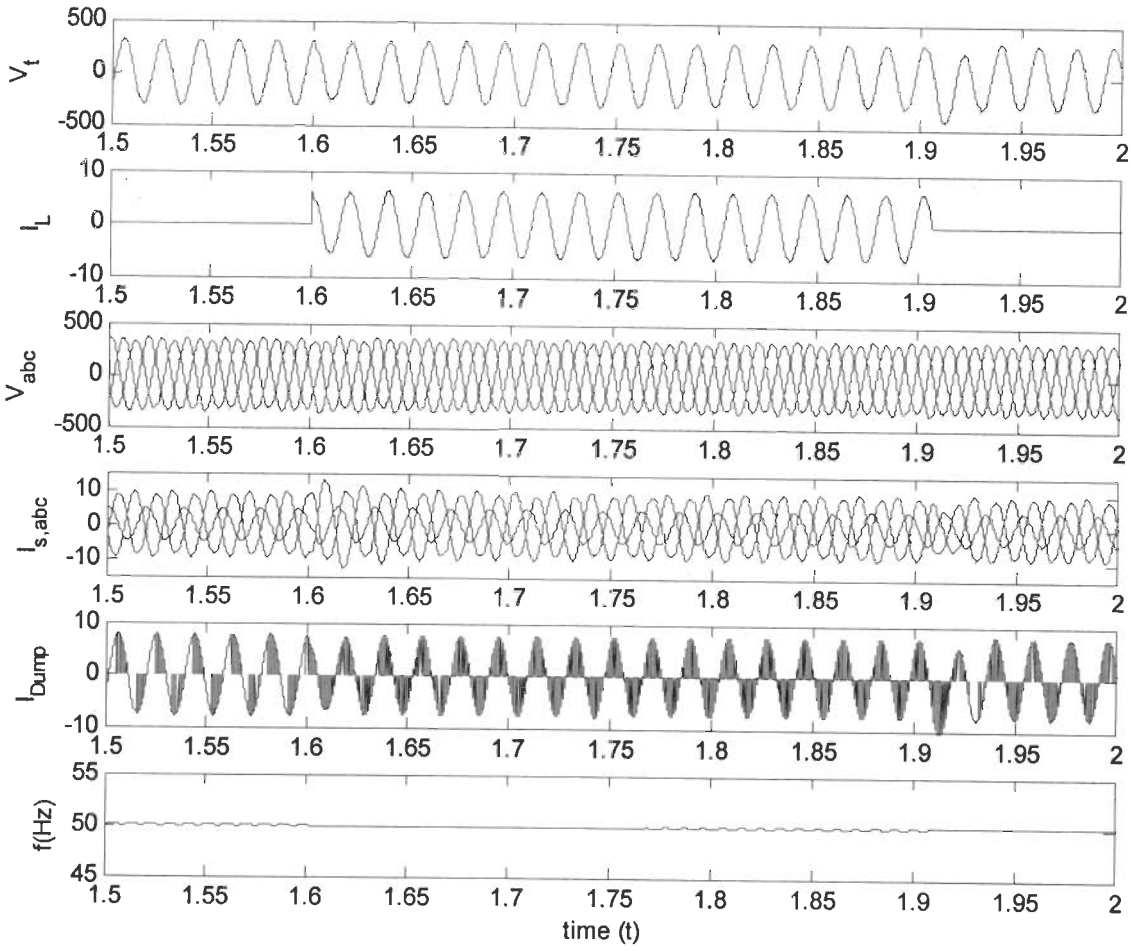


**Figure 3.21: Transient waveform of SEIG load controller system on application and removal of resistive load**

On application and removal of load the terminal voltage remains constant. On application of resistive load, main load current increases and dump load current decreases so that power transfers from dump load to consumer load and SEIG experiences constant load on it. Figure 3.24(a) Figure 3.24(b) shows the voltage and current transient waveforms on application 300 W, 0.8 pf load. Figure 3.24(c) shows the voltage and current trends on application and removal of 300 W, 0.8 pf load. On application and removal of load the terminal voltage remains constant. The load controller is a non-linear system and feeds harmonics in the SEIG. With application of resistive main load, power dissipating in dump load reduces therefore less harmonics are generated and SEIG voltages and currents are close to sinusoidal. Capacitive current also decreases due to less reactive burden. Table 3.2 shows the harmonics at different loads.

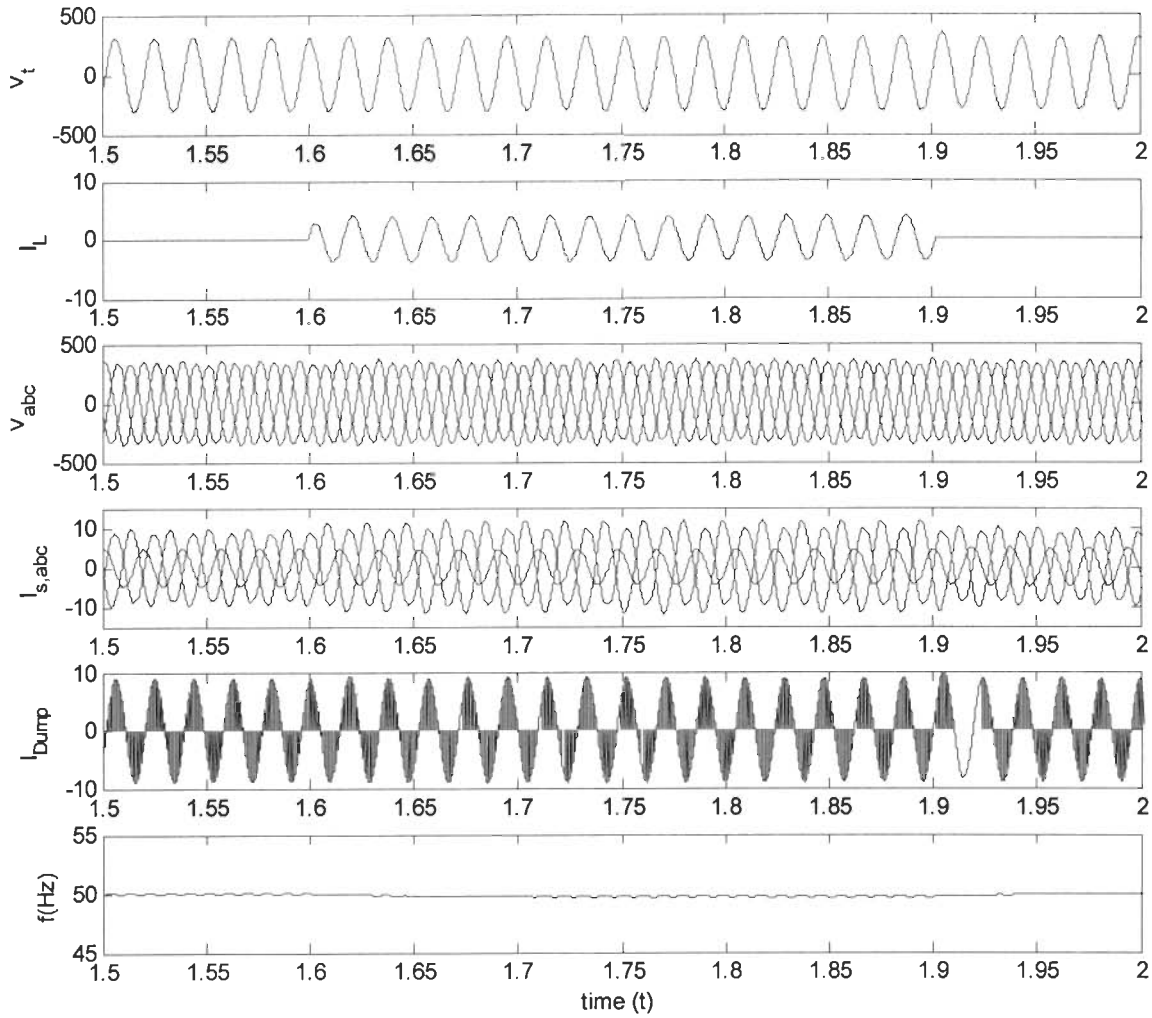


**Figure 3.22: Transient waveform of SEIG load controller system on application and removal of reactive load**

**Table 3.2 : Terminal voltage, frequency and voltage THD at different load applications**

| Main load (W) | Terminal Voltage (V) | | Frequency (Hz) | | Voltage THD (%) | |
|---|---|---|---|---|---|---|
| | Sim. | Meas. | Sim. | Meas. | Sim. | Meas. |
| 0 | 220.1 | 219.1 | 49.86 | 49.16 | 3.5 | 9.8 |
| 300 | 220.0 | 217.3 | 49.91 | 48.23 | 4.7 | 12.4 |
| 500 | 220.2 | 218.6 | 49.93 | 48.37 | 4.3 | 11.3 |
| 1000 | 220.2 | 219.3 | 49.94 | 49.20 | 4.2 | 10.4 |
| 1500 | 220.2 | 219.6 | 49.95 | 49.80 | 4.1 | 10.1 |
| 2000 | 220.3 | 220.8 | 49.98 | 49.95 | 4.0 | 9.6 |
| 200W 0.8pf lag | 219.6 | 218.6 | 50.01 | 50.03 | 5.3 | 10.6 |
| 500W 0.8pf lag | 220.1 | 219.3 | 50.35 | 51.14 | 5.1 | 9. 3 |

Sim.:- Simulated; Meas.:- Measured;

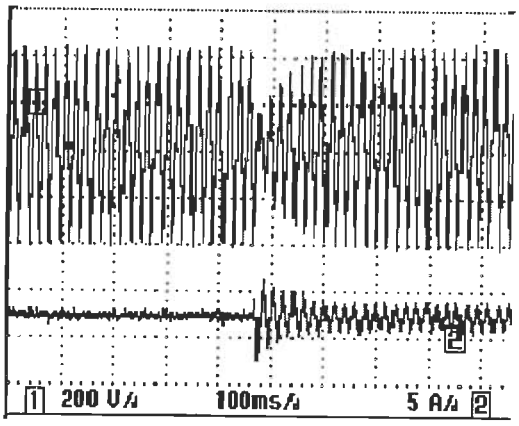


(a)

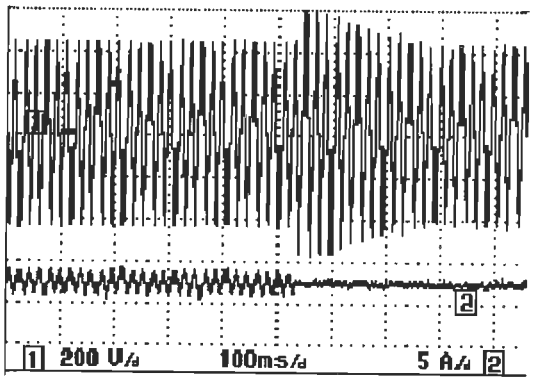


(b)

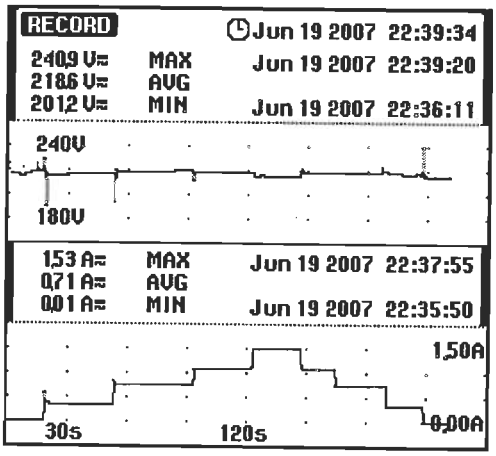


(c)

Figure 3.23: Voltage and current at (a)Application of 500 W resistive load (b)Removal of 500 W resistive load (c)Voltage and current trends at application and removal of 800 W restive load in step of 200 W

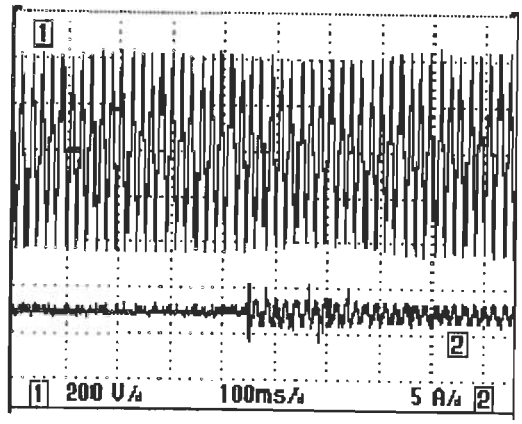


(a)

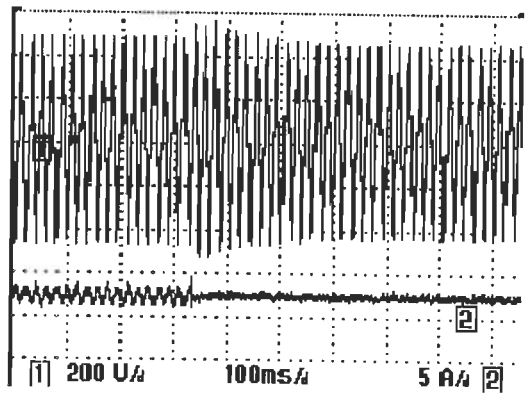


(b)

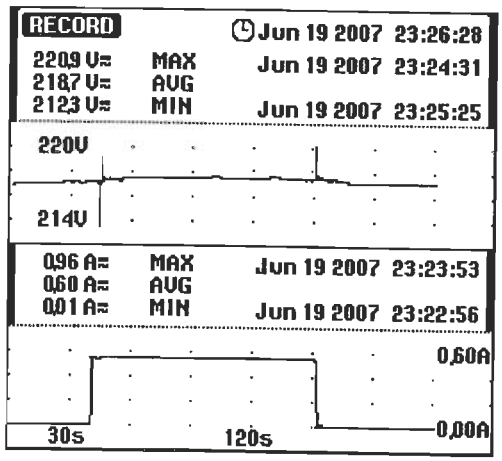


(c)

Figure 3.24: Voltage and current at (a)Application of 300 W 0.8 pf lagging load (b)Removal of 300 W 0.8 pf lagging load (c)Voltage and current trends at application and removal of 300 W 0.8 pf lagging load.

## 3.4 CONCLUSION

A comprehensive analysis for the use of three phase induction motor as a single phase self excited induction generator has been carried out. Also, a prototype model has been developed to regulate the voltage and frequency of the single phase SEIG. The two type of connection scheme have been considered for analysis namely C-2C delta connected single phase SEIG and $C_P$ –$C_S$ star connected single phase SEIG. Form the analysis and experimentation; the following conclusion are drawn.

(i) The use of three phase induction motor as a single phase SEIG is a case of extreme unbalanced operation of the machine. The analysis reveals that in C-2C connection scheme the voltage and current of the SEIG converge to balanced point at certain resistive load and fixed value of excitation capacitance.

(ii) The SEIG is operated at that point with DSP based mark space ratio controlled load controller delivers constant voltage and frequency with varying consumer loads. In spite of the change in consumer load the generator current remains balanced.

(iii) The $C_P$ –$C_S$ connection scheme has balanced voltage and phase current at no load. As the load on the machine increases they tend to become unbalanced. The phase currents are kept below the rated value by de-rating the generator operation as not to cause the temperature rise.

(iv) The developed prototype DSP based single phase SEIG-load controller for $C_P$–$C_S$ connection scheme gives constant voltage and frequency with varying consumer load.

(v) The frequency remains constant on application of resistive load. There is a slight increase in frequency on application of reactive load. The variation in frequency is found within satisfactory limits.

(vi) The simulation of both the connection scheme has been carried out on MATLAB/ Simulink environment. The simulated and experimental results are in close proximity.

# CHAPTER-4

# SINGLE PHASE IM AS SINGLE PHASE SEIG WITH LOAD CONTROLLER

## 4.1 INTRODUCTION

The use of three phase induction motor as three phase SEIG and as single phase SEIG have been discussed in previous two chapters. The SEIG has poor voltage and frequency regulation. To overcome this problem, the application of load controller has also been discussed. Further, the unbalanced single phase operation of three phase induction motor as a single phase SEIG shows that with load controller a satisfactory balanced operation with good voltage and frequency regulation can be achieved. In remote location or hilly areas where grid power is not accessible and economical, the electrical energy from local resources like micro-hydro with unregulated turbines could be a cost effective source of electrical energy. Such areas are characterized by sparsely scattered inhabitants with electrical load of single phase. The single phase power supply is preferred over three phase in order to render the distribution system simple and cost effective.

Single-phase induction motors can be used as single phase self excited induction generators for single phase power generation for the purpose of supplying smaller loads of less than 5kW. Single phase induction machine when used as a motor is an unsymmetrical machine in which two phase windings are connected to a single phase power supply. These two windings are normally unbalanced and classified as the main and auxiliary windings. The auxiliary winding is used for the starting purpose or remains in operation after the machine is started in order to improve performance. When it is used as the SEIG, it has the flexibility of using the main and/or the auxiliary windings both for excitation and loading. If only one winding is used for both excitation and loading it is called one winding induction generator. When both the windings are used for excitation and loading, it is referred as two winding induction generator. This chapter deals with the performance analysis and use of single phase two winding induction motor as the single phase SEIG and its voltage and frequency regulation with load controller.

The available literature [11, 36, 43, 86, 132, 135, 136, 142, 143, 145, 146, 147, 148, 149, 150, 156, 171, 173, 184, 187] divulge the use of two winding single phase induction motor as single phase self excited induction generator. The steady state analysis [43, 132, 135, 136, 156, 171] helps to find appropriate choice of excitation capacitance necessary in order to initiate voltage build-up and to maintain a given terminal voltage, when the SEIG is loaded.

The poor voltage and frequency regulation is the major bottleneck in SEIG application as a stand alone portable power generator. A battery supported PWM inverter based excitation and control [86, 147, 148, 149, 150] require a separate DC source for excitation and control. The voltage regulation using shunt and series connected excitation capacitor [146, 171] involve an iterative procedure to find appropriate capacitor for voltage and frequency regulation. The series connected capacitor may cause sub synchronous resonance and not suitable for dynamic loads. Electronic load controller based voltage regulation [184] has been reported in the literature. The load controller provides an effective voltage and frequency regulation by keeping load on the SEIG constant. For remote and far flung location such control scheme must be cost effective, low maintenance and reliable. This chapter is an effort to establish the steady state model and DSP based voltage and frequency regulation of single phase SEIG. The use of DSP is a cost effective, single chip and reliable implementation for load controller.

## 4.2 MATHEMATICAL MODELING

Figure 4.1 shows the connection scheme of two winding single phase self excited induction generator.

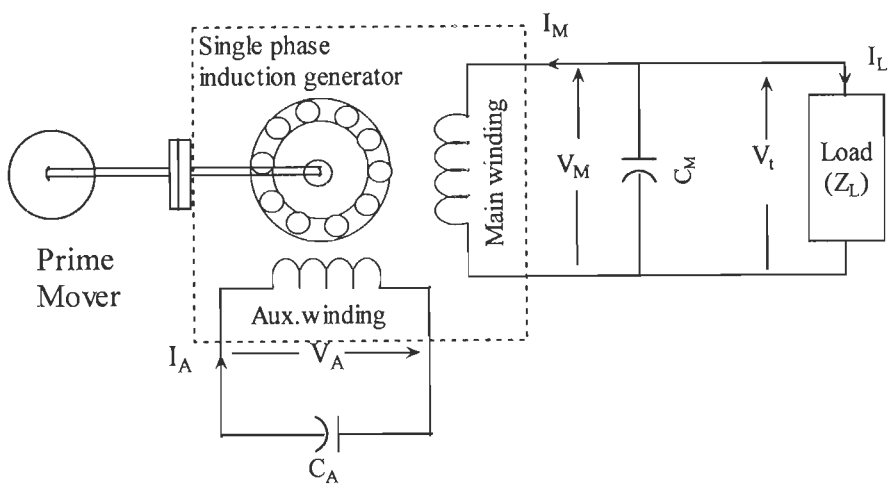


**Figure 4.1: Schematic diagram of capacitor excitation of two winding single phase self excited induction generator.**

The excitation capacitors are connected in shunt to main and auxiliary winding as shown in Figure 4.1. The load is connected across the main winding. The shunt capacitor ($C_A$) across auxiliary winding provides the excitation current for the voltage build up. The Capacitor ($C_M$) across main winding is connected in parallel with load. When the excitation capacitor ($C_A$) is connected across the auxiliary winding and load are connected to main winding, the burden of exciting the machine is taken by auxiliary winding, leaving the main winding to supply more load before reaching its heating limit. The shunt capacitor ($C_M$) is connected to regulate the terminal voltage. The Figure 4.2 shows the equivalent circuit of the generator system of a two winding single phase induction generator based on the double rotating field theory.

Applying KVL in the circuit of Figure 4.2(c)

$$I_M(Z_{1M} + Z_f + Z_{12b}) = 0 \tag{4.1}$$

where, $Z_{1M} = R_{1M} + jFX_{1M} + \dfrac{(R_L + jFX_L)\left(-\dfrac{jX_{C_M}}{F}\right)}{R_L + j\left(FX_L - \dfrac{X_{C_M}}{F}\right)}$

$$Z_f = \frac{Z_{mf} Z_{2f}}{Z_{mf} + Z_{2f}}$$

$$Z_{12b} = \frac{(Z_{1M} + Z_b) Z_{12}}{Z_{1M} + Z_b + Z_{12}}$$

$$Z_{mf} = \frac{R_c . jFX_m}{R_c + jFX_m}$$

$$Z_{2f} = \frac{R_2 F}{F - u} + jFX_2$$

$$\frac{Z_{1A}}{a^2} - Z_{12} = \frac{Z_{1M}}{2}$$

$$Z_{1A} = R_{1A} + jFX_{1A} - \frac{jX_{C_A}}{F}$$

$$Z_b = \frac{Z_{mb} Z_{2b}}{Z_{mb} + Z_{2b}}$$

$$Z_{mb} = \frac{R_c . jFX_m}{R_c + jFX_m}$$

$$Z_{2b} = \frac{R_2 F}{F + u} + jFX_2$$

$$V_A = I_A\left(-j\frac{X_{C_A}}{F}\right)$$

$$P_O = I_L^2 R_L$$

Based on the mathematical formulation, the values of shunt capacitors are selected for rated voltage at rated load.

## 4.3 PERFORMANCE ANALYSIS

The performance study has been carried out for single phase 1.5 kW, 190/240 V, 9.5 A, 50Hz, 1440 rpm squirrel cage induction machine as a single phase self-excited induction generator. The SEIG is driven by 220 V, 20 A, 5 HP, 1500 rpm shunt wound DC machine used as a prime mover. From the steady state model of the generator, it has been found that to generate 1000 W at 220 V and rated speed, 40 μF and 36 μF capacitors of 400 V are connected as $C_M$ and $C_A$ across the main and auxiliary winding. The parameters of the single phase induction machine and its magnetization characteristic obtained from open circuit, locked rotor, DC resistance and synchronous speed test [135] are summarized in Appendix A. The single phase SEIG performance with load is shown in Figure 4.3(a) and Figure 4.3(b). Figure 4.3(a) shows the variation of auxiliary winding voltage ($V_A$) and main winding voltage ($V_M$) or terminal voltage ($V_t$) with increasing load. As the load on SEIG increases the drop in terminal voltage is observed. Figure 4.3(b) shows the variation in main winding and auxiliary winding current with increase in load. Since the single phase SEIG is an unsymmetrical machine, the system observes small vibration and noise which may be attributed to interaction of forward and backward fields in the machine due to unbalanced winding currents. It is interesting to observe that machine can deliver the power output up to 1.5 times of its rated capacity without exceeding the current limit in main winding. Further, in most of the single phase commercially available motors, auxiliary winding is made up of thin wire with more number of turns. Its basic aim is to provide split phase. During running it may or may not be cutoff. It is preferable to retain the auxiliary winding in the circuit for efficient operation of single phase induction motor. However, for operation of single phase induction motor as a SEIG, both the windings are excited simultaneously. The current limit is then decided by the current rating of auxiliary winding. It is necessary to remove centrifugal or SINPAC switch before motor to be operated as SEIG.

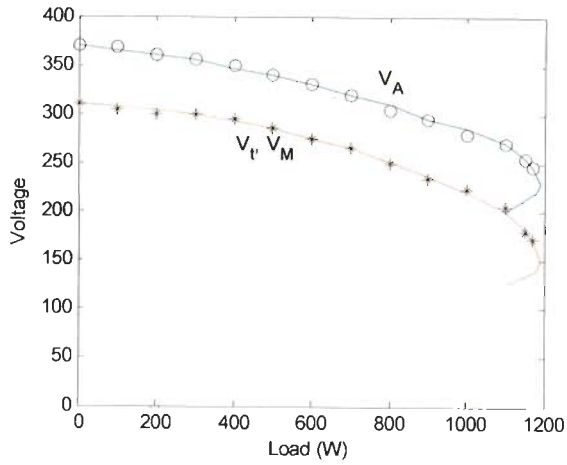


**Figure 4.3(a): Variation of main winding and auxiliary winding voltage with load**

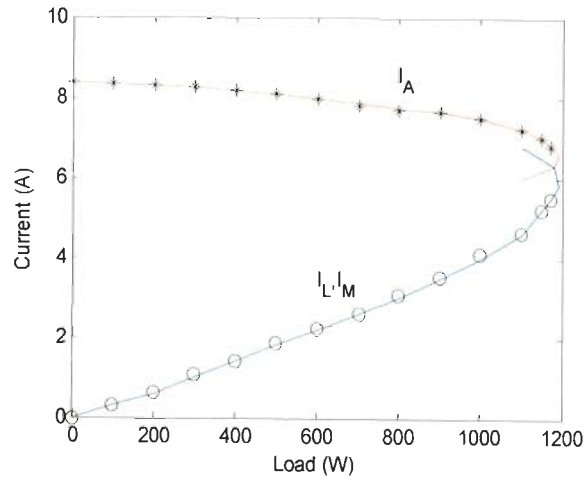


**Figure 4.3(b): Variation of main winding or load current and auxiliary winding current with load**

## 4.4 SINGLE PHASE SEIG WITH LOAD CONTROLLER

The performance analysis shows that the single phase SEIG observe poor voltage regulation at fixed capacitor excitation. The variation in voltage is due to variable reactive VAR demand with variation in load. The single phase SEIG may deliver constant voltage and frequency if the load is maintained constant at its terminals. A load controller connected in parallel with consumer load keeps the load constant through a dump load. Now, SEIG feeds two loads in parallel such that the total power $P_{out} = P_c + P_d$ is constant, Where, $P_{out}$ is the generated power of the generator (which must be kept constant), $P_c$ is the consumer load power, and $P_d$ is the dump load power. A schematic diagram of the SEIG-Load controller system is shown in Figure 4.4. It consists of single phase two winding (main and auxiliary) squirrel cage induction motor (working as SEIG) driven by a

constant power prime mover. The excitation capacitors are connected at the terminals of auxiliary ($C_A$ ) and main winding ($C_M$ ) as shown in Figure 4.4, which have a fixed value to result in rated terminal voltage at rated load. Consumer load and load controller are connected in parallel at generator terminals. The load controller consist of an uncontrolled rectifier, a filtering capacitor ($C_f$), IGBT based chopper and a series resistive dump load ($R_D$). The uncontrolled rectifier converts the SEIG AC terminal voltage to DC. The output ripples are filtered by filter capacitor. An IGBT is used as a chopper switch. When gate pulse to IGBT is high, the current flows through the dump load and the power is consumed. The pulse width or duty cycle of chopper is decided by the difference of power generation to consumer load.

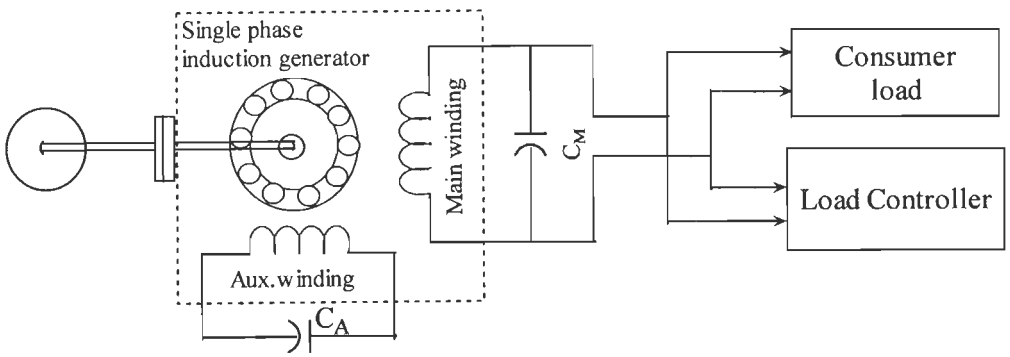


**Figure 4.4(a): Schematic diagram single phase SEIG-load controller system**

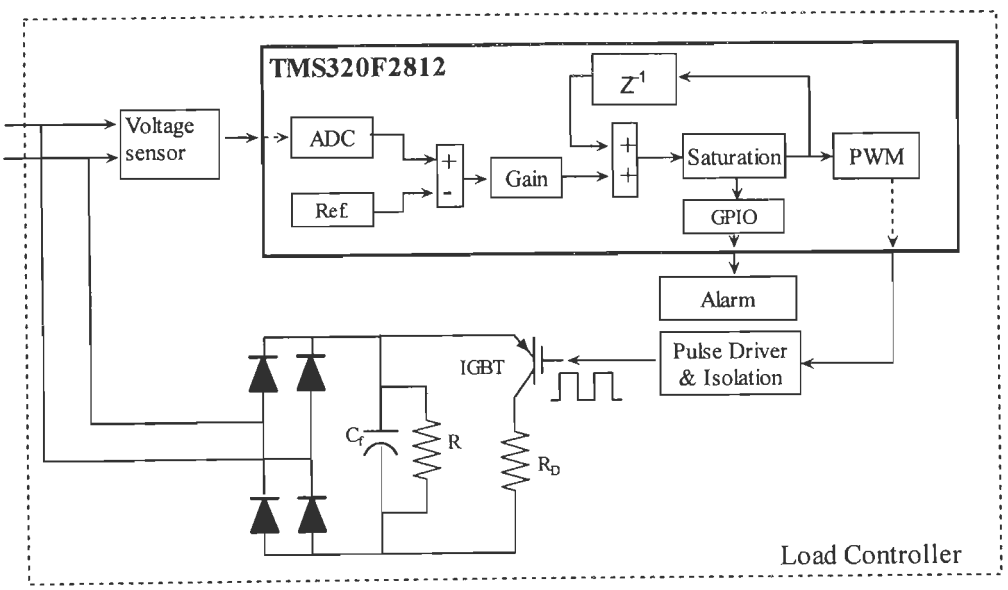


**Figure 4.4(b): Schematic diagram DSP based load controller for single phase SEIG.**

The excitation capacitors are connected in shunt to main and auxiliary winding as shown in Figure 4.1. The load is connected across the main winding. The shunt capacitor ($C_A$) across auxiliary winding provides the excitation current for the voltage build up. The Capacitor ($C_M$) across main winding is connected in parallel with load. When the excitation capacitor ($C_A$) is connected across the auxiliary winding and load are connected to main winding, the burden of exciting the machine is taken by auxiliary winding, leaving the main winding to supply more load before reaching its heating limit. The shunt capacitor ($C_M$) is connected to regulate the terminal voltage. The Figure 4.2 shows the equivalent circuit of the generator system of a two winding single phase induction generator based on the double rotating field theory.

Applying KVL in the circuit of Figure 4.2(c)

$$I_M(Z_{1M} + Z_f + Z_{12b}) = 0 \tag{4.1}$$

where, $Z_{1M} = R_{1M} + jFX_{1M} + \dfrac{(R_L + jFX_L)\left(-\dfrac{jX_{C_M}}{F}\right)}{R_L + j\left(FX_L - \dfrac{X_{C_M}}{F}\right)}$

$$Z_f = \frac{Z_{mf} Z_{2f}}{Z_{mf} + Z_{2f}}$$

$$Z_{12b} = \frac{(Z_{1M} + Z_b)Z_{12}}{Z_{1M} + Z_b + Z_{12}}$$

$$Z_{mf} = \frac{R_c . jFX_m}{R_c + jFX_m}$$

$$Z_{2f} = \frac{R_2 F}{F - u} + jFX_2$$

$$\frac{Z_{1A}}{a^2} - Z_{12} = \frac{Z_{1M}}{2}$$

$$Z_{1A} = R_{1A} + jFX_{1A} - \frac{jX_{C_A}}{F}$$

$$Z_b = \frac{Z_{mb} Z_{2b}}{Z_{mb} + Z_{2b}}$$

$$Z_{mb} = \frac{R_c . jFX_m}{R_c + jFX_m}$$

$$Z_{2b} = \frac{R_2 F}{F + u} + jFX_2$$

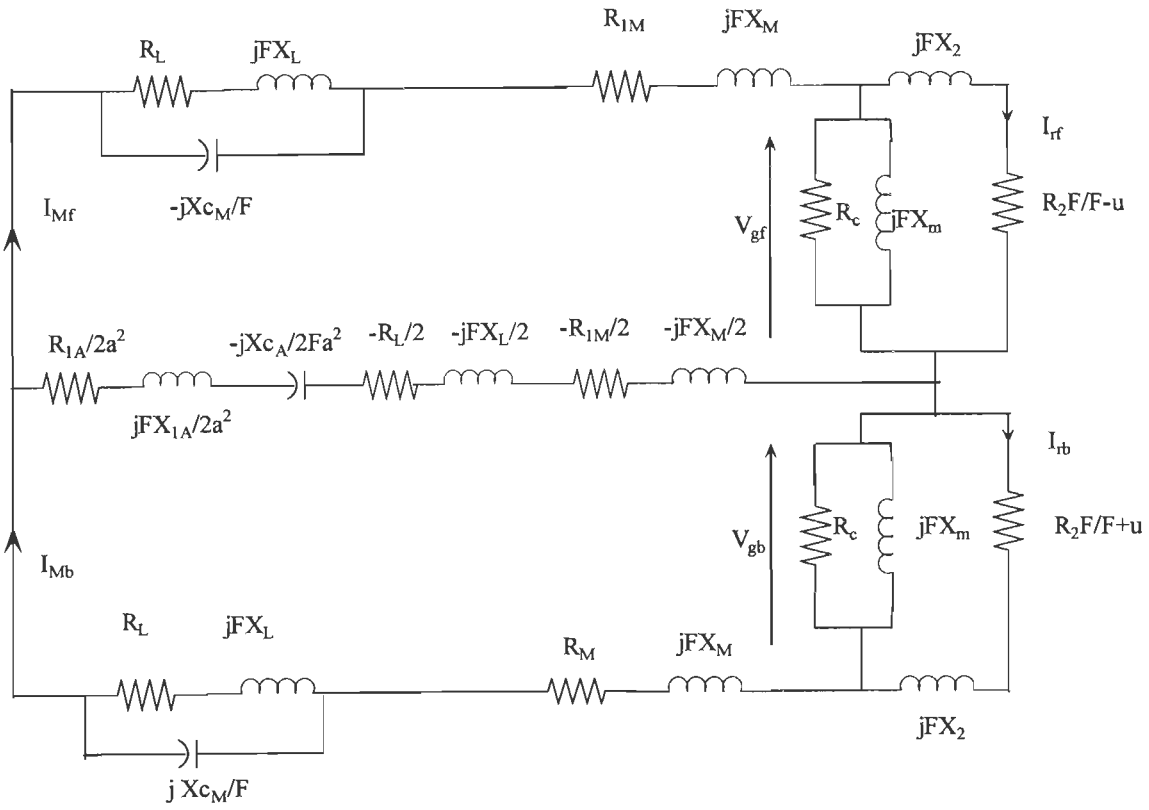


(a)

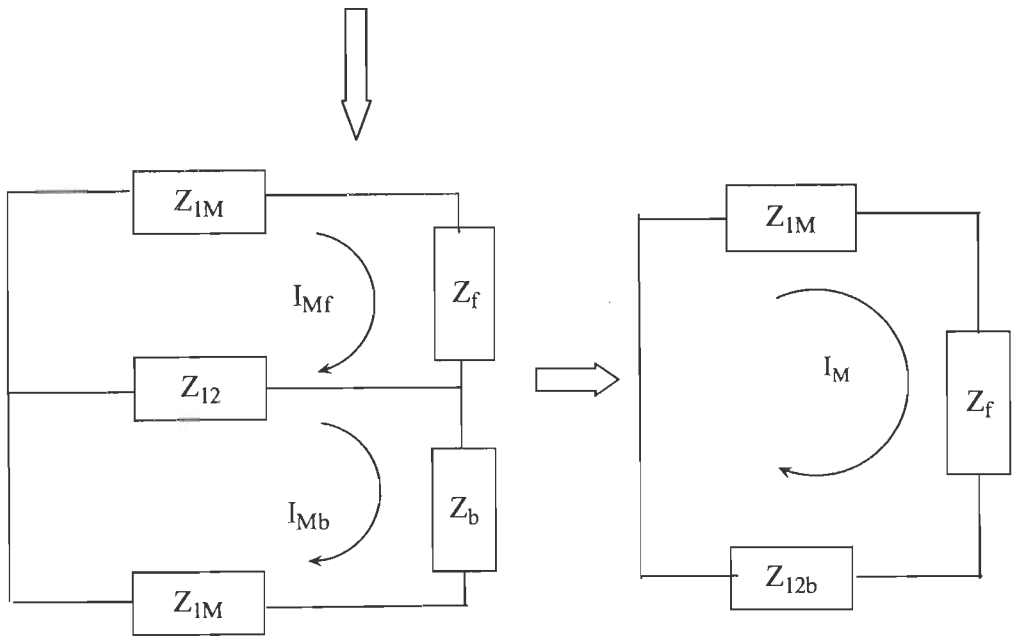


(b) (c)

**Figure 4.2: Equivalent circuit of two winding single phase self excited induction generator**

Under Steady state, $I_M$ can not be zero and hence from Equation (4.1) we have

$$Z_{1M} + Z_f + Z_{12b} = 0 \tag{4.2}$$

For performance analysis under steady-state with fixed values of capacitances, $X_m$ and F are the two unknowns in equation (4.2) and $(Z_{1M} + Z_f + Z_{12b})$ can be represented in functional form as:

$$f(X_m, F) = \left| Z_{1M} + Z_f + Z_{12b} \right| \tag{4.3}$$

For solving the equation (4.2) to determine the variables $X_m$ and F by minimization technique, the function $f(X_m, F)$ is taken as an objective function and the optimization problem is stated as:

Minimize $f(X_m, F)$

such that, $X_{ml} \leq X_m \leq X_{mu}$ and $F_l \leq F \leq F_u$

where subscripts 'l' and 'u' denote lower and upper limits imposed on the variables respectively. This is minimized by sequential unconstrained minimization technique (SUMT) in conjunction with Rosenbrock's method of rotating coordinates. The function must converge to zero and the value of tolerance to check the convergence is taken quite small, say equal to 0.0001.

Once $V_{gf}/F$, $X_m$ and F are known, the quantities that describe the performance characteristics of the system are computed as

$$I_{Mf} = \frac{V_{gf}}{Z_f}$$

$$I_{Mb} = \frac{I_{Mf} Z_{12}}{Z_{12} + Z_{1M} + Z_b}$$

$$I_M = I_{Mf} + I_{Mb}$$

$$I_A = \frac{j(I_{Mf} - I_{Mb})}{a}$$

$$I_L = I_M \frac{\left( -\frac{jX_{C_M}}{F} \right)}{\left( R_L + j(FX_L - \frac{X_{C_M}}{F}) \right)}$$

$$V_M = V_t = I_L (R_L + jX_L)$$

$$V_A = I_A\left(-j\frac{X_{C_A}}{F}\right)$$

$$P_O = I_L^2 R_L$$

Based on the mathematical formulation, the values of shunt capacitors are selected for rated voltage at rated load.

## 4.3 PERFORMANCE ANALYSIS

The performance study has been carried out for single phase 1.5 kW, 190/240 V, 9.5 A, 50Hz, 1440 rpm squirrel cage induction machine as a single phase self-excited induction generator. The SEIG is driven by 220 V, 20 A, 5 HP, 1500 rpm shunt wound DC machine used as a prime mover. From the steady state model of the generator, it has been found that to generate 1000 W at 220 V and rated speed, 40 μF and 36 μF capacitors of 400 V are connected as $C_M$ and $C_A$ across the main and auxiliary winding. The parameters of the single phase induction machine and its magnetization characteristic obtained from open circuit, locked rotor, DC resistance and synchronous speed test [135] are summarized in Appendix A. The single phase SEIG performance with load is shown in Figure 4.3(a) and Figure 4.3(b). Figure 4.3(a) shows the variation of auxiliary winding voltage ($V_A$) and main winding voltage ($V_M$) or terminal voltage ($V_t$) with increasing load. As the load on SEIG increases the drop in terminal voltage is observed. Figure 4.3(b) shows the variation in main winding and auxiliary winding current with increase in load. Since the single phase SEIG is an unsymmetrical machine, the system observes small vibration and noise which may be attributed to interaction of forward and backward fields in the machine due to unbalanced winding currents. It is interesting to observe that machine can deliver the power output up to 1.5 times of its rated capacity without exceeding the current limit in main winding. Further, in most of the single phase commercially available motors, auxiliary winding is made up of thin wire with more number of turns. Its basic aim is to provide split phase. During running it may or may not be cutoff. It is preferable to retain the auxiliary winding in the circuit for efficient operation of single phase induction motor. However, for operation of single phase induction motor as a SEIG, both the windings are excited simultaneously. The current limit is then decided by the current rating of auxiliary winding. It is necessary to remove centrifugal or SINPAC switch before motor to be operated as SEIG.

The output power of the SEIG is kept constant by load controller. The voltage amplitude is determined and compared with reference voltage, which is taken as proportional to the rated terminal voltage of the SEIG. The error is scaled (gain) and algebraically added to previous sample time PWM reference level. As the desired terminal voltage is achieved the error signal becomes zero and PWM reference holds its level. The pulse width references are fed to PWM generator. The PWM generator block have self carrier triangular wave. The carrier frequency is selected according to static switching device. The pulse output is then given to IGBT chopper through an opto isolation and pulse driver circuit.

## 4.5 DIGITAL SIMULATION

Digital simulation of proposed load controller with single phase two winding SEIG system has been carried out with MATLAB Simulink and Power System Blockset. A 1.5 kW, 220 volts, two winding, single phase, 50 Hz, asynchronous machine is used as the SEIG. Figure 4.5 shows the schematic MATLAB model of the single phase SEIG-load controller system. The block rotor test and no load test gives the machine parameters which are summarized in Appendix-A. The dropping torque- speed characteristics of prime mover is given as $T_{shaft} = (K_1 - K_2 w_r)$ where, $K_1$ and $K_2$ are the prime mover constants given in Appendix-A. The excitation capacitors are connected at the terminals of auxiliary winding ($C_A$ ) and main winding ($C_M$ ) of 36 μF and 40 μF respectively. The output is connected with a consumer load of resistive and reactive nature and load controller in parallel. The amplitude is compared with the reference and processed through the controller. The output of the controller is compared with symmetrical triangular wave and through a relational operator to obtain a pulse of suitable duration (width). This pulse is given to gate of the IGBT chopper switch. A universal bridge is used as diode rectifier and filtering capacitor is added for smoothening and filtering. The dump load resistance and filtering capacitance values are selected as per calculation discussed in section 2.3.4. Figure 4.6 shows the voltage build up and steady state ($V_t$), load current ($I_L$) and frequency (Hz). At time t = 1 seconds resistive load of 1000 W in step of 500 W and 250x2 W have been applied. With the application of load, the terminal voltage and frequency remains constant.

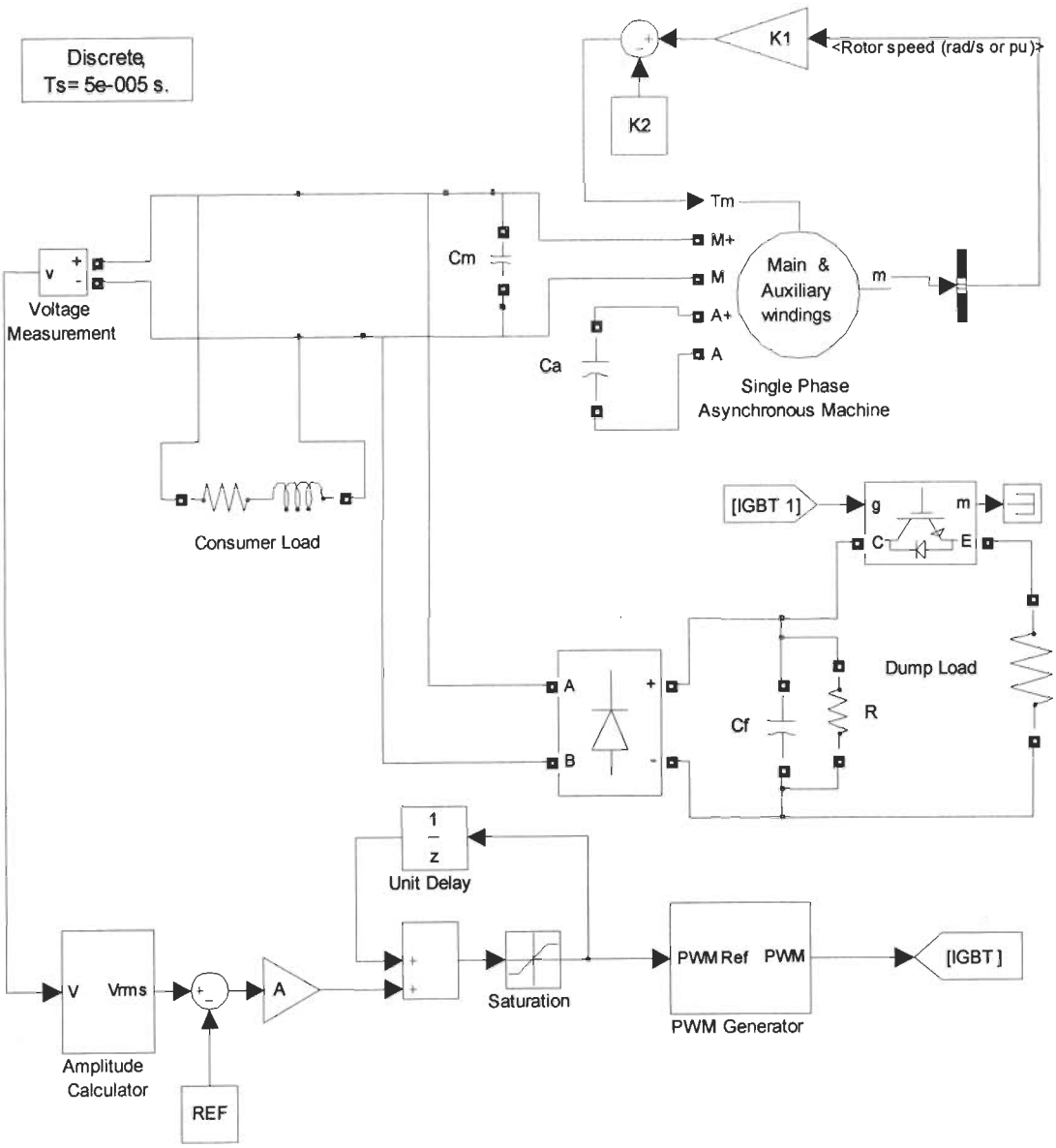


**Figure 4.5: Schematic MATLAB model of the SEIG-load controller system**

Figure 4.7 and Figure 4.8 shows the transient waveform on application of 500W resistive and 400 W, 0.8 lagging power factor reactive load respectively. Waveforms from top to bottom are terminal voltage ($V_t$), load current ($I_L$), dump load current ($I_{Dump}$), SEIG main winding current ($I_{Main}$), voltage across auxiliary winding ($V_{Aux}$), auxiliary winding current ($I_{Aux}$) and frequency (f) respectively. The simulated transient waveform shows that on application of resistive and reactive load, the terminal voltage and frequency remains constant

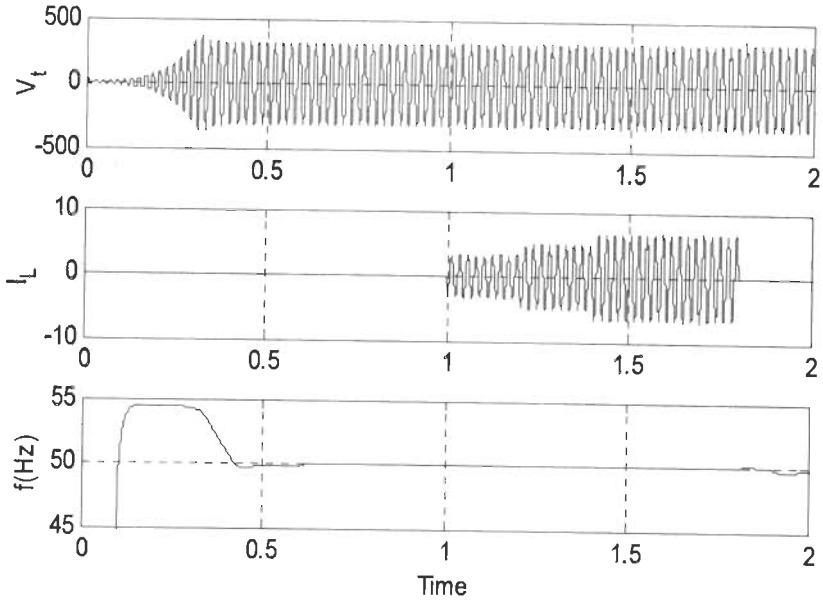


**Figure 4.6: Voltage build up and application of main load in step.**

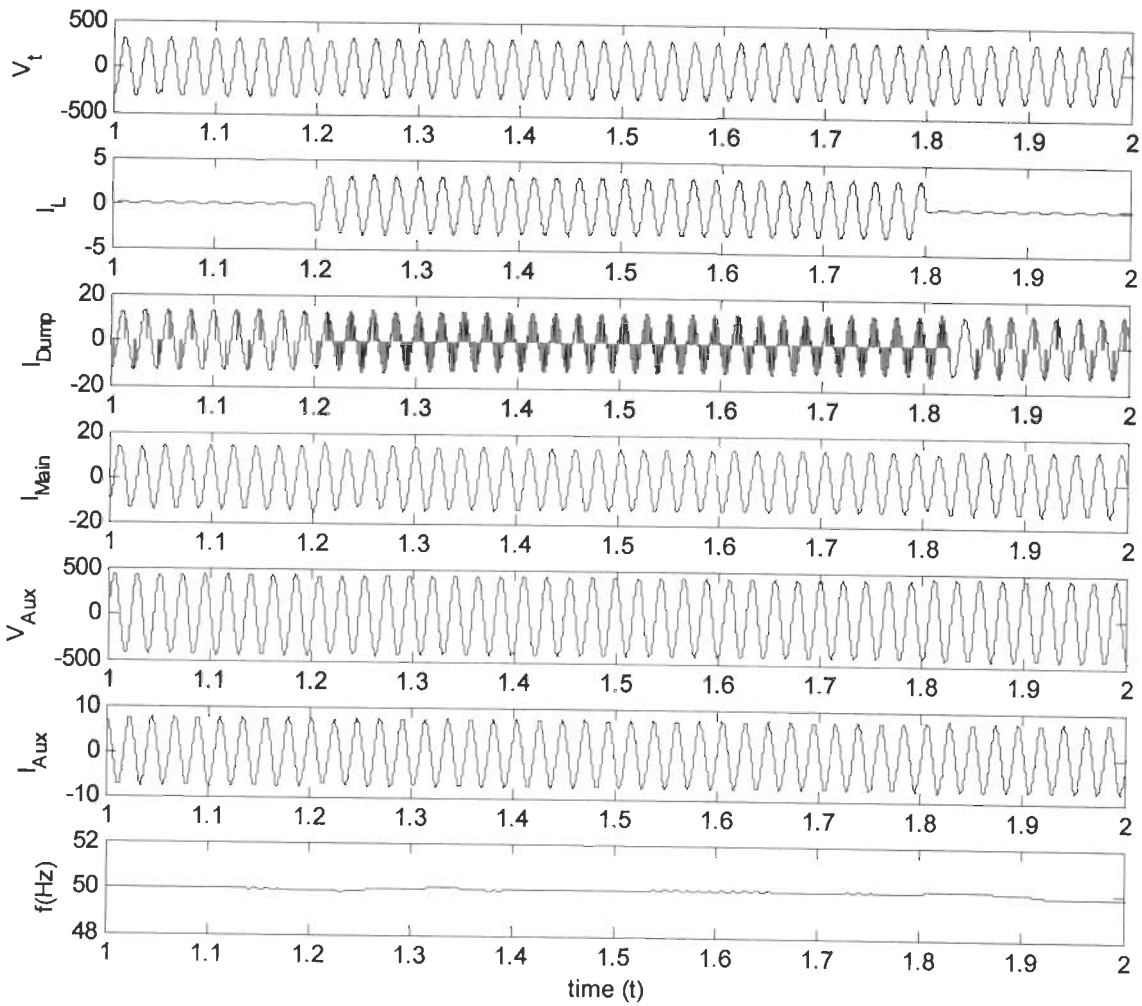


**Figure 4.7: Transient waveform SEIG-load controller system on application of resistive load**

## 4.6 EXPERIMENTATION AND RESULTS

A prototype DSP based load controller with TMS320F2812 processor has been developed and tested in laboratory under various operating conditions. A single phase 1.5 kW, 190/240 V, 9.5 A, 50Hz, 1440 rpm squirrel cage induction machine is used as a single phase self-excited induction generator. The SEIG is driven by 220 V, 20 A, 5 HP, 1500 rpm shunt wound DC machine used as a prime mover. To generate 1000 W at 220 V and rated speed, 40 μF and 36 μF capacitors of 400 V are connected as $C_M$ and $C_A$ across the main winding and auxiliary winding terminals of the SEIG. The test results are carried out with resistive load, 0.8 power factor reactive load and 750 W, 220/230 V, 5.2 A, 50 Hz, 1425 rpm single phase induction motor as dynamic load at developed SEIG-load controller system. The single phase induction machine has start capacitor of 125 μF, 275 V and run capacitor of 10 μF, 400 V. A resistive load of 50 ohm is connected as dump load.

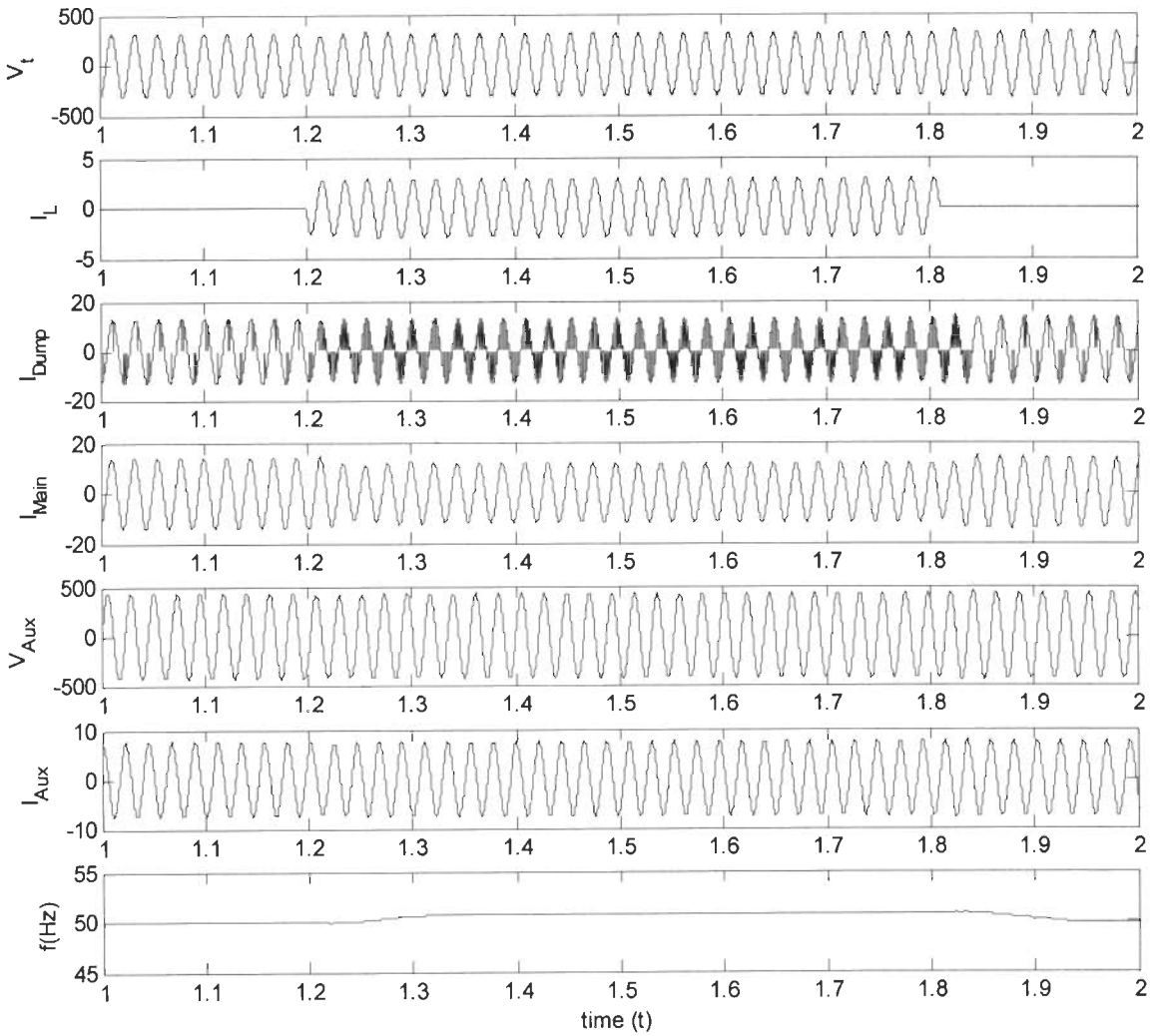


**Figure 4.8: Transient waveform SEIG-load controller system on application of reactive load**

The terminal voltage for feedback is sensed with voltage transducer to achieve a DC value proportional to SEIG output terminal voltage. The voltage transducer converts and linearizes the input AC terminal voltage to output DC voltage. This voltage is given to ADC input of the DSP TMS320F2812. The TMS320F2812 DSP has 16 ADC input channels with an input range of 0-3 Volt. The output values are in the range of 0 to 4095 as the TMS320F2812 DSP ADC is 12-bit converter. The sensed voltage is compared with a reference, which is taken as proportional to the rated terminal voltage of the SEIG and may be altered as and when required. The error is scaled (gain) and algebraically added to previous sample time PWM reference level. As the desired terminal voltage is achieved the error signal becomes zero and PWM reference holds its level. The pulse width references are fed to PWM of DSP. The PWM block have self carrier triangular wave. The carrier frequency is selected according to static switching device. The TMS320F2812 DSP has 6x2 high resolution PWM outputs. The PWM output is then given to IGBT chopper through an opto isolation and pulse driver circuit.

Figure 4.9(a) and 4.9(b) shows the voltage and current transient waveforms of DSP based SEIG-load controller system on application and removal of 500 W resistive load. In Figure 4.9(c), voltage and current trends are shown on successive application and removal of 800 W resistive loads in steps of 200 W. The terminal voltage remains constant at application and removal of resistive load. On application of resistive load, main load current increases and dump load current decreases so that power transfers from dump load to consumer load and SEIG experiences constant load on it. The load controller is a non-linear system and feeds the harmonics in the SEIG. With application of resistive main load, power dissipating in dump load reduces therefore less harmonics are generated and SEIG voltages and currents are close to sinusoidal. Capacitive current also decreases due to less reactive burden.

Figure 4.10(a) and 4.10(b) shows the voltage and current transient waveforms on application and removal of 400 W, 0.8 pf load. Fig 4.10(c) shows the voltage and current trends on application and removal of 400 W 0.8 pf load. On application and removal of load the terminal voltage remains constant. When an inductive load is connected to the SEIG, the voltage will decrease and the load controller responds by reducing the dump load. The reduced load causes an almost instantaneous increase in frequency due to reduced slip and an additional gradual increase in frequency due to rising turbine speed.

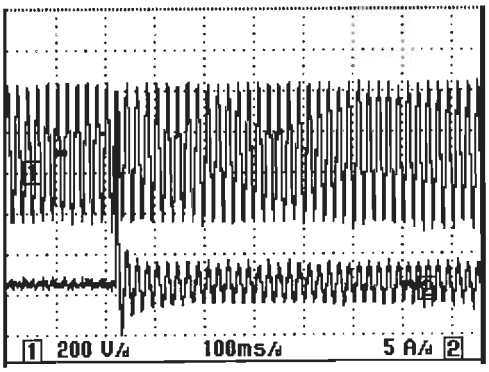


(a)

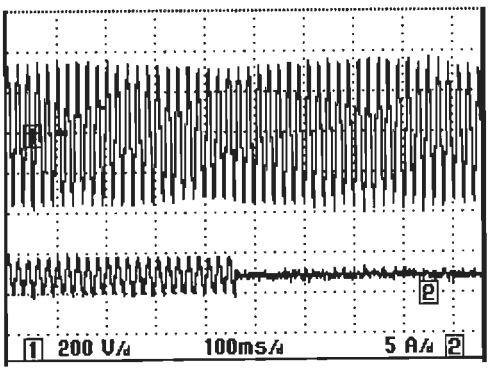


(b)

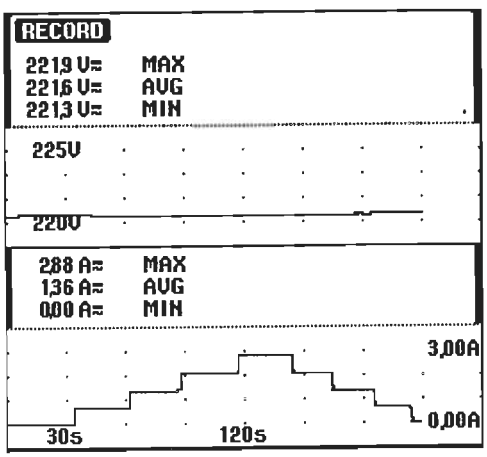


(c)

**Figure 4.9: Voltage and current waveforms at (a) application of 500 W resistive load (b) removal of 500 W resistive load (c) voltage and current trends at successive application and removal of 800 W resistive load in step of 200 W.**

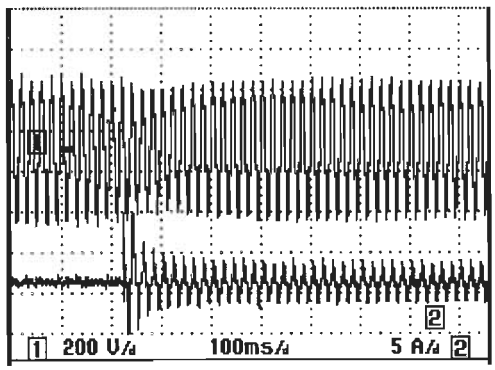


(a)

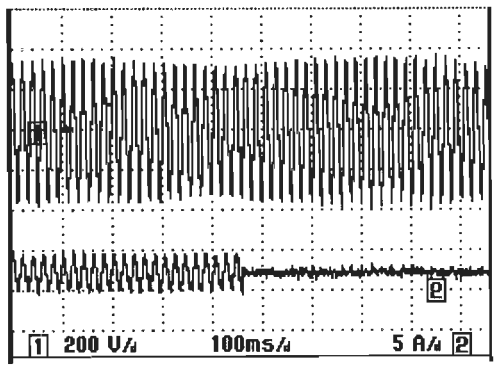


(b)

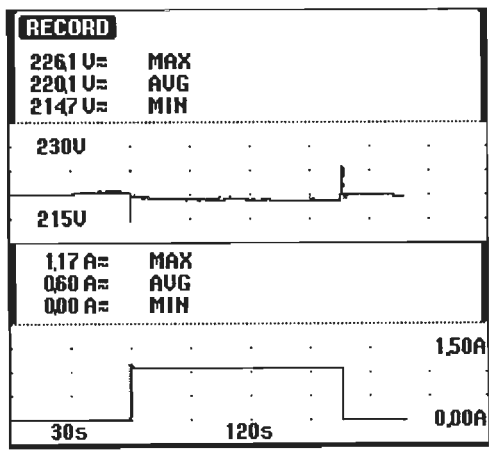


(c)

**Figure 4.10: Voltage and current waveforms at (a) application of 400 W 0.8 lagging pf load (b) removal of 400 W 0.8 lagging pf load (c) voltage and current trends at application and removal of 400 W 0.8 lagging pf load**

The increase in frequency would depend on power factor of the load and the degree of saturation of the SEIG. As modern induction machines tend to be highly saturated, the frequency regulation with variation in load power factor is quite small. A small increase in frequency results in a significant reduction in magnetizing current. In addition, extra VARs are produced by the excitation capacitors due to reduced impedance.

Figure 4.11(a) and 4.11(b) show the transient waveforms of DSP based SEIG-load controller system at starting, running and removal of single phase 1 HP induction motor at no load. An approximate 15% change in voltage is observed for a few cycles and then it recovers very close to rated value. Simultaneously, there is a small increase in frequency to compensate for lagging power factor load due to decrease in magnetizing current and hence generator current. Fig 4.11(c) shows the voltage and current trends on starting, running and removal of single phase induction motor.

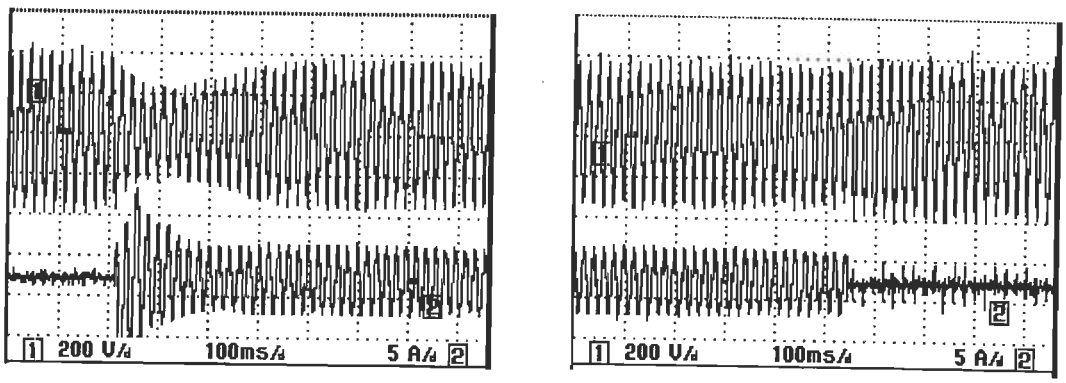


(a) (b)

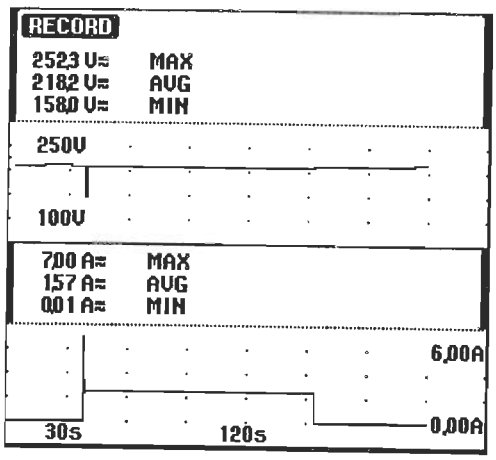


(c)

**Fig: 4.11. Voltage and current waveforms at (a) application of 1 HP single phase IM load (b) removal of 1 HP single phase IM load (c) voltage and current trends at application and removal of 1HP single phase IM load**

The load controller is a non-linear system and feeds harmonics in the SEIG. Table 4.1 summarizes the main load, dump load, terminal voltage, frequency variations, voltage THD and current THD of main load, dump load and generator at various stages. The good voltage and frequency regulation is observed. There is a slight decrease in terminal voltage as the voltage THD in the system increases. A slight increment in frequency is observed for loads of lagging power factor. An increase in voltage and current THD is observed for reactive loads on SEIG.

**Table 4.1 Terminal voltage, frequency, voltage THD and current THD at different load application**

| Main Load | Voltage (V) | | Frequency (Hz) | | Voltage THD (%) | | Current THD(%) | | | | | |
|---|---|---|---|---|---|---|---|---|---|---|---|---|
| | | | | | | | Main load | | Load controller | | Gen. main wdg. | |
| | Sim | Meas | Sim | Meas | Sim | Meas | Sim | Meas | Sim | Meas | Sim | Meas |
| 0 | 220.2 | 221.4 | 50.1 | 50.1 | 2.4 | 3.4 | - | - | 2.2 | 3.2 | 2.8 | 4.8 |
| 200 | 219.6 | 218.1 | 50.0 | 49.8 | 3.4 | 4.6 | 3.1 | 5.0 | 8.1 | 19.1 | 8.3 | 12.4 |
| 400 | 219.8 | 220.2 | 50.0 | 49.9 | 3.2 | 4.2 | 2.7 | 4.5 | 16.3 | 22.7 | 7.4 | 11.1 |
| 600 | 220.1 | 220.0 | 50.0 | 49.9 | 3.1 | 3.8 | 2.5 | 4.4 | 22.5 | 34.3 | 6.4 | 10.0 |
| 800 | 220.1 | 219.8 | 50.0 | 49.9 | 2.6 | 3.6 | 2.4 | 4.4 | 31.7 | 61.1 | 6.2 | 10.0 |
| 1000 | 220.0 | 221.9 | 50.0 | 50.1 | 2.5 | 3.5 | 2.1 | 4.1 | 46.5 | 75.0 | 3.2 | 4.7 |
| 200W 0.8pf lag | 219.2 | 218.6 | 50.5 | 50.8 | 4.5 | 5.7 | 12.1 | 23.9 | 17.1 | 37.9 | 6.8 | 12.6 |
| 300W 0.8pf lag | 218.8 | 216.4 | 50.8 | 51.0 | 6.2 | 7.9 | 15.2 | 27.1 | 32.7 | 77.0 | 11.4 | 29.5 |
| 400W 0.8pf lag | 218.2 | 215.5 | 51.1 | 51.7 | 8.1 | 15.0 | 17.5 | 31.5 | 44.2 | 80.9 | 17.3 | 34.7 |
| 1 HP IM at no load | 218.1 | 215.1 | 50.6 | 50.7 | 4.1 | 4.4 | 5.5 | 7.5 | 41.6 | 80.6 | 15.5 | 35.2 |

Sim:- Simulated; Meas:- Measured

## 4.7 CONCLUSION

A comprehensive analysis of single phase two winding induction motor working as single phase self excited induction generator has been carried out. A DSP based load controller has been designed, developed and implemented for single phase two winding induction motor working as a single phase self excited induction generator. The developed load controller acts as the voltage and frequency regulator for the SEIG. The transient analysis of SEIG load controller system has been carried out for resistive, reactive and dynamic load.

From the analysis, simulation and experimentation, the following conclusions are drawn.

(i) The single phase two winding induction motor can be used as a single phase self excited induction generator for feeding loads up to 5kW in stand alone mode. The terminal voltage reduces with the increase in load.

(ii) The single phase SEIG-load controller system delivers constant voltage and frequency with variable consumer load and fixed capacitor excitation by keeping the load on SEIG constant.

(iii) The terminal voltage remains constant on application and removal of resistive and reactive load. A voltage dip for a few cycles is observed for dynamic load. After few cycle it recovers to rated value.

(iv) The frequency remains constant on application of resistive load application. There is a slight increase in frequency on application of reactive load. The variation in frequency is found within satisfactory limits.

(v) The load controller is a non-linear system and feeds harmonics in the SEIG system. The increase in main load reduces the power to be dissipated in dump load and hence duty cycle of chopper switch decreases which increases the THD in dump load system. The THD of dump load system after passing through filtering capacitor, affect very little to main load. The total harmonic distortion is under satisfactory limits.

(vi) The simulated and the experimental results are in close agreement indicating the effectiveness and accuracy of the developed model.

# CHAPTER-5

# SEIG WITH AC CHOPPER CONTROLLED LOAD CONTROLLER

## 5.1 INTRODUCTION

The economical implementation of digital systems from a hardware complexity standpoint, with the goal of minimizing the computational work load have always been appealing research topic. In recent years self excited induction generators have been identified as a suitable source of power modulator in mini/micro-hydro and wind power stations, due to their reduced unit costs, brushless rotor construction, ruggedness and ease of maintenance. The use of conventional induction machine as a self-excited induction generator (SEIG) for low power applications have been discussed in previous chapters. The induction machine works as a SEIG, if a suitable capacitor bank is connected across its stator terminals and its rotor is driven at a suitable speed by an external prime mover. The induced voltage and its frequency in the winding will increase up and stabilized to a level governed by the magnetic saturation in the machine. The SEIG have good dynamic response, self protection against faults and it can generate power at varying speed. The main disadvantage of these generators in stand-alone operation is the poor voltage and frequency regulation. The inherent poor voltage and frequency regulation in SEIG are due to the difference between the reactive power supplied by the excitation capacitors and that demanded by the load and the machine. This is a bottleneck of its application in stand alone mode.

The generated voltage depends upon the speed, capacitance, load current and power factor of the load. The SEIG can be used to generate constant voltage and frequency if the load is maintained constant at its terminals. Under such operation, SEIG requires fixed capacitance for excitation resulting in a fixed-point operation. For this purpose, a suitable control scheme is to be developed such that the load on the SEIG remains constant despite the change in the consumer load. The SEIG with such control scheme should be cost effective and provide quality power supply with minimum harmonics. In the previous chapters, the electrical load is maintained constant at SEIG

terminals through a mark space ratio controlled load controller. The load controller keeps the total electrical load constant with variable consumer load through a dump load. The power dissipated in dump load is governed by the difference of power generated to consumer load. The load controller with uncontrolled rectifier and series connected chopper switch with mark space ratio chopper control gives unity power factor operation and it requires only one dump load. Such a load controller is nonlinear in nature and injects harmonics in the system. The harmonics generated are random in nature. The SEIG performance is severely affected with these harmonics. A dip in voltage is also observed as the harmonic content increases.

In this chapter, effort has been made to improve performance of the load controller which injects minimum harmonics and makes the dump load control as a linear load. The AC chopper control [34, 59, 60, 76, 88, 139, 140, 157] gives wide control range. Due to symmetrical control of terminal voltage only odd harmonics are present. The harmonics appear as a side band and are the integral multiples of switching frequency. The low order harmonics are eliminated and the order of dominant voltage harmonic can be controlled through change in chopping frequency. It gives the linear control of the fundamental component of the output voltage. In this chapter two different kind of AC chopper have been analyzed based on equal ratio time control (ERTC) AC chopper and on sinusoidal PWM AC chopper control. The digital design and implementation of DSP based SEIG-load controller based on ETRC AC chopper controllable load controller for three phase SEIG and based on sinusoidal PWM AC chopper controllable load controller for single phase two winding SEIG has presented in this chapter.

## 5.2 SEIG WITH ERTC AC CHOPPER CONTROLLED LOAD CONTROLLER

### 5.2.1 System Description

A schematic diagram and digital design of ETRC AC chopper controlled load controller based SEIG system is shown in Figure 5.1. It consist of a three phase SEIG driven by a constant power prime mover. The excitation capacitors are connected at the terminals of the SEIG, which have a fixed value to result in rated terminal voltage at maximum permissible load. Consumer load and load controller are connected in parallel at generator terminals. The load controller consists of three pairs of anti parallel connected static switches (IGBT1-IGBT6), connected in series with a resistive load $R_D$ (dump load).

The SEIG feeds two loads in parallel such that the total power $P_{out}=P_c+P_d$ is constant. where, $P_{out}$ is the generated power of the generator (which must be kept constant), $P_c$ is the consumer load power, and $P_d$ is the dump load power. The amount of dump load power is controlled by IGBT switches. The duty cycle of the gate pulse to switches provides the average conduction period and hence the amount of power to dump load. An equal time ratio control (ETRC) AC chopper approach has been adopted to control dump load.

The IGBT (1, 3, and 5) conducts for positive half cycle and IGBT (2, 4, and 6) conducts for negative half cycle of applied AC input. A symmetrical pulse width is applied for conduction of switches. The amount of conduction through dump load is the difference between generated power and consumer load. The voltage amplitude is determined and compared with reference voltage, which is taken as proportional to the rated terminal voltage of the SEIG. The error is scaled (gain) and algebraically added to previous sample time pulse width reference. As the desired terminal voltage is achieved the error signal becomes zero and pulse width reference holds its level. The pulse width references is compared with symmetrical triangular wave to obtain pulse of suitable width. The frequency of symmetrical triangular wave (Carrier frequency) is selected according to static switching device. The pulse output is then given to IGBT switches through opto isolation and pulse driver circuit.

### 5.2.2 Modeling and Simulation

#### 5.2.2.1 Determination of excitation capacitor

Figure 5.2 shows the per phase equivalent circuit of three phase SEIG with load where $R_s$, $X_{ls}$, $R_r$ , $X_{lr}$ are per phase stator and rotor resistances and reactance respectively; $X_m$ and $X_C$ are per phase magnetizing and capacitive reactance; $I_s$, $I_r$, $I_L$ are per phase stator, rotor and load currents; $V_g$ is air gap voltage and F, v are per unit frequency and speed. Rotor parameters are referred to stator and all reactance are at base frequency.

Applying Kirchhoff's voltage law we have:

$$(Z + Z_L) I_L = 0 \tag{5.1}$$

where, $Z = Z_C \parallel (Z_S + (Z_M \parallel Z_r))$

and $Z_c = -jX_c/F$, $Z_s = R_s+jFX_{ls}$, $Z_r = R_rF/(F-v)+jFX_{lr}$, $Z_M = jFX_m \parallel R_m$.

Under steady state condition, $I_L$ can not be equal to zero and hence,

$$(Z + Z_L) = 0 \tag{5.2}$$

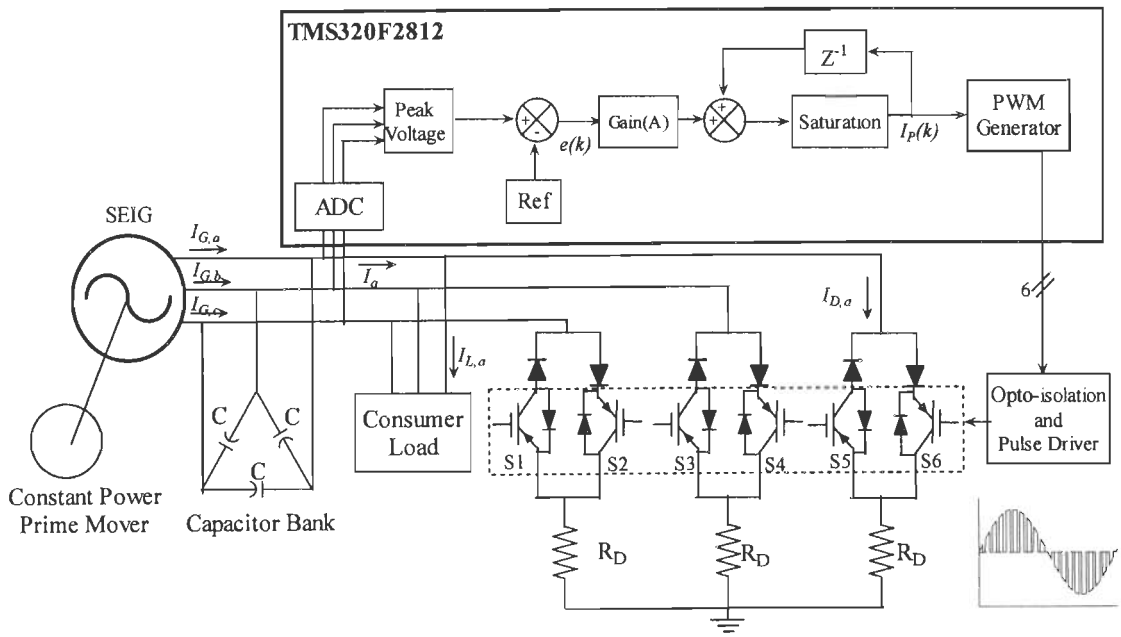


**Figure 5.1: Schematic diagram of three phase SEIG system with load controller**

This can be defined as the function of capacitive reactance (Xc) and per unit frequency( F) as:

$$f(X_c, F) = |Z + Z_L| \tag{5.3}$$

This equation is solved by sequential unconstrained minimization technique (SUMT) in conjunction with Rosenbrock's method of rotating coordinates for Xc and F. The required capacitance is then calculated as:

$$C = \frac{1}{(2\pi f_b X_c)} \tag{5.4}$$

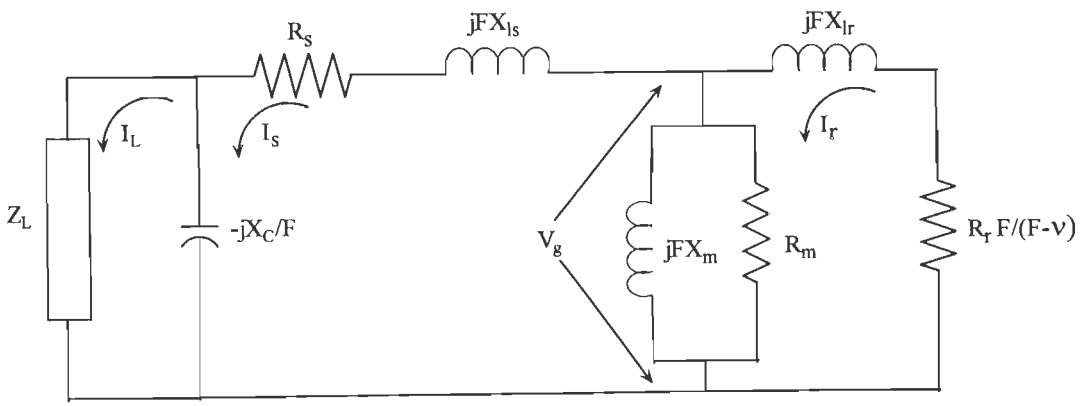


**Figure 5.2 : Steady state equivalent circuit of SEIG with a balanced load**

### 5.2.2.2 Controller design

The schematic diagram of controller is shown in Figure 5.3. To maintain the terminal voltage of the SEIG constant, the terminal voltage error e($k$) at $k^{th}$ sampling instant is computed as:

$$e(k) = V_P(k) - V_{ref} \tag{5.5}$$

where, $V_P(k)$ is the peak amplitude of SEIG terminal voltage and $V_{ref}(k)$ is the reference voltage at $k^{th}$ sampling instant.

The terminal voltage error is processed through a load controller. The output of the load controller at $k^{th}$ sampling instant is given as:

$$I_P(k) = A\,e(k) + I_P(k-1) \tag{5.6}$$

where, A is the gain of the controller to adjust overshoot, $I_P(k\text{-}1)$ is the load controller reference at $(k\text{-}1)^{th}$ sampling instant.

Taking z transform:

$$I_P(z) = AE(z) + z^{-1}I_P(z) \tag{5.7}$$

$$\frac{I_P(z)}{E(z)} = A\frac{1}{1-Z^{-1}} \tag{5.8}$$

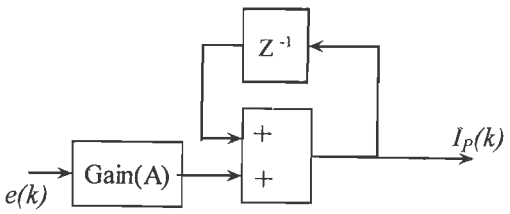


**Figure 5.3: Schematic diagram of controller**

### 5.2.2.3 Preliminary design of dump load

The input AC phase voltage to dump load is given as:

$$v = V_P \sin \omega t \tag{5.9}$$

where, $V_P$ is the peak AC voltage, $\omega$ is the angular frequency.

A Matlab program has been generated which shows that with ETRC, the average conduction period or the rms voltage appearing at the load side is a function of modulation index (m) as:

$$V_o = (V_p/2) \times m \quad \text{for } 0 < m <= 1 \tag{5.10}$$

where, $m = \dfrac{\text{Amplitude of modulating voltage}(A_m)}{\text{Amplitude of carrier triangular wave}(A_c)}$;

For a three phase SEIG of line to line voltage of 400 V, phase voltage is 230.94 V and peak voltage ($V_P$) is $230.94 \times \sqrt{2} = 326.60$ V. Thus rms output voltage for m=1 is:

$$V_O = (326.60 / 2) \times 1 = 163.3 \text{ V} \quad (5.11)$$

Taking an over voltage of 10 % of rated ac voltage for transient condition, the peak voltage is given as:

$$V_{peak} = 1.10 \times 326.60 = 359.3 \text{ V} \quad (5.12)$$

Dump load resistance is given as:

$$R_D = (V_o)^2 / P = (163.3)^2 / 1000 = 26.67\ \Omega \quad (5.13)$$

where, P is the per phase power rating of SEIG.

The AC rms current is given as

$$I_{AC} = (V_o / R_D) \times m \quad \text{for } 0 < m <= 1 \quad (5.14)$$

The maximum AC current for m=1 is given as:

$$I_{AC} = (163.3/26.67) \times 1 = 6.12 \text{ A} \quad (5.15)$$

Taking an creast factor of 1.41 for ac wave and average distortion factor of 0.8 [88], the peak ac current is given as:

$$I_{AC,peak} = 1.41 \times 6.12 / 0.8 = 10.79 \text{ A} \quad (5.16)$$

The maximum voltage and current ratings are 359.3 V and 10.79 A respectively.

#### 5.2.2.4 Simulation

Digital simulation of proposed induction generator controller been carried out with MATLAB Version 7.2 on Simulink Version 6.4. This Power System Blockset facilitates to simulate saturation of asynchronous machines. A 3.73 kW, 400 V, 50 Hz asynchronous machine is used as an SEIG including the machine saturation characteristics which is determined by conducting synchronous speed test. The synchronous speed test specifies the no load saturation curve for induction machine. The voltage and current of synchronous speed test is given in a 2-by-n matrix, where n is the number of points taken from the saturation curve to simulate saturation on MATLAB. The machine parameters are given in Appendix-A. The dropping torque- speed characteristics of prime mover is given as $T_{sh} = K_1 - K_2 \omega_r$; Where, $K_1$ and $K_2$ are the prime mover constants given in Appendix A. The terminals of the machines are connected with delta connected capacitor bank of 25 mf per phase. The output is connected with a controlled dump load and

consumer load of resistive and reactive nature. The voltage amplitude is calculated as $V_p=\{2/3(V_{ab}^2+V_{bc}^2+V_{ca}^2)\}^{1/2}$, where $V_{ab}$, $V_{bc}$, $V_{ca}$ are the line voltage and $V_p$ is the peak amplitude. The peak amplitude is compared with the reference and processed through the proposed sample based controller. The output of the controller is compared with symmetrical triangular wave and through a relational operator to obtain a pulse of suitable duration (width). This pulse is given to gate of the IGBT switches. Figure 5.4 shows the transient waveform of SEIG voltage buildup and application of resistive load ($I_{Load\_}$). The no load voltage generation is around 600 V. With the application of controlled dump load at t=0.5 seconds, the terminal voltage drop to its rated value. At time t=0.7 seconds a resistive load is applied. The terminal voltage and frequency remains constant.

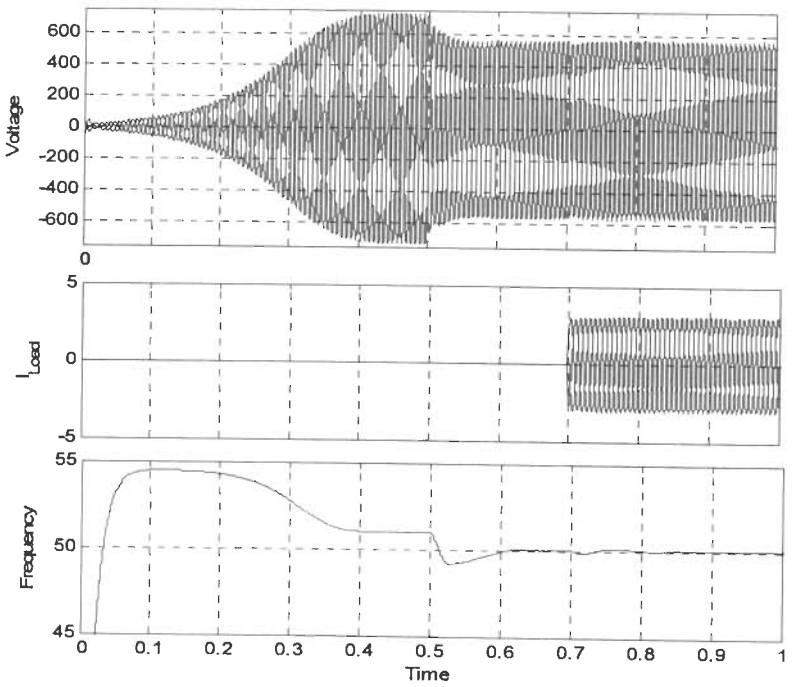


**Figure 5.4: Voltage build up and application of main load**

Figure 5.5 and Figure 5.6 show the transient waveform on application and removal of 1500 W resistive load and 1000 W 0.8 lagging power factor reactive load respectively. The waveform from top to bottom are terminal Voltage ($V_{abc}$), generator winding current ($I_{G,\,abc}$), load current ($I_{L,\,abc}$), dump load current ($I_{D,a}$), line current ($I_a$) and frequency (f) respectively. Figure 5.7 shows the transient waveform on application of dynamic load. On application of load, the average of dump load current decreases and main load current increases. However, the terminal voltage remains constant and so as the frequency.

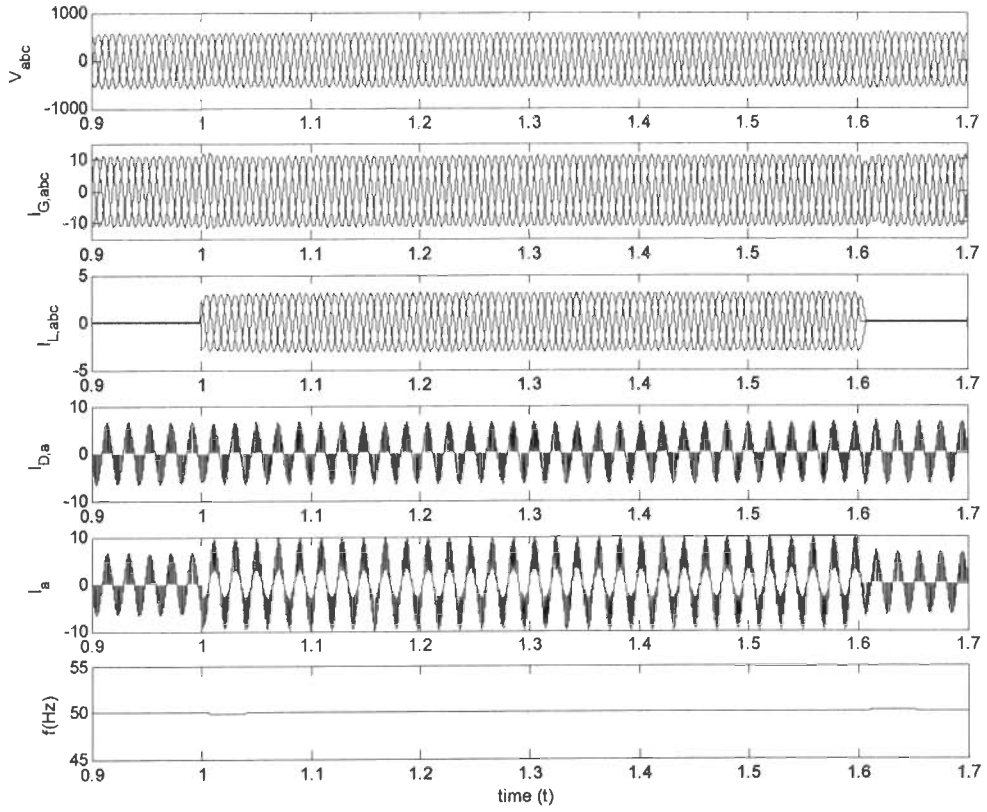


**Figure 5.5: SEIG-load controller system supplying resistive loads**

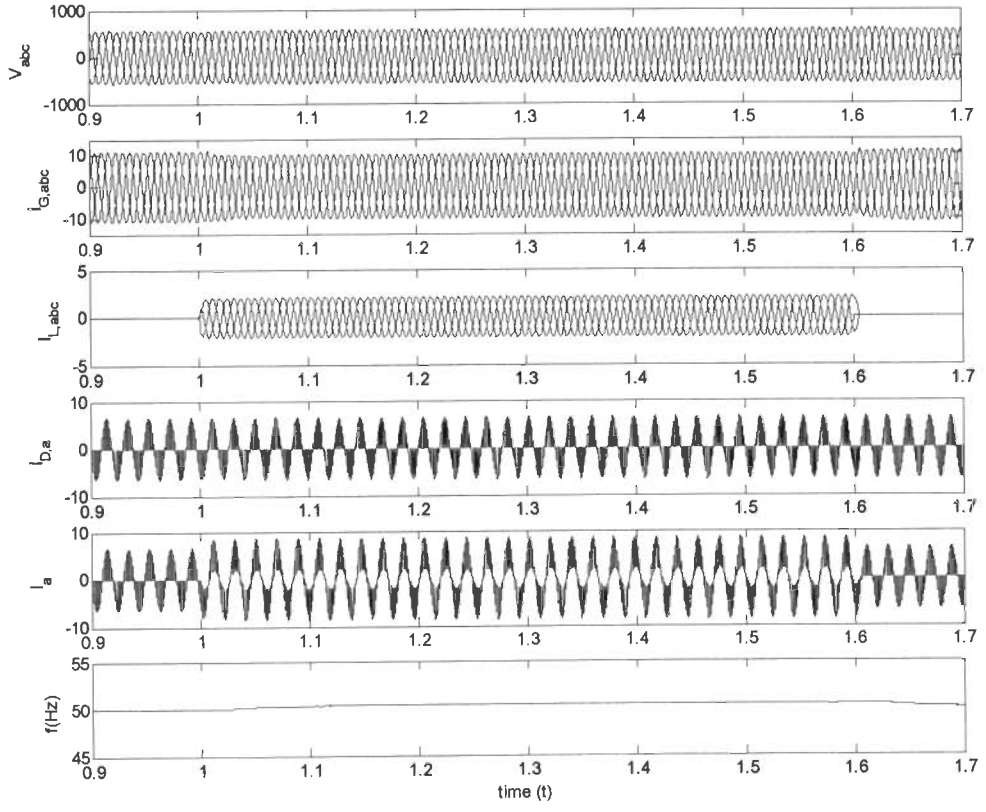


**Figure 5.6: SEIG-load controller system supplying reactive loads**

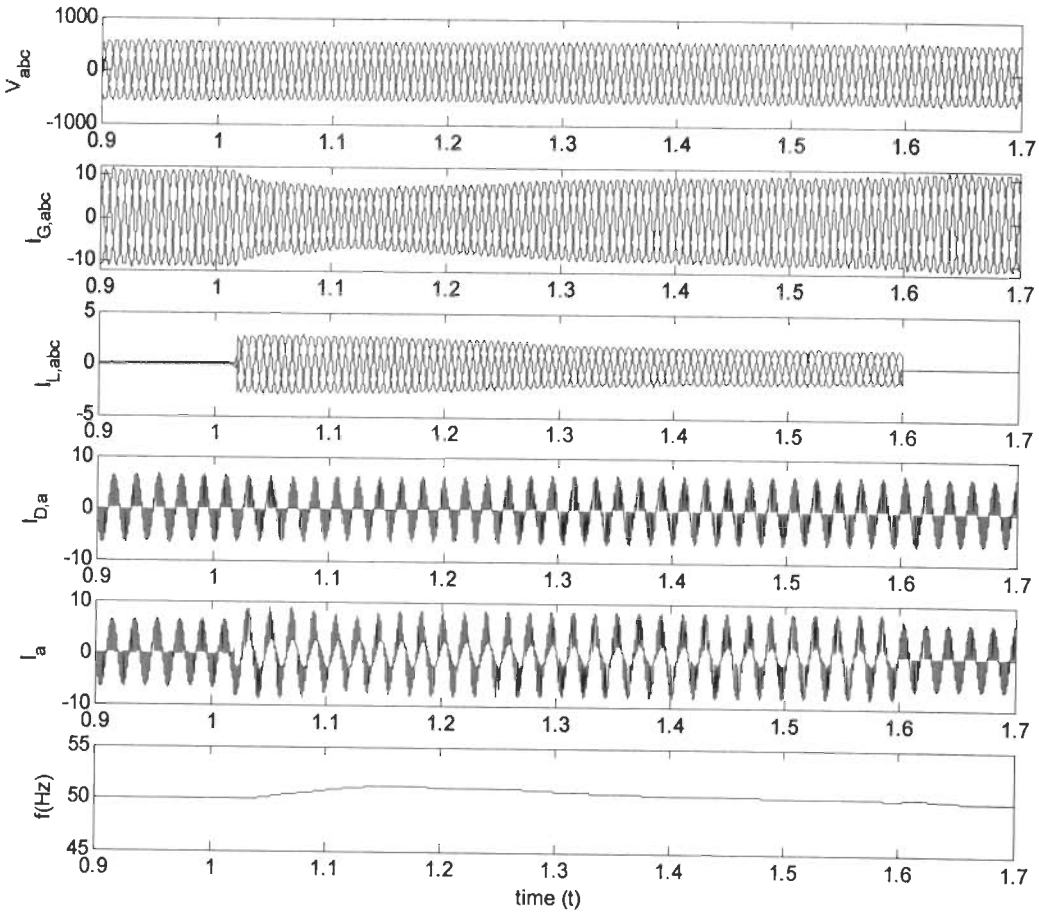


**Figure 5.7: SEIG-load controller system supplying dynamic load.**

### 5.2.3 Implementation

The output power of the SEIG is kept constant by load controller. Figure 5.1 shows the control scheme for voltage regulation of SEIG based on ETRC AC chopper controlled dump load. The AC terminal voltage is sensed through a AC voltage sensor and passed through a signal conditioner. This sensed voltage is read through ADC input of the DSP TMS320F2812. The TMS320F2812 DSP has 16 ADC input channels with an input range of 0- 3 Volt. The output values are in the range of 0 to 4095 as the TMS320F2812 DSP ADC is 12- bit analog to digital converter. It reads the input with a sample rate of 0.0001 seconds (maximum 0.0004 seconds). The input voltage signal contains harmonics. The input signal is passed through a discrete low pass filter. The peak amplitude is compared with the set reference, which is taken as proportional to the rated terminal voltage of the SEIG. The error is scaled (Gain) and algebraically added to previous sample load

controller reference *($I_p(k-1)$)*. The amplitude of generated reference gives the modulation index (m). This reference is then given to PWM block of DSP. The PWM block have self symmetric carrier triangular wave [210]. The carrier frequency is selected according to static switching device. In this particular case a carrier frequency of 3 kHz is selected. Higher switching frequency results in less THD and minimum order of harmonic appearing is of higher order. The TMS320F2812 DSP has 6x2 high resolution PWM outputs. The pulse from DSP is processed through opto-isolation and gate driver circuit. A photocoupler TLP250 is used as gate driver circuit. It includes an opto-isolator, NPN and PNP transistor and the necessary logic to control them, all within an integrated package. Only the addition of two resistors is required to complete the gate driver circuit.

### 5.2.4 Results

Experiments are carried out on developed prototype of ETRC AC chopper controlled load controller based SEIG system. A three phase 3.73 kW, 400 V, 7.5 A 50Hz, 1500 rpm squirrel cage induction machine is used as a self-excited induction generator. The SEIG is driven by 220 V, 20 A, 5 HP, 1500 rpm shunt wound DC machine used as a prime mover. To generate 3 kW at 400 V and rated speed, 25 μF capacitor of 400 V is connected in delta across the SEIG terminals. The test results are carried out with three phase balanced resistive load and 0.8 lagging power factor reactive load. Figure 5.8 shows the experimented transient responses of SEIG-load controller system on application of 1.5 kW three phase balanced resistive load. The waveforms from top to bottom are terminal voltage $V_{ab}$ of SEIG, line current of main load ($I_{L,a}$), line current of dump load ($I_{D,a}$) and line current of SEIG ( $I_a$) respectively. On application of resistive load, main load current increases and dump load current decreases so that power transfers from dump load to consumer load and SEIG experiences constant load on it.

Figure 5.9 shows the transient responses of SEIG system on application of 1kW, 0.8 lagging power factor load. On application and removal of load the terminal voltage remains constant. When an inductive load is connected to the SEIG, it draws a reactive current. Then a part of the excitation capacitance is used to compensate for this reactive current, so less capacitance is available for the SEIG itself. It react to this with an increase in frequency, causing the capacitors to produce some more magnetizing current while the

SEIG needs less so the two balance again and frequency varies as well with the reactive load. The frequency variation caused by reactive load is within acceptable limits. With a SEIG running at a normal degree of saturation, frequency variation would be less. As modern induction machines tend to be saturated, therefore, the frequency regulation with variation in load power factor is quite small. A small increase in frequency results in a significant reduction in magnetizing current. In addition, extra VARs are produced by the excitation capacitors due to reduced impedance. Figure 5.10 shows the transient responses on application of three phase 1 HP induction motor load. A good voltage and frequency regulation is observed. There is a slight decrease in terminal voltage as the voltage THD in the system increases. The frequency remains constant with the application of resistive load. A slight increment in frequency is observed for loads of lagging power factor which is within acceptable limits.

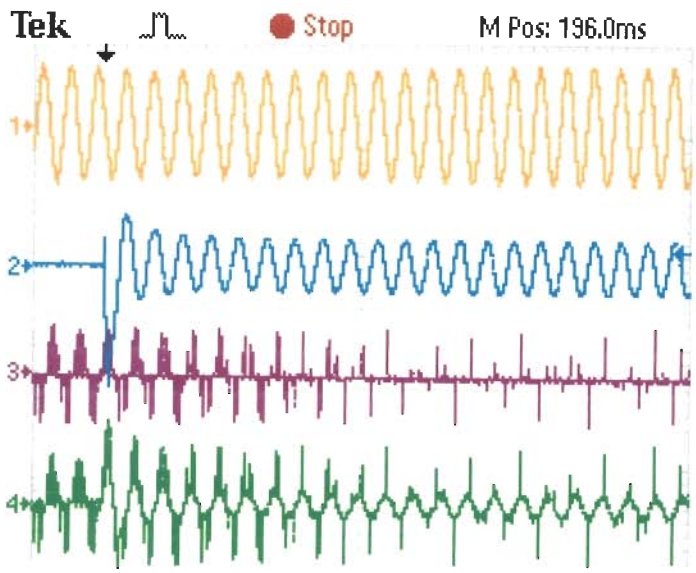


Horizontal scale:-Time 50msec/Div
Vertical scale from ch1 to ch4:-$V_{ab}$ (600V/Div)
$I_{L,a}$ (8A/Div), $I_{D,a}$(8A/Div), $I_{a}$(8A/Div)

**Figure 5.8: Transient waveform on application of balanced three phase resistive load**

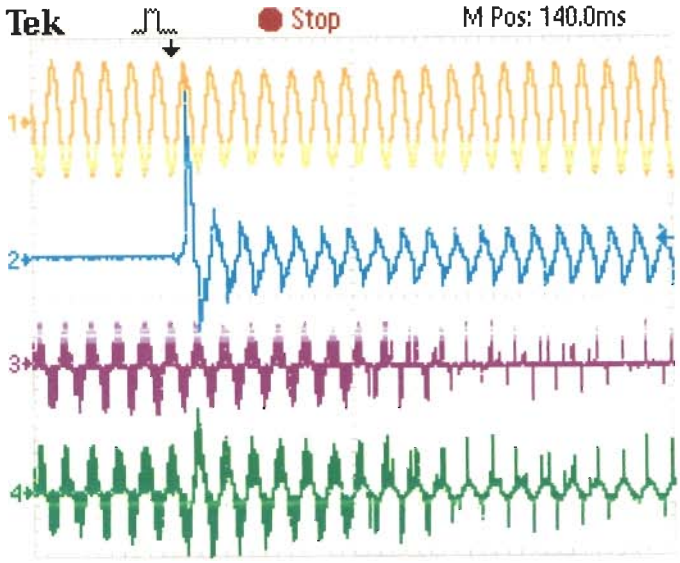


Horizontal scale:-Time 50msec/Div
Vertical scale from ch1 to ch4:-$V_{ab}$ (600V/Div)
$I_{L,a}$ (8A/Div), $I_{D,a}$(8A/Div), $I_a$(8A/Div)

Figure 5.9: Transient waveform on application of balanced three phase reactive load

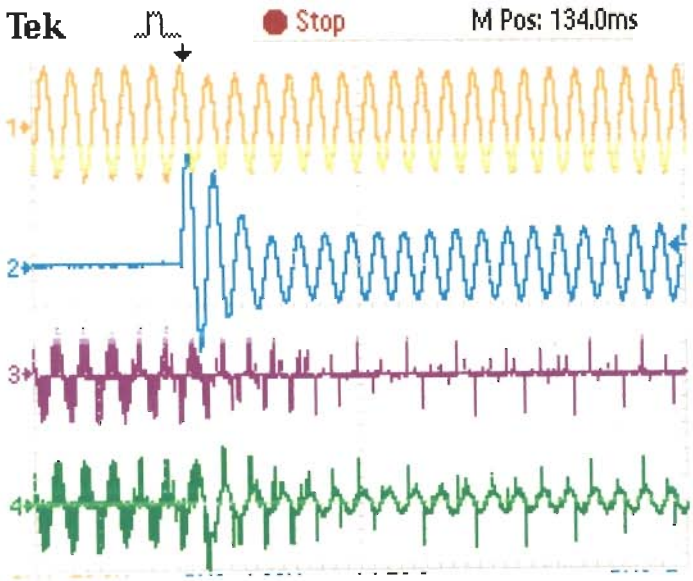


Horizontal scale:-Time 50msec/Div
Vertical scale from ch1 to ch4:-$V_{ab}$ (600V/Div)
$I_{L,a}$ (8A/Div), $I_{D,a}$(8A/Div), $I_a$(8A/Div)

Figure 5.10: Transient waveform on starting and running of induction motor load

### 5.2.5 Harmonic analysis

The equal ratio time control (ERTC) AC chopper circuit is controlled by the switching function *h(t)*, which is generated by comparing a control signal ($I_P(k)$) by a triangular wave ($v_{tri}$) as shown in Figure 5.11. As a result, the output voltage may be found from

$$v_o(t) = h(t).v_s(t) \tag{5.17}$$

where, $v_s(t) = V_P \sin \omega_s t$ and $V_P$ is the peak AC voltage, $\omega_s$ is the angular frequency

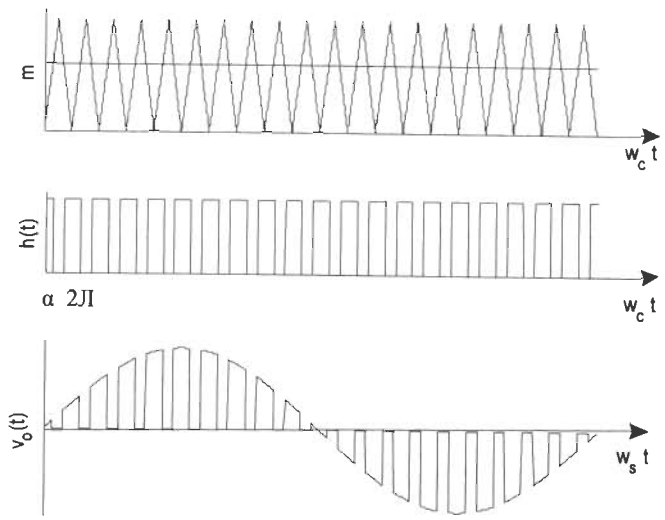


**Figure 5.11: Generation of ETRC output voltage**

The switching function *h(t)* may be expressed in Fourier series as

$$h(t) = C_o + \sum_{n=1}^{\infty} C_n \sin(pn\omega_c t + \phi_n) \tag{5.18}$$

where, $\omega_c$ is the carrier triangular wave angular frequency and p is the frequency ratio of carrier triangular wave to source wave.

$$A_n = \frac{1}{\pi}\int_0^{\alpha}(\cos n\omega t)\, d\omega t$$

$$= \frac{1}{\pi}\frac{\sin(n\alpha)}{n} \tag{5.19}$$

$$B_n = \frac{1}{\pi}\int_0^{\alpha}(\sin n\omega t)\, d\omega t$$

$$= \frac{1}{\pi}[1-\cos n\alpha] \tag{5.20}$$

therefore, $C_n = A_n^2 + B_n^2$

$$= \frac{\sqrt{2}}{\pi n}[1-\cos n\alpha]^{1/2} \tag{5.21}$$

Using the identity, $\cos 2x = 1-2\sin^2 x$ and as $\alpha = 2\pi m$, where $m$ is the time ratio or modulation index. The equation (5.20) may be written as

$$C_n = \frac{2}{\pi n}\sin(n\pi m) \tag{5.22}$$

The phase angle

$$\phi_n = \tan^{-1}\frac{A_n}{B_n} = \frac{\pi}{2} - nm\pi \tag{5.23}$$

From equation (5.18), *h(t)* may be expressed in Fourier series as

$$h(t) = m + \frac{2}{\pi}\sum_{n=1}^{\infty}\frac{1}{n}\sin(nm\pi)\cos(np\omega_s t - nm\pi) \tag{5.24}$$

The output voltage from equation (5.17) and (5.24) is given as

$$v_o(t) = V_P\, m\, \sin(\omega_s t) + \frac{V_P}{\pi}\sum_{n=1}^{\infty}\frac{1}{n}\sin(nm\pi)\times\sin[\{(np+1)\omega_s t - nm\pi\} + \sin\{(1-np)\omega_s t + nm\pi\}] \tag{5.25}$$

The equation (5.25) reveals the following features of this technique.

(i) The fundamental component of $v_o$ *(t)* is in phase with $v_s$ *(t)*.

(ii) Only odd harmonics are present.

(iii) Harmonics are side band of $np\omega_s$ with amplitude equal to $V_P C_n$.

(iv) Increasing p shifts the lowest order harmonics far from fundamental, making it easy to filter.

(v) The amplitude of the fundamental component of $v_o$ *(t)* depends only on the DC value of *h(t)* or modulation index 'm'.

The developed ETRC AC chopper controllable SEIG-load controller behaves as linear dump load as compared to mark space ratio controlled dump load. The dump load current profile follows the dump load voltage profile. The harmonics appearing in mark space ratio control are random in nature and harmonic contents are more while in proposed scheme the harmonics appeared in dump load voltage and current are of the same order and only odd harmonics are present. The THD appearing in the proposed

scheme are less as compared to mark space ratio control despite it doesn't involve any filter capacitor. The change in main load will change the modulation index consequently the pulse width and average period of conduction of load controller. The change in pulse width will change the THD appearing in the system. The dominant order of harmonics is the order of $2P \pm 1$. Where, P is the number of pulse per half cycle. For the present system the carrier frequency is chosen to 3 kHz. Hence minimum order of harmonics appearing is $29^{th}$ and $31^{st}$. Table 5.1 summarizes the main load, terminal voltage, voltage THD and current THD of main load, dump load and generator at different step of resistive and reactive load application. The harmonic contents are less in the proposed system despite of that it does not involve any filter.

**Table 5.1 Terminal voltage, voltage and current THD at different main load**

| S.No. | Main Load (W) | Terminal Voltage (V) | | Voltage THD (%) | | Current THD (%) | | | | | |
|---|---|---|---|---|---|---|---|---|---|---|---|
| | | | | | | Main Load | | Dump Load | | Generator | |
| | | Sim. | Meas. | Sim. | Meas. | Sim. | Meas. | Sim. | Meas. | Sim. | Meas. |
| 1 | 0 | 401.8 | 399.8 | 3.1 | 4.7 | - | - | 5.6 | 12.0 | 8.0 | 11.30 |
| 2 | 1000 | 401.7 | 397.2 | 3.5 | 4.8 | 2.58 | 4.4 | 9.0 | 14.7 | 5.6 | 9.98 |
| 3 | 2000 | 399.1 | 397.3 | 3.4 | 4.5 | 2.63 | 4.4 | 11.9 | 18.4 | 6.2 | 10.70 |
| 4 | 3000 | 398.7 | 396.4 | 3.5 | 4.3 | 2.64 | 4.6 | 18.6 | 23.3 | 7.7 | 8.37 |
| 5 | 500 0.8pf lag | 398.2 | 396.3 | 3.2 | 4.7 | 2.98 | 5.1 | 8.2 | 17.4 | 6.8 | 10.90 |
| 6 | 1000 0.8pf lag | 397.6 | 395.5 | 3.9 | 5.6 | 3.76 | 6.0 | 15.6 | 22.2 | 8.0 | 11.24 |
| 7 | 1 HP IM at no load | 396.6 | 395.1 | 4.2 | 5.1 | 3.84 | 6.4 | 16.7 | 24.3 | 8.1 | 10.94 |

Sim. :- Simulated Meas. :- Measured

## 5.3 SEIG WITH SINUSOIDAL AC CHOPPER CONTROLLED LOAD CONTROLLER

### 5.3.1 System Description

A schematic diagram of the developed DSP based load controller for SEIG system is shown in Figure 5.12. It consists of single phase two winding (main and auxiliary) squirrel cage induction motor (working as SEIG) driven by a constant power prime mover (typically, an un-regulated micro-hydro turbine). The excitation capacitors are connected at the terminals of auxiliary ($C_A$ ) and main windings ($C_M$ ) as shown in Figure 5.12,

which have the fixed value to result in rated terminal voltage at full load. Since the input power is nearly constant, the output power of the SEIG must be held constant at varying consumer load. Any decrease in consumer load may accelerate the SEIG and raise the voltage and frequency level and vice versa. The power at SEIG terminal is kept constant by connecting a dump load in parallel to consumer load such that the total power remains constant i.e. $P_{out} = P_C + P_D$, where $P_{out}$ is the generated power of the generator, $P_C$ is the consumer load power and $P_D$ is the dump load power. The amount of dump load power is the difference of power generated to consumer load. The dump load power is controlled through load controller such that the output power of the SEIG remains constant under varying consumer load resulting in constant voltage and constant frequency output power.

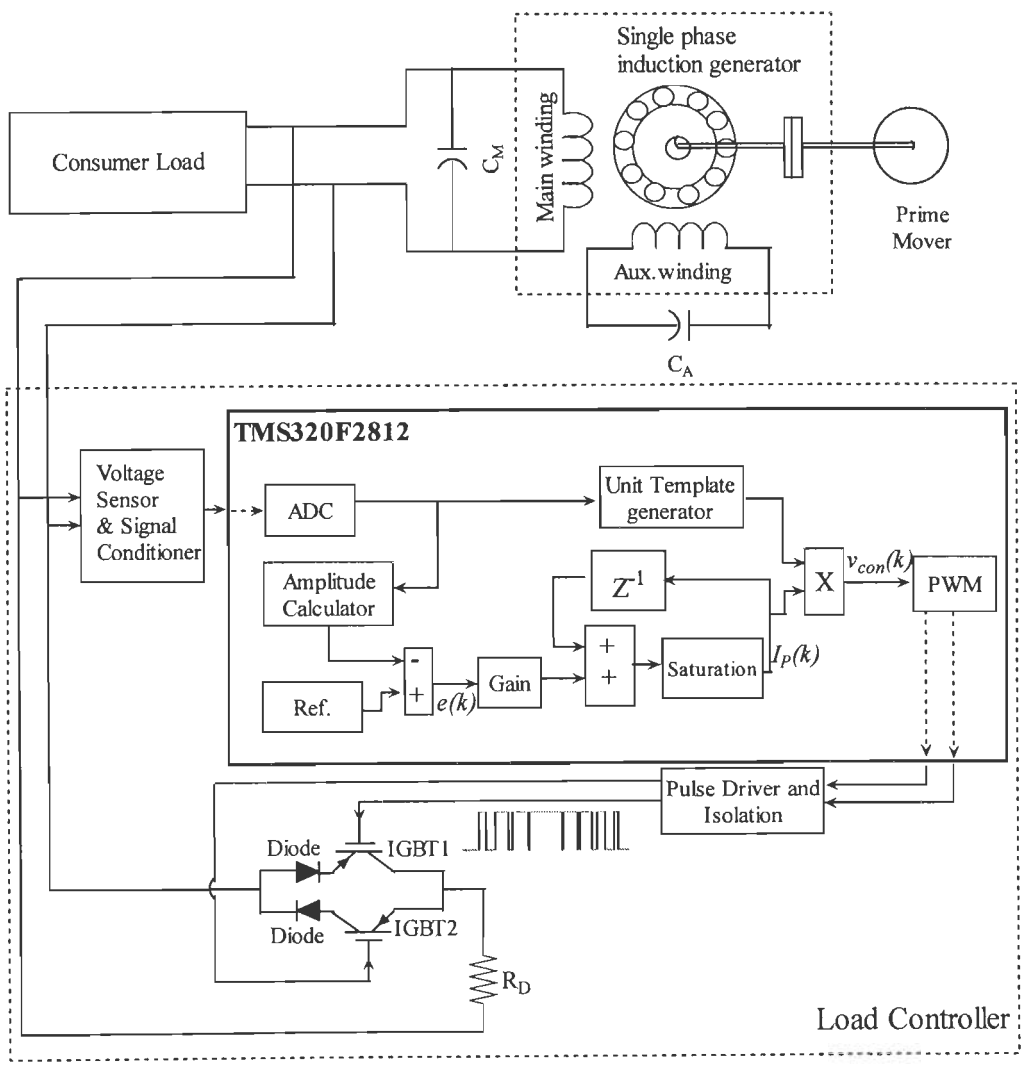


**Figure 5.12:- Schematic diagram of single phase SEIG with load controller**

The load controller consists of two back to back connected IGBT and series resistive dump load resistance. The two IGBT are connected through a series connected diodes which allows only the forward direction flow of current. The IGBT conducts for positive half and negative half of AC cycle respectively on application of gate pulse. The gate pulse is sinusoidally modulated and its modulation index is decided by the difference of power generation to consumer load. The fixed point digital signal processor TMS320F2812 (32-bit, 150 MIPS) is used for generation of suitable pulse width in accordance with changing consumer load. The DSP reads the terminal voltage through a voltage transducer as a feedback signal via its ADC input. The amplitude of ac voltage (V) is computed from sensed instantaneous ac terminal voltage. This amplitude of ac voltage (V) is compared with set reference and the error is processed through a sample based controller. The output of controller is multiplied with unit sine template derived from sensed instantaneous ac terminal voltage. The obtained sine wave is compared with symmetrical triangular wave to obtain a suitable modulated pulse. The generated pulse is then given to IGBTs via photo-coupler isolation and pulse driver circuit.

### 5.3.2 Modeling and Simulation

#### 5.3.2.1 Design of dump load

The input AC voltage to uncontrolled rectifier of load controller is given as:

$$v_s = V_P \sin \omega t \tag{5.26}$$

where, $V_P$ is the peak AC voltage, $\omega$ is the angular frequency.

A Matlab program has been generated which shows that with sinusoidal pulse width modulation the average conduction period or the rms voltage ($V_o$) appearing at the load side is a function of modulation index (m) as:

$$V_o = (V_p/2) \times m \quad \text{for } 0 < m <= 1 \tag{5.27}$$

where, $m = \dfrac{\text{Amplitude of modulating sine wave}(A_m)}{\text{Amplitude of carrier triangular wave}(A_c)}$;

For a single phase SEIG, main winding voltage of 220 V and peak voltage ($V_P$) is $220 \times \sqrt{2} = 311.12$ V. Thus rms output voltage for m=1 is:

$$V_O = (311.12/2) \times 1 = 155.56 \text{ V} \tag{5.28}$$

Taking an over voltage of 10 % of rated ac voltage for transient condition, the peak voltage is given as:

$$V_{peak} = 1.10 \times 311.12 = \ 342.2 \ V \tag{5.29}$$

Dump load resistance is given as:

$$R_D = (V_o)^2 / P = (155.56)^{\ 2} / 1000 = 24.20\ \Omega \tag{5.30}$$

where, P is the power rating of SEIG.

The AC rms current is given as

$$I_{AC} \ = (V_o / R_D) \times m \ \ \text{for} \ \ 0 < m <= 1 \tag{5.31}$$

The maximum AC current for m=1 is given as:

$$I_{AC} = (155.56/24.20) \times 1 = 6.43 \ A \tag{5.32}$$

Taking a creast factor of 1.41 for ac wave and average distortion factor of 0.8 [88], the peak ac current is given as:

$$I_{AC,peak} = 1.41 \times 6.43 / 0.8 = 11.33 \ A \tag{5.33}$$

The maximum voltage and current ratings are 342.2V and 11.33A respectively. Commercially available rating of diodes and IGBT switches are selected of 600V and 15A.

### 5.3.2.2 Controller design

The schematic diagram of controller is shown in Figure 5.12. To maintain the terminal voltage of the SEIG constant, the terminal voltage error e($k$) at $k^{th}$ sampling instant is computed as:

$$e(k) = V_P(k) - V_{ref} \tag{5.34}$$

where, $V_P(k)$ is the peak amplitude of SEIG terminal voltage

and $V_{ref}(k)$ is the reference voltage at $k^{th}$ sampling instant.

The unit template is computed as

$$u(k) = \frac{v_s(k)}{V_p(k)} \tag{5.35}$$

where, $v_s(k)$ is the input voltage at $k^{th}$ sampling instant.

The terminal voltage error is processed through controller. The output of the controller at $k^{th}$ sampling instant is given as:

$$I_P(k) = A\,e(k) + I_P(k-1) \tag{5.36}$$

where, $A$ is the gain of the controller to adjust overshoot, $I_P\ (k\text{-}1)$ is the load controller reference at $(k\text{-}1)^{th}$ sampling instant.

The control signal for PWM generation is given as

$$v_{con}(k) = u(k) \times I_P(k) \tag{5.37}$$

The overshoot of the system is governed by change in controller gain (A).

### 5.3.2.3 Simulation

Digital simulation of the proposed induction generator controller is carried out with MATLAB Version 7.2 on Simulink Version 6.4. A 1.492 kW, 220V, 9.5 A, 50 Hz, 4 pole main and auxiliary winding single phase asynchronous machine modeled in d-q stator reference frame is as a single phase self-excited induction generator. The machine parameters are summarized in Appendix. Shunt capacitor of 40 $\mu$f and 36 $\mu$f is connected across main and auxiliary winding to get the rated voltage at rated speed and load. The dropping torque- speed characteristics of prime mover is given as $T_{sh} = K_1 - K_2\omega_r$; Where, $K_1$ and $K_2$ are the prime mover constants given in Appendix A.

The main winding terminals are connected to consumer load and in parallel with load controller. The voltage amplitude is computed. The unit template is determined through dividing by its peak magnitude. The voltage amplitude is compared with the reference and processed through the controller. The output of the controller is multiplied with unit templates. The obtained sinusoidal PWM reference is compared with symmetrical triangular wave of 3 kHz through a relational operator to obtain a sinusoidal modulated pulse of suitable duration (width). This pulse is given to the gates of back to back connected IGBT. The dump load resistance value is selected as given in section 5.3.2.2.

Figure 5.13 shows the simulated waveform of terminal voltage, load current, dump load current, generator main winding and auxiliary winding current on application and removal of 400 W resistive load.

Figure 5.14 shows the waveform on application and removal of 300 W 0.8 lagging power factor load.

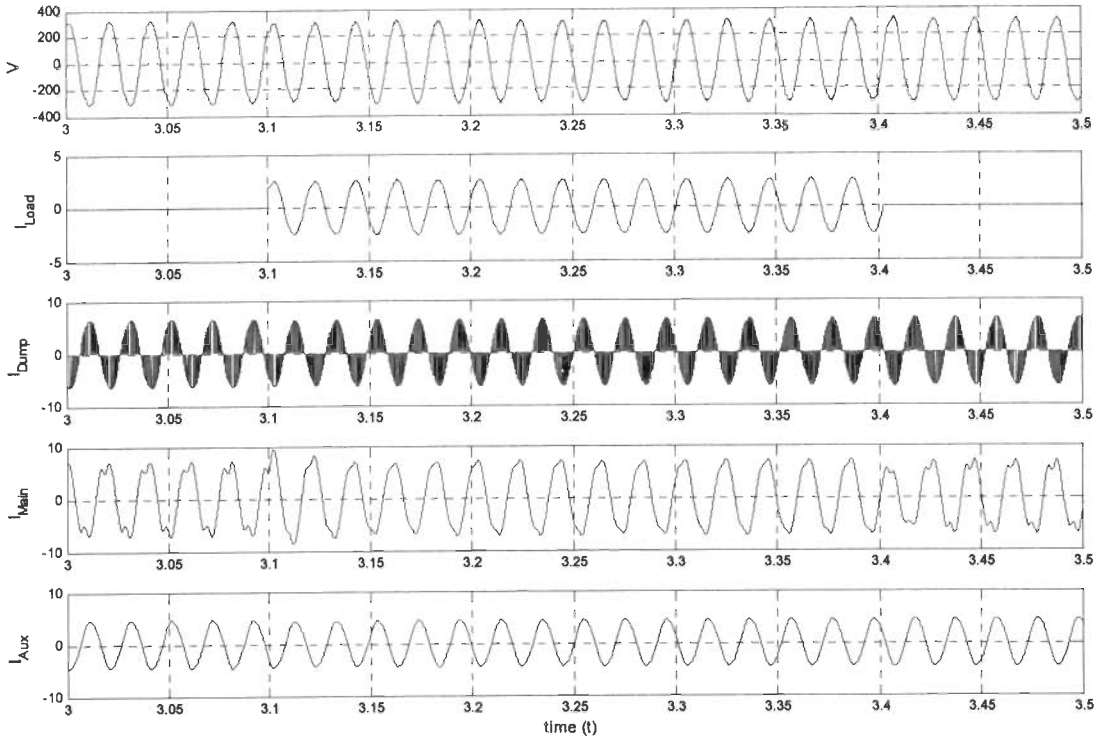


**Figure 5.13: Simulated transient waveform for SEIG-load controller system on application of resistive load**

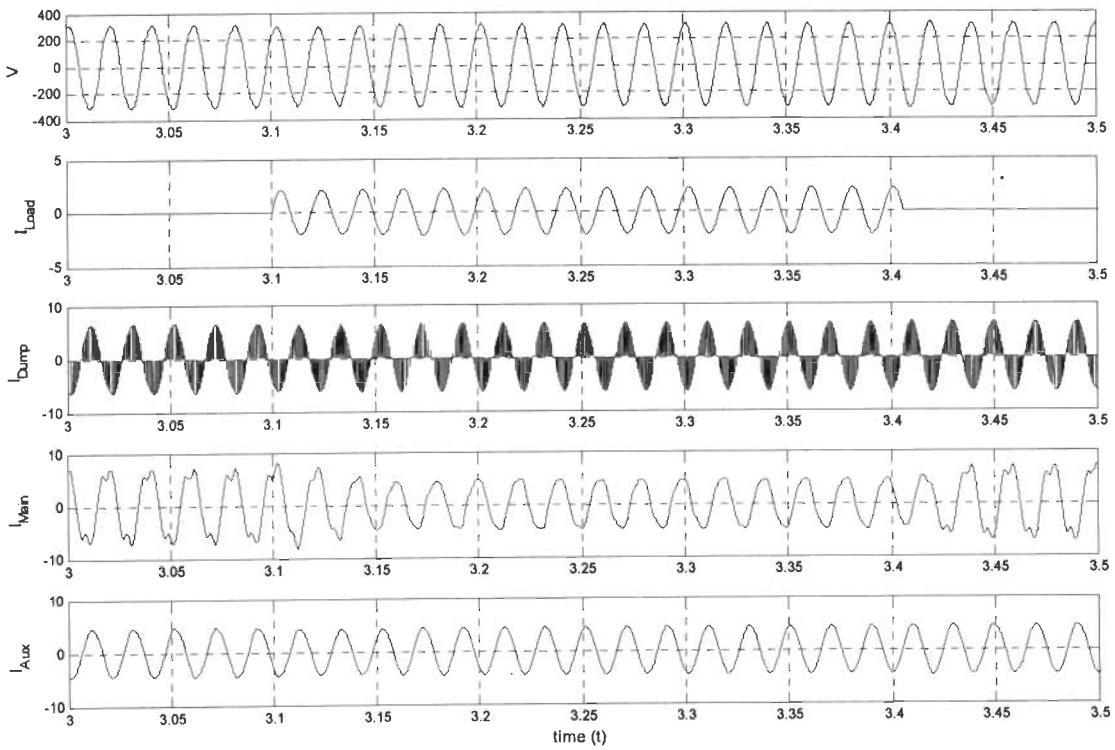


**Figure 5.14: Simulated transient waveform of SEIG-load controller system on application of reactive load**

### 5.3.3 Implementation

The output power of the SEIG is kept constant by load controller. Figure 5.12 shows the control scheme for voltage regulation of SEIG based on sinusoidal PWM AC chopper controlled dump load. The AC terminal voltage is sensed through a AC voltage sensor and passed through a signal conditioner. This sensed voltage is read through ADC input of the DSP TMS320F2812. The unit template is generated through dividing the input signal from its peak value. The input voltage signal contains harmonics. The input signal is passed through a discrete band pass filter. The mean value of input signal is computed. The frequency is varying on switching of loads. The discrete estimation of mean value depends upon the fundamental frequency. The multiple mean is taken to have smooth mean calculation and compared with the set reference, which is taken as proportional to the rated terminal voltage of the SEIG. Figure 5.15 shows the Matlab based model for automatic code generation for CCS link IDE. The error is scaled (Gain) and algebraically added to previous sample load controller reference $(I_p(k-1))$. The generated reference is then multiplied by unit template to generate reference sinusoidal wave ($v_{con}$). The amplitude of generated reference sinusoidal PWM wave gives the modulation index (m).

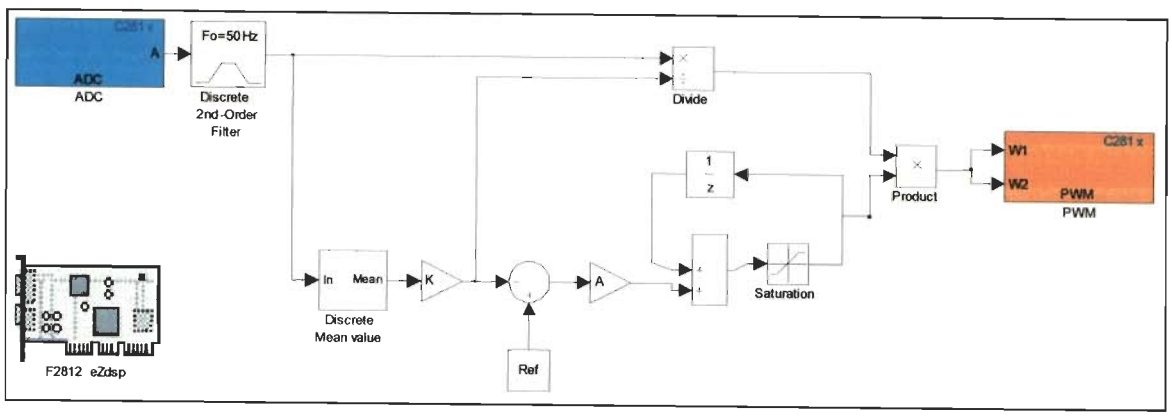


**Figure 5.15: MATLAB CCS project for automatic code generation**

This reference sinusoidal wave is then given to PWM block of DSP. The PWM block have self symmetric carrier triangular wave. The carrier frequency is selected according to static switching device. In this particular case a carrier frequency of 3 kHz is selected. Higher switching frequency results in less THD as well as minimum order of harmonic is high. The TMS320F2812 DSP has 6x2 high resolution PWM outputs. The pulse from DSP is processed through opto-isolation and gate driver circuit. A photocoupler TLP250 is used as gate driver circuit. It includes an opto-isolator, NPN and

PNP transistor and the necessary logic to control them, all within an integrated package. Only the addition of two resistors is required to complete the gate driver circuit.

### 5.3.4 Results

A prototype DSP based load controller with TMS320F2812 processor has been developed and tested in laboratory under various operating conditions. A single phase 1.492 kW, 190/240 V, 9.5 A, 50Hz, 1440 rpm squirrel cage induction machine is used as a single phase self-excited induction generator. The SEIG is driven by 220 V, 20 A, 5 HP, 1500 rpm shunt wound DC machine used as a prime mover. To generate 1000 W at 220 V and rated speed, 40 μF and 36 μF capacitors of 400 V are connected as $C_M$ and $C_A$ across the main winding and auxiliary winding terminals of the SEIG. The test results are carried out with resistive load, 0.8 power factor reactive load and 1 HP, 220/230 V, 5.2 A, 50 Hz, 1425 rpm single phase induction motor with start capacitor of 125 μF, 275 V and run capacitor of 10 μF, 400 V as dynamic load at developed SEIG system with load controller.

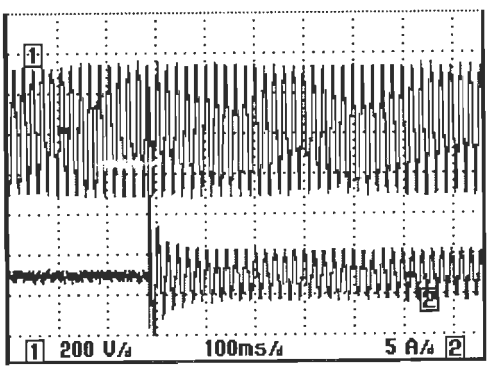


(a)

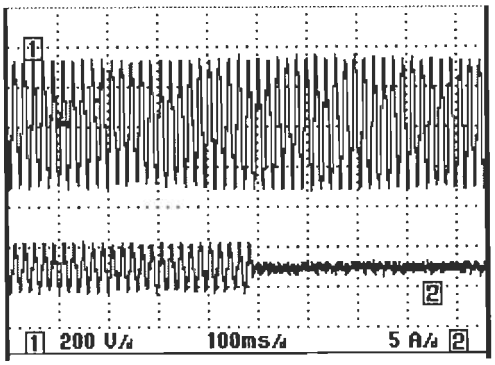


(b)

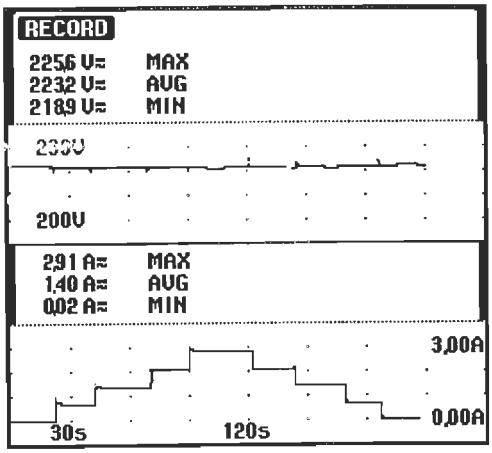


(c)

**Figure5.16: Transient terminal voltage and load current on (a) application (b) removal of 400 W resistive load (c) steady state terminal voltage and load current profile on application and removal of 800 W resistive load in steps of 200 W.**

Figure 5.16(a) and Figure 5.16 (b) shows the load voltage and load current transient waveforms of DSP based load controller for SEIG system on application and removal of 400 W resistive load. In Figure 5.16 (c), steady state load voltage and load current trends are shown on successive application and removal of resistive loads of 800 W in steps of 200 W. The load voltage remains constant at application and removal of resistive load. On application of resistive load, main load current increases and dump load current decreases so that power transfers from dump load to consumer load and SEIG experiences constant load on it.

Figure 5.17(a) and Figure 5.17 (b) shows the load voltage and load current transient waveforms on application and removal of 300 W, 0.8 pf load. Figure 5.17 (c) shows the voltage and current trends on application and removal of 300 W 0.8 pf load.

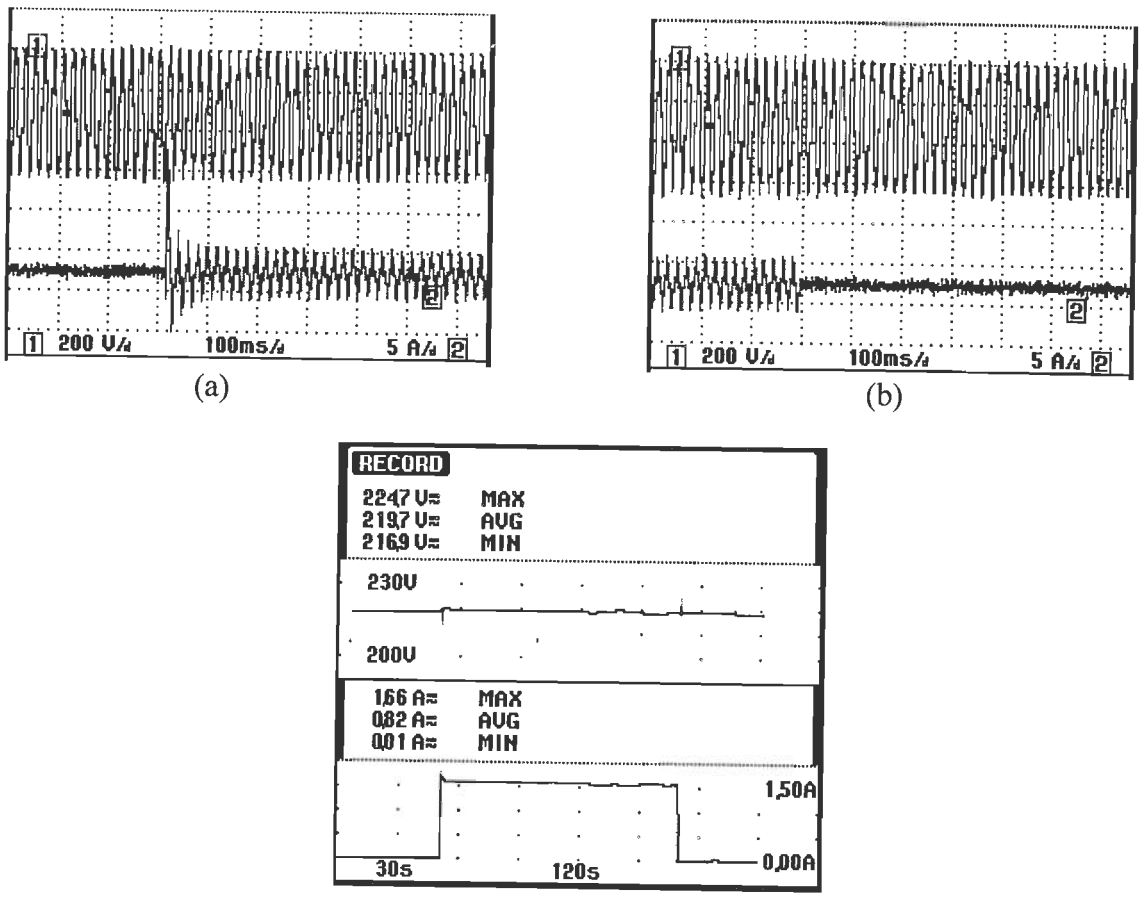


**Figure 5.17: Transient terminal voltage and load current on (a) application (b) removal of 300 W, 0.8 lagging power factor reactive load (c) steady state terminal voltage and load current profile on application and removal of 300 W, 0.8 lagging power factor reactive load.**

On application and removal of load the terminal voltage remains constant. When an inductive load is connected to the SEIG, the voltage will decrease and the load controller responds by reducing the dump load. The reduced load causes an almost instantaneous frequency increase due to reduced slip and an additional gradual increase in frequency due to rising turbine speed. A small increase in frequency results in a significant reduction in magnetizing current. In addition, extra VARs are produced by the excitation capacitors due to reduced impedance which may result in increase of frequency.

Figure 5.18(a) and Figure 5.18 (b) show the transient load voltage and load current waveforms of DSP based load controller for SEIG system at starting, running and removal of single phase 1 HP induction motor at no load. An approximate 15% change in voltage is observed for a few cycles and then it recovers very near to rated value.

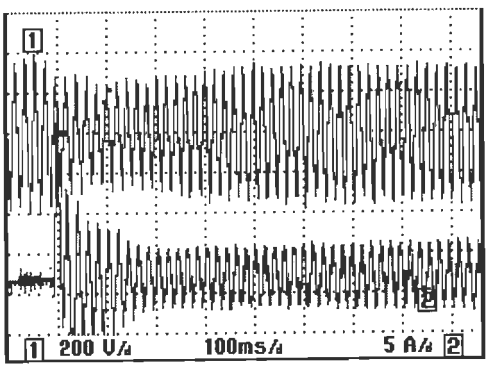


(a)

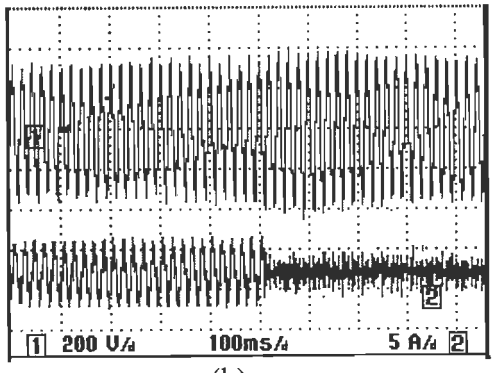


(b)

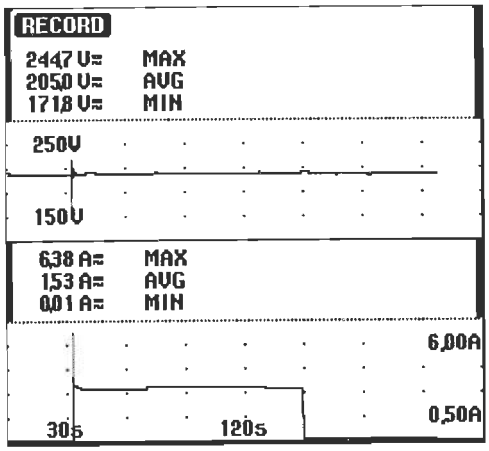


(c)

**Figure 5.18: Transient terminal voltage and load current on (a) application (b) removal of 1 HP induction motor on no load (c) steady state terminal voltage and load current profile on starting , running and removal of 1 HP single phase induction motor on no load.**

Simultaneously, there is a small increase in frequency to compensate for lagging power factor load due to decrease in magnetizing current and hence generator current. Figure 5.18 (c) shows the steady state load voltage and load current trends on starting, running and removal of single phase induction motor. Figure 5.19 and Figure 5.20 shows the measured and simulated frequency under resistive and 0.8 lagging power factor reactive load application respectively. The frequency remains constant with the application of resistive load.

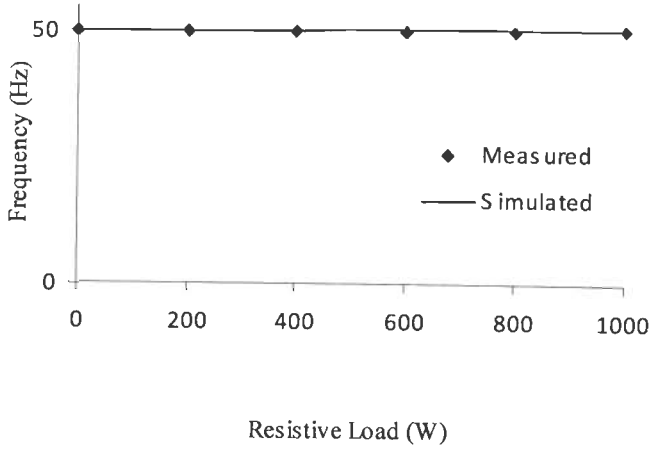


**Figure 5.19: Frequency characteristic of SEIG load controller with resistive load**

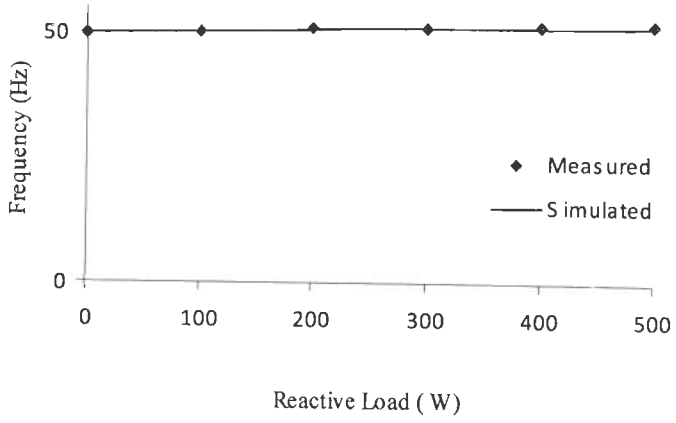


**Figure 5.20: Frequency characteristic of SEIG load controller with reactive load**

### 5.3.5 Harmonic Analysis

The sinusoidal PWM AC chopper circuit is controlled by the switching function *h(t)*, which is generated by comparing a sinusoidal control signal ($v_{con}(k)$) by a triangular wave ($v_{tri}$) as shown in Figure 5.21. As a result, the output voltage may be found from

$$v_o(t) = h(t).v_s(t) \tag{5.38}$$

where, $v_s(t) = V_P \sin \omega_s t$ and $V_P$ is the peak AC voltage, $\omega_s$ is the angular frequency

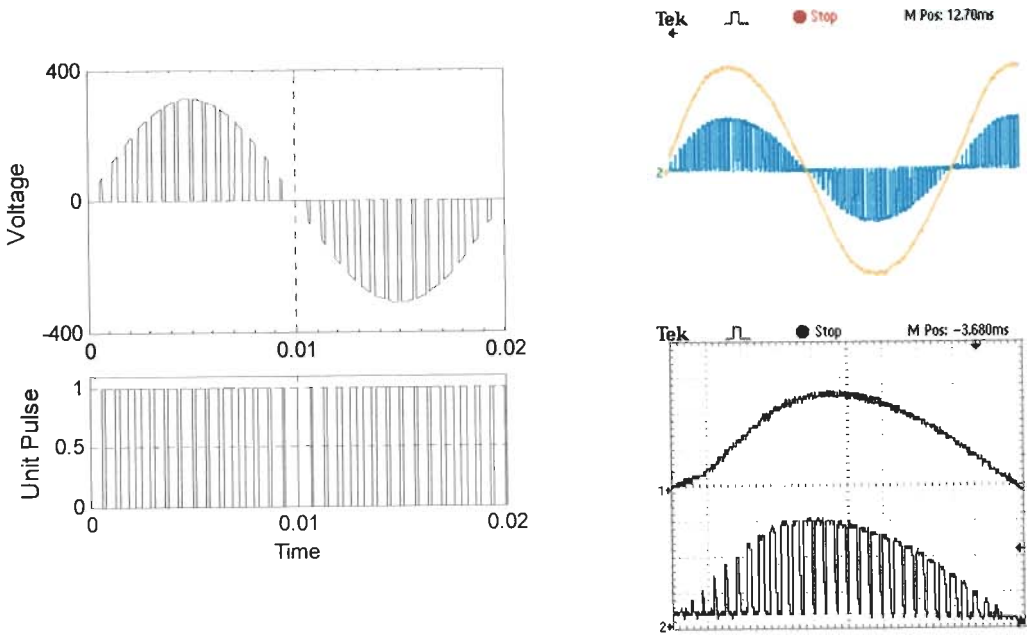


(a) Simulated (b) Experimental

**Figure 5.21: Simulated and experimental sinusoidal PWM sine wave**

The switching function *h(t)* may be expressed in Fourier series as

$$h(t) = C_o + \sum_{n=1}^{\infty} C_n \sin(pn\omega_c t + \phi_n) \tag{5.39}$$

where, $\omega_c$ is the carrier triangular wave angular frequency and p is the frequency ratio($\omega_c/\omega_s$) of carrier triangular wave to source wave.

The output voltage may be expressed as

$$v_o(\omega t) = V_P C_o \sin \omega_s t + \frac{V_P}{2} \sum_{n=1}^{\infty} C_n \cos\{(pn-1)\omega_s t + \phi_n\} - \cos\{(pn+1)\omega_s t + \phi_n\} \tag{5.40}$$

The equation (5.41) reveals the following features of this technique.

(i) The fundamental component of $v_o(t)$ is in phase with $v_s(t)$.

(ii) Only odd harmonics are present.

(iii) Increasing p shifts the lowest order harmonics far from fundamental, making it easy to filter.

(iv) The amplitude of the fundamental component of $v_o(t)$ depends only on the DC value of $h(t)$.

The developed sinusoidal PWM AC chopper controllable SEIG-load controller for single phase SEIG behaves as linear dump load as compared to mark space ratio controlled dump load. The harmonics appeared in dump load voltage and current are of the same order and only odd harmonics are present. The THD appearing in the proposed scheme are less as compared to mark space ratio control despite it doesn't involve any filter capacitor. The change in main load will change the modulation index consequently the pulse width and average period of conduction of load controller. The change in pulse width will change the THD appearing in the system. The dominant order of harmonics is the order of $2P \pm 1$. Where, P is the number of pulse per half cycle. For the present system the carrier frequency is chosen to 3 kHz. Hence minimum order of harmonics appearing is $29^{th}$ and $31^{st}$. Table 5.2 summarizes the main load, terminal voltage, voltage THD and current THD of main load, dump load and generator at different step of resistive and reactive load application. . An increase in voltage and current THD is observed for reactive loads on SEIG.

**Table 5.2 Terminal voltage, voltage THD and current THD at different main load application**

| Load (W) | Voltage (V) | | Voltage THD (%) | | Current THD(%) | | | | | |
|---|---|---|---|---|---|---|---|---|---|---|
| | | | | | Load | | Load Controller | | Gen. Main Winding | |
| | Sim. | Meas. | Sim. | Meas. | Sim. | Meas. | Sim. | Meas. | Sim. | Meas. |
| 0 | 220.2 | 220.5 | 2.36 | 3.1 | - | - | 14.40 | 19.6 | 12.33 | 16.4 |
| 200 | 220.3 | 219.3 | 2.18 | 2.7 | 4.18 | 4.5 | 16.52 | 19.5 | 9.78 | 11.8 |
| 400 | 220.3 | 219.7 | 2.16 | 2.6 | 3.16 | 3.8 | 18.96 | 21.2 | 7.30 | 9.7 |
| 600 | 220.5 | 220.9 | 1.84 | 2.5 | 2.84 | 3.6 | 19.56 | 23.1 | 5.36 | 6.9 |
| 800 | 220.6 | 221.1 | 1.74 | 2.3 | 2.74 | 3.6 | 20.60 | 23.4 | 4.42 | 5.4 |
| 1000 | 220.7 | 221.6 | 1.12 | 2.2 | 2.12 | 3.2 | 24.33 | 25.5 | 4.18 | 5.1 |
| 200W 0.8pf lag | 219.6 | 219.1 | 3.1 | 4.4 | 6.3 | 5.0 | 20.40 | 22.5 | 6.41 | 8.2 |
| 300W 0.8pf lag | 219.1 | 218.1 | 4.3 | 5.2 | 8.3 | 8.6 | 21.10 | 26.6 | 7.36 | 11.4 |
| 400W 0.8pf lag | 218.6 | 217.6 | 4.4 | 6.2 | 11.4 | 12.3 | 24.79 | 29.0 | 11.21 | 16.6 |

Sim.:- Simulated ; Meas.:- Measured; pf lag:- power factor lagging; Gen.:- Generator

## 5.4 CONCLUSION

A DSP based load controller has been designed, developed and implemented for three phase induction motor working as a self excited induction generator and single phase induction motor working as single phase SEIG. The two type of AC chopper controller i.e. equal ratio time control (ERTC) and sinusoidal PWM AC chopper controlled load controller have been designed, developed and implemented. The developed load controller acts as the voltage and frequency regulator for the SEIG. AC chopper control shows the reduction in SEIG-load controller system harmonics. The transient analysis of SEIG load controller system has been carried for resistive, reactive and dynamic load. Form the analysis and experimentation, the following conclusions are drawn.

(i) The terminal voltage remains constant on application and removal of resistive and reactive load. A voltage dip for a few cycles is observed for dynamic load. After few cycle it recovers to rated value.

(ii) The frequency remains constant on application of resistive load . There is a slight increase in frequency on application of reactive load. The variation in frequency is found within satisfactory limits.

(iii) The developed sample based controller is simple as compare to conventional PI controller. The PI controller need to tune for proportional gain ($K_p$) and integral gain ($K_I$) for its dynamic responses while proposed sample based controller need to tune for gain (A) only.

(iv) The load controller based on AC chopper controller is linear in nature. The fundamental component of load controller and source voltage are in phase.

(v) The harmonics appears as the side band and as the integral multiple of switching frequency. The minimum order of harmonic appearing is of higher order. Only odd harmonics are present.

(vi) The THD appearing in SEIG with AC chopper controlled load controller system are less as compare to mark space ratio control despite of it doesn't involve any filter. The total harmonic distortion is under satisfactory limits.

(v) The simulated and the experimental results are in close agreement indicating the effectiveness and accuracy of the developed model.

# CHAPTER-6

# SEIG WITH FUZZY CONTROL LOAD CONTROLLER

## 6.1 INTRODUCTION

The self excited induction generator is one of the suitable choice for harnessing renewable energy such as mini or micro hydro with unregulated turbines. The reduced unit cost, brushless construction, ruggedness and ease of maintenance favors the choice of SEIG as stand alone generator. The SEIG has good dynamic response, self protection against faults and it can generate power at varying speed. The self excited induction generator has poor voltage regulation and frequency regulation. The inherent poor voltage regulation of the SEIG is due to the difference between the reactive power supplied by the excitation capacitors and that demanded by the load and the machine. This is a major bottleneck of its application in isolated mode. In the previous chapters, efforts have been made to regulate the voltage and frequency of the SEIG constant by regulating the load at SEIG terminal. It has also been perceived that a SEIG can supply three phase loads and single phase loads with three phase SEIG single phase SEIG. Such power generating units are suitable for far flung areas where grid connection is not economical and renewable energy can be harnessed from local resources. Hence they must comprise of operational simplicity, less maintenance and can be operated in unattended mode with automatic control. They should have an low-cost controller design with minimum human intervention.

The analytical and experimental study from previous chapters reveals that the use of DSP results in low cost controller design. The fast response, high performance, multiple feature implementations on single processor and flexible solution are other added advantages with DSPs. The digital sample based controller has been developed and implemented which gives speedy response. The sample based controller is simple as compared to traditional PI controller based application. The PI controller is to be tuned for proportional ($K_p$) and integral gain ($K_i$) for acceptable dynamic response, where as in the sample based controller only gain (A) is to be adjusted for a given system to regulate overshoot.

The load controller regulates the voltage and frequency of the SEIG system. The load controller injects harmonics into the system due to its chopping control. Performance of the SEIG is affected by these harmonics. In the previous chapter, effort has been made to reduce these harmonics by introducing AC chopper control. The AC chopper control makes the dump load linear, reduces THD and increases the order of harmonic. The harmonics appear as the side band in odd order and integral multiple of number of pulse in a cycle.

In this chapter, the design and implementation of fuzzy logic controller based on equal time ratio control (ETRC) AC chopper controllable load for SEIG is presented. The fuzzy logic [31, 32, 101, 102, 206] based load controller gives nonlinear control with fast response and virtually no overshoot. The ETRC AC chopper load controller regulates the dump load as linear load with minimum harmonics and excellent dynamic response. A prototype SEIG-load controller system with TMS320F2812 Digital Signal Processor (DSP) has been developed and its transient performance is investigated at different operating conditions such as application and removal of static (resistive and reactive) and dynamic loads.

## 6.2 SYSTEM DESCRIPTION

A schematic diagram of the SEIG-load controller system is shown in Figure 6.1. It consist of a three phase delta connected SEIG driven by a constant power prime mover. The excitation capacitors are connected at the terminals of the SEIG, which have a fixed value to result in rated terminal voltage at rated load. Consumer load and load controller are connected in parallel at generator terminals. The load controller consists of three pair of anti parallel connected static switches (IGBT1-IGBT6), connected in series with a resistive load $R_D$ (dump load).

The SEIG feeds two loads in parallel such that the total power $P_{out}=P_c+P_d$ is constant, Where, $P_{out}$ is the generated power of the generator (which must be kept constant), $P_c$ is the consumer load power, and $P_d$ is the dump load power. This dump load power ($P_d$) may be used for non priority loads such as heating, battery charging, cooking etc. The amount of dump load power is controlled by IGBT switches. The duty cycle of the gate pulse to switches provides the average conduction period and hence the amount of

power to dump load. An equal time ratio control (ETRC) AC chopper approach has been adopted to control dump load.

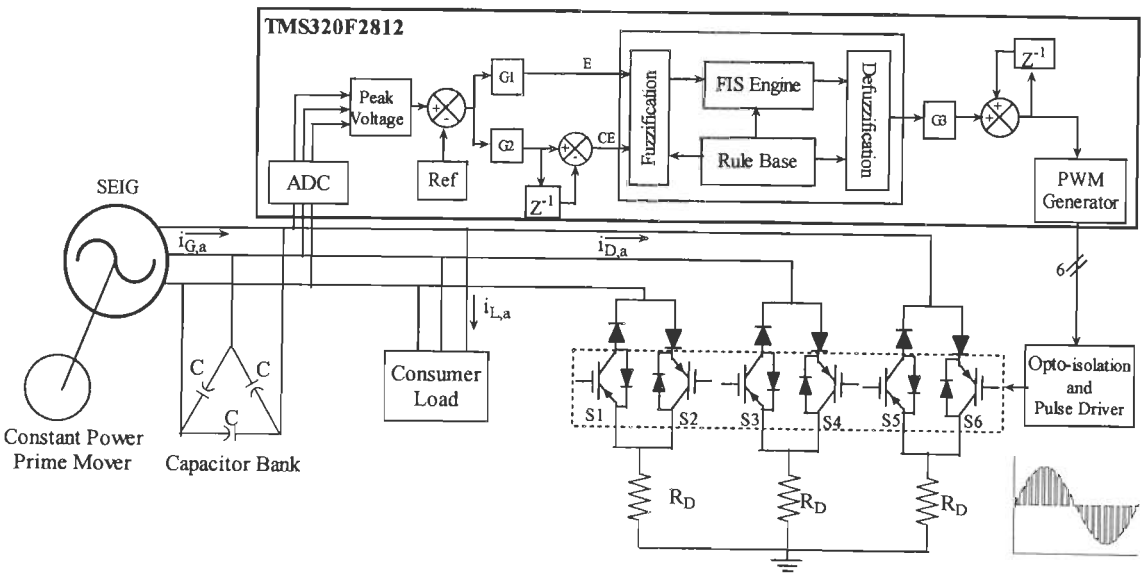


**Figure 6.1: Schematic diagram of three phase SEIG load controller system**

The IGBT (1, 3, and 5) conduct for positive half cycle and IGBT (2, 4, and 6) conduct for negative half cycle of applied AC input. A symmetrical pulse width is applied for conduction of switches. The amount of conduction through dump load is the difference between generated power and consumer load. The voltage amplitude is determined and compared with reference voltage, which is taken as proportional to the rated terminal voltage of the SEIG. The error and change is error is determined. The error and change in error is scaled that transfers the input variables into corresponding universes of discourse. The function of fuzzification converts the input data into suitable linguistic values. These linguistic values are processed through fuzzy inference engine with data base. The data base and rule base characterizes the control goals and control policy of the domain experts by means of a set of linguistic control rules. The defuzzification interface performs a scale mapping, which converts the range of values of output variables into corresponding universe of discourse. The output obtained is the pulse width reference and processed through a PWM generator where it is compared with symmetrical triangular wave to obtain suitable pulse. The pulse generated is given to IGBT switches through opto isolation and amplification.

## 6.3 FUZZY LOGIC CONTROL

The internal structure of the Fuzzy logic controller is shown in Figure 6.1. It comprises of three functional blocks namely, the fuzzzifier, inference system, and the defuzzifier. The fuzzifer converts crisp data into linguistic format. The inference system decides in linguistic format with the help of logical linguistic rules supplied by the rule base and the relevant data supplied by the data base. The output of the inference system passes through the defuzzifier wherein the linguistic format signal is converted back into the numeric form or crisp form. The inference system block uses the rules in the format of "if-then-else".

The error ($e$) and change in error ($ce$) are the two input variables to the fuzzy controller as

$$e(k) = V_t(k) - V_{ref}(k) \tag{6.1}$$

and $$ce(k) = e(k) - e(k-1) \tag{6.2}$$

where, $V_t$ and $V_{ref}$ are terminal voltage and reference voltages at $k^{th}$ sampling time. The essential scaling brings input values into a numeric interval in which the fuzzy variables described known as universe of discourse. The input variables are converted into labels of fuzzy sets in terms of suitable linguistic values, this is called fuzzification process. The scaled inputs are crisp values limited to the universe of discourse of input variables. Triangular membership function (MF) is chosen to evaluate the degree of membership of the input crisp values.

The five level input and seven level output variables and triangular membership functions are shown in Figure 6.2. The Figure 6.3 shows the fuzzy control surface for the defined membership functions and rules. The output MFs are asymmetrical because near the origin (steady state), the signal requires more precision. There are five MFs for error ($e(pu)$), change in error ($ce(pu)$) and seven MFs for output($du(pu)$) signal. The Table 6.1 shows the corresponding rule table for the controller. The top row and left column of the matrix indicate the fuzzy sets of the variable $e(pu)$ and $ce(pu)$ respectively and the MFs of the output variable du are shown in the elements of the matrix. The abbreviation NB, NM, NS, Z, PS, PM, PB are negative big, negative medium, negative small, equal to zero, positive small, positive medium and positive big respectively. There are 5x5 =25 possible rules in the matrix, where a rule read as

IF $e(pu)=PS$ AND $ce(pu)=NB$ THEN $du(pu) = NS$

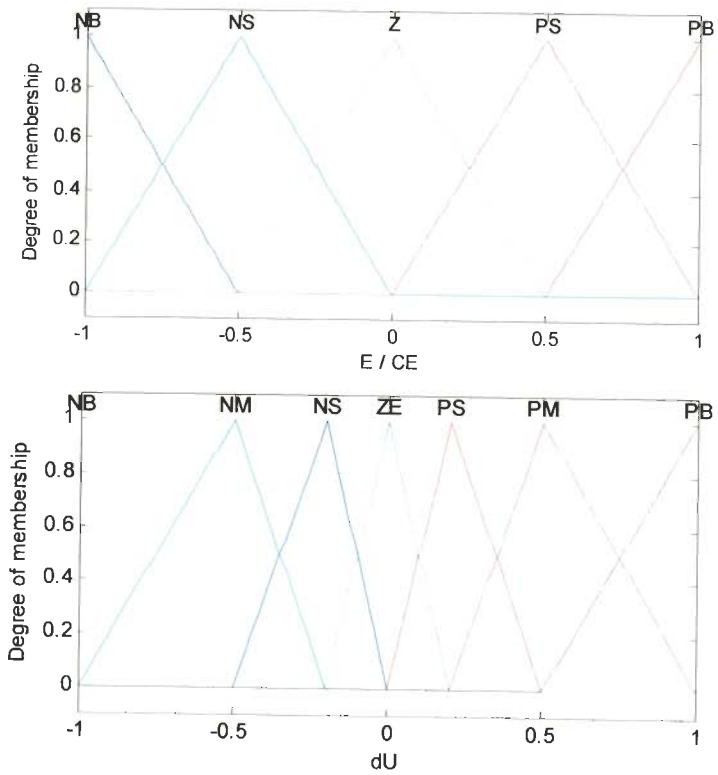


**Figure 6.2: Input and output Membership functions**

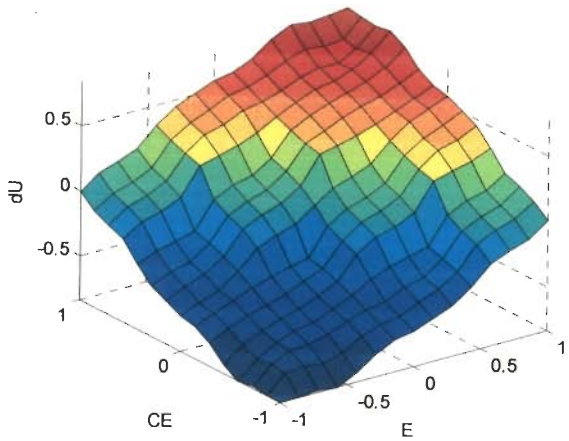


**Figure 6.3: Fuzzy control surface view**

**Table 6.1 Fuzzy rule base matrix**

| e(pu) / ce(pu) | NB | NS | Z | PS | PB |
|---|---|---|---|---|---|
| NB | NB | NB | NM | NS | Z |
| NS | NB | NM | NS | Z | PS |
| Z | NM | NS | Z | PS | PM |
| PS | NS | Z | PS | PM | PB |
| PB | Z | PS | PM | PB | PB |

The value of output signal is determined in accordance with the linguistic rules. The required rules and data are supplied by the rule base. The linguistic output data is converted back into crisp output data by defuzzification. The membership of the corresponding output is taken as minimum membership value for the two respective inputs. Mathematically,

$$\alpha = \min [\mu(\text{input1}), \mu(\text{input2})] \quad (6.3)$$

$$\text{Crisp value} = \{\Sigma p(m)\, \alpha\} / \Sigma \alpha \quad (6.4)$$

where, $\mu$ refers to membership value, the output membership is stored in $\alpha$ and p(m) refer to location of peak of membership function. The defuzzifed (crisp) value multiplied by a scale factor and integrated to obtain the output ($U$).

## 6.4 DIGITAL SIMULATION

Digital simulation of the proposed fuzzy load controller been carried out with MATLAB Version 7.2 on Simulink Version 6.4 with Power System Blockset which facilitates to simulate saturation of asynchronous machines. A 3.73 kW, 400 V, 50 Hz asynchronous machine is used as a SEIG including the machine saturation characteristics which is determined by conducting synchronous speed test. The synchronous speed test specifies the no load saturation curve for induction machine. The voltage and current of synchronous speed test is given in a 2-by-n matrix, where n is the number of points taken from the saturation curve to simulate saturation on MATLAB. The machine parameters are given in Appendix-A. The dropping torque- speed characteristics of prime mover is given as $T_{sh} = k_1 - k_2 \omega_r$; where, $k_1$ and $k_2$ are the prime mover constants given in Appendix A. The terminals of the machines are connected with delta connected capacitor bank of 25 $\mu$F per phase. The output is connected with a controlled dump load and consumer load of resistive and reactive nature. The voltage amplitude is calculated as $V_p = \{2/3(V_{ab}^2 + V_{bc}^2 + V_{ca}^2)\}^{1/2}$ , where $V_{ab}$, $V_{bc}$ , $V_{ca}$ are the line voltage and $V_p$ is the peak amplitude. The peak amplitude is compared with the reference and error is computed. The error and change in error is determined. The error and change in error is scaled that transfers the input variables into corresponding universes of discourse. The function of fuzzification converts the input data into suitable linguistic values. These linguistic values processed through fuzzy inference engine with data base. The fuzzy interface engine has been implemented with MATLAB Fuzzy Logic Toolbox and mamdani method. The MF editor and rule editor defines the MF and rules. The center of area (COA) method has been

used for defuzzification. The defuzzification interface performs a scale mapping, which converts the range of values of output variables into corresponding universe of discourse. The output obtained is the pulse width reference and processed through a PWM generator. The output PWM reference is compared with symmetrical triangular wave through a relational operator to obtain a pulse of suitable duration (width). This pulse is given to gate of the IGBT switches. Figure 6.4 shows the simulation transient waveform of SEIG voltage build up and application of resistive load. The waveform form top to bottom is line voltage ($V_{abc}$), generator current ($I_{abc}$), load current ($I_{L,abc}$) and frequency(f). The no load voltage generation is around 600 V. At time t=0.8 seconds the load controller is switched in, which brings the voltage and frequency to rated value. At time t=1.1 seconds a resistive load of 1500 W is applied. The terminal voltage and frequency remains constant on application of load.

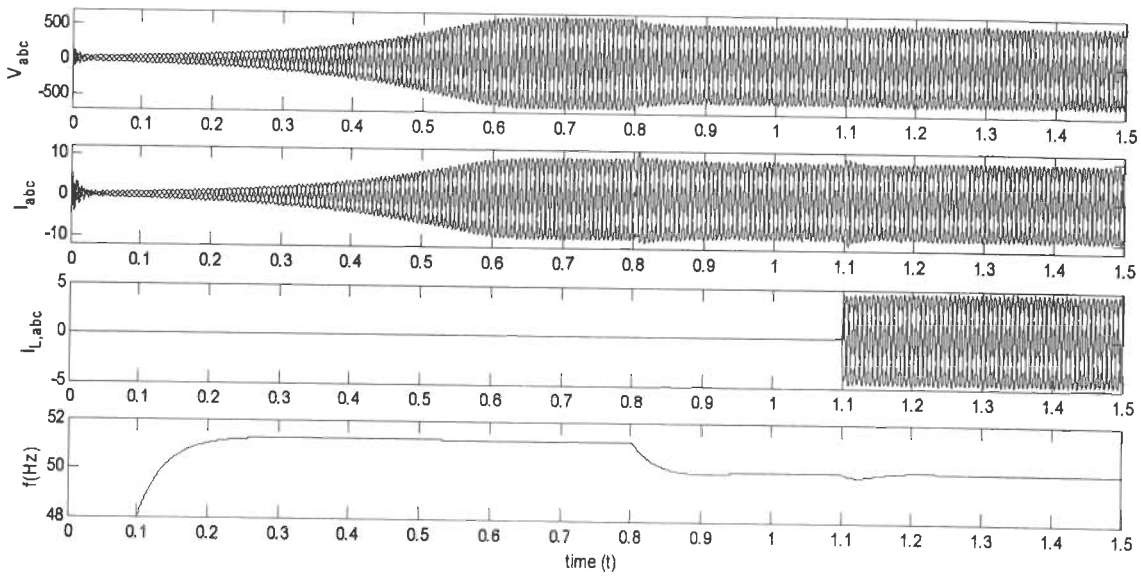


**Figure 6.4: Voltage build up and load controller application**

Figure 6.5 and Figure 6.6 show the transient waveform on application and removal of 1500 W resistive load and 1000 W 0.8 lagging power factor reactive load respectively. The waveform from top to bottom are terminal voltage ($V_{abc}$), generator winding current ($I_{G,abc}$), load current ($I_{L,\ abc}$), dump load current ($I_{D,a}$), and frequency (f). On application of load, the average of dump load current decreases and main load current increases. However, the terminal voltage and frequency remains constant. Figure 6.7 shows the transient waveform on application of dynamic load. On application of reactive load, the terminal voltage remains constant. There is a slight increase in frequency to compensate for reactive power demanded by the load and simultaneously decrease in generator stator current.

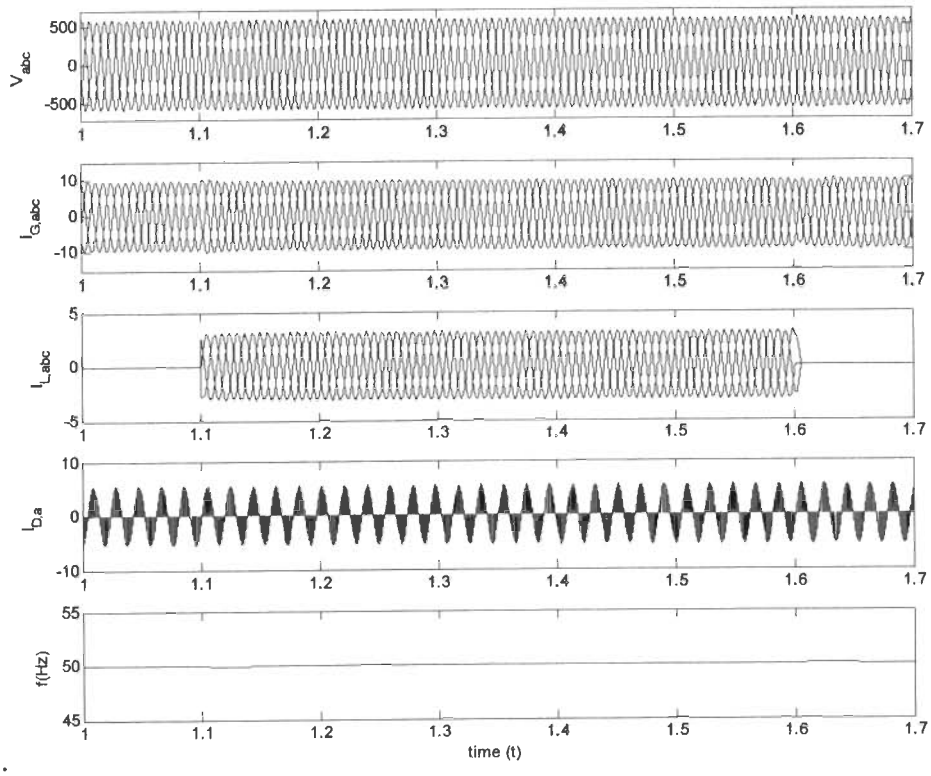


**Figure 6.5: Transient waveform on application of balanced three phase resistive load.**

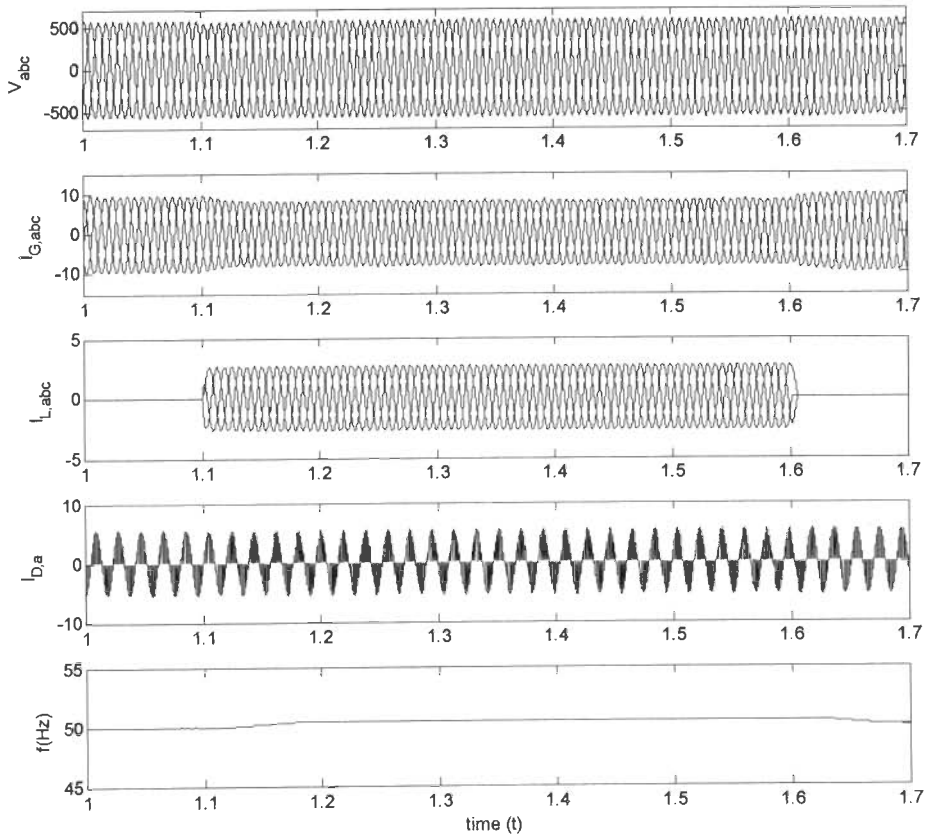


**Figure 6.6: Transient waveform on application of reactive load**

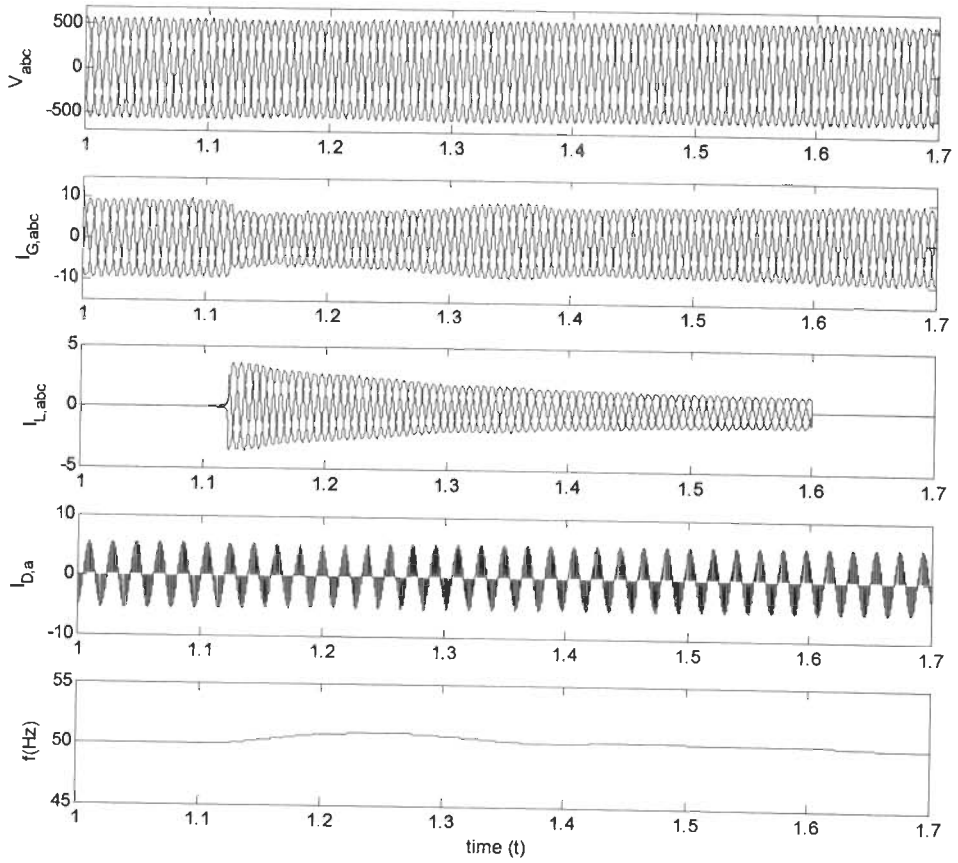


**Figure 6.7: Transient waveform on application of three phase dynamic load.**

## 6.5 IMPLEMENTATION

Figure 6.1 shows the control scheme for voltage regulation of SEIG based on ETRC AC chopper controlled dump load through fuzzy load controller. The AC terminal voltage is sensed through a AC voltage sensor and passed through a signal conditioner. The AC voltage sensor converts AC voltage into corresponding scaled DC voltage. This sensed voltage is read through ADC input of the DSP TMS320F2812. The TMS320F2812 DSP has 16 ADC input channels with an input range of 0-3 Volt. The output values are in the range of 0 to 4095 as the TMS320F2812 DSP ADC is 12- bit analog to digital converter. It reads the input with a sample rate of 0.0001 seconds. The input voltage signal contains peak to peak ripples. A discrete mean is taken to smooth it. The peak amplitude is compared with the set reference, which is taken as proportional to the rated terminal voltage of the SEIG. The error processed through fuzzy controller. The architecture of the TMS320F2812 does not directly support floating-point maths. However, fixed-point

numbers can be converted to floating-point for fuzzy implementation. This reduces the development process, but the application run slower. The amplitude of generated PWM reference gives the modulation index (m). This reference is then given to PWM block of DSP. The PWM block have self symmetric carrier triangular wave. The carrier frequency is selected according to static switching device. In this particular case a carrier frequency of 3 kHz is selected. Higher switching frequency results in less THD and minimum order of harmonic appeared is of higher order. The TMS320F2812 DSP has 6x2 high resolution PWM outputs. Figure 6.8 shows the Matlab based model for automatic code generation to create CCS project for DSP. The pulse out from DSP is processed through opto-isolation and gate driver circuit.

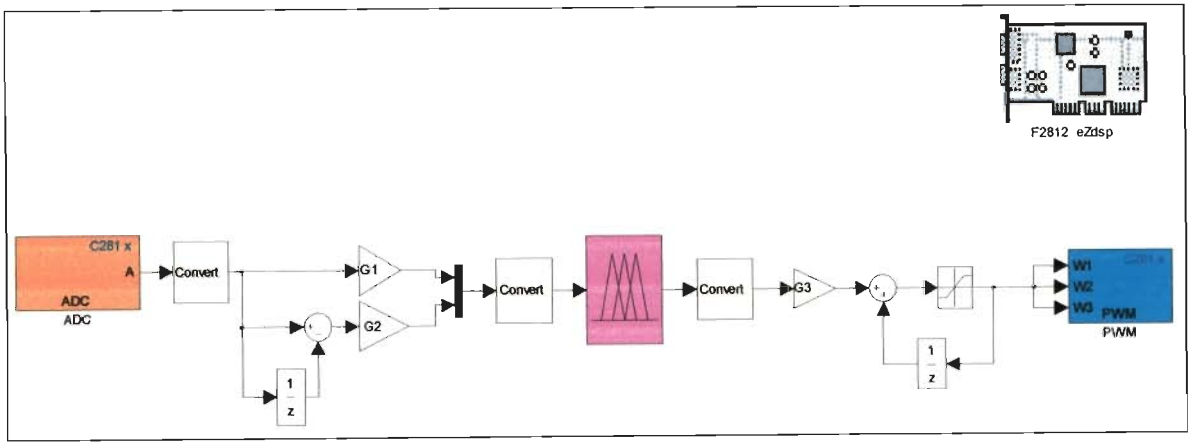


**Figure 6.8: MATLAB model for automatic code generation.**

## 6.6 RESULTS

The prototype of fuzzy ETRC AC chopper controlled load controller based SEIG system has been developed in laboratory and results are obtained for application of static and dynamic loads. A three phase 3.73 kW, 400 V, 7.5 A 50Hz, 1500 rpm squirrel cage induction machine is used as a self-excited induction generator. The SEIG is driven by 220 V, 20 A, 5 HP, 1500 rpm shunt wound DC machine used as a prime mover. To generate 3 kW at 400 V and rated speed, 25 μF capacitor of 400 V is connected in delta across the SEIG terminals. On application of resistive load the terminal voltage and frequency remains constant.

The experimental test results are carried out with three phase balanced resistive load, 0.8 lagging power factor reactive load and induction motor load as dynamic load.

Figure 6.9 shows the experimented transient responses of SEIG-load controller system on application of 1.5 kW three phase balanced resistive load. The waveforms from top to bottom are line voltage ($v_{ab}$) of SEIG, line current of main load ($i_{L,a}$), line current of dump load ($i_{D,a}$) and SEIG line current ( $i_a$). On application of resistive load, main load current increases and dump load current decreases so that power transfers from dump load to consumer load and SEIG experiences constant load on it.

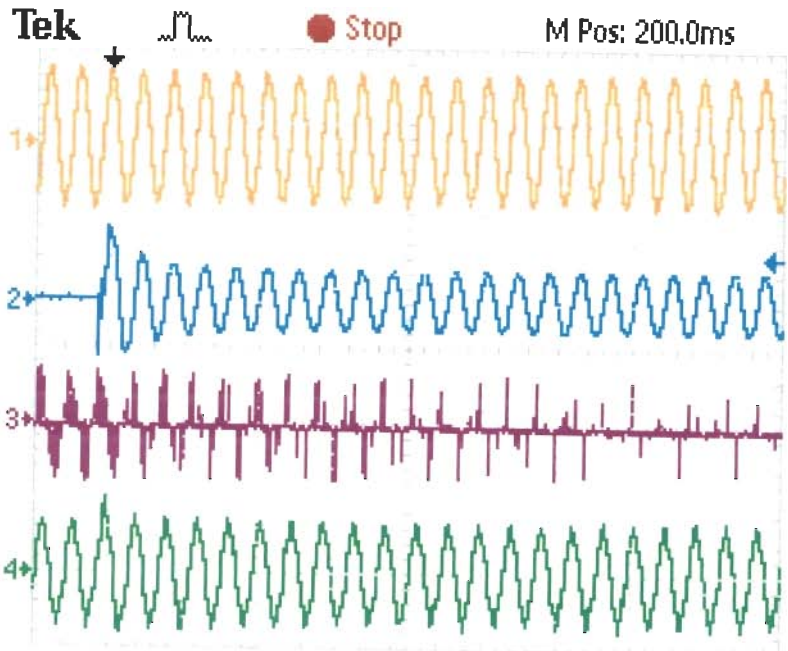


Horizontal scale:-Time 50msec/Div
Vertical scale from ch1 to ch4:-$v_{ab}$ (600V/Div)
$i_{L,a}$ (8A/Div), $i_{D,a}$(8A/Div), $i_a$(8A/Div)

**Figure 6.9: Transient waveform on application of balanced three phase resistive load**

Figure 6.10 shows the transient responses of SEIG system on application of 1kW, 0.8 lagging power factor load. On application and removal of load the terminal voltage remains constant. When an inductive load is connected to the SEIG, it draws a reactive current. Then a part of the excitation capacitance is used to compensate for this reactive current, therefore less capacitive excitation current oscillates between machine winding and excitation capacitor. It react to this with an increase in frequency, causing the capacitors to produce some more magnetizing current while the SEIG needs less so the two balance again and frequency varies as well with the reactive load. The frequency variation caused by reactive load within acceptable range. With SEIG running at a normal degree of saturation, frequency variation would be less. A small increase in frequency

results in a significant reduction in magnetizing current. In addition, extra VARs are produced by the excitation capacitors due to reduced impedance. Figure 6.11 shows the transient responses on application of three phase 1 HP induction motor load at no load.

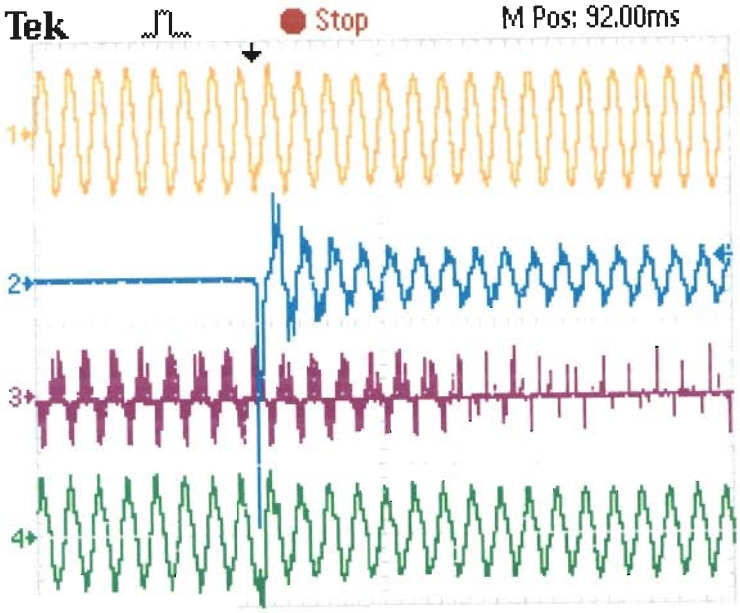


Horizontal scale:-Time 50msec/Div
Vertical scale from ch1 to ch4:-$v_{ab}$ (600V/Div)
$i_{L,a}$ (8A/Div), $i_{D,a}$(8A/Div), $i_a$(8A/Div)

**Figure 6.10: Transient waveform on application of balanced three phase reactive load**

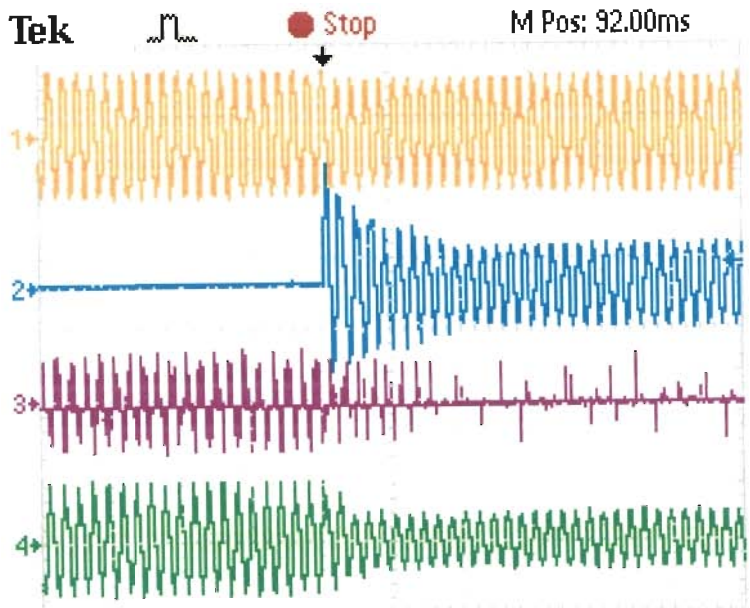


Horizontal scale:-Time 100 msec/Div
Vertical scale from ch1 to ch4:-$v_{ab}$ (600V/Div)
$i_{L,a}$ (4A/Div), $i_{D,a}$(8A/Div), $i_a$(8A/Div)

**Figure 6.11: Transient waveform on starting and running of induction motor load**

## 6.7 HARMONIC ANALYSIS

The output voltage of ETRC AC chopper is comprising of AC voltage, dc reference and triangular carrier wave. The detail expression is given in previous chapter (sec. 5.2.5). The output voltage equation may be written as:

$$v_o(t) = V_P\, m\, \sin(\omega_s t) + \frac{V_P}{\pi}\sum_{n=1}^{\infty}\frac{1}{n}\sin(n m \pi)\times\sin[\{(np+1)\omega_s t - n m \pi\} + \sin\{(1-np)\omega_s t + n m \pi\}] \quad (6.5)$$

The Fourier analysis of output voltage of AC chopper reveals that only odd harmonics are present. The dump load is comprised of resistive load only. The current profile follows the voltage profile. The minimum order of harmonic is integral multiple of $2P \pm 1$ where, P is the number of pulse per half cycle. The P=30 for 3kHz carrier frequency, the minimum order of harmonic is of the order of $29^{th}$ and $31^{st}$ and so on. The change in main load will change the modulation index consequently the pulse width and average period of conduction of load controller. The change in pulse width will change the THD appearing in the system. A suitable design of dump load minimizes the THD variations. The AC chopper is directly connected at the terminals of SEIG. The SEIG terminals are shunt connected with delta connected capacitor bank. The SEIG stator winding comprises of self inductance. The combination works as a passive filter for generated harmonic. The consumer load is not affected with AC controller harmonics as they are of higher order, low in magnitude and filtering effect of SEIG system.

## 6.8 CONCLUSION

A DSP based Fuzzy ETRC AC chopper controllable load controller has been designed, developed and implemented for induction motor working as a self excited induction generator. The developed load controller system acts as the voltage and frequency regulator for the SEIG. The load controller presented in previous chapters is based on sample based controller. The sample based controller based application is simple as compared to traditional PI controller based application and only gain (A) need to be adjusted for acceptable dynamic response. The tuning of gain (A) depends upon the motor parameters. In this chapter, an auto tuned fuzzy logic based load controller is presented. The simulation is carried out in MATLAB/SIMULINK environment. The performance of fuzzy logic based SEIG load controller has been tested for different operating conditions

such as application and removal of static and dynamic loads. From analysis and experimentation following conclusions are drawn:

(i) The terminal voltage remains constant on application and removal of resistive and reactive load. A voltage dip for a few cycles is observed for dynamic load. After few cycle it recovers at rated value.

(ii) The frequency remains constant on application of resistive load. There is a slight increase in frequency on application of reactive load. The variation in frequency is found within satisfactory limits.

(iii) The Fuzzy logic based controller gives nonlinear control with fast response and virtually no overshoot. The fuzzy logic control has advantage of coping with larger parameter variation of the system and it provides improved performances in terms of overshoot limitation and sensitivity to parameter variation.

(iv) The proposed Fuzzy based load controller has been designed and implemented using TMS320F2812 fixed point processor. The architecture of the TMS320F2812 does not directly support floating-point maths. However, fixed-point numbers can be converted to floating-point for fuzzy implementation. This reduces the development process, but the application run slower.

(v) The load controller based on AC chopper controller is linear in nature. The fundamental component of load controller and source voltage are in phase.

(vi) The harmonics appear as the side band and are the integral multiple of switching frequency. Only odd harmonics are present.

(vii) The THD appearing in SEIG with AC chopper controlled load controller system are less as compared to mark space ratio control despite of it doesn't involve any filter. The total harmonic distortion is within acceptable limits.

(viii) The simulated and the experimental results are in close agreement indicating the effectiveness and accuracy of the developed controller.

# CHAPTER-7

# STATCOM BASED VOLTAGE AND FREQUENCY REGULATION OF SEIG

## 7.1 INTRODUCTION

In the previous chapters, efforts have been made to regulate the voltage and frequency of the SEIG constant by keeping the load at SEIG terminal constant through a load controller and dump load in parallel with consumer load. The load controller does not compensate for variable reactive power demand. The performance of SEIG is largely affected by power factor of the load as it draws the reactive current. Then, a part of the excitation capacitance is used to compensate for this reactive current, thus less leading VARs are available for the SEIG itself. The other part of load controller is that it injects harmonics in the SEIG system. The AC chopper based load controller reduces the harmonics in the system up to satisfactory level. In practice, with the increased used of electronic equipments, a large number of consumer load are nonlinear in nature and therefore, they inject harmonics in the system. The SEIG's performance is also affected by these harmonics. Hence there is a need to develop a control scheme to regulate the voltage and frequency of the SEIG with variable reactive power compensation and harmonic elimination.

The literature review reveals that several attempts have been made to maintain the constant terminal voltage by switched capacitor [64, 65], and thyristor controlled inductor as static VAR compensator (SVC) [1, 2, 4, 7, 33], saturable core reactor [129], long and short shunt connections of capacitors [167]. The voltage regulation or reactive power compensation provided by these schemes is stepped in nature and injects harmonic in the SEIG system. The static VAR compensator uses either thyristor switched capacitors (TSCs) or thyristor controlled reactor (TSR) with fixed capacitor but it require large valued capacitors and reactors. Marra et al. [125, 126] have reported a pulse width modulation bidirectional voltage-fed converter for voltage and frequency regulation. It proposes a chopper controlled dump resistance to regulate the voltage and VSI inverter for reactive power compensation. Kuo and wang [96, 98] have described a method of voltage

control of SEIG under unbalanced, nonlinear load using a current controlled voltage source inverter. Bhim Singh et al. [177, 178, 179, 185, 186] have presented a design procedure to compensate for reactive power of SEIG through static compensator (STATCOM). Larsen et al [100] have described the benefits of STATCOM over the SVC system. STATCOM employees a voltage source inverter with self supporting DC bus and coupling inductor, which provide capacitive and inductive reactive power compensation.

The generated voltage of the SEIG depends upon the speed, excitation capacitance, load current and power factor of the load. The prime mover may be micro hydro low head unregulated turbine, biomass or oil driven engine which have constant power input. The terminal voltage depends upon the excitation capacitance and load current. The steady state performance characteristics of three phase SEIG can be computed using steady state model and given in section 2.3.2. Figure 7.1(a) shows the terminal voltage variation with different capacitor value connected in delta at 5 HP induction motor working as SEIG. There is a drop in terminal voltage as the load on SEIG terminal increases. When a reactive load is connected to the SEIG, it draws a reactive current. Then a part of the excitation capacitance is used to compensate for this reactive current, so less capacitance is available for the SEIG itself. Figure 7.1(b) shows the effect of load power factor on SEIG performance. The output power as well as terminal voltage decreases as there is drop in load power factor. The static compensator (STATCOM) compensate for reactive power with increase in load current. STATCOM comprises a current controlled voltage source inverter with self sustained DC bus capacitor and coupling inductor. The DC bus capacitor and coupling inductor together works as a second order filter and eliminates harmonics in the system. STATCOM balances the phase current and thus works as a load balancer.

In this chapter a digital control algorithm for STATCOM based SEIG system has been presented. The control algorithm has been first co-simulated with processor in the loop (PIL) using TMS320F2812 fixed point DSP and then experimentally validated. The Processor-in-the-loop (PIL) provides one verification capability in development process. It is a co-simulation technique which helps to evaluate as how well a control algorithm operates on the fixed point digital signal processor selected for the application. The transient behaviour of SEIG-STATCOM system at different operating conditions such as

application and removal of balanced/unbalanced, nonlinear and dynamic load is investigated.

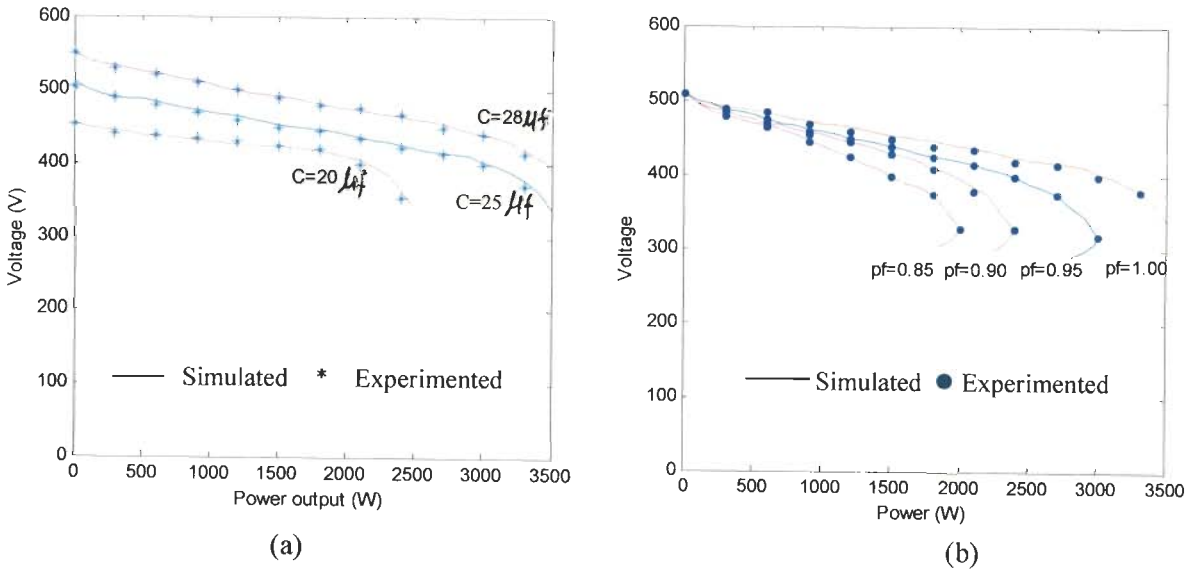


**Figure 7.1: Variation of terminal voltage with output power at different excitation capacitor and load power factor**

## 7.2 STATCOM BASED SEIG SYSTEM WITH LOAD CONTROLLER

### 7.2.1 System Description

The schematic diagram of the SEIG with excitation capacitor, current controlled voltage source inverter with DC bus capacitor (STATCOM), consumer load and chopper controlled dump load is shown in Figure 7.2. The excitation capacitors are connected at the terminals of the SEIG, which have a fixed value to result in rated terminal voltage at no load. The SEIG generate constant voltage and power at fixed value of excitation capacitor when load is kept constant. Consumer load and chopper controlled dump load are connected in parallel at generator terminals. The chopper controlled dump load consists of an uncontrolled rectifier, a filtering capacitor, IGBT based chopper and a series resistive (dump) load. The uncontrolled rectifier converts the SEIG AC terminal voltage to DC. The output ripples are filtered by filter capacitor ($C_f$). An IGBT is used as a chopper switch. When gate pulse to IGBT is high, the current flows through the dump load and the power is consumed. The pulse width or duty cycle of chopper is decided by the difference of output power to consumer load. The performance of SEIG is largely affected by power factor of the load. The nonlinear consumer load and chopper control injects harmonics in

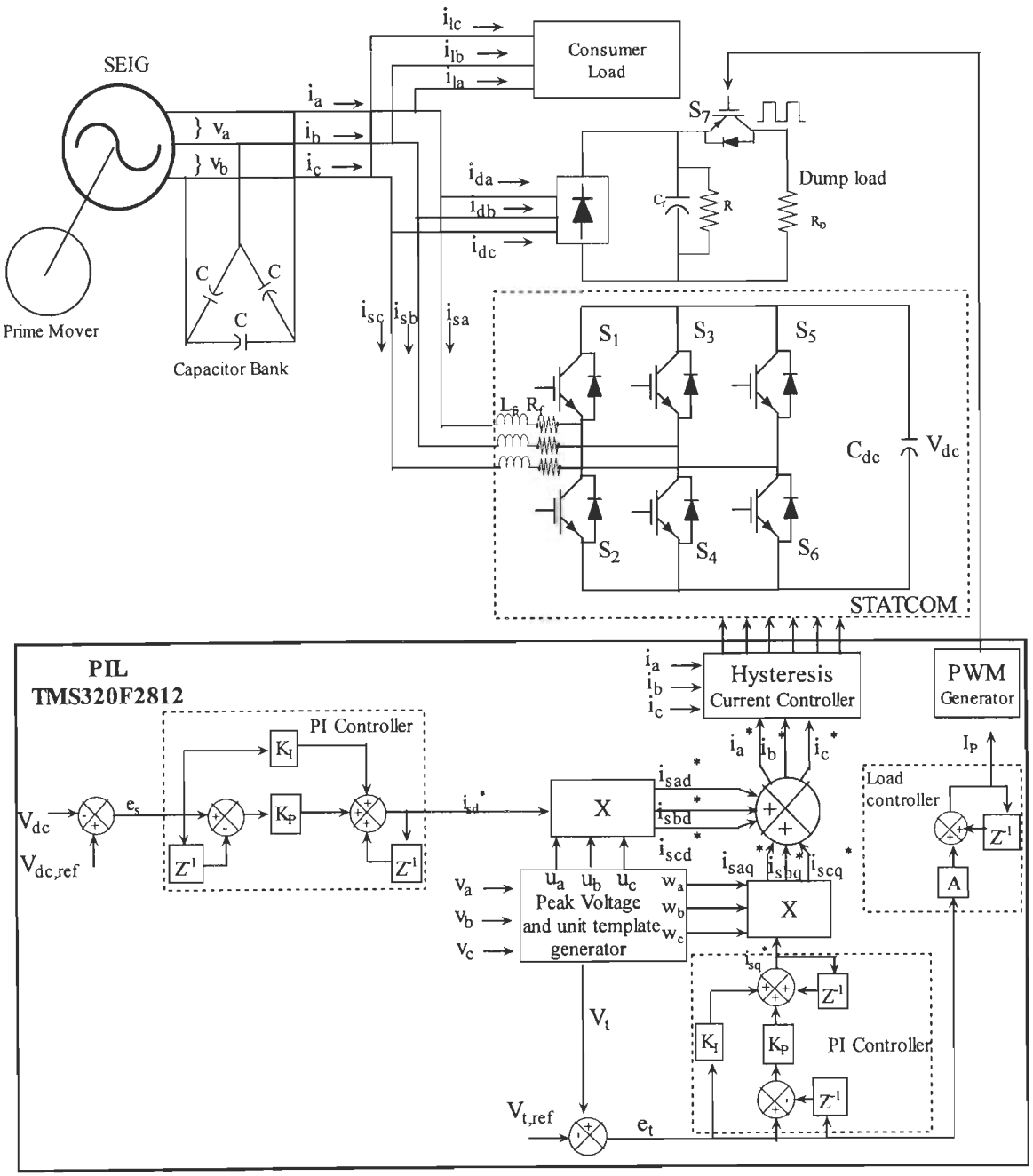


**Figure 7.2: Schematic diagram of three phase SEIG-STATCOM system.**

the system. The SEIG's performance is affected by these harmonics. A current controlled voltage source inverter (CC-VSI) working as STATCOM is used for harmonic elimination, load balancing, and reactive power compensation. It consist of three phase IGBT based inverter, DC bus capacitor, and AC inductors. The output of the inverter is connected through the AC filtering inductor to the SEIG terminals. The DC bus capacitor is used to filter voltage ripples and provide self-supporting DC bus.

### 7.2.2 Processor-in-the-loop

Processor-in-the-loop provides one verification capability in development process [227]. It is a co-simulation technique which helps to evaluate as how well a control algorithm operates on the fixed point digital signal processor selected for the application. The term co-simulation is a division of process in which Simulink software models the system, while code generated from the controller subsystem runs on the processor hardware. This bridges the gap between simulation and final system configuration.

In the PIL co-simulation, Real-Time Workshop software generates an executable application for the PIL algorithm. This code runs (in simulated time) on a processor platform. The system model remains in Simulink software without the use of code generation. Figure 7.3 shows the PIL co-simulation process. The simulink software simulates the SEIG-STATCOM model for one sample interval and exports the output signals ('Yout' of the system) to the processor platform via code composer studio integrated dovelopment environment (CCS link IDE). When the processor platform receives signals from the model, it executes the PIL algorithm for one sample step.

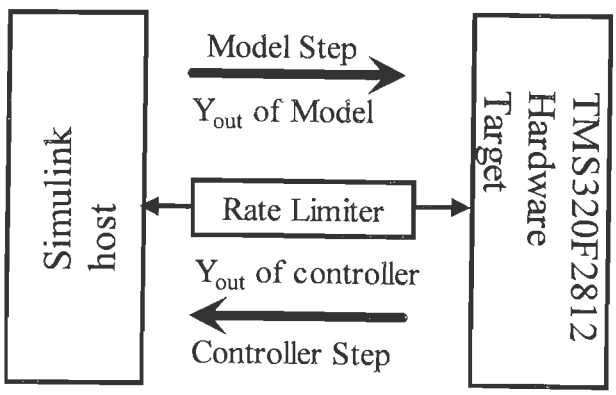


**Figure 7.3:- Process of PIL co-simulation.**

The PIL algorithm returns its output signals ('Yout' of the algorithm) computed during this step to Simulink software, via CCS link IDE interface. At this point, one sample cycle of the simulation is complete and the system model proceeds to the next sample interval. The process repeats and the simulation progresses. After each sample period, the simulation halts to ensure that all data has been exchanged between the Simulink and object code. PIL co-simulation is a slow process. The simulink software simulates the SEIG-STATCOM model for one sample interval and exports the output signals to the processor platform. When the processor receives signals from the model, it executes the PIL algorithm for one sample step. The code runs in simulated time on a processor.

### 7.2.3 Control Scheme

The schematic diagram of the STATCOM based SEIG system is shown in Figure 7.2. The control scheme to regulate the terminal voltage, frequency, load balancing, reactive power compensation and harmonic elimination of the SEIG system is based on the controlling of source currents and the load at SEIG. The peak voltage amplitude ($V_t$) is calculated and amplitude is compared with the reference. The error ($e_t$) is processed through the load controller. The output of the controller is compared with symmetrical triangular wave to obtain a pulse of suitable duration (width). This pulse is given to gate of the IGBT chopper switch. The unit templates ($u_a, u_b$, and $u_c$) quadrature unit template ($w_a$, $w_b$ and $w_c$ ) are computed by AC line voltages ($v_a$, $v_b$, and $v_c$) and their peak amplitude ($V_t$). The error ($e_t$) is processed through digital PI controller based on backward difference method and output quadrature reference ($i_{sq}$) is obtained. The DC bus voltage ($V_{dc}$) is compared with the reference ($V_{dc,ref}$) and error($e_s$) is processed through digital PI controller and output ($i_{sd}$) is obtained. The output references ($i_{sd}$, $i_{sq}$) is multiplied with unit templates and algebraically added to obtain reference source currents ($i_a^*$, $i_b^*$, and $i_c^*$). The reference source current are compared with actual line current ($i_a$, $i_b$, and $i_c$) and processed through the hysteresis current controller to obtain the pulse for STATCOM.

The peak amplitude of voltages ($V_t$) is computed as

$$V_t = \{(2/3)(v_a^2 + v_b^2 + v_c^2)\}^{1/2} \tag{7.1}$$

where, $v_a$, $v_b$ and $v_c$ are the SEIG terminal line voltages.

The unit vectors in phase with $v_a$, $v_b$, $v_c$ are computed as

$$u_a = v_a/V_t; \quad u_b = v_b/V_t; \quad u_c = v_c/V_t; \tag{7.2}$$

the unit vector in quadrature with , $v_a$, $v_b$ and $v_c$ may be derived as:

$$w_a = (-u_b + u_c)/\sqrt{3};$$

$$w_b = \sqrt{3}u_a/2 + (u_b - u_c)/2\sqrt{3};$$

$$w_c = -\sqrt{3}u_a/2 + (u_b - u_c)/2\sqrt{3} \tag{7.3}$$

the AC voltage error at k[th] sampling instant is computed as:

$$e_t(k) = V_{t,ref}(k) - V_t(k) \tag{7.4}$$

where, $V_{t,ref}(k)$ is the reference peak amplitude of AC voltage. For digital implementation, PI controller is discretised using the backward difference method. The output of the digital PI controller for maintaining the AC terminal voltage of the STATCOM at $k^{th}$ sampling instant is:

$$i_{sq}(k) = i_{sq}(k-1) + K_P[e_t(k) - e_t(k-1)] + K_I e_t(k) \tag{7.5}$$

where, $K_P$ and $K_I$ are the proportional and integral gain constants of the PI controller, $e_t(k)$ and $e_t(k\text{-}1)$ are the AC peak voltage errors at the $k^{th}$ and $(k\text{-}1)^{th}$ sampling instant, and $i_{sq}(k\text{-}1)$ is the amplitude of the reference source current at $(k\text{-}1)^{th}$ sampling instant.

The quadrature component of the reference source current is estimated as:

$$i^*_{saq} = i_{sq}w_a; \quad i^*_{sbq} = i_{sq}w_b; \quad i^*_{scq} = i_{sq}w_c; \tag{7.6}$$

To maintain the DC bus voltage of the CC-VSI constant, the DC bus voltage error, $e_s(k)$ at $k^{th}$ sampling instant is computed as:

$$e_s(k) = V_{dc,ref}(k) - V_{dc}(k) \tag{7.7}$$

where, $V_{dc,ref}(k)$ is the reference DC voltage and $V_{dc}(k)$ is the DC link voltage of CC-VSI at $k^{th}$ sampling instant.

The output of the digital PI controller for maintaining the dc bus voltage of the STATCOM at $k^{th}$ sampling instant is:

$$i_{sd}(k) = i_{sd}(k-1) + K_P[e_s(k) - e_s(k-1)] + K_I e_s(k) \tag{7.8}$$

where, $K_P$ and $K_I$ are the proportional and integral gain constants of the PI controller, $e_s(k)$ and $e_s(k\text{-}1)$ are the dc voltage errors at the $k^{th}$ and $(k\text{-}1)^{th}$ sampling instant, and $i_{sd}(k\text{-}1)$ is the amplitude of the reference source current at $(k\text{-}1)^{th}$ sampling instant.

The in-phase component of reference source current are estimated as

$$i^*_{sad} = i_{sd}u_a; \quad i^*_{sbd} = i_{sd}u_b; \quad i^*_{scd} = i_{sd}u_c; \tag{7.9}$$

The reference source current from equation (7.6) and equation (7.9) is given as

$$i_a^* = i_{sad}^* + i_{saq}^*; \qquad i_b^* = i_{sbd}^* + i_{sbq}^*; \qquad i_c^* = i_{scd}^* + i_{scq}^*; \tag{7.10}$$

The estimated reference source current is compared with the actual load current and error is processed through hysteresis controller for obtaining the switching pulses.

The terminal voltage error ($e_t$) is processed through a load controller. The output of the load controller at $k^{th}$ sampling instant is given as:

$$I_P(k) = A\, e_t(k) + I_P(k-1) \tag{7.11}$$

where, A is the gain of the controller to adjust overshoot, $I_P$ *(k-1)* is the load controller reference at $(k\text{-}1)^{th}$ sampling instant. The generated reference $I_P$ is compared with symmetrical triangular carrier wave to generate pulses to compensate for variation in consumer load.

### 7.2.4 PIL Co-Simulation

Digital simulation of the proposed SEIG-STATCOM system has been carried out with MATLAB Version 7.6 on Simulink Version 7.1. This Power System Blockset facilitates to simulate saturation in asynchronous machines. A 3.73 kW, 400 V 50 Hz star connected asynchronous machine is used as an SEIG including the machine saturation characteristic which is determined by conducting synchronous speed test. The synchronous speed test specifies the no load saturation curve for the induction machine. The machine parameters are summarized in Appendix-A. The drooping torque- speed characteristic of prime mover is given as $T_{sh} = k_1 - k_2\omega_r$; where, $k_1$ and $k_2$ are the prime mover constants given in Appendix-A. A delta connected capacitor of 25 μF per phase is connected across machine terminals to maintain rated terminal voltage at rated speed as shown in Figure 7.4. The consumer load, chopper controlled dump load and STATCOM are connected in parallel with the generator terminals.

The control algorithm is objected to TMS320F2812 fixed point digital signal processor which supports the fixed point data and fixed point algorithm. The control algorithm is created in a subsystem with target preference to F2812 eZdsp from Matlab embedded target support library for TI C2000. The subsystem is then build from real time workshop to create PIL block. The generated s-function PIL block is then placed with system model with appropriate rate limiter and data type converter blocks replacing existing subsystem as shown in Figure 7.5.

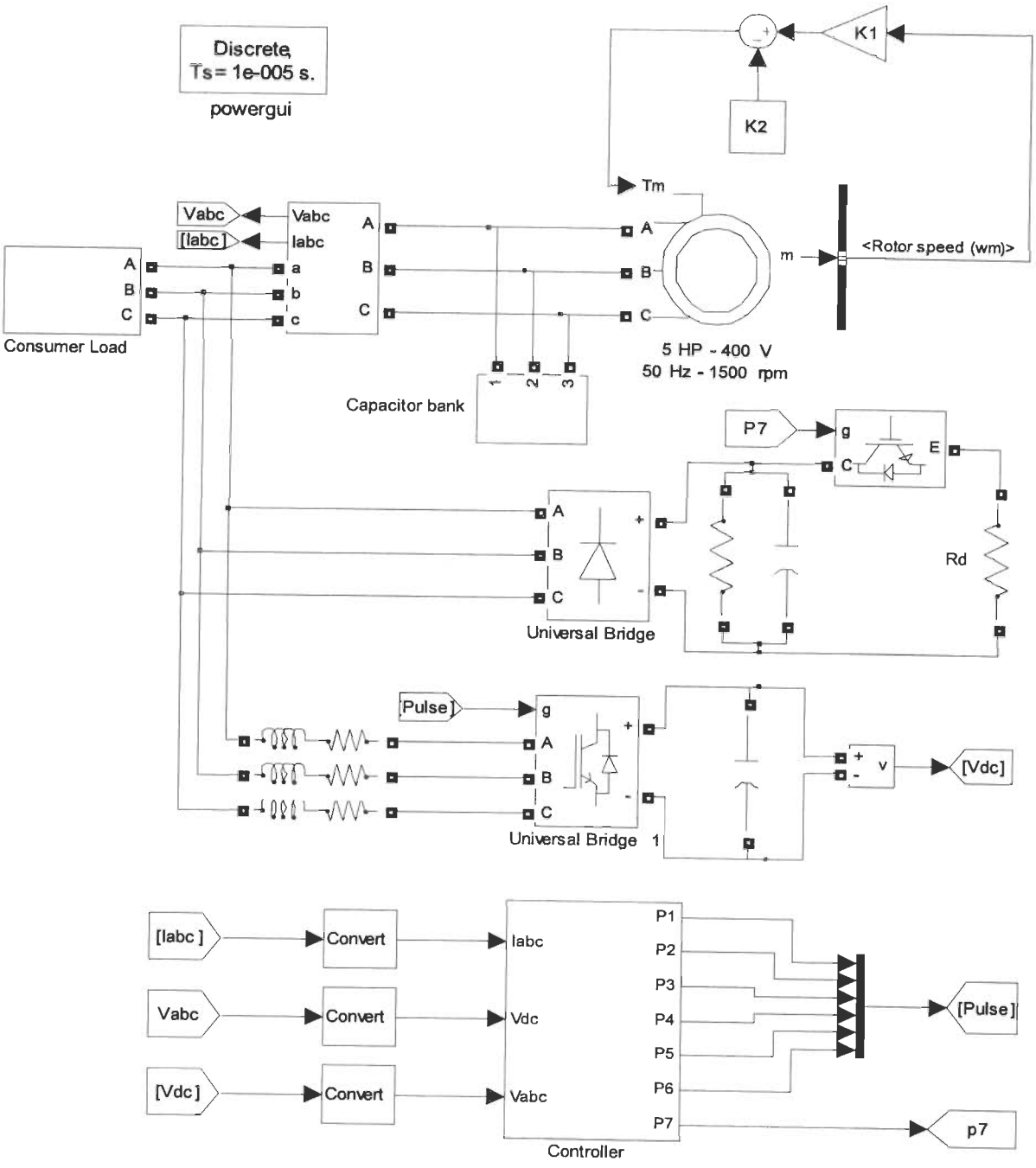


**Figure 7.4: Schematic diagram of MATLAB based model of SEIG-STATCOM**

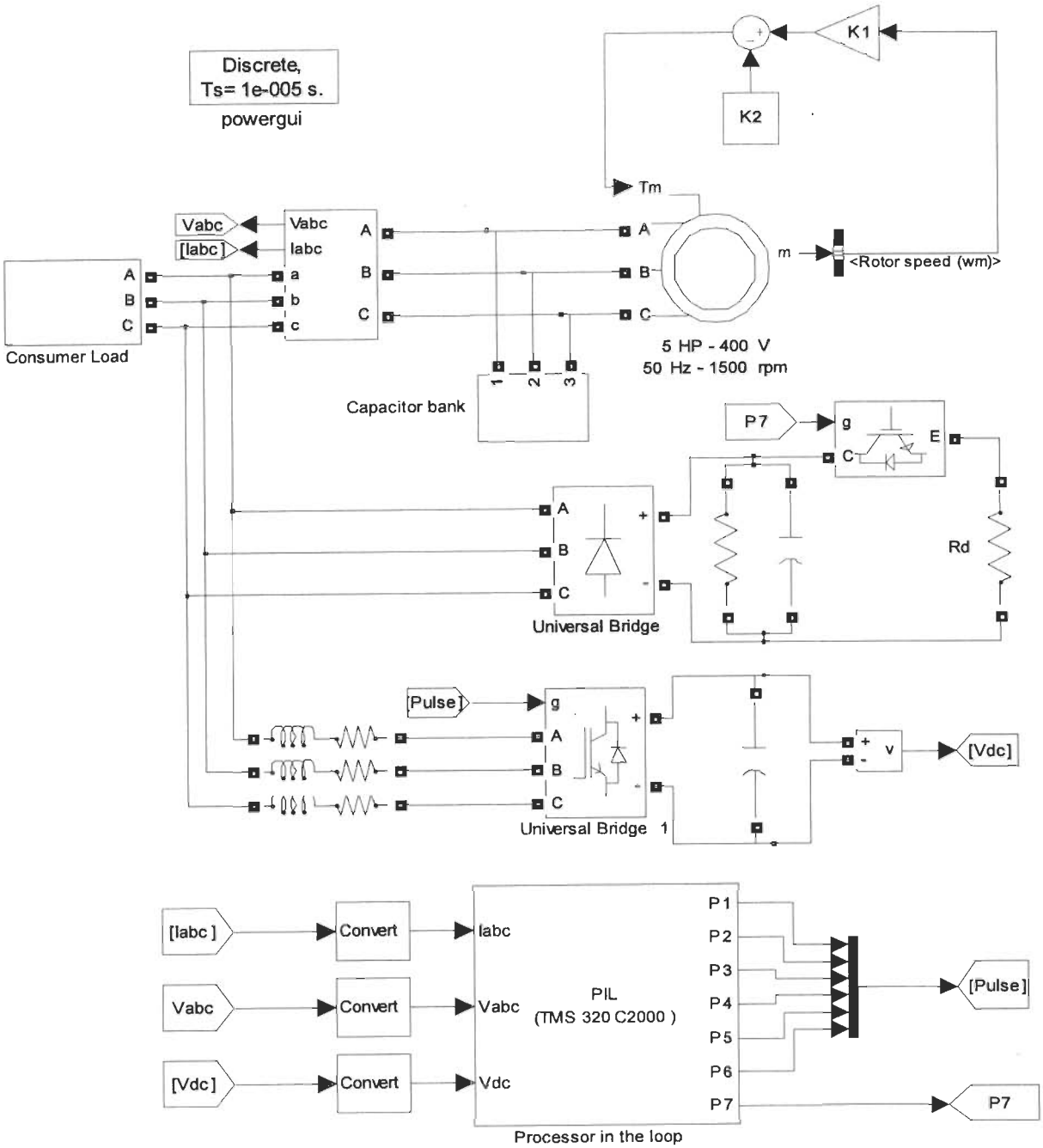


**Figure 7.5: Schematic diagram of MATLAB based model of SEIG-STATCOM with PIL co-simulation**

The PIL block contains the controller algorithm. IQN math library support is taken for fixed point algebric calculations. The peak amplitude is compared with the reference and processed through the controller. The output of the controller is compared with symmetrical triangular wave and through a relational operator to obtain a pulse of suitable duration (width).

This pulse is given to gate of the IGBT chopper switch. A universal bridge is used as a diode rectifier and filtering capacitor is added for smoothening and filtering. The DC bus voltage is compared with reference and error is processed through digital PI controller. The obtained reference is multiplied with unit template to generate reference currents. The reference currents are then compared with system model current and error is processed through a hystersis band to generate appropriate pulses for STATCOM.

### 7.2.5 Results

The SEIG-STATCOM system for voltage and frequency regulation supplying balance, unbalanced and non-linear loads is co-simulated and real time simulation results are shown. Figure 7.6 shows the transient waveforms of voltage buildup and switching in of the STATCOM and chopper controlled dump load working as a voltage and frequency regulator for three phase balanced resistive load. Waveforms from top to bottom are SEIG ac line voltages ($v_{abc}$) , line currents ($i_{abc}$), STATCOM currents ($i_{s,abc}$), dump load currents ($i_{D,abc}$), balanced resistive load currents ($i_{l,abc}$), dc bus voltage ($V_{dc}$), peak amplitude of ac terminal voltage($V_t$) and frequency (f). The process of voltage build up start with remnant field. An initial stator current is assumed to initiate the process. The dc bus capacitor is charged through the anti-parallel diodes of VSI. At time t = 0.55 seconds gate pulses are given to IGBTs of STATCOM and chopper controlled dump load. The STATCOM behaves as a source of the reactive power and draws the active power from the generator to charge its dc bus capacitor to reference voltage of 680 V. There is a dip in terminal voltage which recovers to rated 400 V (565 V- peak). The frequency also drops to 50 Hz rated. At time t = 0.7 seconds, a balance three phase resistive load of 1500 W is applied. On application of load, terminal voltage and frequency remains constant to their rated value. The STATCOM and dump load current are adjusted accordingly.

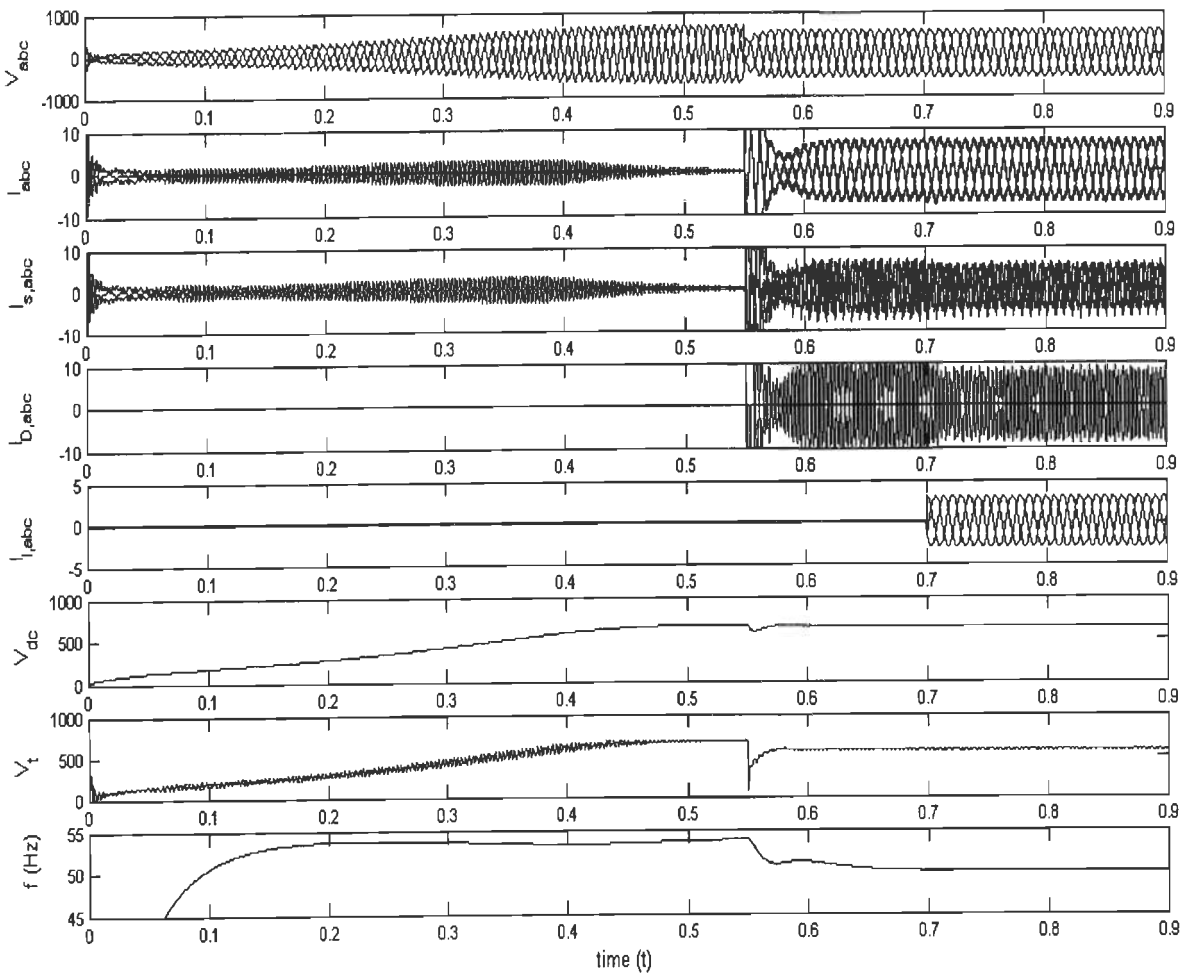


**Figure 7.6: Waveforms for SEIG voltage build up, switching in of STATCOM and balanced three phase resistive load**

Figure 7.7 shows the transient waveforms during switching of reactive balanced and resistive unbalanced load. At time t=0.8 seconds a balanced three phase reactive load of 1000 W, 0.8 lagging power factor have been applied. On application of load terminal voltage and frequency remains constant. The additional reactive power demanded by load is fulfilled by STATCOM. At time t=0.85 seconds a single phase resistive load of 1500 W have been switched in to introduce load unbalance. After the application of unbalanced load, the SEIG voltages and currents remains balanced. Also, dc bus voltage of STATCOM remain constant.

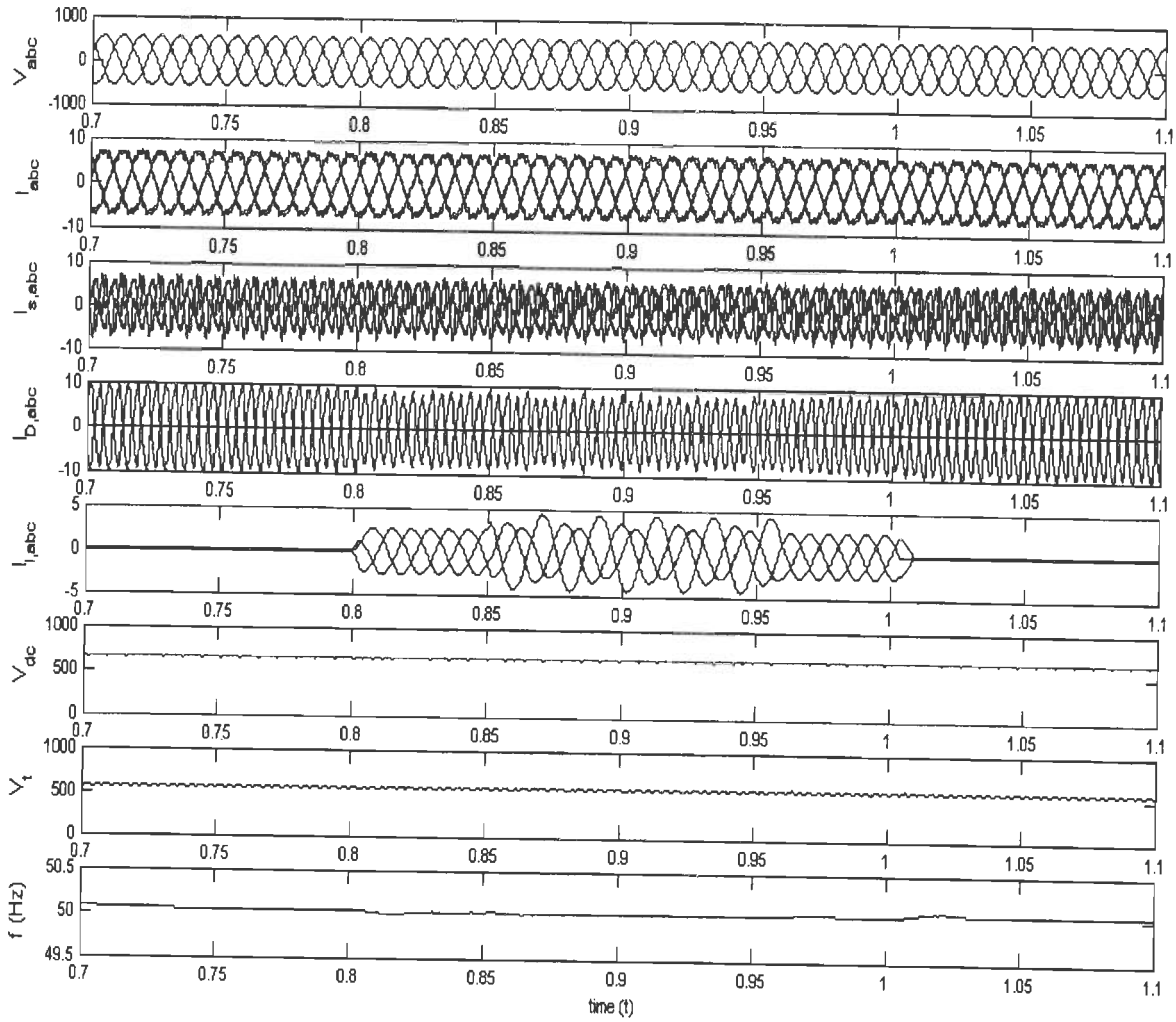


**Figure 7.7: Waveforms of SEIG-STATCOM system supplying unbalanced reactive loads**

Figure 7.8 shows the transient waveforms on application of nonlinear load. At time t=0.8 seconds a three phase diode rectifier having 100 ohms resistance and 100 mH inductance as a load is switched in. The diode rectifier produces quasi square wave of load current. With the application of rectifier load, terminal voltage and frequency remains constant. The voltage and current profile of SEIG remain sinusoidal. Figure 7.9 shows the steady state waveforms and harmonic spectrum of SEIG voltage ($v_a$), SEIG current ($i_a$), dump load current ($i_{D,a}$) and load current ($i_{l,a}$) with three phase diode rectifier with resistive and inductive load. The load current and dump load current THD are 13.12% and 26.52% respectively while SEIG voltage and current THD are 4.96% and 5.54% only. This shows that the proposed controller eliminates the harmonic injected in the system.

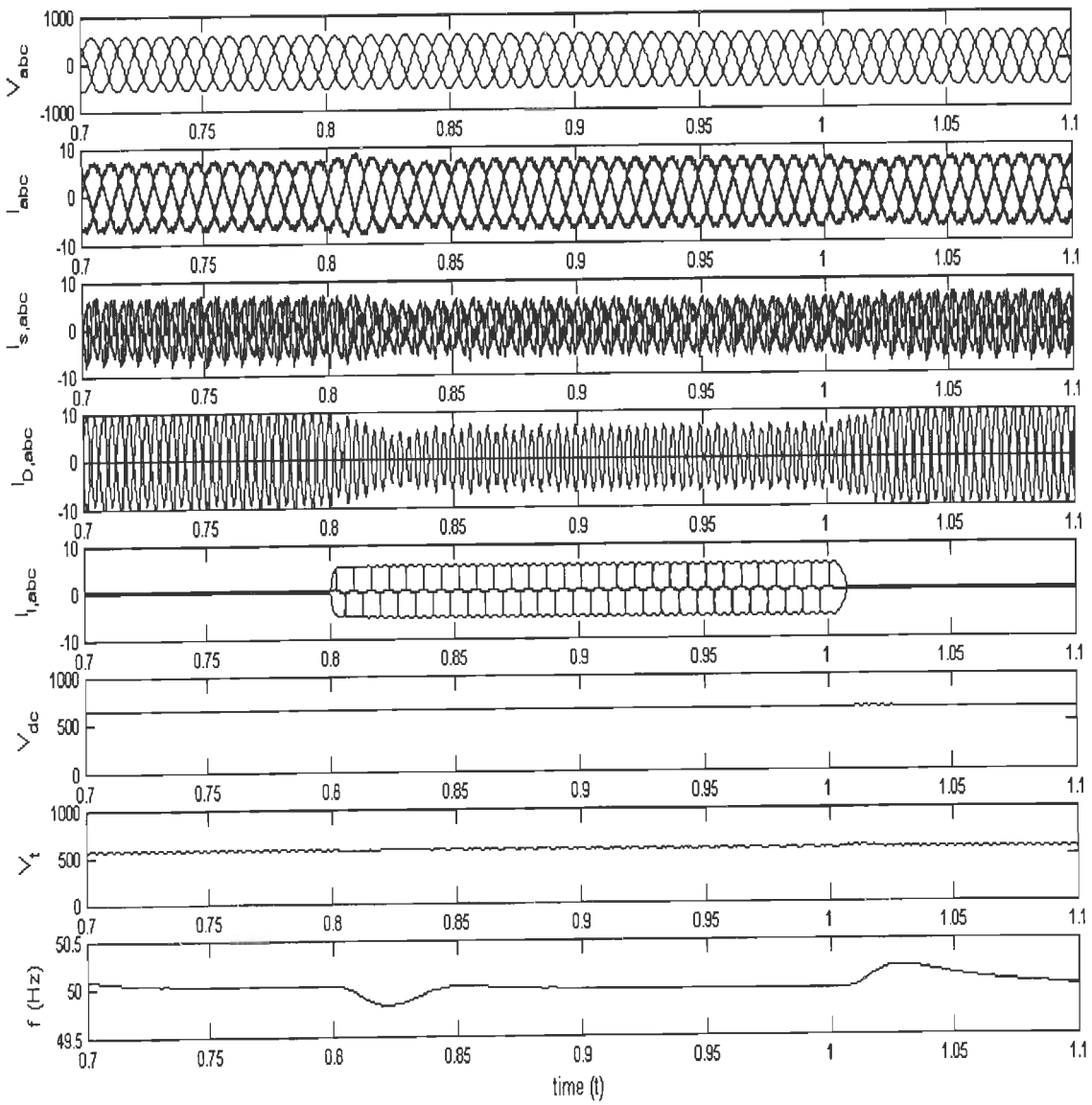


**Figure 7.8: Waveforms of SEIG-STATCOM system supplying nonlinear diode rectifier load**

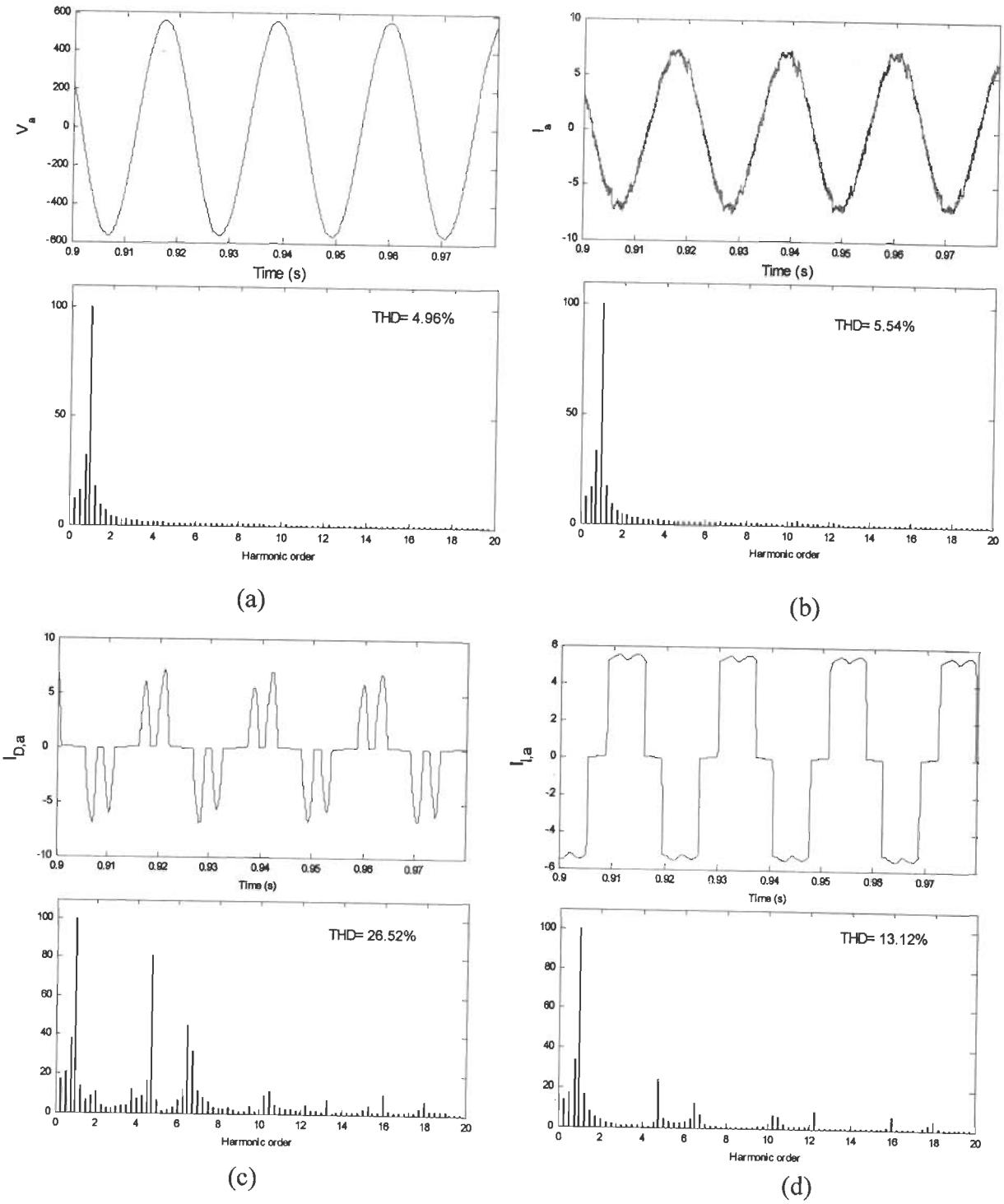


**Figure 7.9: Steady state waveforms and harmonic spectrum of SEIG-STATCOM system**

## 7.3 STATCOM BASED SEIG WITH DC CHOPPER CONTROL

The SEIG with STATCOM and load controller has been discussed in previous section. The STATCOM compensate for reactive power, eliminate harmonics in the system and works as a load balancer for three phase unbalanced load. The load at SEIG terminals has been kept constant by a load controller with mark space ratio controlled dump load. The self supporting DC bus of STATCOM filters voltage ripples. It is typical to maintain a self supporting DC bus as it requires a fine tuning of PI controller. A different topology has been discussed in this section, having a chopper controlled dump load connected in parallel with DC bus capacitor. Such configuration removes the need for a separated load controller and its associate hardware. The DC bus voltage is kept constant by controlling the pulse width of DC chopper and thus the AC terminal voltage.

### 7.3.1 System Description

The schematic diagram of the SEIG with excitation capacitor, current controlled voltage source inverter with DC bus capacitor (STATCOM), chopper controlled dump load and consumer load is shown in Figure 7.10. The excitation capacitors are connected at the terminals of the SEIG, which have a fixed value to result in rated terminal voltage at no load. The SEIG generate constant voltage and power at fixed value of excitation capacitor when load is kept constant. DC bus capacitor and chopper controlled dump load are connected in parallel. The chopper controlled dump load consist a series resistive (dump) load. An IGBT is used as a chopper switch. When gate pulse to IGBT is high, the current flows through the dump load and the power is consumed. The pulse width or duty cycle of chopper is decided by the difference of DC bus voltage to reference DC voltage. When there is an increase in SEIG terminal voltage, the DC bus voltage increases and error in DC bus voltage increases. Thus pulse width in DC chopper increases and power dissipated in dump load increases which increase the total load on SEIG and regulates the terminal voltage. The performance of SEIG is largely affected by power factor of the load. Usually the consumer load is of lagging power factor in nature. When reactive load is connected to the SEIG, it draws reactive current. Then a part of the excitation capacitance is used to compensate for this reactive current hence affect the excitation capacitive reactance required for SEIG to generate rated terminal voltage. Increasing use of static converters in consumer utilities injects harmonics in the system. The SEIG's performance is affected by these harmonics. A current controlled voltage source inverter (CC-VSI) working as

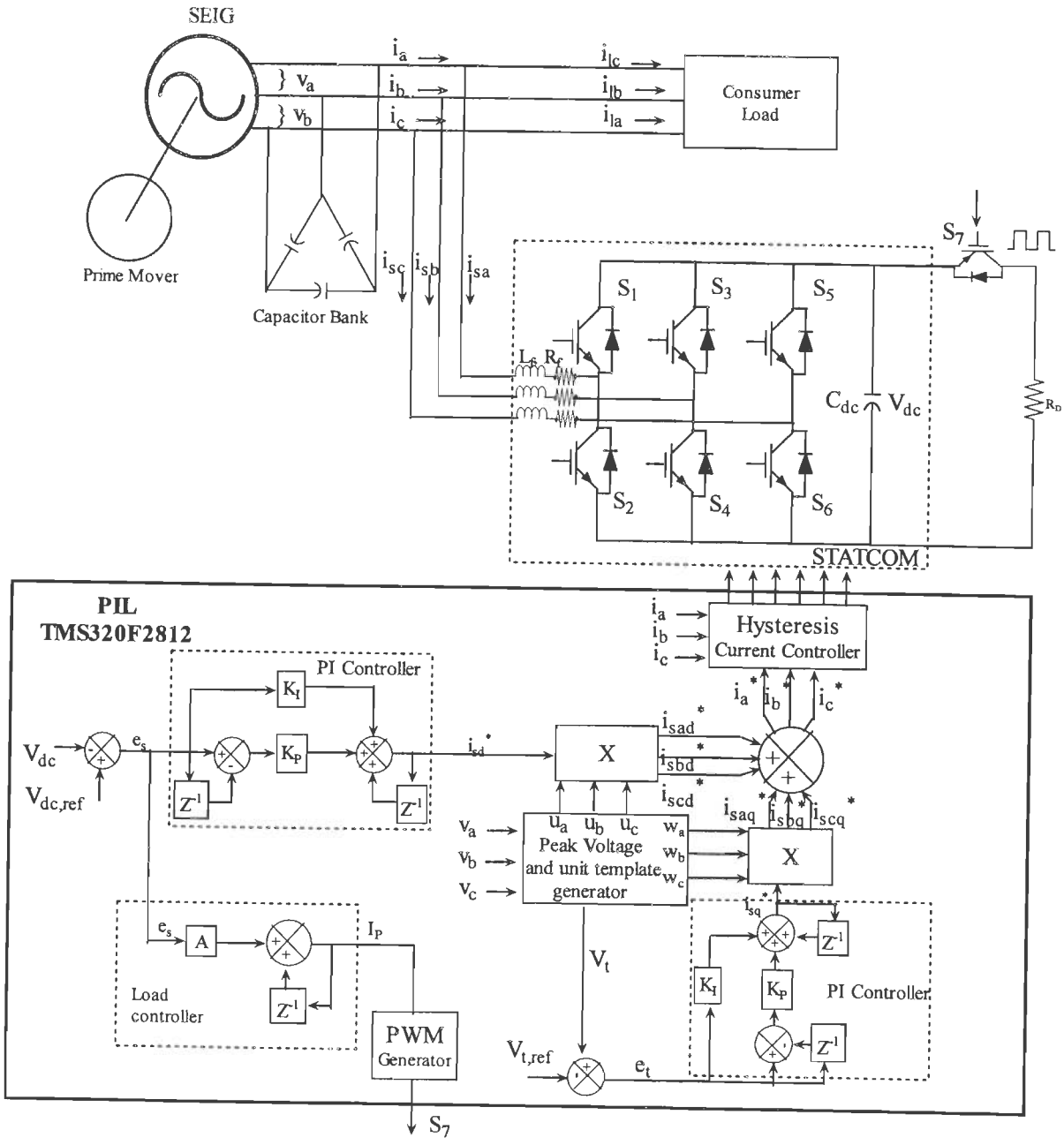


**Figure 7.10: Schematic diagram of three phase SEIG-STATCOM system.**

STATCOM is used for harmonic elimination, load balancing, and reactive power compensation. It consists of three phase IGBT based inverter, DC bus capacitor, and AC filtering inductors. The output of the inverter is connected through the AC filtering inductor to the SEIG terminals. The DC bus capacitor is used to filter voltage ripples.

### 7.3.2 Control Scheme

The schematic diagram of the STATCOM based SEIG system is shown in Figure 7.11. The control scheme to regulate the terminal voltage, frequency, load balancing, reactive power compensation and harmonic elimination of the SEIG system is based on the controlling of source current, voltage and the load at SEIG. The process of generating reference source current is similar to discussed in previous section except the method of controlling the DC bus voltage. The process has again given here for completeness of control scheme.

The peak voltage amplitude ($V_t$) is calculated. The peak voltage amplitude is compared with the reference and error ($e_t$) is computed. The unit templates ($u_a, u_b$, and $u_c$) quadrature unit template ($w_a$, $w_b$ and $w_c$ ) are computed by AC line voltages ($v_a$, $v_b$, and $v_c$) and their peak amplitude ($V_t$). The error ($e_t$) is processed through digital PI controller based on backward difference method and output quadrature reference ($i_{sq}$) is obtained. The DC bus voltage ($V_{dc}$) is compared with the reference ($V_{dc,ref}$) and error($e_s$) is processed through digital PI controller and output ($i_{sd}$) is obtained. The output references ($i_{sd}$, $i_{sq}$) is multiplied with unit templates and algebraically added to obtain reference source currents ($i_a^*$, $i_b^*$, and $i_c^*$). The reference source current are compared with actual line current ($i_a$, $i_b$, and $i_c$) and processed through the hysteresis current controller to obtain the pulse for STATCOM. The error ($e_s$) is processed through the load controller. The output of the controller is compared with symmetrical triangular wave to obtain a pulse of suitable duration (width). This pulse is given to gate of the IGBT chopper switch.

The peak amplitude of voltages ($V_t$) is computed as

$$V_t = \{(2/3)(v_a^2 + v_b^2 + v_c^2)\}^{1/2} \tag{7.12}$$

where, $v_a$, $v_b$ and $v_c$ are the SEIG terminal line voltages.

The unit vectors in phase with $v_a$, $v_b$, $v_c$ are computed as

$$u_a = v_a/V_t; \quad u_b = v_b/V_t; \quad u_c = v_c/V_t; \tag{7.13}$$

the unit vector in quadrature with , $v_a$, $v_b$ and $v_c$ may be derived as:

$$w_a = (-u_b + u_c)/\sqrt{3};$$

$$w_b = \sqrt{3}u_a/2 + (u_b - u_c)/2\sqrt{3};$$

$$w_c = -\sqrt{3}u_a/2 + (u_b - u_c)/2\sqrt{3} \tag{7.14}$$

The AC voltage error at k[th] sampling instant is computed as:

$$e_t(k) = V_{t,ref}(k) - V_t(k) \tag{7.15}$$

where, $V_{t,ref}(k)$ is the reference peak amplitude of AC voltage.

For digital implementation, PI controller is discretised using the backward difference method. The output of the digital PI controller for maintaining the AC terminal voltage of the STATCOM at $k^{th}$ sampling instant is:

$$i_{sq}(k) = i_{sq}(k-1) + K_P[e_t(k) - e_t(k-1)] + K_I e_t(k) \tag{7.16}$$

where, $K_P$ and $K_I$ are the proportional and integral gain constants of the PI controller, $e_t(k)$ and $e_t(k\text{-}1)$ are the AC peak voltage errors at the $k^{th}$ and $(k\text{-}1)^{th}$ sampling instant, and $i_{sq}(k\text{-}1)$ is the amplitude of the reference source current at $(k\text{-}1)^{th}$ sampling instant.

The quadrature component of the reference source current is estimated as:

$$i^*_{saq} = i_{sq}w_a; \quad i^*_{sbq} = i_{sq}w_b; \quad i^*_{scq} = i_{sq}w_c; \tag{7.17}$$

To maintain the DC bus voltage of the CC-VSI constant, the DC bus voltage error, $e_s(k)$ at $k^{th}$ sampling instant is computed as:

$$e_s(k) = V_{dc,ref}(k) - V_{dc}(k) \tag{7.18}$$

where, $V_{dc,ref}(k)$ is the reference DC voltage and $V_{dc}(k)$ is the DC link voltage of CC-VSI at $k^{th}$ sampling instant.

The output of the digital PI controller for maintaining the dc bus voltage of the STATCOM at $k^{th}$ sampling instant is:

$$i_{sd}(k) = i_{sd}(k-1) + K_P[e_s(k) - e_s(k-1)] + K_I e_s(k) \tag{7.19}$$

where, $K_P$ and $K_I$ are the proportional and integral gain constants of the PI controller, $e_s(k)$ and $e_s(k\text{-}1)$ are the dc voltage errors at the $k^{th}$ and $(k\text{-}1)^{th}$ sampling instant, and $i_{sd}(k\text{-}1)$ is the amplitude of the reference source current at $(k\text{-}1)^{th}$ sampling instant.

The in phase component of reference source current are estimated as

$$i^*_{sad} = i_{sd}u_a; \quad i^*_{sbd} = i_{sd}u_b; \quad i^*_{scd} = i_{sd}u_c; \tag{7.20}$$

The reference source current from equation (7.17) and equation (7.20) is given as

$$i^*_a = i^*_{sad} + i^*_{saq}; \qquad i^*_b = i^*_{sbd} + i^*_{sbq}; \qquad i^*_c = i^*_{scd} + i^*_{scq}; \tag{7.21}$$

The estimated reference source current is compared with the actual load current and error is process through hysteresis controller for obtaining the switching pulses.

The DC voltage error ($e_s$) is processed through a load controller. The output of the load controller at $k^{th}$ sampling instant is given as:

$$I_P(k) = A\, e_s(k) + I_P(k-1) \tag{7.22}$$

where, A is the gain of the controller to adjust overshoot, $I_P$ *(k-1)* is the load controller reference at $(k\text{-}1)^{th}$ sampling instant. The generated reference $I_P$ is compared with symmetrical triangular carrier wave to generate pulses to compensate for variation in consumer load.

### 7.3.3 Digital Simulation

Digital simulation of the proposed SEIG-STATCOM system has been carried out with MATLAB Version 7.6 on Simulink Version 7.1. This Power System Blockset facilitates to simulate saturation in asynchronous machines. A 3.73 kW, 400 V 50 Hz star connected asynchronous machine is used as an SEIG including the machine saturation characteristics which is determined by conducting synchronous speed test. The synchronous speed test specifies the no load saturation curve for the induction machine. The voltage and magnetizing current of synchronous speed test is given in a 2-by-n matrix, where n is the number of points taken on magnetization curve to simulate saturation on MATLAB. The block rotor test and no load test give the machine parameters which are summarized in Appendix A. The drooping torque- speed characteristic of prime mover is given as $T_{sh}= k_1\omega_r - k_2$; where, $k_1$ and $k_2$ are the prime mover constants given in Appendix-A. A delta connected capacitor of 25 μF per phase is connected across machine terminals to maintain rated terminal voltage at rated speed as shown in Figure 7.11. The STATCOM controller with chopper controlled dump load is connected in shunt with generator terminals.

The control algorithm is objected to TMS320F2812 fixed point digital signal processor. A Spectrum Digital TMS320F2812 DSP starter kit with XDS510 USB JTAG emulator and code composer studio V3.3 with MATLAB is used for automatic code generation and verification. The control algorithm is created in a subsystem with target preference to F2812 eZdsp from Matlab embedded target support library for TI C2000. The subsystem is then build from real time workshop to create PIL block. The generated s-function PIL block is then placed with system model with appropriate rate limiter and data type converter blocks replacing existing subsystem as shown in Figure 7.12.

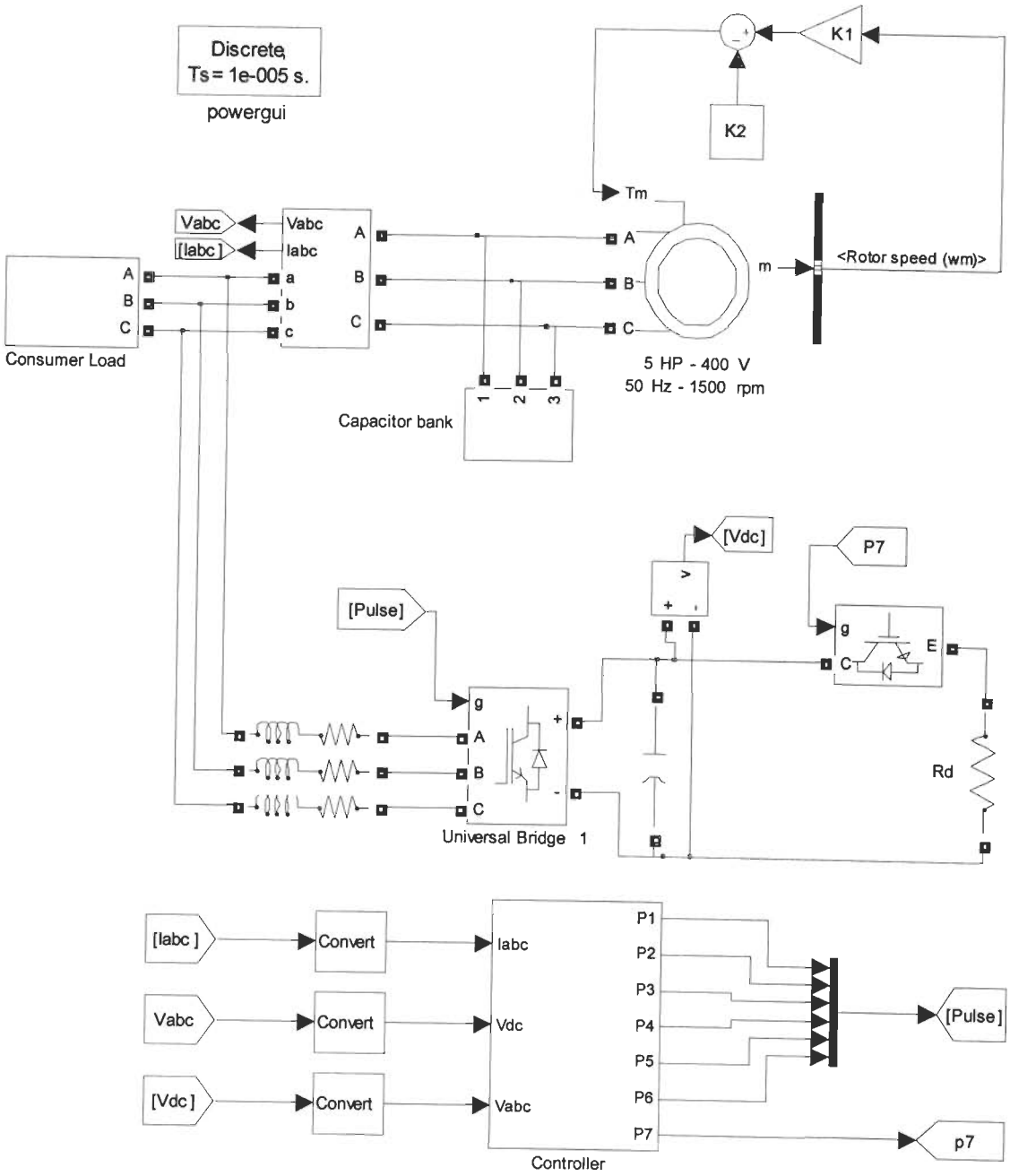


**Figure 7.11: Schematic diagram of MATLAB based model of SEIG-STATCOM**

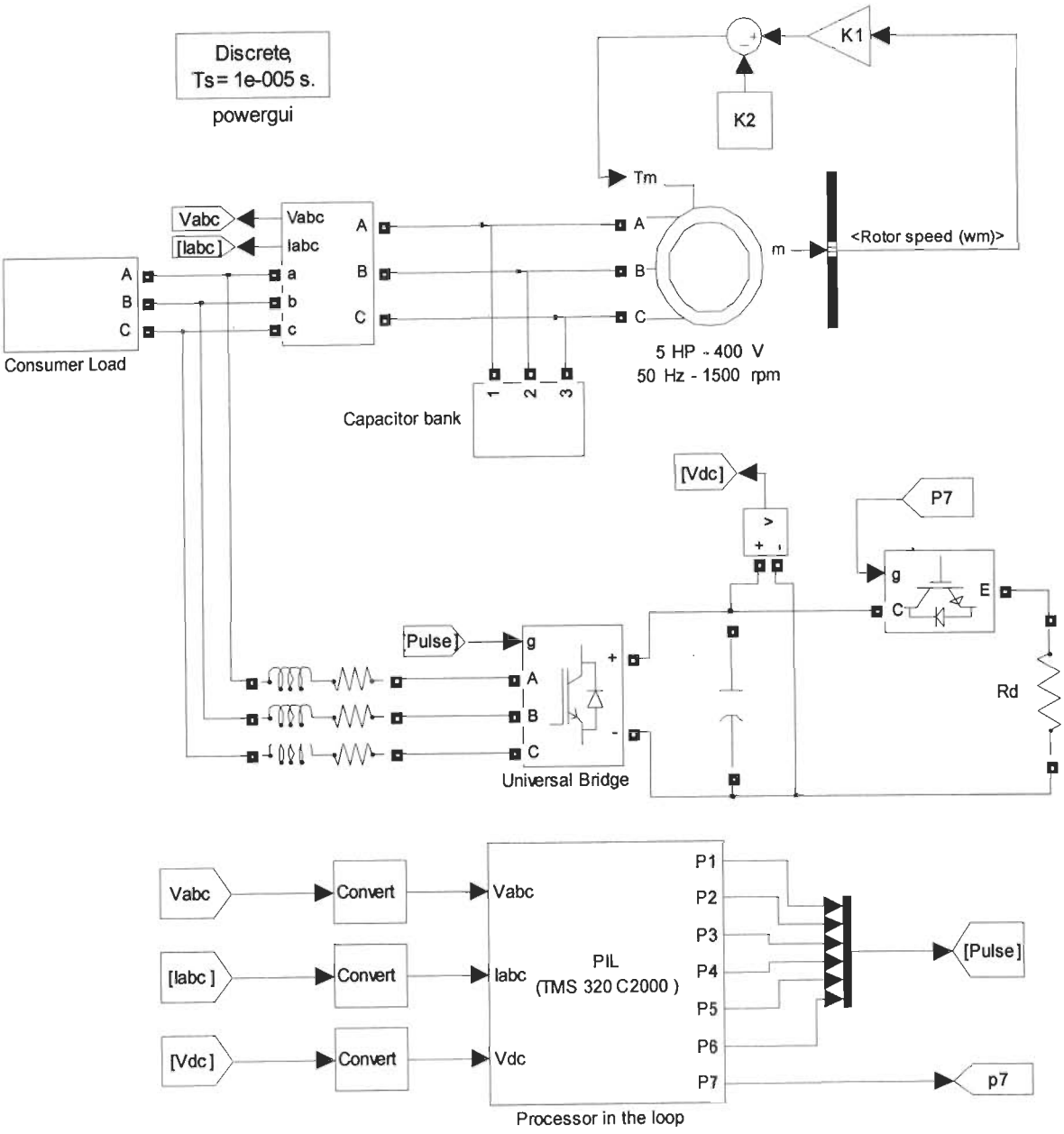


**Figure 7.12: Schematic diagram of MATLAB based model of SEIG-STATCOM with PIL co-simulation**

The PIL block contains the controller algorithm. IQN math library support is taken for fixed point algebric calculations. The peak amplitude is compared with the reference and processed through the load controller. The output of the controller is compared with symmetrical triangular wave and through a relational operator to obtain a pulse of suitable duration (width). This pulse is given to gate of the IGBT chopper switch. The DC bus voltage and AC peak voltage is compared with reference and error is processed through digital PI controller. The obtained reference is multiplied with in phase and quadrature unit template respectively to generate reference currents. The reference currents are then compared with system model current and error is processed through a hystersis controller to generate appropriate pulses for STATCOM.

The SEIG-STATCOM system is co-simulated and real time simulation results are shown. Figure 7.13 shows the transient waveforms of voltage buildup and switching in the STATCOM controller working as a voltage and frequency regulator for three phase balanced resistive load. Waveforms from top to bottom are SEIG line voltages ($v_{abc}$) , line currents ($i_{abc}$), STATCOM currents ($i_{s,abc}$), Generator currents ($i_{G,abc}$), load currents ($i_{l,abc}$), dc bus voltage ($V_{dc}$), peak amplitude of ac terminal voltage ($V_t$) and frequency (f).

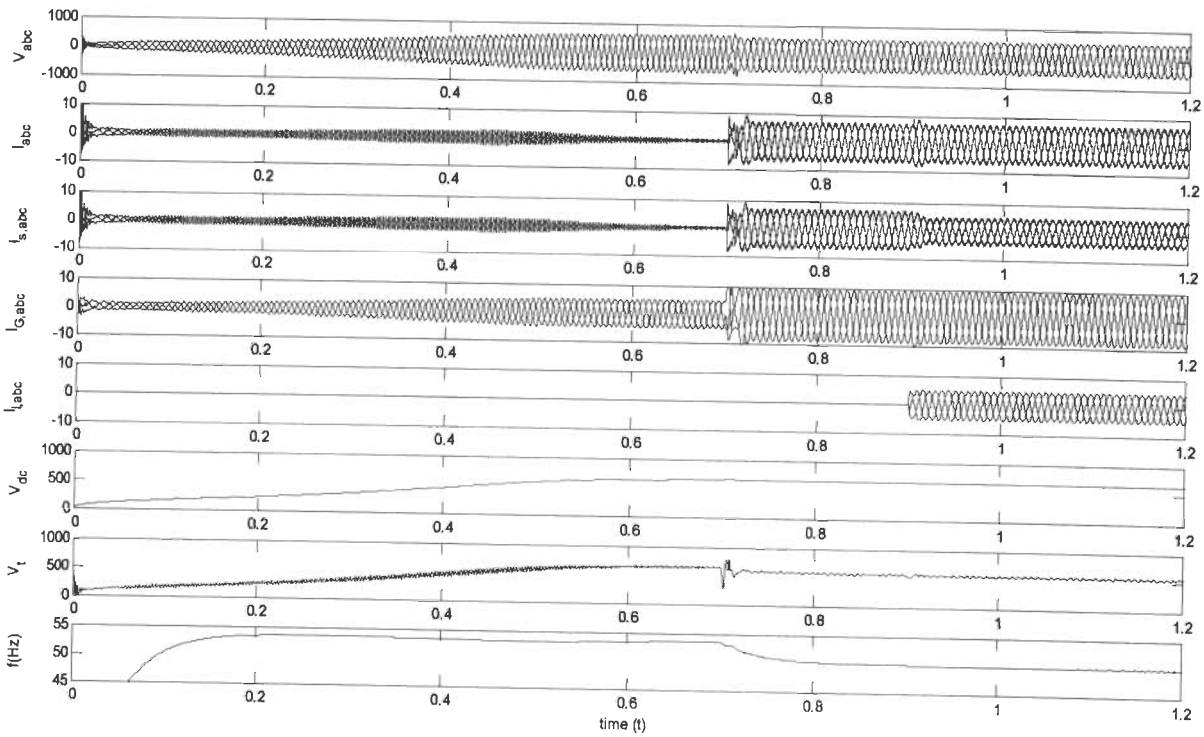


**Figure 7.13: Voltage build up of SEIG, switching in of STATCOM and balanced three phase resistive load**

The process of voltage build up start with remnant field. A initial stator current is assumed to initiate the process. The dc bus capacitor is charge through the anti-parallel diodes of VSI. At time t=0.7 seconds gate pulses are given to IGBTs of STATCOM and dc chopper switch. The STATCOM behaves as a source of the reactive power and draws the active power from the generator to charge its dc bus capacitor to reference voltage of 650 V. There is a dip in terminal voltage which recovers to rated 400 V (565 V- peak). The frequency also drops to 50 Hz rated. At time t=0.9 seconds a balance three phase resistive load of 2 kW is applied. On application of load, terminal voltage and frequency remains constant to their rated value. The STATCOM current is adjusted accordingly.

Figure 7.14 shows the transient waveforms during switching of unbalanced load. At time t=1.1 second an three phase reactive load of 1000 W, 0.8 lagging power factor and single phase 1500 W resistive load have been applied. The terminal voltage and frequency remain constant on application of unbalanced reactive load. The additional reactive power demand by load is fulfilled by STATCOM. After the application of unbalanced load, the SEIG voltages and currents remain balanced. Also, dc bus voltage of STATCOM remains constant.

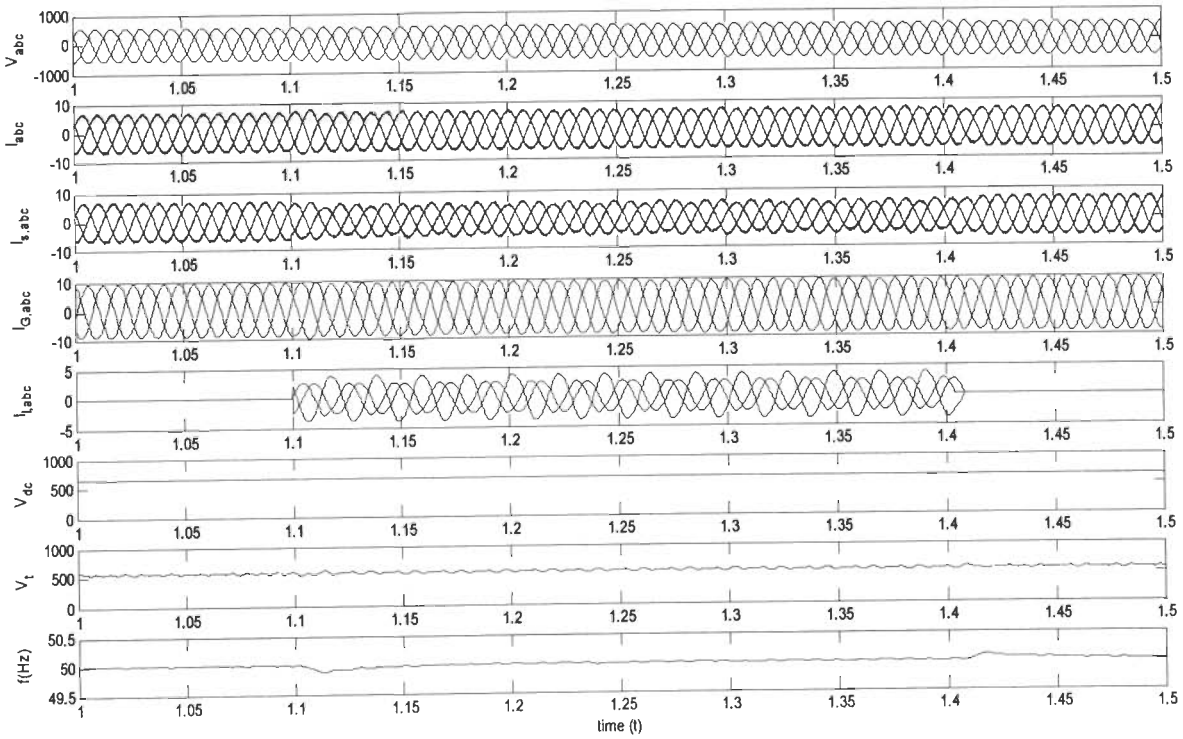


**Figure 7.14: Transient waveform of SEIG-STATCOM system supplying unbalanced reactive loads**

Figure 7.15 shows the transient waveforms on application of nonlinear load. At time t=1.1 second a three phase diode rectifier having 100 ohms resistance and 100 mH inductance as a load is switched in. The diode rectifier produces quasi square wave of load current. With the application of rectifier load, terminal voltage and frequency remains constant. The voltage and current profile of SEIG remain sinusoidal. The STATCOM controller works as harmonic eliminator. Table 7.1 shows the load current THD, SEIG current THD and SEIG voltage THD for different nonlinear load application. This shows that the proposed controller eliminates the harmonic injected in the system.

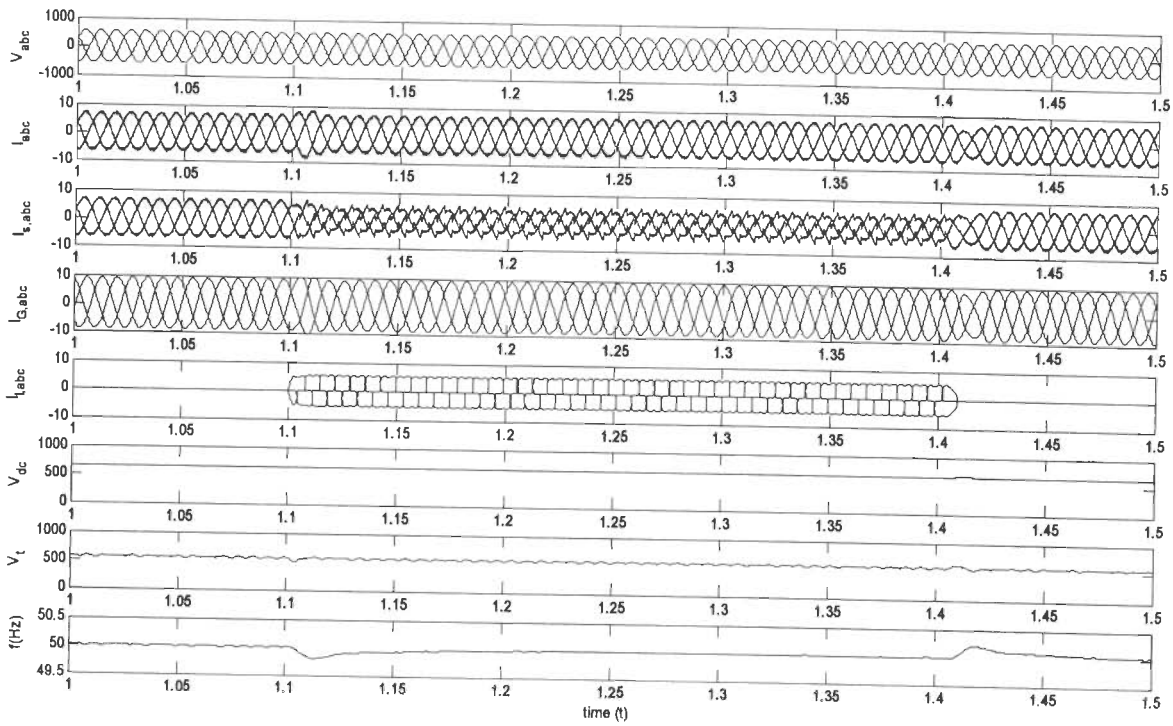


**Figure 7.15: SEIG-STATCOM system supplying nonlinear diode rectifier load**

**Table 7.1 SEIG voltage, current and load current THD for nonlinear load**

| Type of load | SEIG voltage (rms) | SEIG voltage THD (%) | SEIG current THD (%) | Load Current THD (%) |
|---|---|---|---|---|
| Three phase diode rectifier with resistive load | 400 | 1.64 | 2.16 | 24.22 |
| Three phase diode rectifier with resistive and reactive load | 400 | 2.12 | 2.56 | 26.52 |
| Three phase diode rectifier with resistive load and capacitive filter | 400 | 2.14 | 3.14 | 29.16 |
| Three phase thyristorized converter with resistive load and delay angle of 45 degree | 400 | 2.74 | 4.26 | 44.24 |

### 7.3.4 Implementation

The PIL co-simulation technique helps to evaluate as how well a control algorithm operates on the fixed point digital signal processor selected for the application. The term co-simulationis a division of process in which Simulink software models the system, while code generated from the controller subsystem runs on the processor hardware. This bridge the gap between simulation and final system configuration. In the PIL co-simulation, Real-Time Workshop software generates an executable application for the PIL algorithm. This code runs (in simulated time) on a processor platform. The system model remains in Simulink software without the use of code generation. The simulink software simulates the SEIG-STATCOM model for one sample interval and exports the output signals to the processor platform via code composer studio integrated dovelopment environment (CCS link IDE). When the processor platform receives signals from the model, it executes the PIL algorithm for one sample step. The PIL algorithm returns its output signals computed during this step to Simulink software, via CCS link IDE interface. At this point, one sample cycle of the simulation is complete and the system model proceeds to the next sample interval. The process repeats and the simulation progresses.

However, a real time application differs from PIL co-simulation. During real time appliction, the input signal is received through on board analog to digital converter (ADC) channel and output is received from general purpose input output-digital output (GPIO-DO) and pulse width modulation (PWM) channels. The input signal via ADC is received through voltage and curent sensors. The output signal of PWM and GPIO-DO is obtained in pulse form and given to IGBT switches throgh suitable isolation and pulse driver circuit. Unlike PIL application, this code run in real time on a processor platform.

The real time implementation require few compensation before put into operation. Figure 7.16 shows the MATLAB simulink model for automatic code generation. The on board ADC is 12-bit 0-3 V unipolar operation. The voltage and current signals are bipolar AC signals. The ADC calibration is require to read these signals though on board ADC channel. The input voltage and current signals of ±1.5 V (max.) is clamped to 0-3 V (max.) unipolar. The hardware associated to clamp the signal is given in Appendix- D. The Figure 7.17 (a) and (b) show the real time sensed voltage and voltgae signal clamped with 1.5 V. Figure 7.18 shows the current signals before and after clamping with 1.5 V.

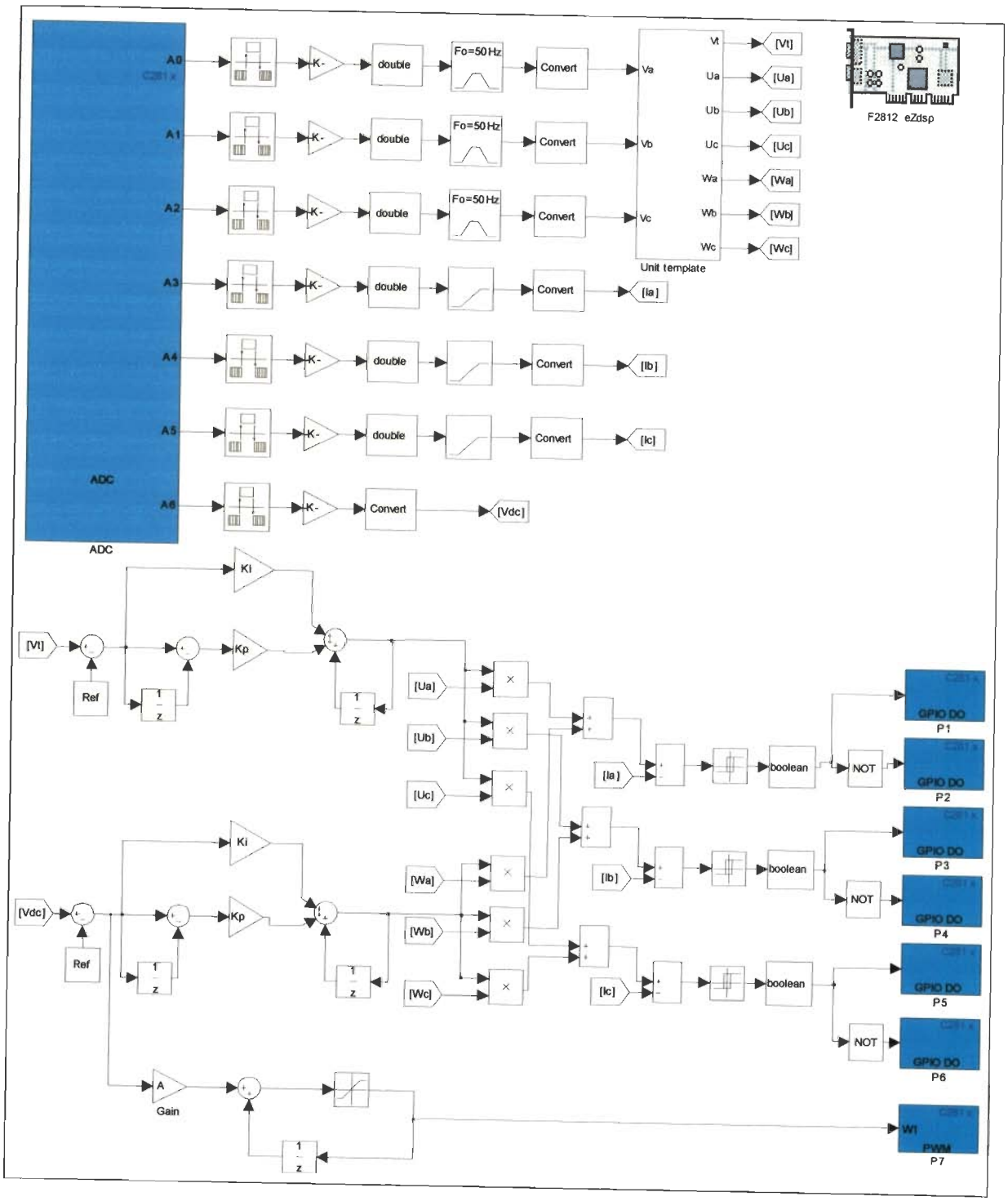


**Figure 7.16: MATLAB model for automatic code generation**

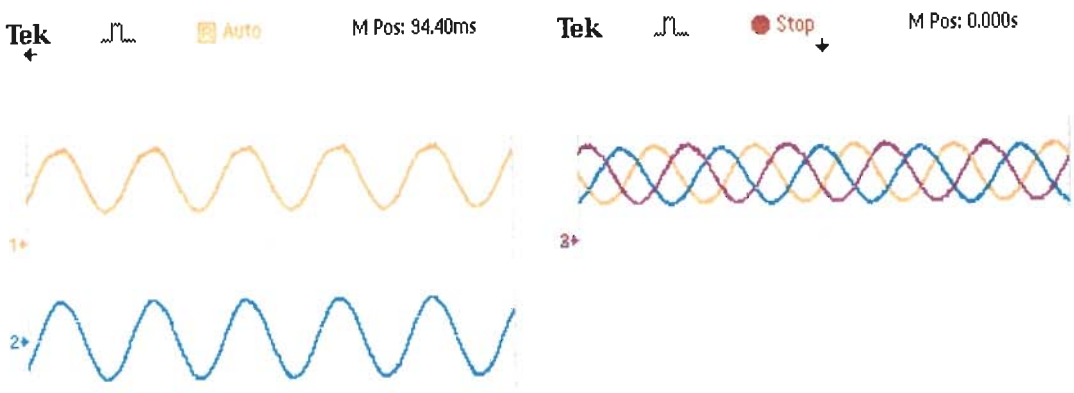


(a) (b)

**Figure 7.17: (a) Bipolar and clamped unipolar line voltage (b) clamped three phase line voltage**

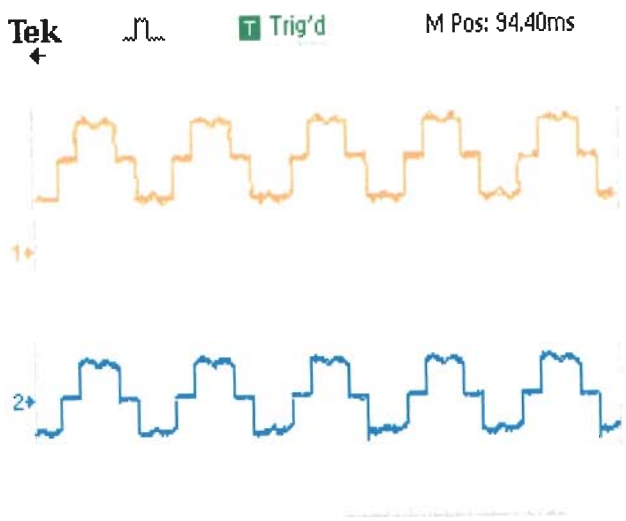


**Figure 7.18: Bipolar to clamped unipolar line current**

The output of voltage and current sensors are limited to ±1.5 V peak to peak. Clamping it with 1.5V makes the signal 0-3V peak to peak. The three line voltages, three line currnets and one DC bus voltage are input signal sensed through voltage and current sensors, clamped and read through on board 12 bit ADC channel with a sample rate of 0.0001 second (0.0004 second, max.). The model is build and downloaded onto processor thrhough CCS (code composer studio). The ADC channel has the maximum sample rate of 0.0004 seconds and input signal is read at 0.0001 seconds, while the doveloped algorithm is on sample rate of 0.000001 seconds. The first step is to match the two

different rate signals, hence a rate limiter is placed. The signal is normalized to actual through a gain. The ADC input is read as unsigned interger data. To work on fixed point processor, we need to convert the data to fixed point data. Hence a data converter block is added.

The input unipolar voltage and current signals need to be converted back to bipolar. The DC clamp is added to make bipolar signal to unipolar is removed through a first order high pass filter. The line current signal is passed through a high pass filter with a cutoff frequency of 5 Hz. This blocks the DC component and allows the AC signal. The magnitude and phase response of high pass filter is shown in Figure 7.19(a). The line voltage is used for unit template generation. The voltages should be sinusoidal and must not contain harmonics. The voltage signal is passed through a second order band pass filter with pass frequency of 50 Hz and a damping factor of 0.707. The magnitude and phase response of second order band pass filter is shown in Figure 7.19(b). This eliminates the DC component and higher order frequency from the voltage signal. The filter application run for double type data, hence a data converter is added before and after to convert data to double and back to fixed point. The architecture of the TMS320F2812 does not directly support floating-point maths. However, fixed-point numbers can be converted to floating-point for implementation.

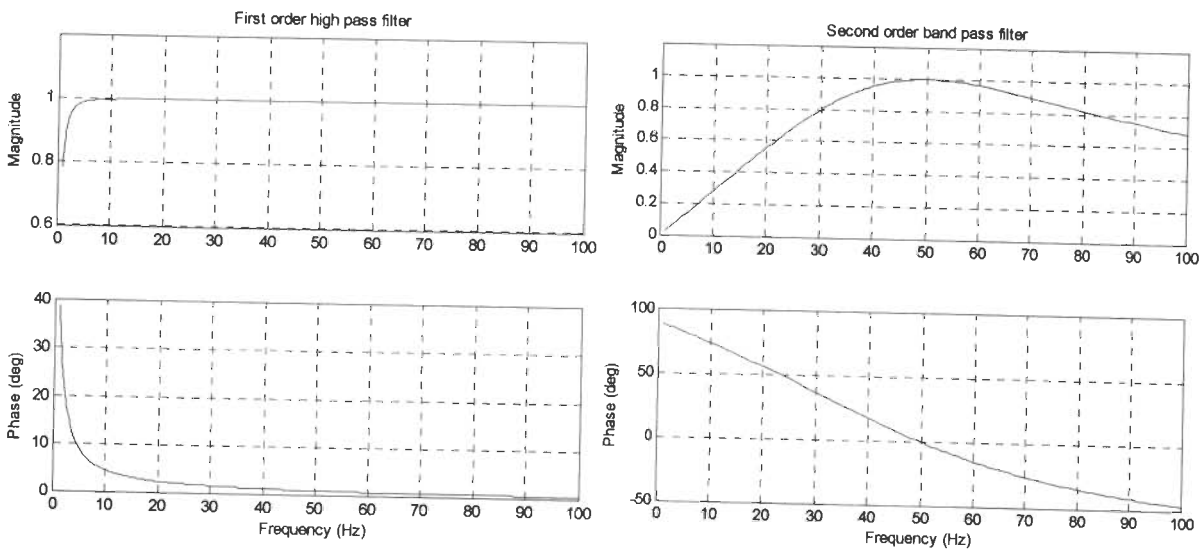


(a) (b)

**Figure 7.19: Magnitude and phase response of (a) first order high pass filter (b) second order band pass filter.**

The in phase, quadrature unit templates and peak voltage are computed from input line voltages. The DC bus voltage and peak AC voltage is compared with reference and error is processed through digital PI controllers. The outputs of PI controllers are multiplied with in phase and quadrature unit templates. The obtained current references are algebraically added and compared with actual current. The error is processed though a relay operator within a specified band. The output of relay is given to one lag of voltage source inverter. The NOT gate operator gives the negative part of the pulse. The pulse is given to general purpose digital output pin of TMS320F2812 DSP. The DC voltage error is processed through load controller. The output of load controller is processed through PWM and pulse is obtained.

### 7.3.5 Experimentation and results

A prototype DSP based SEIG-STATCOM system with TMS320F2812 processor has been developed and tested in laboratory under various operating conditions. A three phase 3.73 kW, 400 V, 7.5 A, 50 Hz, 1500 rpm delta connected squirrel cage induction machine is used as a self-excited induction generator. The SEIG is driven by 220 V, 20 A, 5 HP, 1500 rpm shunt wound DC machine is used as a prime mover. To generate 3 kW at 400 V and rated speed, 25 μF capacitor of 400 V is connected in delta across the SEIG terminals. The test results are carried out with three phase balanced resistive load and diode rectifier with resistive load as nonlinear load. The pulse output from TMS320F2812 DSP is digitally isolated and amplified through pulse driver circuit. A TLP250 photocoupler is used for isolation and pulse driver. The pulse are given to voltage source inverter having coupling inductor and DC bus capacitor. The input coupling inductor is taken of 4mH per phase and DC bus capacitor of 1500 μF has been connected. A SEMIKRON make IGBT based inverter with built-in driver card is used as voltage source inverter. The built-in driver takes care of dead band control for positive and negative group conduction of IGBT. An individual IGBT switch is used for load controller with series resistive dump load. LEM make voltage and current sensors are used for voltage and current sensing. The hardware associated for sensors and ADC calibrations are given in Appendix E.

Figure 7.20 shows the transient waveform on application of 1500 W balanced resistive load. Waveform from the top to bottom are line voltage ($v_a$), SEIG stator current ($I_a$), STATCOM with dump load current ($I_{s,a}$) and load current ($I_a$). On application of resistive load the current in the dump load decreases. The generator current and voltage remains constant. Figure 7.21(a) and Figure 7.21 (b) shows the transient waveform on application of diode rectifier based nonlinear load. The diode rectifier produces quasi square wave of load current. With the application of rectifier load, terminal voltage and frequency remains constant. The voltage and current profile of SEIG remain sinusoidal. The STATCOM controller works as harmonic eliminator. The Figure 7.22 shows harmonic spectrum of SEIG voltage ($v_a$), SEIG stator current ($i_a$) and load current ($i_{l,a}$) with three phase diode rectifier with resistive load. The load current THD are 28.00% while SEIG voltage and current THD are 2.30% and 5.80% respectively. This shows that the proposed controller eliminates the harmonic injected in the system.

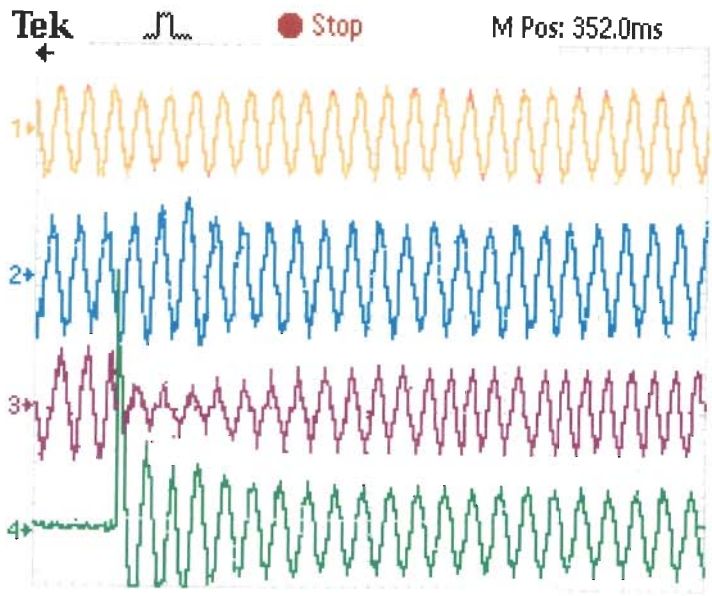


Horizontal scale:-Time 50 msec/Div
Vertical scale from ch1 to ch4:-$V_a$ (1000V/Div)
$I_a$ (8 A/Div), $I_{s,a}$(8A/Div), $I_{L,a}$(4A/Div)

**Figure 7.20 : Transient waveform on application of balanced three phase reactive load**

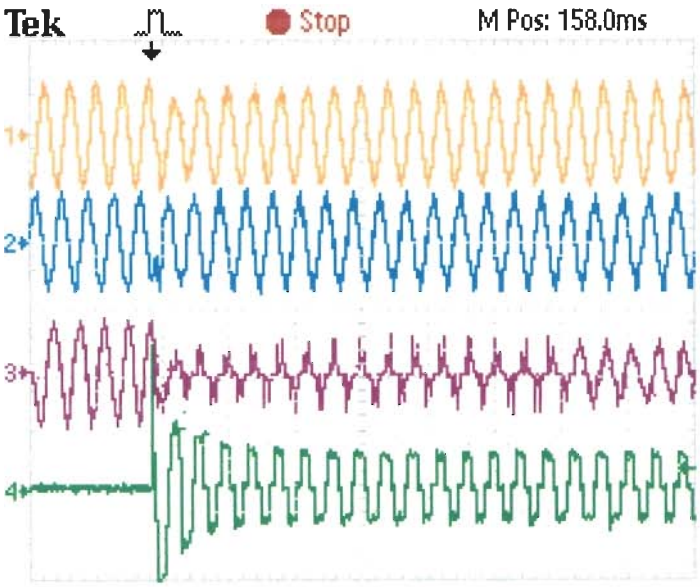


Horizontal scale:-Time 50 msec/Div
Vertical scale from ch1 to ch4:-$V_a$ (1000V/Div)
$I_a$ (8 A/Div), $I_{s,a}$(8A/Div), $I_{L,a}$(4A/Div)

**Figure 7.21(a): Transient waveform on application of diode rectifier non linear load**

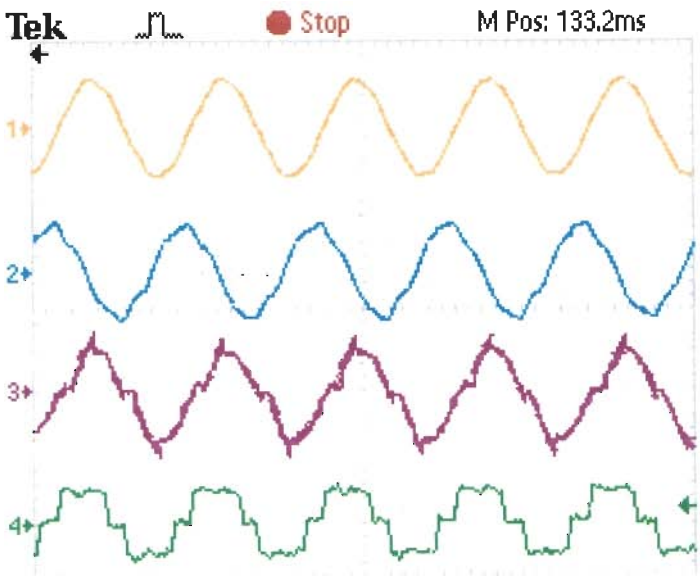


Horizontal scale:-Time 50 msec/Div
Vertical scale from ch1 to ch4:-$V_a$ (1000V/Div)
$I_a$ (8 A/Div), $I_{s,a}$(8A/Div), $I_{L,a}$(4A/Div)

**Figure 7.21(b): Transient waveform with non linear load**

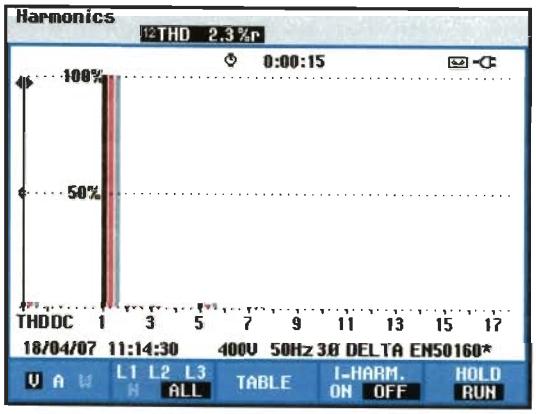


(a)

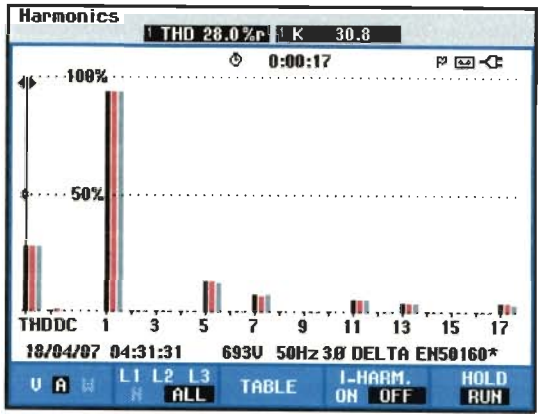


(b)

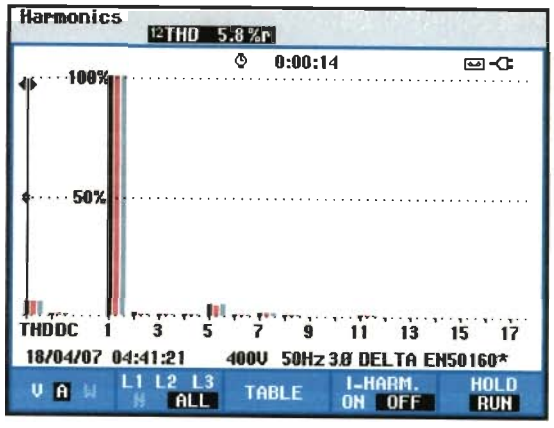


(c)

**Figure 7.22 : SEIG (a) Voltage (b) *load* current (c) *stator* current THD with STATCOM controller.**

## 7.4 CONCLUSION

The developed STATCOM controller regulates the terminal voltage and frequency of the SEIG under balance and unbalanced load application. The results show that the SEIG terminal voltage and frequency remains constant while supplying resistive loads. The controller compensate for the additional VAR required when reactive load is connected. The controller balances the SEIG currents and voltage under unbalanced load and act as load balancer. The harmonic generated by nonlinear load are compensated by proposed STACOM based controller. Therefore it acts as harmonic compensator. The SEIG generates constant power. The chopper controlled dump load operates according to the

changes in consumer load. The PIL co-simulation evaluates how well control algorithm operates on the fixed point digital signal processor. From analysis and experimentation following conclusions are drawn:

(i) The STATCOM based controller ragulates the terminal voltage and frequency with varying consumer load.

(ii) The STATCIM based controller compensate for additional VAR required when consumer load is increased or reactive load is connected.

(iii) The proposed controller balances the SEIG current and voltage under application of unbalanced load and act as load balancer.

(iv) The harmonics generated due to application of nonlinear load are eleiminated by proposed STATCOM based controller.

(v) The digital design of proposed controller with backward differnce PI controller and load controller shows its application with Fixed Point Processors.

(vi) The co-simulation with processor in the loop (PIL) validate the algorithm for fixed point processor application. This bridge the gap between simulation and final system configuration.

(vii) The proposed controller design has been experimentally vaidated with application of linear and nonlinear loads. The voltage and current transients on application of resistive load and nonlinear load are found under satisfactory limits. The harmonics content are also reduced from load current to SEIG current.

# CHAPTER-8

# WIND DRIVEN SEIG WITH VOLTAGE & FREQUENCY REGULATION AND ENERGY STORAGE SYSTEM

## 8.1 INTRODUCTION

In the previous chapters, the detailed investigation of SEIG for stand alone power generation has been carried out. The SEIG have relative advantage over conventional synchronous generator for harnessing renewable energy in stand alone mode, however, the poor voltage and frequency regulation is basic drawback for its application. The effort has been made to regulate the voltage and frequency of the SEIG system with load controllers. The load controller does not compensate for variable reactive power demand. The performance of SEIG is largely affected by power factor of the load as it draws a reactive current. The design and development of static compensator (STATCOM) reactive power compensation, voltage and frequency regulation with increase in load current has been examined in previous chapter. The STATCOM works as a second order filter and eliminates harmonics in the system. The STATCOM balances the phase current and thus works as a load balancer.

The stand alone wind energy conversion system using a squirrel cage self excited induction generator is could be one of the attractive option for small and medium power generation system. The SEIG can harness the power from constant as well as variable speed prime mover such as variable head hydro and wind turbines. There is a need to develop a suitable control scheme to regulate the output voltage and frequency with fixed excitation capacitor and variable speed prime mover using squirrel cage induction motor. Stand alone operation of SEIG-WECS [82,170] with regulated output and frequency requires either an asynchronous ac-dc-ac link power converter or a matrix converter. In [131], a series connected pulse width modulated VSI with a battery bank is used to regulate the voltage and frequency. However, this scheme presents low frequency harmonics at low rotor speeds. The concept of terminal impedance controller has been proposed by Bonert and Hoops [29]. A bidirectional VS-PWM with a capacitor and switched resistor at dc bus has been proposed in [125]. This provides a reference voltage

and frequency for the induction generator. The converter can compensate for reactive power to regulate the terminal voltage. However, it can only absorb the active power.

In this chapter an effort has been made to introduce a bidirectional active and reactive power flow control scheme. The proposed bidirectional converter compensate for variable reactive power to regulate the terminal voltage. It absorbs the active power during light load or higher wind speed and delivers the active power during high load or lower wind speed with an energy storage system for SEIG-wind energy conversion system.

## 8.2 SYSTEM DESCRIPTION

The schematic diagram and control scheme of the SEIG- Wind energy conversion system under consideration is shown in Figure 8.1. The wind turbine is connected to the rotor of the SEIG through step-up gear box. At the stator side of the induction generator, there is an excitation capacitor bank in parallel with voltage source converter (VSC), and the consumer load. The VSC consists of three phase IGBT based inverter, DC bus capacitor, AC coupling inductors and battery bank. The output of the inverter is connected through the AC filtering inductor to the SEIG terminals. The DC bus capacitor is connected in parallel with battery bank. The DC bus capacitor suppresses the ripples appearing at the DC side of VSC. The VSC absorbs or injects the active power depending upon the frequency error. The VSC absorbs the active power that is stored in the battery bank when the system frequency is above the reference value. Conversely, the VSC injects active power when system frequency decreases due to increase in load or decrease in wind speed. Reactive power is also compensated from VSC as a function of terminal voltage error. The generated voltage of the SEIG depends upon the amount of excitation capacitance. A delta connected capacitor bank is connected at the generator terminals to generated rated voltage at no load, while additional demand of excitation to regulated voltage is met by the VSC controller. As the terminal voltage drops, the terminal voltage error makes the VSC converter to inject reactive power. Thus the VSC provide bidirectional flow of active and reactive power.

## 8.3 CONTROL SCHEME

The schematic diagram of the SEIG- wind energy conversion system is shown in Figure 8.1. The control scheme to regulate the terminal voltage, frequency, load balancing, reactive power compensation, harmonic elimination and battery current for SEIG-WECS

system is based on the controlling of source currents. The peak voltage amplitude ($V_t$) is calculated and amplitude is compared with the reference. The error ($e_t$) is processed through voltage PI controller and quadrature current reference ($i_{sq}^*$) output is obtained for reactive component of reference current.

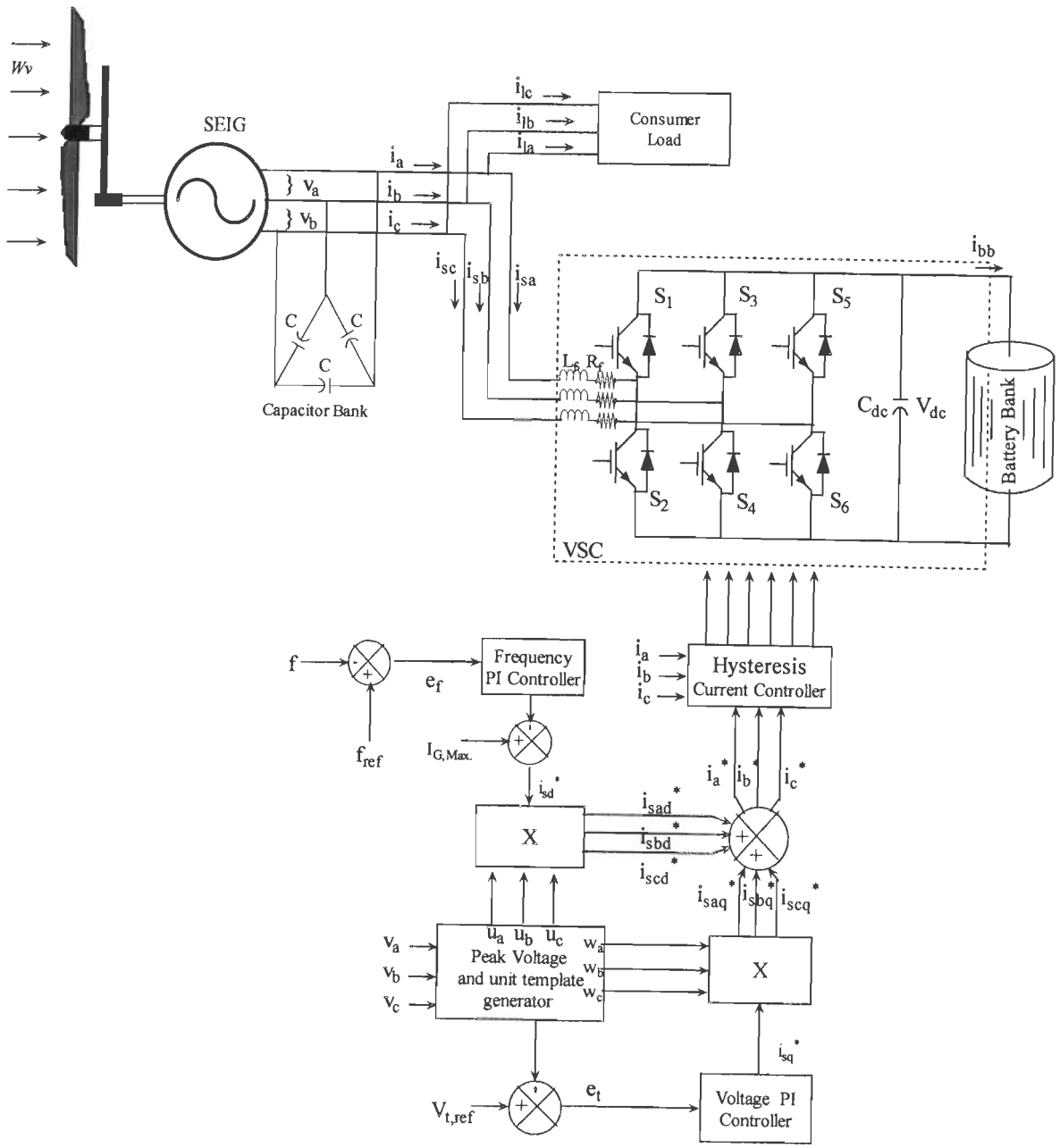


**Figure 8.1: Schematic diagram of three phase SEIG-wind energy conversion system**

The unit templates ($u_a$, $u_b$, and $u_c$) quadrature unit template ($w_a$, $w_b$ and $w_c$ ) are computed by AC line voltages ($v_a$, $v_b$, and $v_c$) and their peak amplitude ($V_t$). The instantaneous value of frequency (f) is estimated using phase locked loop control. The

frequency error ($e_f$) is estimated by subtracting estimated frequency (f) from reference frequency ($f_{ref}$). The frequency error is processed through a frequency PI controller. The maximum generator current ($I_{G,Max.}$) is calculated by division of rated power output of SEIG to rated terminal voltage. For generating active component of reference current ($i_{sd}^*$), the output of frequency PI controller is subtracted from maximum generator current. The output references ($i_{sd}^*$, $i_{sq}^*$) is multiplied with unit templates and algebraically added to obtain reference source currents ($i_a^*$, $i_b^*$, and $i_c^*$). The reference source currents are compared with actual line currents ($i_a$, $i_b$, and $i_c$) and processed through the hysteresis current controller to obtain the pulse VSC.

The peak amplitude of voltages ($V_t$) is computed as

$$V_t = \{(2/3)(v_a^2 + v_b^2 + v_c^2)\}^{1/2} \tag{8.1}$$

where, $v_a$, $v_b$ and $v_c$ are the SEIG terminal line voltages.

The unit vectors in phase with $v_a$, $v_b$, $v_c$ are computed as

$$u_a = v_a/V_t; \quad u_b = v_b/V_t; \quad u_c = v_c/V_t; \tag{8.2}$$

The unit vector in quadrature with, $v_a$, $v_b$ and $v_c$ may be derived as:

$$\begin{aligned} w_a &= (-u_b + u_c)/\sqrt{3}; \\ w_b &= \sqrt{3}u_a/2 + (u_b - u_c)/2\sqrt{3}; \\ w_c &= -\sqrt{3}u_a/2 + (u_b - u_c)/2\sqrt{3} \end{aligned} \tag{8.3}$$

The AC voltage error at k $^{th}$ sampling instant is computed as:

$$e_t(k) = V_{t,ref}(k) - V_t(k) \tag{8.4}$$

where, $V_{t,ref}(k)$ is the reference peak amplitude of AC voltage.

The output of the voltage PI controller for maintaining the AC terminal voltage of the SEIG at $k^{th}$ sampling instant is:

$$i_{sq}(k) = i_{sq}(k-1) + K_P[e_t(k) - e_t(k-1)] + K_I e_t(k)$$

where, $K_P$ and $K_I$ are the proportional and integral gain constants of the PI controller, $e_t(k)$ and $e_t(k\text{-}1)$ are the AC peak voltage errors at the $k^{th}$ and $(k\text{-}1)^{th}$ sampling instant, and $i_{sq}(k\text{-}1)$ is the amplitude of the reference source current at $(k\text{-}1)^{th}$ sampling instant.

The quadrature reactive component of the reference source current is estimated as:

$$\begin{aligned} i_{saq}^* &= i_{sq} w_a \\ i_{sbq}^* &= i_{sq} w_b \\ i_{scq}^* &= i_{sq} w_c \end{aligned} \tag{8.5}$$

The frequency error is defined as

$$e_f(k) = f(k) - f_{ref}(k) \tag{8.6}$$

where, $f(k)$and $f_{ref}(k)$ is the system frequency and reference frequency at k[th] sampling instant.

The frequency error is processed through frequency PI controller and output at $k$ [th] sampling instant is given as

$$i_{sd}(k) = i_{sd}(k-1) + K_P[e_f(k) - e_f(k-1)] + K_I e_f(k) \tag{8.7}$$

where, $K_P$ and $K_I$ are the proportional and integral gain constants of the frequency PI controller, $e_f(k)$ and $e_f(k\text{-}1)$ are the frequency errors at the $k$ [th] and $(k\text{-}1)^{th}$ sampling instant, and $i_{sd}(k\text{-}1)$ is the output of the frequency PI controller at $(k\text{-}1)$ [th] sampling instant.

The output of frequency PI controller is subtracted from maximum generator current and active component of reference is obtained as

$$I_{sd}^{*}(k) = I_{G,Max.}(k) - I_{sd}(k) \tag{8.8}$$

The instantaneous in phase active component of reference source current are estimated as

$$\begin{aligned} i_{sad}^{*} &= i_{sd} u_a \\ i_{sbd}^{*} &= i_{sd} u_b \\ i_{scd}^{*} &= i_{sd} u_c \end{aligned} \tag{8.9}$$

The reference source current from equation (8.5) and equation (8.9) is given as

$$\begin{aligned} i_a^{*} &= i_{sad}^{*} + i_{saq}^{*} \\ i_b^{*} &= i_{sbd}^{*} + i_{sbq}^{*} \\ i_c^{*} &= i_{scd}^{*} + i_{scq}^{*} \end{aligned} \tag{8.10}$$

The estimated reference source current is compared with the actual load current and error is process through hysteresis controller for obtaining the switching pulses.

## 8.4 MODELING AND SIMULATION

Digital simulation of the proposed SEIG-WECS with energy storage system has been carried out with MATLAB Version 7.6 and Simulink Version 7.1. The synchronous speed test data for air gap voltage and magnetizing current is experimentally estimated for simulation of saturation in asynchronous machine. The synchronous speed test specifies the no load saturation curve for the induction machine. Figure 8.2 and Figure 8.3 shows the MATLAB based model of SEIG-wind energy conversion system. A 7.5 kW, 400 V, 50 Hz, delta connected asynchronous machine is used as a SEIG. A delta connected capacitor

bank of 36 μF per phase is connected at the terminals of machine to obtain a 6kW power output at rated voltage and rated speed.

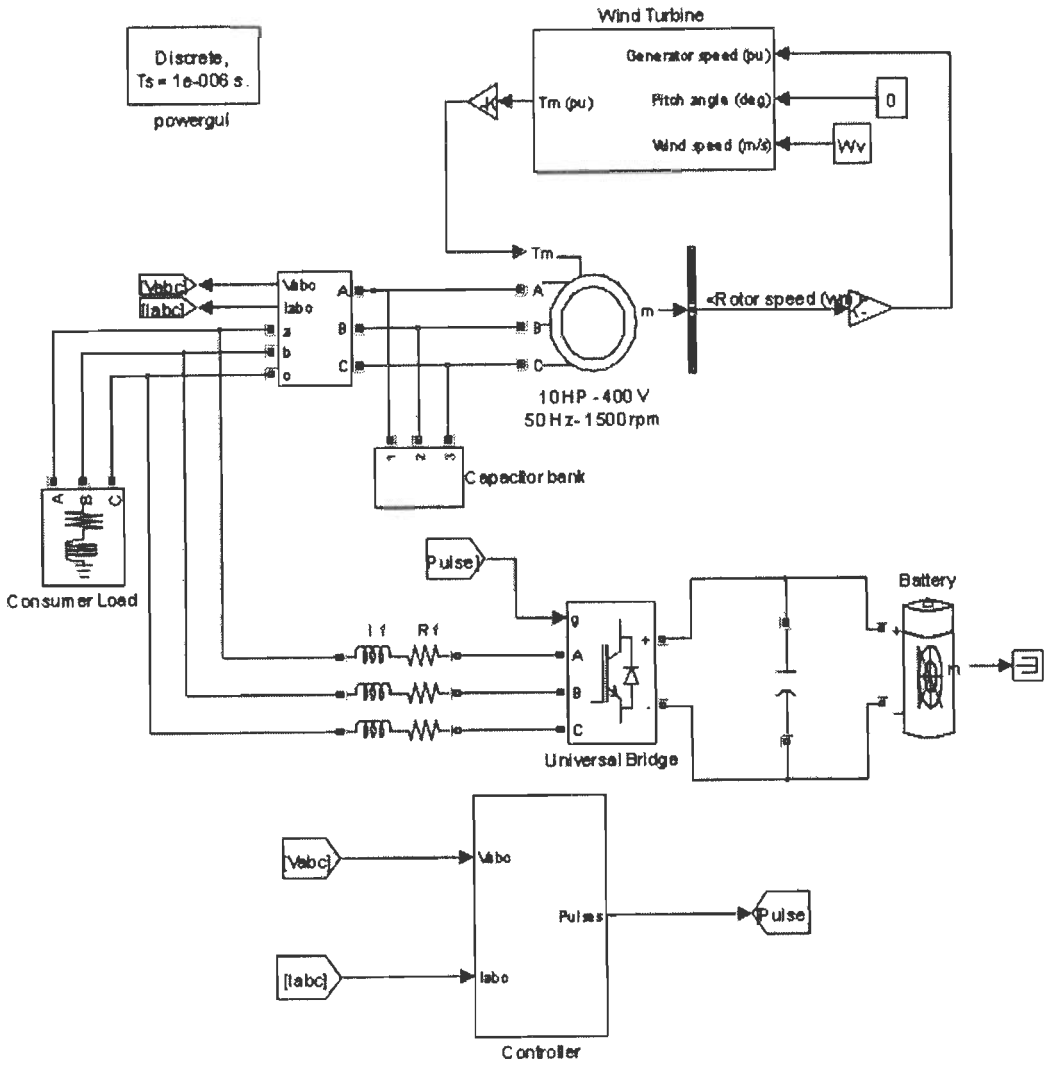


**Figure 8.2: MATLAB based model of SEIG-wind energy conversion system**

The consumer load and VSC are connected in parallel. The VSC consist of input coupling inductor, IGBT based universal bridge, output DC capacitor and battery bank. The terminal voltage and line current are measured with three phase VI measurement block and given to controller subsystem. The controller subsystem is shown in Figure 8.3. The unit template, frequency, peak terminal voltages are estimated. The voltage error and frequency error are processed through PI controller and output is multiplied with unit templates to obtain reference currents. The reference current are compared with the measured line currents and processed through hystersis controller to obtain the suitable pulse.

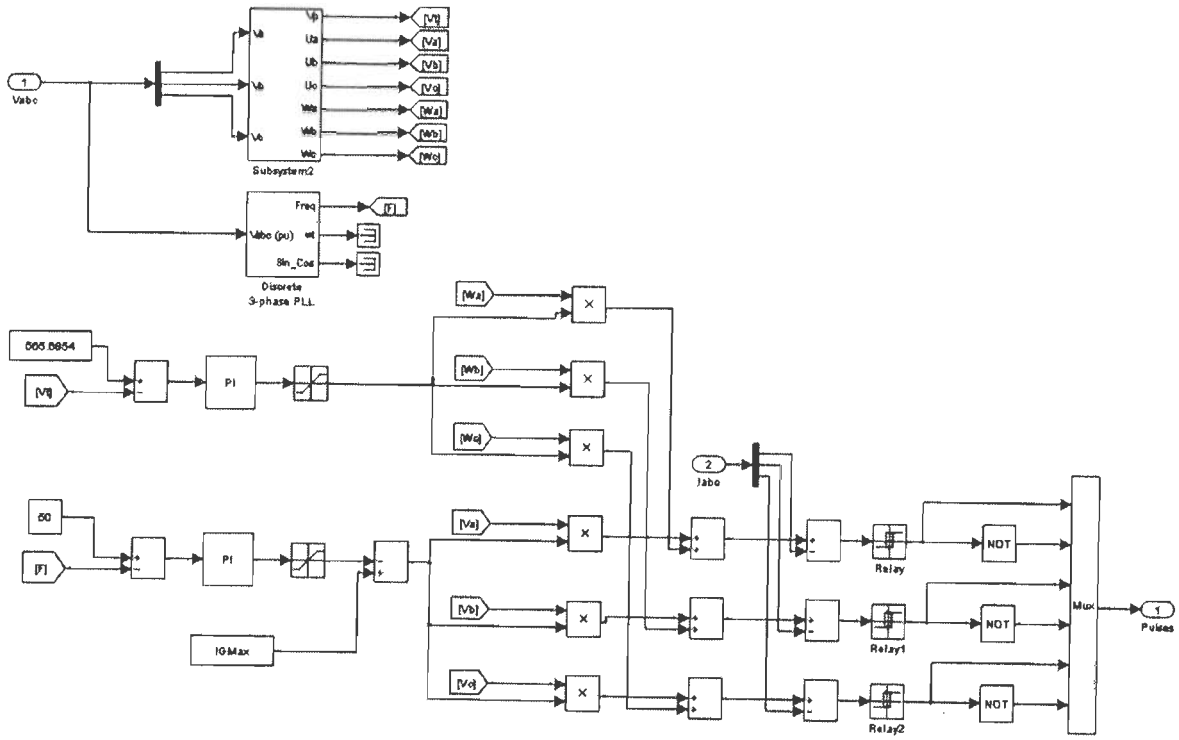


**Figure 8.3: MATLAB based Controller subsystem of SEIG-wind energy conversion system**

### Modeling of mechanical system

The power generated by the wind turbine can be expressed as:

$$P = 0.5\rho A C_P w_v^3 \tag{8.11}$$

where, $\rho$ is specific density of the air, $A$ is swept area of the blades, $C_P$ is the power coefficient and $w_v$ is the wind speed in m/s.

The power coefficient $C_p$ is the function of tip speed ratio (TSR, λ) and for a constant pitch angle ($\beta$) it may be given as:

$$C_P = C_1\{(C_2/\lambda_i) - C_3\beta - C_4\}e^{-(C/\lambda_i)} + C_6\lambda \tag{8.12}$$

$$\text{where, } 1/\lambda_i = [1/(\lambda + C_7\beta)] - \{C_8/(\beta^3 + 1)\} \text{ and } \beta = 0^0 \tag{8.13}$$

and constants $C_1$ = 0.5176, $C_2$ = 116, $C_3$ = 0.4, $C_4$ = 5, $C_5$ = 21, $C_6$ = 0.0068, $C_7$ = 0.08, $C_8$ = 0.035;

The polynomial relationship curve between $C_P$ and λ at a fixed degree pitch angle ($\beta$ = 0) is shown in Figure 8.4. The $C_P$ reaches a maximum value of 0.48 for a maximum TSR 8.1, which gives the maximum mechanical power available in the wind turbine. The Figure 8.5 shows the relationship between turbine output power to turbine speed at variable wind speed for the MATLAB library wind turbine model.

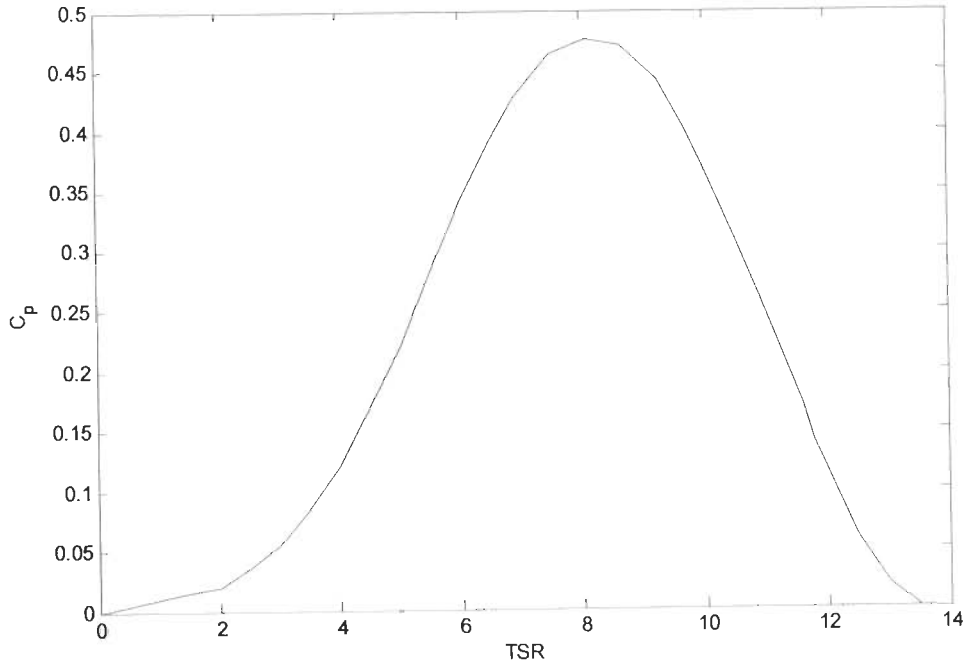


**Figure 8.4: Power coefficient ($C_P$) versus TSR (λ) curve of the wind turbine**

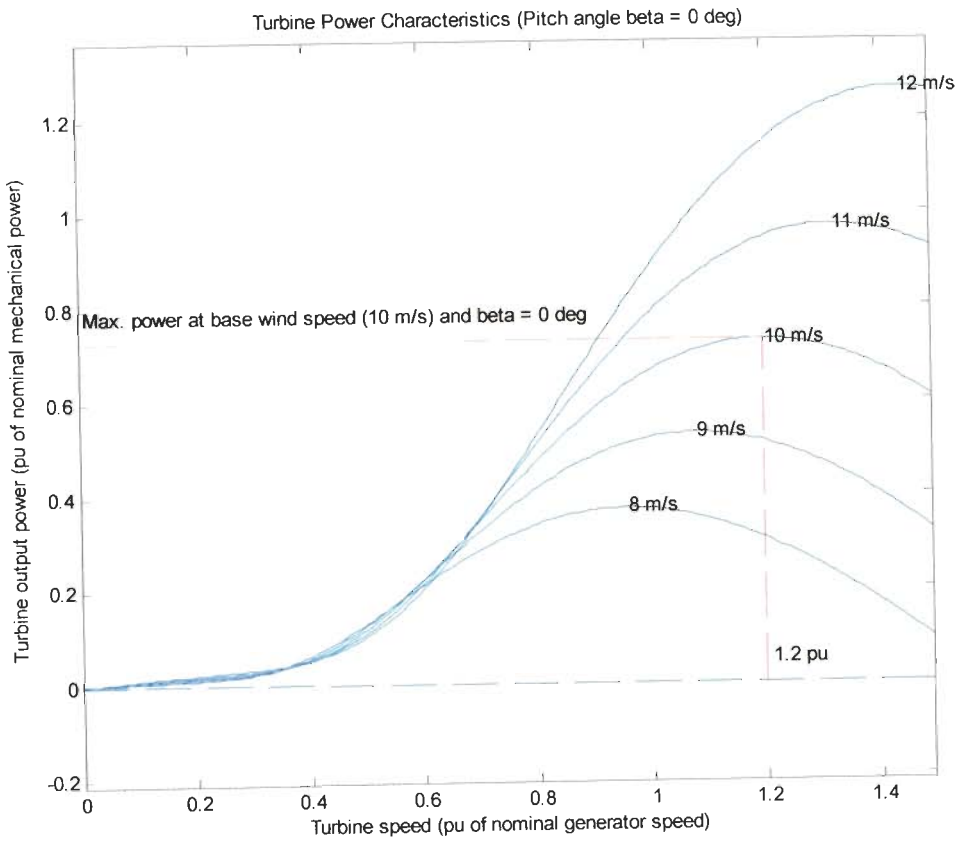


**Figure 8.5: Wind turbine power characteristics.**

**Modeling of battery bank**

A MATLAB battery bank model has been used as energy storage system for SEIG-WECS. The characteristic equation based on equivalent circuit may be given as:

$$E = E_o - \frac{KQ}{Q - it} + A\exp(-B.it) \tag{8.14}$$

where, E = No load voltage (V)

$E_0$ = Constant voltage (V)

K = Polarization voltage (V)

Q = Battery capacity (Ah)

A = Exponential voltage (V)

B = Exponential capacity (1/Ah)

i = Discharge current (A)

t = Time( seconds)

Figure 8.6 shows the nominal current discharge characteristics of the battery. The first section represents the exponential voltage drop when the battery is fully charged. The second section represents the charge that can be extracted from the battery until the voltage drops below the battery nominal voltage and the third section represents the total discharge of the battery, when the voltage drops rapidly.

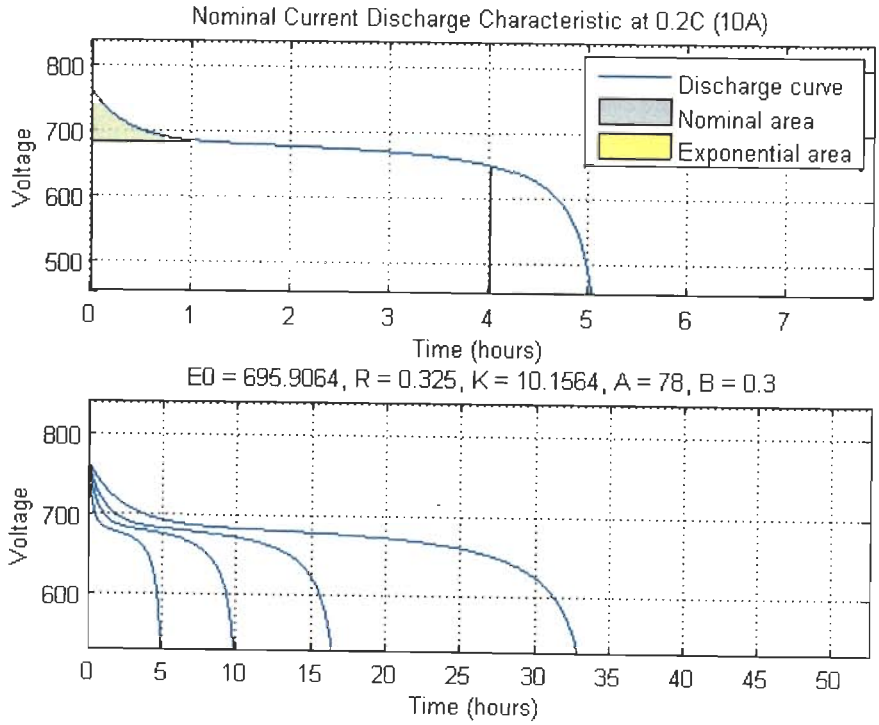


**Figure 8.6: Current discharge characteristics**

## 8.5 RESULTS AND DISCUSSION

The SEIG-WECS with energy storage system with varying consumer load and wind speed has been simulated and results are shown. Figure 8.7 shows the SEIG WECS supplying the balanced three phase resistive load. Transient waveform from top to bottom are SEIG line voltage ($V_{abc}$), SEIG line current ($I_{abc}$), load current ($I_{L,abc}$), VSC current ($I_{s,abc}$), peak terminal voltage ($V_t$), frequency (f), wind velocity ($w_v$), battery current ($I_{bb}$), DC bus voltage ($V_{dc}$) and generator, load & battery power (P). The SEIG has connected with excitation capacitor to generate 6kW at rated speed. At time t=1.55 sec. a resistive load of 4kW has been connected. On application of resistive load the voltage and frequency remains constant and current supplying to battery bank reduces subsequently VSC current reduces. At time t=1.7 sec., a resistive load of 4kW has more been connected which make the total load connected to SEIG-WECS system to 8kW. The additional 2kW load is then supplied from battery bank and battery bank current becomes negative. The power curve relation shows that the generated power remains constant at 6kW while power to battery bank becomes positive when load is less then 6kW and become negative when load power is more then 6kW.

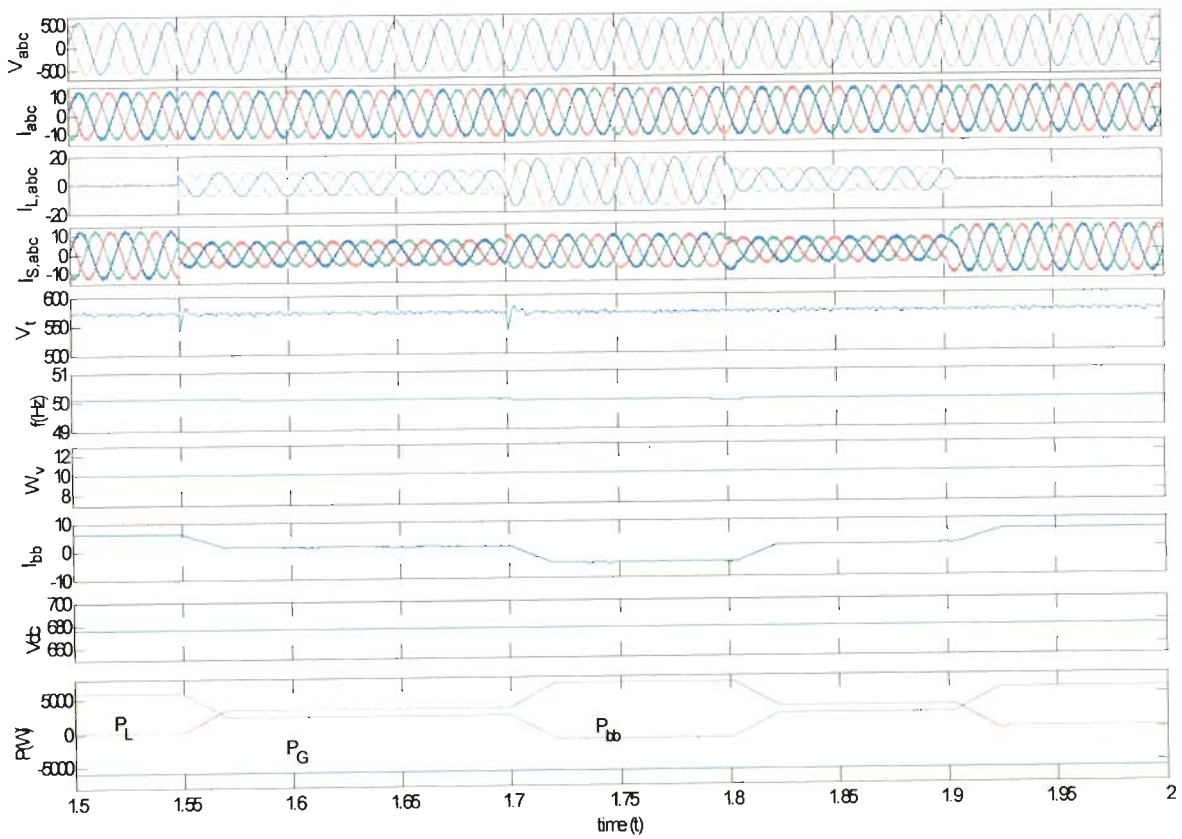


**Figure 8.7: Transient waveform of SEIG-WECS for application of 8kW resistive load application.**

Figure 8.8 shows the transient waveform of SEIG-WEC system on application of unbalanced reactive load. A 3kW, 0.8 lagging power factor balanced reactive load has been applied at t=1.55 sec. At t=1.65 sec., a single phase resistive load have been added and make the total load unbalanced. With the application of reactive unbalanced load, the voltage and frequency remains constant. The SEIG currents also remain balanced. The VSC compensated for reactive power demand of load. It also works as load balancer.

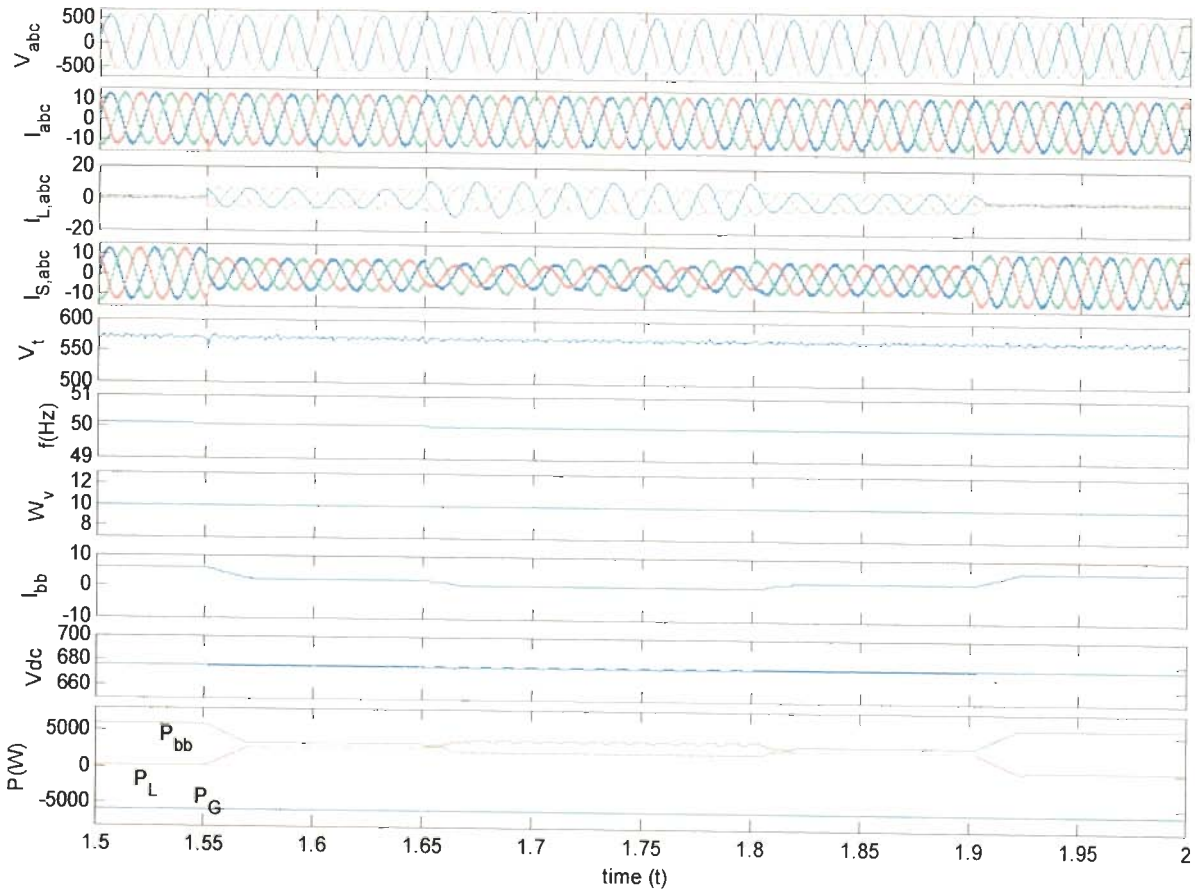


**Figure 8.8: Transient waveform of SEIG-WECS for application of unbalanced reactive load.**

Figure 8.9 shows the transient waveform on the application of nonlinear diode rectifier load with 100ohm and 100mH at DC side. Another three phase balanced resistive load of 4kW has been added at time t=1.7 sec. With application of nonlinear load, the voltage and frequency of the SEIG system remains constant similar to the case of linear and unbalanced load application. The SEIG voltage and current remains sinusoidal and VSC eliminates the harmonic generated by the nonlinear load. The generated output power remains constant and the additional active power demand is supplied form battery bank. The harmonic analysis shows that the total harmonic distortion (THD) SEIG voltage and current is obtained as 1.6% and 2.2% respectively while the load current THD is 26.2%.

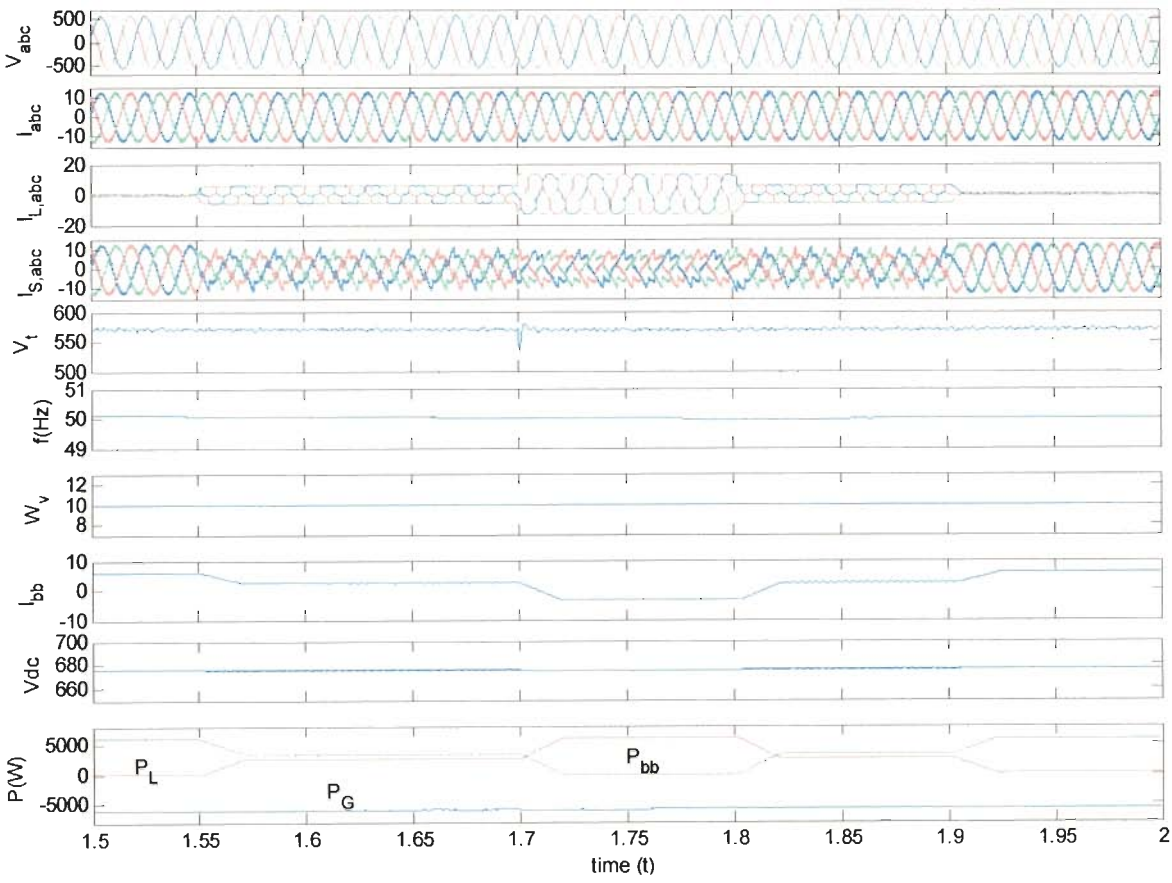


**Figure 8.9: Transient waveform of SEIG-WECS for application of nonlinear load**

Figure 8.10 shows the performance of the controller with varying wind speed and constant resistive load. At time t=1.55 sec., a balanced three phase resistive load of 4kW is applied. At time t=1.65 sec., the wind velocity is changed form 10 m/s to 12 m/s. The increase in wind speed increases the power output of the generator while voltage and frequency remains constant. The generator current also increases. At time t=1.85 sec. the wind speed is reduced form 12 m/s to 8 m/s which is below the base speed. The reduction in wind speed reduces the power output of the SEIG. The generator current also reduces accordingly. At time t=2.1 sec., load is fully removed. The voltage and frequency remains constant with the change in wind speed and with the change in consumer load. The battery bank absorbs the additional active power and delivers when load demand is increased from rated generation.

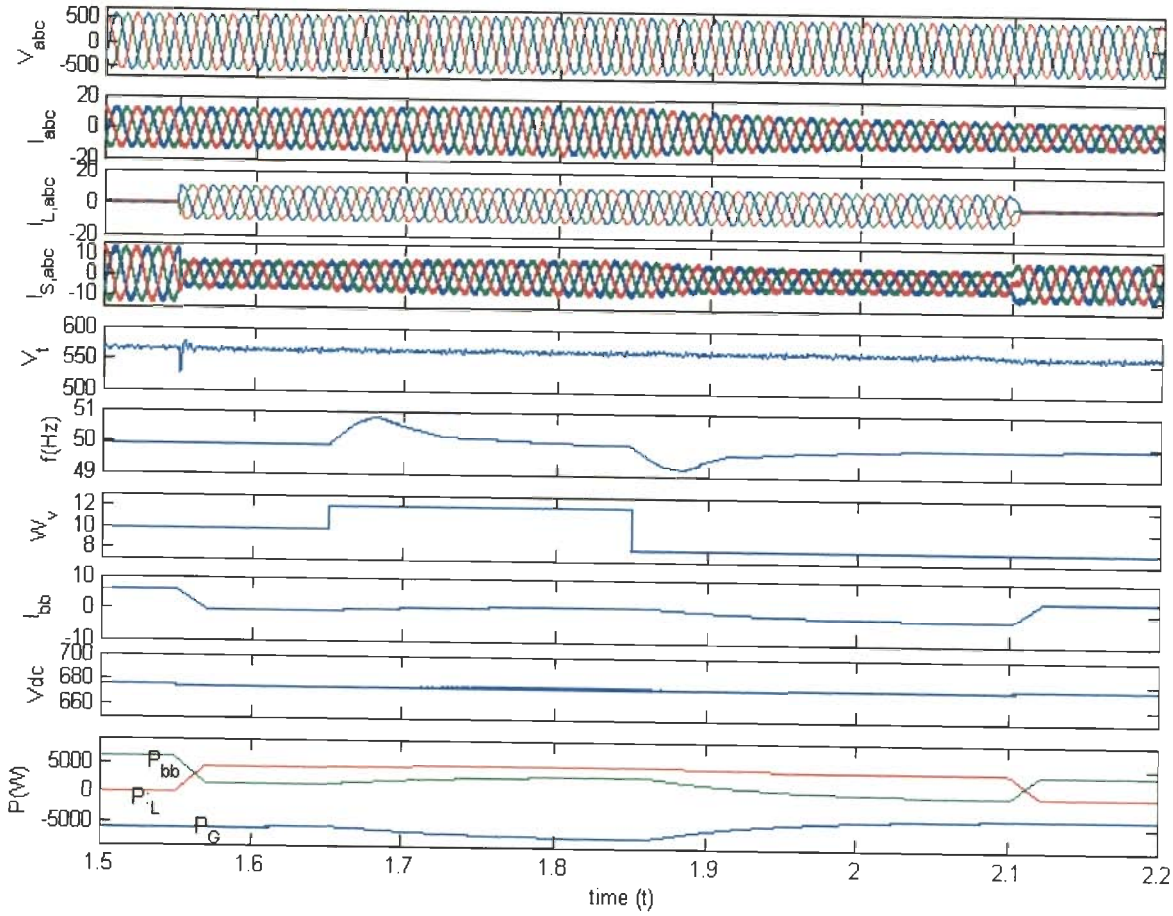


**Figure 8.10: Transient waveform of SEIG-WECS for variable wind speed and resistive load**

## 8.6 CONCLUSION

The application of SEIG for wind energy conversion system has been designed and analyzed under varying load and wind speed. A VSC based voltage and frequency regulation through a function of frequency control using a battery storage system have been designed and validated with simulation for stand alone WECS with SEIG. The proposed controller has bidirectional power flow capability of active and reactive power by which it regulates the system voltage and frequency with variation in consumer load and the speed of the wind. The VSC also act as harmonic eliminator and load balancer for non linear unbalanced consumer load. The following are the main conclusion drawn.

(i) A VSC based voltage and frequency regulation through a function of frequency control using a battery storage system have been examined and validated with simulation for stand alone WECS with SEIG.

(ii) The voltage and frequency remains constant with application of resistive, reactive, balanced, unbalanced, nonlinear loads under varying wind speed and consumer load.

(iii) The proposed controller is has bidirectional active and reactive power flow capability by which it controls the system voltage and frequency with variation of consumer load and the speed of the wind.

(iv) The VSC acts as a voltage regulator, harmonic eliminator, load balancer for varying consumer load and varying wind speed.

# CHAPTER-9

# CONCLUSIONS AND SUGGESTIONS FOR FUTURE WORK

## 9.1 GENERAL

Considering the importance of electrification of remote rural areas for sustainable development of a country, autonomous, small-scale power generation schemes are required to be developed utilizing locally available renewable energy resources such as small/mini hydro, wind, bio-mass etc. for supplying power in isolated mode. The self excited induction generator (SEIG) is found to one of the suitable option for such applications to generate power from renewable energy resources due to its inherent advantages. In remote areas, the population is sparsely distributed and the most of the electric loads are of single-phase type. The single-phase supply is preferred over three-phase upto a load of 20 kW to make the distribution system cost effective. Beyond this power rating, the power is supplied with three-phase distribution system. In the range of 5 kW to 20 kW, the three-phase induction machines being inexpensive, readily available and more efficient than single-phase machines of equivalent rating and may be used for single-phase power generation. Single phase induction motor can be used as a single phase SEIG for supplying smaller load of rating less then 5 kW. The SEIG has major drawback of poor voltage and frequency regulation. This is a major bottleneck of its application.

In view of the above, the research work has been directed for the performance analysis and voltage, frequency regulation of the SEIG. Such power generating units are suitable for far flung areas where grid connection is not economical and renewable energy can be harnessed from local resources. They must comprise of operation simplicity, less maintenance and should be operated in unattended mode with automatic control. Hence, a single chip based digital controller has been designed and developed for the economical implementation of SEIG system with reduced hardware complexity.

## 9.2 MAIN CONCLUSIONS

A comprehensive analysis of three-phase induction motor working as a three phase self excited induction generator has been carried out. Dynamic models for predicting transient responses have been developed in d-q axes stationary reference frame incorporating the effect of cross-saturation. The steady-state model is developed and the equivalent impedance of the generator and load is computed. For the minimization of closed loop equivalent impedance of the steady-state equivalent circuit, the sequential unconstrained minimization technique (SUMT) has been used in conjunction with Rosenbrock's method of rotating coordinates. The variations of output voltage, stator phase voltages and phase currents with output power have been presented from the steady-state model. The minimum capacitance required for self-excitation of the SEIG has also been determined from the steady-state model.

A digital load controller system has been designed and developed for regulating the voltage and frequency of the SEIG using DSP. The use of DSP gives cost effective solution and can eliminate the use of complicated control circuit. A single chip provides flexible solution, multiple features fast processing to implement advanced and complex algorithm. Accordingly, a DSP based load controller has been designed, developed and implemented using a new sample based controller. The proposed sample based controller is simple as compared to traditional PI controller as it requires only one parameter to be tuned for optimal operation. Experiments are carried out on developed prototype of DSP based load controller for SEIG system. The mark space ratio control resistive load is used as a dump load with static switch, in parallel with consumer load to regulate the output power at SEIG terminals. The transient behavior of DSP TMS320F2812 based load controller for SEIG system at different operating conditions such as application and removal of static (resistive and reactive) and dynamic load is investigated to demonstrate the capabilities of the proposed load controller. The MATLAB based digital simulation of the transient responses for different operating conditions have been compared with the experimental results to validate the developed model.

It is possible to use a three-phase induction motor as a single-phase SEIG and thus become the preferred approach for providing a single-phase supply. Beyond 5 kW load, the three phase induction machine, being inexpensive and readily available in the market with higher efficiency than equivalent rating single phase induction machine has become attractive proposition for supplying single phase power up to 20 kW. Three phase SEIG

supplying single phase load is the case of unbalanced operation and it is required to operate the machine at de-rated power output so that the temperature rise in the machine is restricted within permissible limits. The two type of excitation scheme have been considered for study. Two capacitor excitation of three phase delta connected induction motor to work as single phase SEIG, known as the *'C-2C'* connection. This connection gives optimum output at 415 V phase voltage for 415 V delta connected induction machine. The three capacitor excitation scheme for three phase star connected induction machine working as single phase SEIG known as '$C_p$-$C_s$' is also been analyzed. This connection gives 220 V single phase voltage output for 415 V star connected three phase induction machine. The steady-state model for both the connections has been developed individually and the equivalent impedance of the generator and load is computed. The minimum capacitance required for self-excitation and also the performance of the system at steady-state is determined from the steady-state model.

The use of three phase induction motor as a single phase SEIG is a case of extreme unbalanced operation of the machine. The analysis and MATLAB based digital simulation reveals that in '*C-2C*' connection scheme the voltage and current of the SEIG converge to balanced point at certain resistive load and fixed value of excitation capacitance. The '$C_p$-$C_s$' connection scheme has balanced voltage and phase current at no load. As the load on the machine increases they tend to become unbalanced. The phase currents are kept within the rated value by de-rating the generator operation so as not to cause the temperature rise. A detailed study supported with MATLAB based digital simulation and application of load controller to regulate the voltage and frequency of single phase SEIG using three phase induction machine have been examined. A DSP based load controller is designed, developed and implemented for single phase SEIG using three phase induction motor. The developed prototype single phase SEIG-load controller system has been extensively tested for application of static and dynamic load. The terminal voltage and frequency remains constant on application and removal of loads. The simulated results have been validated with experimental results.

Single-phase induction motors can be used as single phase self excited induction generator for single phase power generation for the purpose of supplying smaller loads of less than 5kW. Single phase induction machine is an unsymmetrical machine having two phase windings. The steady-state model of two winding single phase induction motor working as a single phase SEIG based on the double rotating field theory has been

developed. The equivalent impedance of the generator and load is used to computation the minimum capacitance required for self-excitation and also the performance of the system. The MATLAB based digital simulation is used for the performance analysis along with the experimentation, which shows the variation of terminal voltage and winding current with increase in load. The digital simulation of single phase load controller based on mark space ratio control using sample based controller has been carried out. A prototype DSP based load controller has been designed, developed and implemented in laboratory for single phase two winding induction motor working as a single phase SEIG to regulate the terminal voltage and frequency. The transient analysis of the SEIG load controller system has been carried out for resistive, reactive and dynamic load application. The MATLAB simulated transient responses has been compared with the experimental results to validate the developed model.

The SEIG can be used to generate constant voltage and frequency if the load is maintained constant at its terminals. The electrical load is maintained constant at SEIG terminals through a mark space ratio controlled load controller. The load controller keeps the total electrical load constant with variable consumer load through a dump load. The power dissipated in dump load is governed by the difference of power generated to consumer load. The load controller with uncontrolled rectifier and series connected chopper switch with mark space ratio chopper control gives unity power factor operation and it requires only one dump load. Such a load controller is nonlinear in nature and injects harmonics in the system. The harmonics generated are random in nature. The SEIG performance is severely affected with these harmonics. A dip in voltage is also observed as the harmonic content increases. Further, effort has been made to improve performance of the load controller with ac chopper control which injects minimum harmonics and makes the dump load control as a linear load. Due to symmetrical control of terminal voltage only odd harmonics are present. The harmonics appear as a side band and are the integral multiples of switching frequency. The low order harmonics are eliminated and the order of dominant voltage harmonic can be controlled through change in chopping frequency. It gives the linear control of the fundamental component of the output voltage. Two different kind of AC chopper have been analyzed based on equal time ratio control (ETRC) AC chopper and sinusoidal PWM AC chopper control. The digital design and implementation of DSP based SEIG-load controller based on ETRC AC chopper controllable load controller for three phase SEIG and based on sinusoidal PWM AC

chopper controllable load controller for single phase two winding SEIG has been examined. The transient analysis of SEIG load controller system has been carried for resistive, reactive and dynamic load and experimental results are compared with MATLAB based digital simulation results to validate the model.

The developed sample based controller is simple as compared to traditional PI controller based application. The PI controller is to be tuned for proportional ($K_p$) and integral gain ($K_i$) for dynamic responses, where as in the developed sample based controller only gain (A) is to be adjusted for a given system to regulate overshoot. A fuzzy logic based load controller have also been analyzed and implemented. A fuzzy logic based load controller gives nonlinear control with fast response and virtually no overshoot. The ETRC AC chopper load controller regulates the dump load as linear load with minimum harmonics and excellent dynamic response. A prototype SEIG-load controller system through fuzzy logic based controller with TMS320F2812 DSP has been developed, implemented and its transient behavior is investigated at different operating conditions such as application and removal of static (resistive and reactive) and dynamic loads.

The application of load controller to SEIG system is a simple and cost effective approach to regulate the voltage and frequency but the load controller does not compensate for variable reactive power demand with varying consumer load. The terminal voltage depends upon the excitation capacitance and load current. The performance of SEIG is largely affected by power factor of the load as it draws a reactive current and harmonics present in the system. A digital control algorithm for static compensator (STATCOM) based SEIG system has been designed and developed. The STATCOM compensate for reactive power with increase in load current. The control algorithm has been first co-simulated with processor in the loop (PIL) using TMS320F2812 fixed point DSP and then experimentally validated. The transient behaviour of SEIG-STATCOM system at different operating conditions such as application and removal of balanced/unbalanced, nonlinear and dynamic load is investigated. The results show that the SEIG terminal voltage and frequency remains constant while supplying balanced resistive loads. The controller compensate for the additional VAR required when reactive load is connected and keeps the terminal voltage and frequency constant. The controller balances the SEIG currents and voltage under unbalanced load application and act as load balancer. The harmonic generated by nonlinear load are compensated by proposed STACOM based controller. Therefore it acts as harmonic eliminator. The MATLAB based

digital simulation of the transient response has been compared with the experimental results to validate the developed model.

The SEIG can harness the power from constant as well as variable speed prime mover such as variable head hydro and wind turbines. The application of SEIG for wind energy conversion system has been designed and analyzed under varying load and wind speed with fixed excitation capacitance. A voltage source converter (VSC) based voltage and frequency regulation through a function of frequency control using a battery storage system have been designed and validated with MATLAB based simulation for stand alone WECS with SEIG. The voltage and frequency remains constant with application of resistive, reactive, balanced, unbalanced, nonlinear loads under varying wind speed and consumer load. The proposed controller has bidirectional active and reactive power flow capability which it regulates the system voltage and frequency with variation in consumer load and the speed of the wind. The VSC also act as harmonic eliminator and load balancer for non linear unbalanced consumer load.

## 9.3 RECOMMENDATIONS AND FUTURE SCOPE OF WORK

Research is a continuous process. An end of a research project is in fact a beginning of a lot of other avenues for future work. A door to new research issues is opened upon the end of a research project. Following aspects are identified for future research work in this area:

(i) The SEIG output power regulated with dump load controller employ resistive dump load. The resistive dump load can be replaced by energy storage device like battery or fuel cell.

(ii) The use of high power converters for dump load control can give power factor correction to the main load and thus can compensate for reactive power demand.

(iii) The SEIG-STATCOM system can further be improved with self tuning filter, digital PLL system and PWM techniques.

(iv) The SEIG-WECS with energy storage can be further explored for maximum power from wind, fuzzy logic control and vector control.

(v) The DSPs can be configured for network based applications with TCP/IP stack. Such configuration can provide remote control network applications.

# REFERENCES


[1] **Ahmed T. and Nakaoka M.,** "Static VAR compensator based terminal voltage control for stand-alone AC and DC outputted self-excited induction generator", *Proc. of IEEE International Conference on Power Electronics, Machines and Drives*, Vol. 1, pp. 40-45, 2004.

[2] **Ahmed T. Nishida K. Soushin K. and Nakaoka M.,** "Static VAR compensator based voltage control implementation of single phase self excited induction generator", *IEE Proc. Generation, Transmission & Distribution*, Vol. 152, No. 2, pp. 145-156, 2005.

[3] **Ahmed T. Nishida K., Nakaoka M. and Noro O.,** "Self excited induction generator with regulated DC voltage scheme for wind power applications", *Proc. of IEEE annual conference and Exposition on Applied Power Electronics*, Vol. 3, pp. 1831-1837, 2005.

[4] **Ahmed T., Nishida K. and Nakaoka M.,** "Static VAR compensator based voltage regulation implementation of single-phase self-excited induction generator", *Proc. of IEEE Conference on Industry Applications*, Vol. 3, pp. 2069-2076, 2004.

[5] **Ahmed T., Nishida K. and Nakaoka M.,** "Wind energy DC supply based induction generator with static VAR compensator and AC voltage regulator", *Proc. of IEE Annual International Conference on Telecommunications Energy*, pp. 689-696, 2004.

[6] **Ahmed T., Nishida K., Nakaoka M. and Woo L. H.,** "SVC and AC load voltage regulation scheme for DC outputted three-phase induction generator", *Proc. of IEEE International Conference on Power Electronics and Motion Control*, Vol. 3, pp. 1189-1194, 2004.

[7] **Ahmed T., Noro O., Hiraki E. and Nakaoka M.,** "Terminal voltage regulation characteristics by static VAR compensator for a three-phase self-excited induction generator", *IEEE Trans. on Industry Applications*, Vol. 40, No. 4, pp. 978- 988, July/August 2004.

[8] **Ahmed T., Noro O., Hiraki E. and Nakaoka M.,** "Three-phase self-excited induction generator driven by variable speed prime-mover for clean renewable energy utilization and its terminal voltage regulation characteristics by static VAR compensator", *Proc. of IEEE Conference on Industry Applications,*, Vol. 2, pp. 693-700, 2003.

[9] **Ahmed T., Noro O., Matsuo K., Shindo Y. and Nakaoka M.,** "Wind turbine coupled three-phase self-excited induction generator voltage regulation scheme with static VAR compensator controlled by PI controller", *Proc. of IEEE International Conference on Electrical Machines and Systems*, Vol. 1, pp. 293-296, 2003.

[10] **Ahmed T., Noro O., Matsuo K., Shindo Y. and Nakaoka M.,** "Minimum excitation capacitance requirements for wind turbine coupled stand-alone self-excited induction generator with voltage regulation based on SVC", *Proc. of International Conference on Telecommunications Energy*, pp. 396-403, 2003.

[11] **Ahmed T., Ogura K., Soshin K., Hiraki E. and Nakaoka M.,** "Small scale wind turbine coupled single-phase self-excited induction generator with SVC for isolated renewable energy utilization", *Proc. of IEEE International Conference on Power Electronics and Drive Systems*, Vol. 1, pp. 781-786, 2003.

[12] **Alan I., Lipo T. A.,** "Control of polyphase induction generator/induction motor power conversion system completely isolated from the utility", *IEEE Trans. on Industry Applications*, Vol. 30, No. 3, pp. 636-647, 1994.

[13] **Al-Bahrani A. H., Malik N. H.,** "Voltage control of parallel operated self-excited induction generators", *IEEE Trans. on Energy Conversion*, Vol. 8, pp. 236-242, 1993.

[14] **Al-bahrani A. H., Malik N. H.,** "Steady-state analysis and performance characteristics of a three-phase induction generator self-excited with a single capacitor", *IEEE Trans. on Energy Conversion*, Vol. 5, No. 4, pp. 725-732, 1990.

[15] **Al-Bahrani A. H., Malik N. H.,** "Steady-state analysis of parallel operated self-excited induction generators", *IEE Proc., Generation, Transmission and Distribution*, Vol. 140, No. 1, pp. 49-55, 1993.

[16] **Alexandrovitz A., Katz D.** "Analysis of transient phenomena in three phase induction motor represented in phase axes by digital simulation", *Electric Machines and Electromechanics*, Vol. 7, pp. 305-324, 1982.

[17] **Alghuwainem S. M.,** "Steady-state analysis of an isolated self-excited induction generator driven by regulated and unregulated turbines", *IEEE Trans. on Energy Conversion*, Vol. 14, No. 3, pp. 718-723, 1999.

[18] **Alghuwainem S. M.,** "Steady-state analysis of an isolated self-excited induction generator supplying an induction motor load", *Proc. of IEEE International Conference on Electric Machines and Drives*, pp. 351-353, 1999.

[19] **Al-Jabri A. K., Alolah A. I.,** "Limits on the performance of the three-phase self-excited induction generators", *IEEE Trans. on Energy Conversion*, Vol. 5, No.2, pp. 350-356, 1990.

[20] **Al-Jabri A. K., Alolah A. I.,** "Capacitance requirement for isolated self-excited induction generator", *IEE Proc., Pt. B*, Vol. 137, No. 3, pp. 154-159, 1990.

[21] **Al-Jabri A.,** "Direct evaluation for the output frequency and the magnetizing reactance of three-phase isolated self-excited induction generators", *Electric Machines and Power Systems*, Vol. 18, No. 2, pp. 113-121, 1990.

[22] **Alolah A. I., Alkanhal M. A.,** "Excitation requirements of three-phase self-excited induction generator under single-phase loading with minimum unbalance", *Proc. of IEEE Power Engineering Society Winter Meeting*, Vol. 1, pp. 257-259, January 2000.

[23] **Bailey J. D.,** "Factor influencing the protection of small to medium size induction generators", *IEEE Trans. on Industry Applications*, Vol. 24, No. 5, pp. 955-964, September/October 1988.

[24] **Bansal R. C., Bhatti T. S. and Kothari D. P.,** "Bibliography on the application of induction generators in nonconventional energy systems", *IEEE Trans. on Energy Conversion*, Vol. 18, No. 3, pp. 433-439, September 2003.

[25] **Barkle J. E., Ferguson R. W.,** "Induction generator theory and application", *AIEE Trans. on Electrical Engineering*, Vol. 73, pp. 12-19, 1954.

[26] **Bassett , Potter F. M.,** "Capacitive excitation for induction generators", *AIEE Trans. (Elect. Engg.)*, Vol. 54, pp. 540-545, 1935.

[27] **Bhattacharya J. L., Woodward J. L.,** "Excitation balancing of self-excited induction generator for maximum power output", *IEE Proc., Generation, Transmission and Distribution*, Vol. 135, No. 2, pp. 88-97, 1988.

[28] **Bim E., Szajner J. and Burian Y.,** "Voltage compensation of an induction generator with long shunt connection", *IEEE Trans. on Energy Conversion*, Vol. 4, No. 3, pp. 526-530, 1989.

[29] **Bonert R., Hoops G.,** "Stand-alone induction generator with terminal impedance controller and no turbine controls", *IEEE Trans. on Energy Conversion*, Vol. 5, No. 1, pp. 28-31, 1990.

[30] **Bonert R., Rajakaruna S.,** "Self-excited induction generator with excellent voltage and frequency control", *IEE Proc., Generation, Transmission and Distribution*, Vol. 145, No. 1, pp. 33-39, 1990.

[31] **Bose B. K.,** "Modern power electronics and AC drives", *Pearson Education Inc.*, Vol. , pp. , 2002..

[32] **Bose B. K.,** "Expert systems, fuzzy logic and neural network applications in power electronics and motion control", *IEEE Proc.*, Vol. 82, pp. 1302-1323, 1994.

[33] **Brennen M. B., Abbondati A.,** "Static exciter for induction generators", *IEEE Trans. on Industrial Application*, Vol. 13, No. 5, pp. 422-428, 1977.

[34] **Case M. J. , Van Resburg J. F. J. and Nicolae D. V.,** "Alternating current source to Volltage source converter", *Proc. of International Confrerence on Power Systems Transients*, pp. , June 19-23, 2005.

[35] **Chakraborty C., Bhadra S. N. and Chattopadhyay A. K.,** "Excitation requirements for stand alone three-phase induction generator", *IEEE Trans. on Energy Conversion*, Vol. 13, No. 4, pp. 358-365, December 1998.

[36] **Chakraborty C., Bhadra S. N., Chattopadhyay A. K. and Biswas S. K.,** "A novel two-phase self-excited induction generator- series connected converter system as DC power supply", *Proc. of IEEE Industry Applications Society Annual Meeting*, Vol. 1, pp. 374-379, 2-8 October 1993.

[37] **Chakraborty C., Bhadra S. N., Das S. P. and Chattopadhyay A. K.,** "Analysis of parallel operated self-excited induction generators", *IEEE Trans. on Energy Conversion*, Vol. 14, No.2, pp. 209-216, 1999.

[38] **Chan T. F., Lai L. L.,** "A novel excitation scheme for a stand-alone three-phase induction generator supplying single-phase loads", *IEEE Trans. on Energy Conversion*, Vol. 19, No. 1, pp. 136-143, 2004.

[39] **Chan T. F., Lai L. L.,** "A novel single-phase self-regulated self-excited induction generator using a three-phase machine", *IEEE Trans. on Energy Conversion*, Vol. 16, No. 2, pp. 204-208, 2001.

[40] **Chan T. F., Lai L. L.,** "Steady-state analysis and performance of a single-phase self-regulated self-excited induction generator", *IEE Proc., Generation, Transmission and Distribution*, Vol. 149, No. 2, pp. 233-241, 2002.

[41] **Chan T. F.,** "Capacitance requirements of induction generators", *IEEE Trans. on Energy Conversion*, Vol. 8, No. 2, pp. 304-311, 1993.

[42] **Chan T. F.,** "Performance analysis of a three-phase induction generator connected to a single-phase power system", *IEEE Trans. on Energy Conversion*, Vol. 13, No. 3, pp. 205-213, 1998.

[43] **Chan T. F.,** "Analysis of single-phase self-excited induction generator", *Electric Machines and Power Systems*, Vol. 23, No. 2, pp. 149-162, 1995.

[44] **Chan T. F.,** "Steady state analysis of self-excited induction generators using an iterative method", *IEEE Trans. on Energy Conversion*, Vol. 10, No. 3, pp. 502-507, 1995.

[45] **Chan T. F.,** "Steady-state analysis of self-excited induction generators", *IEEE Trans. on Energy Conversion*, Vol. 9, No. 2, pp. 288-296, June 1994.

[46] **Chan T. F.,** "Self-excited induction generators driven by regulated and unregulated turbines", *IEEE Trans. on Energy Conversion*, Vol. 11, No. 2, pp. 338-343, June 1996.

[47] **Chan T. F., Lai L. L.,** "A novel single-phase self-regulated self-excited induction generator using a three-phase machine", *Proc. of IEEE International Conference on Electric Machines and Drives*, pp. 616-618, 1999.

[48] **Chan T. F., Lai L. L.,** "Capacitance requirements of a three-phase induction generator self-excited with a single-capacitance and supplying a single-phase load", *IEEE Trans. on Energy Conversion*, Vol. 17, No. 1, pp. 90-94, March 2002.

[49] **Chan T. F., Lai L. L.,** "Single-phase operation of a three-phase induction generator using a novel line current injection method", *Proc. of IEEE International Conference on Electric Machines and Drives*, Vol. 2, pp. 715-720, 2003.

[50] **Chan T. F., Lai L. L.,** "Single-phase operation of a three-phase induction generator using a novel line current injection method", *IEEE Trans. on Energy Conversion*, Vol. 20, No. 2, pp. 308-315, 2005.

[51] **Chan T. F., Nigim K. A. and Lai L. L.,** "Voltage and frequency control of self-excited slip-ring induction generators", *IEEE Trans. on Energy Conversion*, Vol. 19, No. 1, pp. 81-87, 2004.

[52] **Chan T. F., Nigim K. and Lai L. L.,** "Voltage and frequency control of self-excited slip-ring induction generators", *Proc. of IEEE International Conference on Electric Machines and Drives*, pp. 410-414, 2001.

[53] **Chatterjee Jayanta K., Venkatesa Perumal B. and Reddy Gopu Naveen,** "Analysis of operation of a self-excited induction generator with generalized impedance controller", *IEEE Trans. on Energy Conversion*, Vol. 22, No. 2, pp. 307-315, June 2007.

[54] **Chirgwin M. and Stratton L. J.,** "Variable speed constant frequency generation system for air-craft", *AIEE Trans. on Electrical Engineering*, Vol. 78, pp. 304-310, 1959.

[55] **Colak I., Garvey S. D. and Wright M. T.** "Simulation of induction machine using phase variable and the explicit inverse inductance matrix", *Zinternational Journal of Elect. Engg. Edu.*, Vol. 32, pp. 354-365, 1995.

[56] **Daly S. A., Paor A. M. D. and Simpson R. J.,** "Modelling and control of wind driven wind-driven induction generator for water storage heating", *IEE Proc.Pt. A*, Vol. 130, No. 9, pp. 596-603, 1987.

[57] **Datta R., Ranganathan V. T.,** "Variable-speed wind power generation using doubly fed wound rotor induction machine – a comparison with alternative schemes", *IEEE Trans. on Energy Conversion*, Vol. 17, No. 3, pp. 414-421, September 2002.

[58] **Datta R., Ranganathan V. T.,** "A method of tracking the peak power for a variable speed wind energy conversion system", *IEEE Trans. on Energy Conversion*, Vol. 18, No. 1, pp. 163-168, March 2003.

[59] **Do-Hyun Jang, Gyu-Ha Choe,** "Step up/down AC voltage regulator using transformer with tap changer and PWM AC chopper", *IEEE Trans. on Industrial Electronics*, Vol. 45, No. 6, pp. 905-911, December 1998.

[60] **Do-Hyun Jang, Gyu-Ha Choe and Mehraded Ehsani,** "Asymmetrical PWM Technique with harmonic elimination and power factor control in AC choppers", *IEEE Trans. on Power Electronics*, Vol. 10, No.2, pp. 175-184, March 1995.

[61] **Donescu V., Charelte A., Yao Z. and Rajgopalam V.,** "Modelling and simulation of saturated induction motor in phase qualities", *IEEE Trans. on Energy Conversion*, Vol. 14, No. 3, pp. 386-393, 1999.

[62] **Doxey B. C.,** "Theory and application of capacitor-excited induction generator", *The Engineer*, Vol. 29, pp. 893-897, 1963.

[63] **Elder J. M., Boys J. T. and Woodward J. L.,** "Integral cycle control of stand-alone generators", *IEE Proc., generation, Transmission and Distribution*, Vol. 132, No. 2, pp. 57-66, 1985.

[64] **Elder J. M., Boys J. T. and Woodward J. L.,** "Self-excited induction machine as low cost generator", *IEE Proc., Generation, transmission and Distribution*, Vol. 131, No. 2, pp. 33-40, 1984.

[65] **Elder J. M., Boys J. T. and Woodward J. L.,** "Integral cycle control of stand-alone generators", *IEE Proc., generation, Transmission and Distribution*, Vol. 132, No 2, pp. 57-66, 1985.

[66] **Elder J. M., Boys J. T. and Woodward J. L.,** "The process of self-excitation in induction generators", *IEE Proc., Electric Power Applications*, Vol. 130, No. 2, pp. 103-108, March 1983.

[67] **Eltamaly A. M.,** "New formula to determine minimum capacitance required for self-excited induction generator", *Proc. of IEEE Annual Conference of Power Electronics Specialists, PESC 02*, Vol. 1, pp. 106-110, 2002.

[68] **Erdelyi E., Kolatorowicz E. E. and Miller W. R.,** "The limitations of induction generator in constant frequency aircraft system", *AIEE Trans. on Electrical Engineering*, Vol. 77, pp. 348-351, 1958.

[69] **Erisa T., Takata S. and Ueda R.,** "Dynamic performance of self-excited induction generator with voltage controller", *IEEE Trans. on Industry Applications*, Vol. 2, pp. 508-513, 1980.

[70] **Faiz J.,** "Design and implementation of a solid state controller for regulation of output voltage of a wind driven self excited three phase squirrel cage induction generator", *Proc. of 8th International Conf. on Electr. Mach. System*, Vol. 3, pp. 2384-2388, 2005.

[71] **Farret F. A., Palle B. and Simoes M. G.,** "State-space modeling of parallel self-excited induction generators for wind farm simulation", *Proc. of IEEE Conference on Industry Applications*, Vol. 4, pp. 2801-2807, 2004.

[72] **Farret F. A., Palle B. and Simoes M. G.,** "Full expandable model of parallel self-excited induction generators", *IEE Proc., Electric Power Applications*, Vol. 152, No. 1, pp. 96-102, 2005.

[73] **Fukami T., Imamura M., Kaburaki Y. and Miyamoto T.,** "A new self-regulated self-excited single-phase induction generator using a squirrel-cage three-phase induction machine", *Proc. of Int. Conf. on Energy Management and Power Delivery*, Vol. 1, pp. 308-312, 1995.

[74] **Fukami T., Kaburaki Y., Kawahara S. and Miyamoto T.,** "Performance analysis of a self-regulated self-excited single-phase induction generator using a three-phase machine", *IEEE Trans. on Energy Conversion*, Vol. 14, No. 3, pp. 622-627, September 1999.

[75] **Fukami T., Kaburaki Y., Kawahara S. and Miyamoto T.,** "Performance analysis of a self-regulated self-excited single-phase induction generator using a three-phase machine", *Proc. of IEEE International Conference Record on Electric Machines and Drives*, pp. TD2/3.1 - TD2/3.3, 1997.

[76] **Gamal M. Hashem,** "Generalized symmetrical angle PWM technique for ac voltage controller", *39th International Universities Power Engineering Conference UPEC 2004.*, Vol. 2, pp. 898- 901, 2004..

[77] **Goyal H., Bhatti T. S. and Kothari D. P.,** "A novel technique proposed for automatic control of small hydro power plants", *International Journal of Global Energy Issues*, Vol. 24, No. 1/2, pp. 29-46, 2005.

[78] **Grantham C., Sutanto D. and Mismail B.,** "Steady-state and transient analysis of self-excited induction generators", *IEE Proc., Electric Power applications*, Vol. 136, No. 2, pp. 61-68, 1989.

[79] **Hallenius K. E., Vas P. and Brown J. E.,** "The analysis of a saturated self-excited asynchronous generator", *IEEE Trans. on Energy Conversion*, Vol. 6, No. 2, pp. 336-344, 1991.

[80] **Harrington R. J., Bassiouny F. M. M.,** "New approach to determine the critical capacitance for self-excited induction generators", *IEEE Trans. on Energy Conversion*, Vol. 13, No. 3, pp. 244-249, 1998.

[81] **Henderson D.,** "An advanced electronic load governor for control of micro hydroelectric generation", *IEEE Trans. on Energy Conversion*, Vol. 13, No. 3, pp. 300-304, September 1998.

[82] **Hillowala R. M., Sharaf A. M.,** "A utility interactive wind energy conversion scheme with an asymchronous DC link using a supplementary control loop", *IEEE Trans. on Energy Conversion*, Vol. 9, No. 3, pp. 558-563, 1994.

[83] **Jain S. K., Sharma J. D. and Singh S. P.,** "Transient performance of three-phase self-excited induction generator during balanced and unbalanced faults.", *IEE Proc., Generation, Transmission and Distribution*, Vol. 149, No. 1, pp. 50-57, January 2002.

[84] **Jayaramaiah G. V., Fernandes B. G.,** "Novel Voltage Controller for Stand-alone Induction Generator using PWM-VSI", *Proc. of IEEE Conference on Industry Applications*, Vol. 1, pp. 204-208, October 2006.

[85] **Jayaramaiah G. V., Fernandes B. G.,** "Voltage controller for stand-alone induction generator using instantaneous power control", *Proc. of IEEE International Conference on Power Electronics Systems and Applications*, pp. 102-106, 2004.

[86] **Jimoh A. A., Ojo O.,** "Self-excitation in PWM inverter excited single-phase induction generator", *Proc. of IEEE AFRICON*, Vol. 2, pp. 871-876, 1999.

[87] **Joshi D., Sandhu K. S. and Soni M. K.,** "Constant voltage constant frequency operation for a self-excited induction generator", *IEEE Trans. on Energy Conversion*, Vol. 21, No. 1, pp. 228-234, March 2006.

[88] **Khaled E. Addoweesh,** "An exact analysis of an ideal static AC chopper", *International Journal of Electronics*, Vol. 75, No.5, pp. 999-1013, 1993.

[89] **Khan P. K. S., Chatterjee J. K., Salam M. A. and Ahmad H.,** "Transient performance of unregulated prime-mover driven stand-alone self-excited induction generator with solid-state lead-lag Var compensator", *Proc. of TENCON 2000*, Vol. 1, pp. 235-239, September 2000.

[90] **Khan P.K.S., Chatterjee J.K.,** "Modelling and control design for self-excited induction generator with solid state lead-lag VAR compensator in micro-hydro energy conversion scheme", *Proc. of IEEE International Conference on Global Connectivity in Energy, Computer, Communication and Control, TENCON '98*, Vol. 2, pp. 398-401, 1998.

[91] **Kormilo S., Robinson P.,** "Electronic control of small hydroelectric schemes using a microcomputer", *IEE Proc., Part-E*, Vol. 131, No. 4, pp. 132-136, 1984.

[92] **Krause P. C., Thomas C. H.,** "Simulation of symmetrical induction machinery", *IEEE Trans. on Power Apparatus and Systems*, Vol. 84, No. 11, pp. 1038-1053, 1965.

[93] **Krause P. C.,** "Analysis of electrical machinery", *McGraw-Hill Book Company*, 1986.

[94] **Kumaresan N.,** "Analysis and control of three-phase self-excited induction generators supplying single-phase ac and dc loads", *IEE Proc., Electric Power Applications*, Vol. 152, No. 3, pp. 739-747, 2005.

[95] **Kuo S. C., Wang L.,** "Steady-state performance and dynamic stability of a self-excited induction generator feeding an induction motor", *IEEE Power Engineering Society Winter Meeting*, Vol. 1, pp. 277-280, 2000.

[96] **Kuo S. C., Wang L.,** "Analysis of isolated self-excited induction generator feeding a rectifier load", *IEE Proc., Generation, Transmission and Distribution*, Vol. 149, No.1, pp. 90-97, 2002.

[97] **Kuo S. C., Wang L.,** "Dynamic eigenvalue analysis of a self-excited induction generator feeding an induction motor", *Proc. of IEEE Power Engineering Society Winter Meeting*, Vol. 3, pp. 1393-1397, 2001.

[98] **Kuo S. C., Wang L.,** "Analysis of voltage control for a self-excited induction generator using a current controlled voltage source inverter (CC-VSI)", *IEE Proc., Generation, Transmission and Distribution*, Vol. 148, No. 5, pp. 431-438, September 2001.

[99] **Kuparman A., Rabinovici R.,** "Shunt voltage regulators for autonomous induction generators. Part1: Principles of operation", *Proc. of IEEE International Conference on Electronics, Circuits and Systems, ICECS*, 2004.

[100] **Larsen E., Miller N., Nilsson S. and Lindgren S.,** "Benefits of GTO based compensation systems for electric utility applications", *IEEE Trans. on Power Delivery*, Vol. 7, No. 4, pp. 2055-2064, 1997.

[101] **Lee C. C.,** "Fuzzy logic in control system: Fuzzy logic controller- part I", *IEEE Trans. on System, Man, and Cybernetics*, Vol. 20,No. 2, pp. 404-418, 1990.

[102] **Lee C. C.,** "Fuzzy logic in control system: Fuzzy logic controller- part II", *IEEE Trans. on System, Man, and Cybernetics*, Vol. 20,No. 2, pp. 419-435, 1990.

[103] **Lee C. H., Wang L.,** "A novel analysis of parallel operated self-excited induction generators", *IEEE Trans. on Energy Conversion*, Vol. 13, No. 2, pp. 117-123, 1998.

[104] **Lee R. J., Pillay P. and Harley R. G.,** "D-Q reference frames for the simulation of induction motor", *Electric Power Systems Research*, Vol. 8, pp. 15-26, 1984.

[105] **Levi E., Rauski D.,** "Modelling of deep-bar and double-cage self-excited induction generators for wind electricity studies", *Electric Power Systems Research*, Vol. 27, pp. 73-81, 1993.

[106] **Levi E.,** "A unified approach to main flux saturation modeling in D-Q axis model of induction machines", *IEEE Trans. on Energy Conversion*, Vol. 10, No. 3, pp. 455-461, September 1995.

[107] **Levi E.,** "Impact of cross saturation on accuracy of saturated induction machine models", *IEEE Trans. on Energy Conversion*, Vol. 12, No. 3, pp. 211-216, September 1997.

[108] **Liao Y. W., Levi E.,** "Modelling and simulation of a stand-alone induction generator with rotor flux oriented control", *Electric Power Systems Research*, Vol. 46, pp. 141-152, 1998.

[109] **Lipo T. A., Consoli A.,** "Modelling and simulation of induction motors with saturable leakage reactance", *IEEE Trans on Industry Application*, Vol. 20, pp. 180-189, 1981.

[110] **Lopes L. A. C., Almeida R. G.,** "Operation aspects of an isolated wind driven induction generator regulated by a shunt voltage source inverter", *Proc. of Conference of IEEE Industry Applications*, Vol. 4, pp. 2277-2282, 2000.

[111] **Lopes L. A. C., Almeida R. G.,** "Wind driven self excited induction generator with voltage and frequency regulated by a reduced rating voltage source inverter", *IEEE Trans. on Energy Conversion*, Vol. 21, No. 2, pp. 297-304, June 2006.

[112] **Mahato S. N., Sharma M. P. and. Singh S. P,** "Excitation capacitance required for self excited single phase induction generator using three phase machine", *International Journal of Energy Conversion and Management*, Vol. 49, No. 5, pp. 1126-1133, 2008.

[113] **Mahato S. N., Sharma M. P. and. Singh S. P,** "Capacitor required for maximum power of a self excited single phase induction generator using a three phase machine", *IEEE Trans. on Energy Conversion*, Vol. 23, No. 2, pp. 372-381, 2008.

[114] **Mahato S. N., Sharma M. P. and. Singh S. P,** "Steady state and dynamic behaviour of a single phase self excited induction generator using a three phase machine", *International Journal of Emerging Electric Power Systems*, Vol. 8, Issue 3, pp. Article 5, August 2007.

[115] **Mahato S. N., Sharma M. P. and. Singh S. P,** "Selection of optimal capacitors for maximum power output of a single phase self excited induction generator using a three phase machine", *Electric power components and systems*, Vol. 35, No. 8, pp. 857-870, August 2007.

[116] **Mahato S. N., Sharma M. P. and. Singh S. P,** "Transient performance of a single phase self regulated self excited induction generator using a three phase machine", *Electric Power Systems Research*, Vol. 77, pp. 839-850, 2007.

[117] **Mahato S. N., Sharma M. P. and. Singh S. P,** "Capacitor required for maximum power of a self excited single phase induction generator using a three phase machine", *IEEE Trans. on Energy Conversion*, Vol. 23, No. 2, pp. 372-381, 2008.

[118] **Mahato S. N., Sharma M. P. and. Singh S. P,** "Excitation capacitance required for self excited single phase induction generator using three phase machine", *International Journal of Energy Conversion and Management*, Vol. 49, No. 5, pp. 1126-1133, 2008.

[119] **Mahato S. N., Sharma M. P. and. Singh S. P,** "Selection of optimal capacitors for maximum power output of a single phase self excited induction generator using a three phase machine", *Electric power components and systems*, Vol. 35, No. 8, pp. 857-870, August 2007.

[120] **Mahato S. N., Sharma M. P. and. Singh S. P,** "Transient performance of sinle phase self regulated self excited induction generator using a three phase machine", *Electric Power Systems Research*, Vol. 77, pp. 839-850, 2007.

[121] **Malik N. H., Haque S. E.,** "Steady state analysis and performance of an isolated self-excited induction generator", *IEEE Trans. on Energy Conversion*, Vol. EC-1, No. 3, pp. 134-139, September 1986.

[122] **Malik N. H., Al-Bahrani A. H.,** "Influence of the terminal capacitor on the performance characteristics of a self-excited induction generator", *IEE Proc., Generation, Transmission and Distribution*, Vol. 137, No. 2, pp. 168-173, March 1990.

[123] **Malik N. H., Mazi A. A.,** "Capacitive requirements for isolated self-excited generators", *IEEE Trans. on Energy Conversion*, Vol. 2, No. 1, pp. 62-69, 1987.

[124] **Margato E., Santana J.,** "Induction generator excited by current source inverter used as a DC power supply – Modelling and behaviour", *Proc. IEEE International Symposium on Industrial Electronics*, Vol. , pp. 814-819, 1996.

[125] **Marra E. G., Pomilio J. A.,** "Self-excited induction generator controlled by a VS-PWM bi-directional converter for rural application", *IEEE Trans. on Industry Applications*, Vol. 35, No. 4, pp. 877-883, July-August 1999.

[126] **Marra E. G., Pomilio J. A.,** "Induction generator based system providing regulated voltage with constant frequency", *IEEE Trans. on Industrial Electronics*, Vol. 47, pp. 908-914, 2000.

[127] **Melkebeek J. A. A., Novotny D. W.,** "Small signal dynamic analysis of regeneration and self-excitation in induction machines", *Electric Machines and Power Systems*, Vol. 8, pp. 259-280, 1983.

[128] **Melkebeek J. A. A.,** "Magnetizing field saturation and dynamic behavior of induction machines, Part-I: Improved calculation method for induction machine dynamics, Part-II: Stability limit of a voltage fed induction motor and self-excited induction generator", *IEE Proc., Electric Power Applications*, Vol. 130, No.1, pp. 1-17, 1983.

[129] **Mishra R. K., Singh B. and Vasantha M. K.,** "Voltage regulator for isolated self-excited cage induction generator", *Electric Machines and Power Systems*, Vol. 24, No.1, pp. 75-83, 1992.

[130] **Moo C. S., Wei C. C., Huang C. L. and Liu C. T.,** "Hybrid model for dynamic simulation of solid state controlled induction machine", *Electric Machines and Power Systems*, Vol. 17, pp. 269-282, 1989.

[131] **Muljadi E., Lipo T. A.,** "Series compensated PWM inverter with battery supply applied to an isolated induction generator", *IEEE Trans. on Industry Applications*, Vol. 30, No. 4, pp. 1073-1082, July-August 1994.

[132] **Murthy S. S.,** "A novel self-excited self-regulated single-phase induction generator Part 1: Basic System and Theory", *IEEE Trans. on Energy Conversion*, Vol. 8, No. 3, pp. 377-382, 1993.

[133] **Murthy S. S., Malik O. P. and Tandon A. K.,** "Analysis of self-excited induction generators", *IEE Proc., Generation, Transmission and Distribution*, Vol. 129, No.6, pp. 260-265, 1982.

[134] **Murthy S. S., Malik O. P. and Walsh P.,** "Capacitive requirements of self-excited induction generator to achieve desired voltage regulation", *Proc. of IEEE Industrial and Commercial Power Systems Conf.*, Milwaukee, 1983.

[135] **Murthy S. S., Rai H. C. and Tandon A. K.,** "A novel self-excited self-regulated single-phase induction generator Part II : Experimental investigation", *IEEE Trans. on Energy Conversion*, Vol. 8, No. 3, pp. 383-388, 1993.

[136] **Murthy S. S., Rai H. C., Singh Bhim, Singh B. P., Goyal N. K. and Vaishya M. O.,** "New experimental finding on a novel two-winding single-phase self-excited induction generator for standby power generation", *Proc. of IEEE International Conference on PEDES*, pp. 674-678, 1996.

[137] **Murthy S. S., Rini Jose and Bhim Singh,** "A practical load controller for stand alone small hydro systems using self excited induction generator", *Proceedings of IEEE International Conference on Power Electronic Drives and Energy Systems for Industrial Growth*, Vol. 1, pp. 359-364, 1998.

[138] **Murthy S. S., Singh B. P., Nagamani C. and Satyanarayana K. V. V.,** "Studies on the use of conventional induction motors as self-excited induction generators", *IEEE Trans. on Energy Conversion*, Vol. 3, No. 4, pp. 842-848, 1986.

[139] **Nabil A. Ahmed, Kenji Amei and Masaaki Sakui,** "A new configuration of single phase symmetrical PWM AC choppwer voltage controller", *IEEE Trans. on Industrial Electronics*, Vol. 46, No. 5, pp. 942-952, 1999.

[140] **Nigim K. A., Heydt G. T.,** "Power quality improvement using intergral PWM control in an AC/AC voltage converter", *Electric Power Systems Research*, Vol. 63, pp. 65-71, 2002.

[141] **Novotny D. W., Gritter D. J. and Studsmann G. H.,** "Self-excitation in inverter driven induction machines", *IEEE Trans. on Power Apparatus and Systems*, Vol. 96, No. 4, pp. 1117-1125, 1977.

[142] **Ojo O., Bhat I.,** "An analysis of single-phase self-excited induction generators: Model development and steady-state calculations", *IEEE Trans. on Energy Conversion*, Vol. 10, No.2, pp. 254-260, 1995.

[143] **Ojo O., Gonoh B.,** "A controlled stand-alone single-phase induction generator", *Proc. of the International Conference on Power Electronics, Drives and Energy Systems for Industrial Growth*, Vol. 2, pp. 694-699, 1996.

[144] **Ojo O.,** "Minimum air-gap flux linkage requirement for self-excitation in stand-alone induction generators", *IEEE Trans. on Energy Conversion*, Vol. 10, No. 3, pp. 484-491, September 1995.

[145] **Ojo O.,** "The transient and qualitative performance of a self-excited single-phase induction generator", *IEEE Trans. on Energy Conversion*, Vol. 10, No. 3, pp. 493-501, 1995.

[146] **Ojo O.,** "Performance of self-excited single-phase induction generators with shunt, short-shunt and long-shunt excitation connections", *IEEE Trans. on Energy Conversion*, Vol. 11, No. 3, pp. 477-482, 1996.

[147] **Ojo O., Omozusi O. and Jimoh A. A.,** "Performance of an autonomous single-phase induction generator with a bi-directional PWM inverter-battery system in the auxiliary winding", *Proc. of IEEE International Symposium on Industrial Electronics*, Vol. 1, pp. 306-311, 1998.

[148] **Ojo O., Omozusi O. and Jimoh A. A.,** "The operation of an inverter-assisted single-phase induction generator", *IEEE Trans. on Industrial Electronics*, Vol. 47, No. 3, pp. 632-640, 2000.

[149] **Ojo O., Omozusi O. and Jimoh A. A.,** "Expanding the operating range of a single-phase induction generator with a PWM inverter", *Proc. of IEEE Industry Applications Conference*, Vol. 1, pp. 205-212, 1998.

[150] **Ojo O., Omozusi O., Ginart A. and Gonoh B.,** "The operation of a stand-alone, single-phase induction generator using a single-phase, pulse-width modulated inverter with a battery supply", *IEEE Trans. on Energy Conversion*, Vol. 14, No. 3, pp. 526-531, 1999.

[151] **Palle B., Simoes M. G. and Farret F. A.,** "Dynamic simulation and analysis of parallel self-excited induction generators for islanded wind farm systems", *IEEE Trans. on Industry Applications*, Vol. 41, No.4, pp. 1099-1106, 2005.

[152] **Park R. H.,** "Two reaction theory of synchronous machines, Part-I: Generalized method of analysis", *AIEE Trans. (Elect. Engg.)*, Vol. 48, pp. 716-727, 1929.

[153] **Quazene L., McPherson G. Jr.,** "Analysis of the isolated induction generator", *IEEE Trans. on Power Apparatus and Systems*, Vol. PAS-102, No. 8, pp. 2793-2798, August 1983.

[154] **Quispe E. C., Arias R. D. and Quintero J. E.,** "A new voltage regulator for self-excited induction generator – design, simulation and experimental results", *IEEE Int. Conf. Record of Electric Machines and Drives*, pp. TB3/7.1-TB3/7.3, 1997.

[155] **Rahim Y. H. A.,** "Excitation of isolated three-phase induction generator by a single capacitor", *IEE Proc., Electric Power Applications*, Vol. 140, No. 1, pp. 44-50, 1993.

[156] **Rahim Y. H. A., Alolah A. I. and Al-Mudaiheem R. I.,** "Performance of single-phase induction generators", *IEEE Trans. on Energy Conversion*, Vol. 8, No. 3, pp. 389-395, 1993.

[157] **Rahmani L., Krim F., Khanniche M. S. and Boufia A.,** "Control for PWM ac chopper feeding nonlinear loads", *International Journal of Electronics*, Vol. 91, N0. 3, pp. 149-163, 2004.

[158] **Rajakaruna S., Bonert R.,** "A technique for the steady-state analysis of a self-excited induction generator with variable speed", *IEEE Trans. on Energy Conversion*, Vol. 8, No. 4, pp. 757-761, 1993.

[159] **Richard G. G., Tan O. T.,** "Simplified models for induction machine transients under balanced and unbalanced conditions", *IEEE Trans. on Industry Applications*, Vol. 17, No. 1, pp. 15-21, 1981.

[160] **Robb D. D., Krause P.C.,** "The self excitation of induction machine with application to motor starting", *IEEE Trans. on Power Apparatus and Systems*, Vol. 90, No. 2, 1971.

[161] **Salama M. H., Holmes P. G.,** "Transient and steady-state load performance of a stand-alone self-excited induction generator", *IEE Proc., Electric Power Applications*, Vol. 143, pp. 50-58, 1996.

[162] **Schauder C., Mehta H.,** "Vector analysis and control of advanced static VAr compensator", *IEE Proc., Generation, Transmission and Distribution*, Vol. 140, No. 4, pp. 299-306, 1993.

[163] **Shaltout A. A., Abdel-Halim M. A.,** "Solid state control of wind driven self excited induction generator", *Electric Machine and Power Systems*, Vol. 23, No. 5, pp. 571-582, 1995.

[164] **Shen D., Lehn P. M.,** "Modeling, analysis and control of a current source inverter based STATCOM", *IEEE Trans. on Power Delivery*, Vol. 17, No. 1, pp. 248-253, 2002.

[165] **Shilpakar L. B., Singh B. and Rao K. S. P.,** "Transient analysis of parallely operated self-excited induction generators", *Proc. of IEEE International Conference on PEDES for Industrial Growth*, Vol. 1, pp. , 1996.

[166] **Shilpakar L. B., Singh B. and Singh B. P.,** "Dynamic behavior of three-phase self-excited induction generator for single-phase power generation", *Electric Power Systems Research*, Vol. 48, pp. 37-44, 1998.

[167] **Shridhar L., Singh B. and Jha C. S.,** "Transient performance of the self-regulated short-shunt self-excited induction generator", *IEEE Trans. on Energy Conversion*, Vol. 10, No. 2, pp. 261-267, 1995.

[168] **Shridhar L., Singh B. and Jha C. S.,** "Options for single-phase power generation in isolated applications using cage generators", *Journal of Institute of Engineers (India)*, Electrical, 1996.

[169] **Simoes M. G., Bose B. K. and Spiegel R. J.,** "Design and performance evaluation of a fuzzy logic based variable speed wind generation system", *IEEE Trans. on Industry Applications*, Vol. 33, No. 4, pp. 956-965, July/August 1997.

[170] **Simoes M. G., Bose B. K. and Spiegel R. J.,** "Fuzzy logic based intelligent control of a variable speed cage machine wind generation system", *IEEE Trans. on Power Electronics*, Vol. 12, No. 1, pp. 87-95, 1997.

[171] **Singh B., Shilpakar L. B.,** "Steady-state analysis of single-phase self-excited induction generator", *IEE Proc., Generation, Transmission and Distribution*, Vol. 146, No. 5, pp. 421-427, September 1999.

[172] **Singh B., Shilpakar L. B.,** "Analysis of a novel solid state voltage regulator for a self-excited induction generator", *IEE Proc., Generation, Transmission and Distribution*, Vol. 145, No. 6, pp. 647-655, 1998.

[173] **Singh B.,** "Optimum utilization of single-phase induction machine as a capacitor self-excited induction generator", *Electric Machines and Power Systems*, Vol. 13, No. 2, pp. 73-85, 1987.

[174] **Singh B.,** "Induction generators – A perspective", *Electric Machines and Power Systems*, Vol. 23, pp. 163-177, 1995.

[175] **Singh B., Kasal G. K.,** "Voltage and frequency controller for a three phase four wire autonomous wind energy conversion system", *IEEE Trans. on Energy Conversion*, Vol. 23, No. 2, pp. 509-518, June 2008.

[176] **Singh B., Mishra R. K. and Vasantha M. K.,** "Development of voltage regulator using saturable core reactor", *Proc. of Thirteen National System Conference*, Kharagpur, 1989.

[177] **Singh B., Murthy S. S., Gupta S.,** "STATCOM-Based Voltage Regulator for Self-Excited Induction Generator Feeding Nonlinear Loads", *IEEE Transactions on Industrial Electronics*, Vol. 53, No.5, pp. 1437-1452, October 2006.

[178] **Singh B., Murthy S. S. and Gupta S.,** "STATCOM based voltage regulator for self-excited induction generator feeding non-linear loads", *Proc. of Annual Conference of the IEEE Industrial Electronics Society*, Vol. 1, pp. , 2003.

[179] **Singh B., Murthy S. S. and Gupta S.,** "An Improved Electronic Load Controller for self-excited induction generator in micro-hydel applications", *Proc. of IEEE Conference of Industrial Electronics Society*, Vol. 3, pp. 2741-2746, 2003.

[180] **Singh B., Murthy S. S. and Gupta S.,** "Analysis and implementation of an electronic load controller for a self-excited induction generator", *IEE Proc., Generation, Transmission and Distribution*, Vol. 151, No. 1, pp. 51-60, 2004.

[181] **Singh B., Murthy S. S. and Gupta S.,** "Transient analysis of self-excited induction generator with electronic load controller (ELC) supplying static and dynamic loads", *IEEE Trans. on Industry Applications*, Vol. 41, No. 5, pp. 1194-1204, 2005.

[182] **Singh B., Murthy S. S. and Gupta S.,** "An electronic voltage and frequency controller for single-phase self-excited induction generators for pico hydro applications", *Proc. of IEEE International Conf. on Power Electronics and Drives Systems, PEDS 2005*, Vol. 1, pp. 240-245, 2005.

[183] **Singh B., Murthy S. S. and Gupta S.,** "Analysis and design of electronic load controller for self-excited induction generators", *IEEE Trans. on Energy Conversion*, Vol. 21, No. 1, pp. 285-293, 2006.

[184] **Singh B., Murthy S. S. and Gupta S.,** "An electronic voltage and frequency controller for single-phase self-excited induction generators for pico hydro applications", *Proc. of IEEE International Conf. on Power Electronics and Drives Systems, PEDS 2005*, Vol. 1, pp. 240-245, 2005.

[185] **Singh B., Murthy S. S. and Gupta S.,** "Modeling and analysis of STATCOM based voltage regulator for self-excited induction generator with unbalanced loads", *Proc. of IEEE Conference on Convergent Technologies for Asia-Pacific Region, TENCON 2003*, Vol. 3, pp. 15-17, 2003.

[186] **Singh B., Murthy S. S. and Gupta S.,** "Analysis and design of STATCOM based voltage regulator for self-excited induction generators", *IEEE Trans. on Energy Conversion*, Vol. 19, No. 4, pp. 783-790, December 2004.

[187] **Singh B., Saxena R. B., Murthy S. S. and Singh B. P.,** "A single-phase self-excited induction generator for lighting loads in remote areas", *International Journal on Elect. Engg. Education*, Vol. 25, pp. 269-275, 1988.

[188] **Singh Bhim, Kasal Gaurav,** "Voltage and frequency controller for isolated asynchronous generators feeding 3-phase 4-wire loads", *Proc. of the IEEE International Conference on Industrial Technology*, pp. 2773-2778, 2006.

[189] **Singh Bhim, Murthy S. S. and Gupta Sushma,** "A voltage and frequency controller for self-excited induction generators", *Electric Power Components and Systems*, Vol. 34, pp. 141-157, 2006.

[190] **Singh Bhim, Singh S. P. and Jain M. P.,** "Design optimization of a capacitor self-excited cage induction generator", *Electric Power Systems Research*, Vol. 22, No. 1, pp. 71-76, 1991.

[191] **Singh Bhim, Sridhar L. and Jha C. S.,** "Transient analysis of self-excited induction generator supplying dynamic load", *Electric Machines and Power Systems*, Vol. 27, pp. 941-954, 1999.

[192] **Singh S. P., Jain S. K. and Sharma J.,** "Voltage regulation optimization of compensated self-excited induction generator with dynamic load", *IEEE Trans. on Energy Conversion*, Vol. 19, No. 4, pp. 724-732, December 2004.

[193] **Singh S. P., Singh B. and Jain M. P.,** "A new technique for the analysis of self-excited induction generator", *Electric Machines and Power Systems*, Vol. 23, No. 6, pp. 647-656, 1995.

[194] **Singh S. P., Singh B. and Jain M. P.,** "Performance characteristics and optimum utilization of a cage machine as capacitor excited induction generator", *IEEE Trans. on Energy Conversion*, Vol. 5, No. 5, pp. 679-685, 1990.

[195] **Singh S. P., Singh B. and Jain M. P.,** "Simplified approach for the analysis of the self-excited induction generator", *Journal of Institute of Engineers (India), Pt. El*, Vol. 76, pp. 14-17, 1995.

[196] **Smith Nigel P. A.,** "Induction generators for stand-alone micro-hydro systems", *Proceedings of IEEE International Conference on Power Electronics, Drives and Energy Systems for Industrial Growth, PEDES – 1996*, Vol. 2, pp. 669-673, 1996.

[197] **Smith O. J. M.,** "Three-phase induction generator for single-phase line", *IEEE Trans. on Energy Conversion*, Vol. 2, No. 3, pp. 382-387, 1987.

[198] **Sousa G. C. D., Martins F. N., Rey J. P. and Bruinsma J. A.,** "An autonomous induction generator system with voltage regulation", *Proc. of IEEE International Conference on Power Electronics and Drive Systems*, Vol. 1, pp. 94-98, 2001.

[199] **Spitsa V., Kuperman A., Weiss G. and Rabinovici R.,** "Design of a robust voltage controller for an induction generator in an autonomous power system using a genetic algorithm", *Proc. of the American Control Conference, USA*, Vol. , pp. 3475-3481, June 2006.

[200] **Sridhar L., Singh B. and Jha C. S.,** "Transient performance of the self regulated short shunt self excited induction generator", *IEEE Trans. on Energy Conversion*, Vol. 6, No. 2, pp. 261-267, 1995.

[201] **Sridhar L., Singh B., Jha C. S., Singh B. P. and Murthy S. S.,** "Selection of capacitors for the self-regulated short-shunt self-excited induction generator", *IEEE Trans. on Energy Conversion*, Vol. 10, No. 1, pp. 10-16, 1995.

[202] **Sridhar L., Singh Bhim, Jha C. S. and Singh B. P.,** "Analysis of self-excited induction generator feeding induction motor", *IEEE Trans. on Energy Conversion*, Vol. 14, No.1, pp. 93-100, 1999.

[203] **Suarez E., Bortolotto G.,** "Voltage frequency control of a self-excited induction generator", *IEEE Trans. on Energy Conversion*, Vol. 14, No. 3, pp. 394-401, 1999.

[204] **Sutanto D., Grantham C. and Mismail B.,** "The simulation of self-excited induction generators for use in remote area power supplies", *Proc. of IEEE International Conference on Energy, Computer, Communication and Control Systems*, Vol. 1, pp. 97-101, 28-30 August 1991.

[205] **Sutanto D., Grantham C. and Rahman F.,** "A regulated self-excited induction generator for use in a remote area power supply", *Proc. of IEEE International Conference on Electrical Machines and Drives*, pp. 234-239, 8-10 September 1993.

[206] **Takagi T., Sugeno M,** "Fuzzy identification of a syustem and its applications to modeling and control", *IEEE Trans. on System, Man, and Cybernetics*, Vol. 15, pp. 116-132, 1985.

[207] **Tandon A. K., Murthy S. S. and Berg G. J.,** "Steady-state analysis of capacitor self-excited induction generators", *IEEE Trans. on Power Apparatus and Systems*, Vol. PAS-103, No. 3, pp. 612-618, March 1984.

[208] **Tandon A. K., Murthy S. S. and Jha C. S.,** "New method of computing steady-state response of capacitor self-excited induction generator", *Journal of Institute of Engineers (India)*, Vol. Pt. El 6, pp. 196-201, 1985.

[209] **Tiwari A. K., Murthy S. S., Singh B. and Sridhar L.,** "Design based performance evaluation of two-winding capacitor self-excited single-phase induction generator", *Electric Power Systems Research*, Vol. 67, pp. 89-97, November 2003.

[210] **Toliyat A. H., Campbell S.,** "DSP based electromechanical motion control", *Power Electronics and Applications Series, CRC Press*, Vol. 3, 2003.

[211] **Vas P., Hallenius K. E. and Brown J. E.,** "Cross-saturation in smooth air-gap electrical machines", *IEEE Trans. on Energy Conversion*, Vol. 1, No. 1, pp. 103-109, March 1986.

[212] **Wang L., Cheng C. M.,** "Excitation capacitance required for an isolated three-phase induction generator under single-phasing mode of operation", *IEEE Power Engineering Society Winter Meeting*, Vol. 3, pp. 1403-1407, 2001.

[213] **Wang L., Cheng C. M.,** "Excitation capacitance required for an isolated three-phase induction generator supplying a single-phase load", *Proc. of IEEE Power Engineering Society Winter Meeting*, Vol. 1, pp. 299-303, 2000.

[214] **Wang L., Deng R. Y.,** "Transient performance of an isolated induction generator under unbalanced excitation capacitor", *IEEE Trans. on Energy Conversion*, Vol. 14, No. 4, pp. 887-893, December 1999.

[215] **Wang L., Lee C. H.,** "Long-shunt and short-shunt connections on dynamic performance of a SEIG feeding an induction motor load", *IEEE Trans. on Energy Conversion*, Vol. 15, No. 1, pp. 1-7, March 2000.

[216] **Wang L., Lee C. H.,** "Dynamic analysis of parallel operated self-excited induction generators feeding an induction motor load", *IEEE Trans. on Energy Conversion*, Vol. 14, No. 3, pp. 479-485, 1999.

[217] **Wang L., Su J. Y.,** "Dynamic performances of an isolated self-excited induction generator under various loading conditions", *IEEE Trans. on Energy Conversion*, Vol. 14, No. 1, pp. 93-100, 1999.

[218] **Wang L., Lee C. H.,** "A novel analysis on the performance of an isolated self-excited induction generator", *IEEE Trans. on Energy Conversion*, Vol. 12, No. 2, pp. 109-117, June 1997.

[219] **Wang L., Su J. Y.,** "Determination of minimum and maximum capacitances of an isolated SEIG using eigenvalue sensitivity approach", *Proc. of IEEE International Conference on Power System Technology, POWERCON '98*, Vol. 1, pp. 610-614, 18-21 August 1998.

[220] **Wang Y. S., Wang L.,** "Unbalanced switching effects on dynamic performance of an isolated three-phase self-excited generator", *Electric Machines and Power Systems*, Vol. 29, No. 4, pp. 375-387, 2001.

[221] **Wanger C. F.,** "Process of Self-excitation of Induction Motors", *IEE Trans. (Electrical Engineering)*, Vol. 58, pp. 47-51, Febuary 1939.

[222] **Wasynczuk O., Diao Y. M. and Krause P. C.,** "Theory and comparision of reduced order models of induction machines", *IEEE Trans. on Power Apparatus and Systems*, Vol. 104, No. 3, pp. 598-606, 1985.

[223] **Watson D. B., Milner I. P.,** "Autonomous and parallel operation of self-excited induction generators", *International Journal on Elect. Engg. Education*, Vol. 8, No. 4, pp. 365-374, 1985.

[224] **Wekhande S., Agarwal V.,** "A variable speed constant voltage controller for self-excited induction generator with minimum control requirements", *Proc. of IEEE International Conference on Power Electronics and Drive Systems*, Vol. 1, pp. 98-103, July 1999.

[225] **Wekhande S., Agarwal V.,** "A new variable speed constant voltage controller for self-excited induction generator", *Electric Power Systems Research*, Vol. 59, pp. 157-164, 2001.

[226] **Wekhande S., Agarwal V.,** "Simple control for a wind driven induciton gererator", *IEEE Industry Application Magazine*, Vol. 7, No.2, pp. 44-53, 2001.

[227] www.mathworks.com/access/helpdesk/help/toolbox/ccslink/index.html.

[228] **Zidani Y., Naciri M.,** "A numerical analytical approach for the optimal capacitor used for the self excited induction generator", *Proc. of IEEE Annual Conference of Power Electronics Specialists, PESC 2001*, Vol. 1, pp. 216-220, 2001.

# APPENDIX-A

## MACHINES SPECIFICATIONS

The specifications of the machines used for simulation and experimentation are given below:

### Machine – I

The parameters of the 3.73 kW, 400 volts, 3 phase, 50 Hz, 4-pole SEIG are:

$R_s = 1.405\Omega$, $R_r = 1.39\Omega$, $L_{ls} = L_{lr} = 0.0078H$,

$J = 0.138$ kg/m$^2$, Base speed 1500 rpm

The magnetizing inductance $L_m$ is related to the magnetizing current in the following manner:

$L_m = A_1 + A_2 I_m - A_3 I_m^2 + A_4 I_m^3$

where, $A_1 = 0.12$, $A_2 = 0.063$, $A_3 = 0.018$, $A_4 = 0.0012$;

### Machine – II

The parameters of the 7.5 kW, 3-phase, 4-pole, 50 Hz, 400 V, 15.13 A, 1440 rpm, star connected induction machine are:

$R_s = 0.76\ \Omega$, $R_r = 1.03\ \Omega$, $L_{ls} = L_{lr} = 0.0048H$,

Base impedance = 15.21 Ω, Base speed = 1500 rpm.

The moment of inertia of the induction machine including the machine (prime-mover) coupled on its shaft is 0.1384 kg-m$^2$.

The magnetizing inductance $L_m$ is related to the magnetizing current in the following manner:

$L_m = A_1 - A_2 I_m + A_3 I_m^2 + A_4 I_m^3$

where, $A_1 = 0.1634$, $A_2 = 0.0087$, $A_3 = 0.00009$, $A_4 = 0.000003$;

### Machine – III

The parameters of the 1.5 kW, 220 volts, single phase, 50 Hz, SEIG are:

Main winding: resistance ($R_s$) = 2.02Ω, leakage inductance ($L_s$) = 0.0074 H

Auxiliary winding: resistance ($R_{as}$) = 7.14Ω, leakage inductance ($L_{as}$) = 0.0085 H

Rotor resistance ($R_r$) = 4.12 Ω, Rotor Leakage Inductance ( $L_r$)= 0.0056H,

Mutual inductance ( $L_m$) = 0.187 H  Inertia (J)=0.0146 kg/m$^2$

**Coefficients of the Prime-mover Characteristics**

***Prime-mover for 3.7 kW three phase SEIG:***

$k_1 = 600$, $k_2 = 3.5$

***Prime-mover for 1.5 kW single phase SEIG:***

$k_1 = 220$; $k_2 = 1.325$

**Controller Parameters**

The controller parameters in chapter 2 are:

Gain (A) = 0.85

Sampling time ($T_s$) = 0.0001 seconds

Switching frequency = 1.18 KHz

The controller parameters in chapter 3 are:

For Delta connected SEIG:

Gain (A) = 0.85

Sampling time ($T_s$) = 0.0001 seconds

Switching frequency = 1.18 KHz

For Star connected SEIG:

Gain (A) = 0.54

Sampling time ($T_s$) = 0.0001 seconds

Switching frequency=1.18 KHz

The controller parameters in chapter 4 are:

Gain (A) = 0.76

Sampling time ($T_s$) = 0.0001 seconds

Switching frequency = 1.18 KHz

The controller parameters in chapter 5 are:

For Three phase ERTC AC chopper:

Gain (A) = 0.65

Sampling time ($T_s$) = 0.0001 seconds

Switching frequency = 3 KHz

For single phase sinusoidal PWM AC chopper:

Gain (A) = 0.35

Sampling time ($T_s$) = 0.0001 seconds

Switching frequency = 3 KHz

The controller parameters in chapter 7 are:

For STATCOM based SEIG with load controller:

AC Voltage PI Controller :

Proportional gain ($K_p$) = 0.05

Integral gain ($K_I$) = 0.045

DC Voltage PI Controller :

Proportional gain ($K_p$) = 0.6

Integral gain ($K_I$) = 0.04

Load controller :

Gain (A) = 0.80

Sampling time ($T_s$) = 10e-6 seconds,

Switching frequency = 3 KHz

For STATCOM based SEIG with DC Chopper control:

AC Voltage PI Controller :

Proportional gain ($K_p$) = 0.05

Integral gain ($K_I$)= 0.045

DC Voltage PI Controller :

Proportional gain ($K_p$) = 0.6

Integral gain ($K_I$)= 0.04

DC Chopper Control :

Gain (A) = 0.80

Sampling time ($T_s$) = 10e-6 seconds

Switching frequency=3 KHz

The controller parameters in chapter 8 are:

Voltage PI Controller :

Proportional gain ($K_p$) = 0.10

Integral gain ($K_I$) = 0.08

Frequency PI Controller :

Proportional gain ($K_p$) = 1.4

Integral gain ($K_I$) = 0.95

Sample time ($T_s$) = 10 e-6 seconds.

# APPENDIX B

## B.1 MINIMIZATION TECHNIQUE

A general non-linear multi-variable constrained minimization problem is stated as:

Find $X(x_1, x_2, \ldots\ldots, x_n)$ such that

F(X) is minimum subject to

$$g_j(X) \geq 0 \qquad j = 1,2,\ldots\ldots,m$$

and $$x_{li} \leq x_i \leq x_{ui} \qquad i = 1, 2, \ldots\ldots, n,$$

where $X(x_1, x_2, \ldots\ldots, x_n)$ is the set of independent variables with their lower and upper bounds as $x_{li}$ and $x_{ui}$ respectively.

F(X) is the objective function to be optimized.

Since the variables are restricted within their bounds, it is considered as constraints $g_j(X)$.

The Sequential Unconstrained Minimization Technique (SUMT) [171, 189] is an indirect search method. In this method, the constrained optimization problem is converted into a series of unconstrained problems and is then solved by Rosenbrock's method of rotating coordinates. The conversion of constrained problem into unconstrained one is done in the following way:

At the beginning of k-th iteration,

$$P(X, r_k) = F(X) + r_k \sum_{j=1}^{m} \frac{1}{G_j(X)}$$

where $P(X, r_k)$ is augmented objective function. The sigma term, called the penalty term, the scalar $r_k$ ($r_k > 0$) is called the penalty factor. $G_j(X)$ is the normalized form of all constraints $g_j(X)$ in such a manner that these should lie between –1.0 and 0.0 only.

The minimization process begins with initial value of variables $X_0$. In order to get fast convergence, the starting value of $r_k$ is considered so that the starting value of $P(X,r_k)$ is twice that of F(X) [171]. Then the augmented function is minimized with the help of a suitable unconstrained minimization technique (the Rosenbrock's method of rotating coordinates) without any constraints to get a point, say, $X_k$. After this, the new augmented function $P(X_k, r_{k+1})$ is formed with $r_{k+1} < r_k$, ($r_{k+1} = c*r_k$) where $0 < c < 1$, and again it is minimized with $X_{k+1}$.

The process of unconstrained minimization is continued for decreasing sequence values of $r_k$, till the convergence criteria is satisfied. The convergence criteria is considered such that the process is continued for either a predetermined number of iterations or until the progress in per unit value of the objective function becomes less than a small specified quantity. The value of 'c' is taken as 0.25. The flowchart of the method is given in Figure B.1.

## B.2 ROSENBROCK'S METHOD OF ROTATING COORDINATES

At the first stage of this method, variables are varied in sequence in both the directions parallel to their axes. When for a particular variable, there is an improvement in the value of the objective function, that is success, the step length corresponding to this variable is magnified by an acceleration factor 'a' ($a > 1$) in the search direction for the next cycle . If there is no improvement in the current value of the objective function, that is a failure, the step length of the variable is decreased by deceleration factor 'b' ($0<b<1$) in the reverse direction. The sequence is repeated until a success and a failure are encountered for all variables at this stage.

In the second stage, the direction of search is given a rotation with respect to the original axes. For computing the appropriate direction, the coordinate system is rotated in such a manner that the first axis is oriented towards the locally estimated direction of a valley and all the other axes are made mutually orthogonal and normal to the first one using Gram-Schmidt orthogonalization The procedure is continued for either a given number of stages or until the progress in per unit value of objective function becomes less than a specified small quantity. The self-explanatory flowchart of the method is given in Figure B.2.

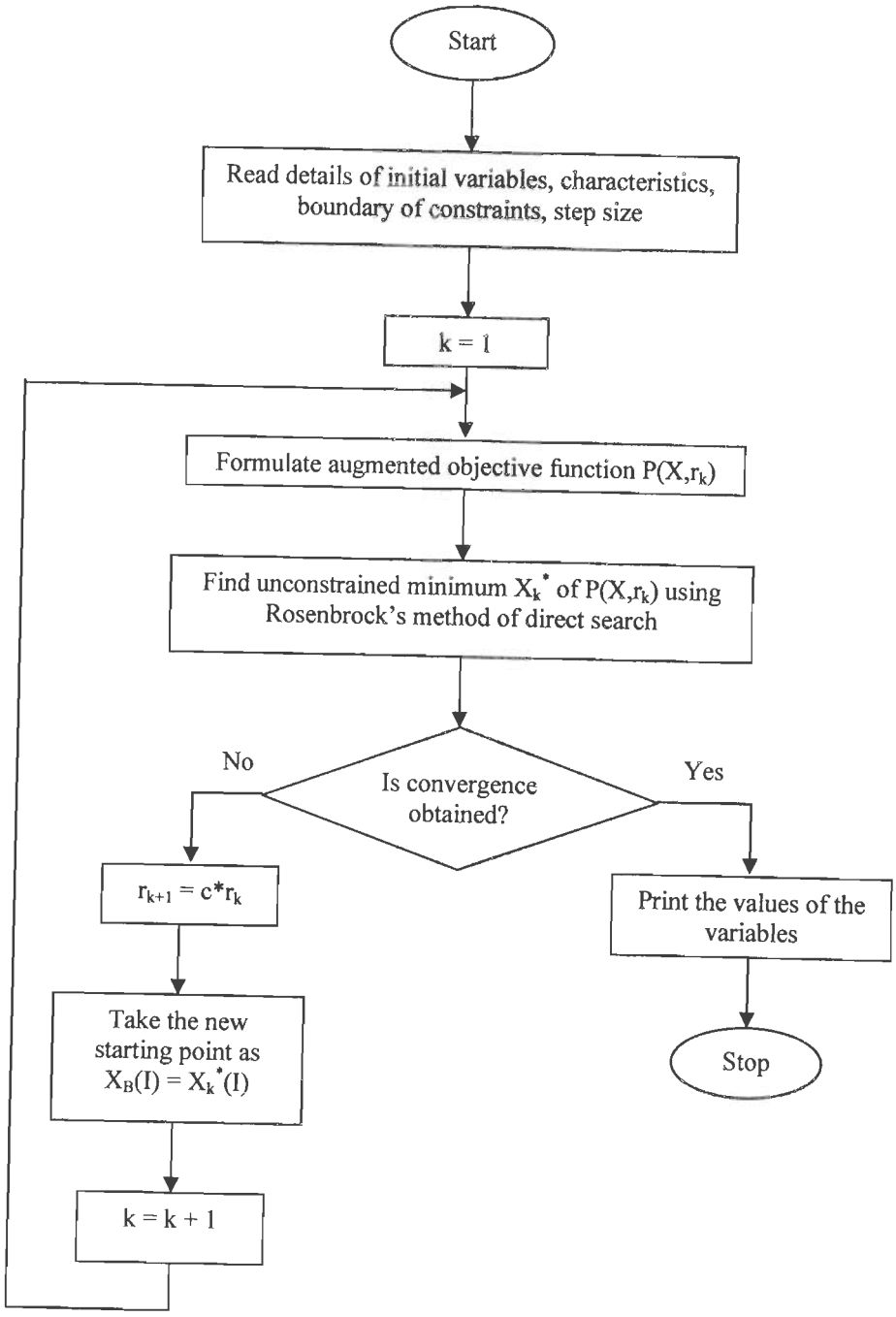


**Figure B.1: Flowchart of sequential unconstrained minimization technique**

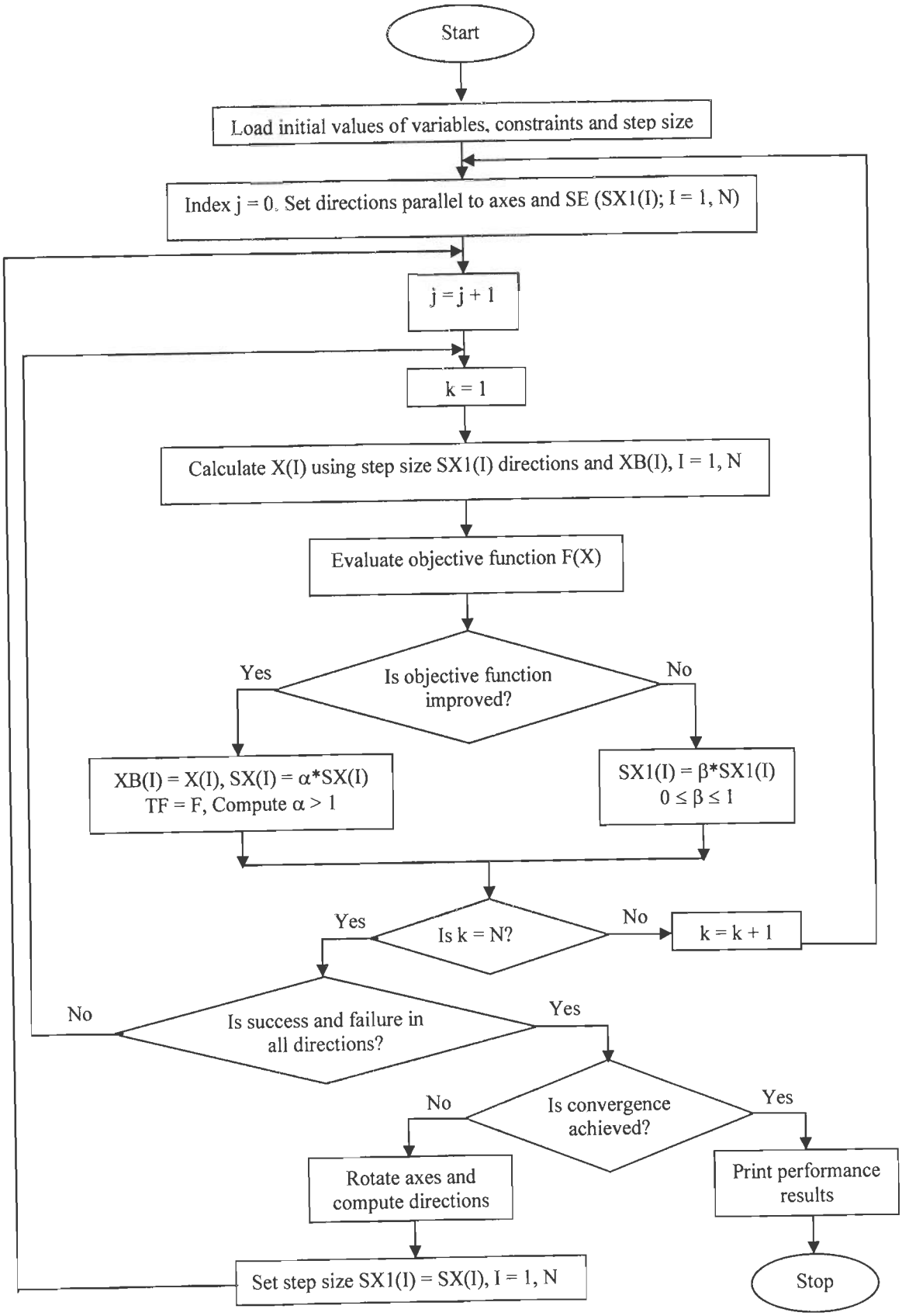


**Figure B.2: Flowchart of Rosenbrock's direct search unconstrained minimization technique**

# APPENDIX-C

## C.1 DYNAMIC MODEL OF THREE-PHASE INDUCTION MACHINE

The d-q variable and hybrid variable (stator in phase variables and rotor in d-q variables) dynamic models of symmetrical three-phase induction machine are derived considering the following assumptions:

- The change in resistance due to the change in frequency and temperature is neglected.
- The MMF space and time harmonics are neglected.
- The core loss is neglected.

### C.1.1 D-Q Variable Model

Figure C.1 shows a schematic diagram of three-phase induction machine with d-q axes superimposed. The q-axis lags the d-axis by $90^0$. $v_{sa}$ is the voltage across the terminals of stator phase A while the current flowing through it is $i_{sa}$. Phases B and C are not shown on the diagram to maintain clarity. The voltage and flux linkage equations in phase variables are:

$$[v_{abcs}] = [R_s][i_{abcs}] + p[\lambda_{abcs}] \quad \text{(C.1a)}$$

$$[v_{abcr}] = [R_r][i_{abcr}] + p[\lambda_{abcr}] \quad \text{(C.1b)}$$

$$[\lambda_{abcs}] = [L_s][i_{abcs}] + [L_{sr}][i_{abcr}] \quad \text{(C.2a)}$$

$$[\lambda_{abcr}] = [L_{sr}]^T[i_{abcs}] + [L_r][i_{abcr}] \quad \text{(C.2b)}$$

where,

$$[v_{abcs}] = [v_{sa}\ v_{sb}\ v_{sc}]^T, \qquad [v_{abcr}] = [v_{ra}\ v_{rb}\ v_{rc}]^T$$

$$[i_{abcs}] = [i_{sa}\ i_{sb}\ i_{sc}]^T, \qquad [i_{abcr}] = [i_{ra}\ i_{rb}\ i_{rc}]^T$$

$$[\lambda_{abcs}] = [\lambda_{sa}\ \lambda_{sb}\ \lambda_{sc}]^T, \qquad [\lambda_{abcr}] = [\lambda_{ra}\ \lambda_{rb}\ \lambda_{rc}]^T$$

$$[R_s] = \text{diag}[R_s], \qquad [R_r] = \text{diag}[R_r]$$

$$[L_s] = \begin{bmatrix} L_{ls}+L_{ms} & -\frac{1}{2}L_{ms} & -\frac{1}{2}L_{ms} \\ -\frac{1}{2}L_{ms} & L_{ls}+L_{ms} & -\frac{1}{2}L_{ms} \\ -\frac{1}{2}L_{ms} & -\frac{1}{2}L_{ms} & L_{ls}+L_{ms} \end{bmatrix}, \quad [L_r] = \begin{bmatrix} L_{lr}+L_{mr} & -\frac{1}{2}L_{mr} & -\frac{1}{2}L_{mr} \\ -\frac{1}{2}L_{mr} & L_{lr}+L_{mr} & -\frac{1}{2}L_{mr} \\ -\frac{1}{2}L_{mr} & -\frac{1}{2}L_{mr} & L_{lr}+L_{mr} \end{bmatrix}$$

$$L_{sr} = \begin{bmatrix} L_{sr}\cos\theta_r & L_{sr}\cos(\theta_r + 120^0) & L_{sr}\cos(\theta_r - 120^0) \\ L_{sr}\cos(\theta_r - 120^0) & L_{sr}\cos\theta_r & L_{sr}\cos(\theta_r + 120^0) \\ L_{sr}\cos(\theta_r + 120^0) & L_{sr}\cos(\theta_r - 120^0) & L_{sr}\cos\theta_r \end{bmatrix}$$

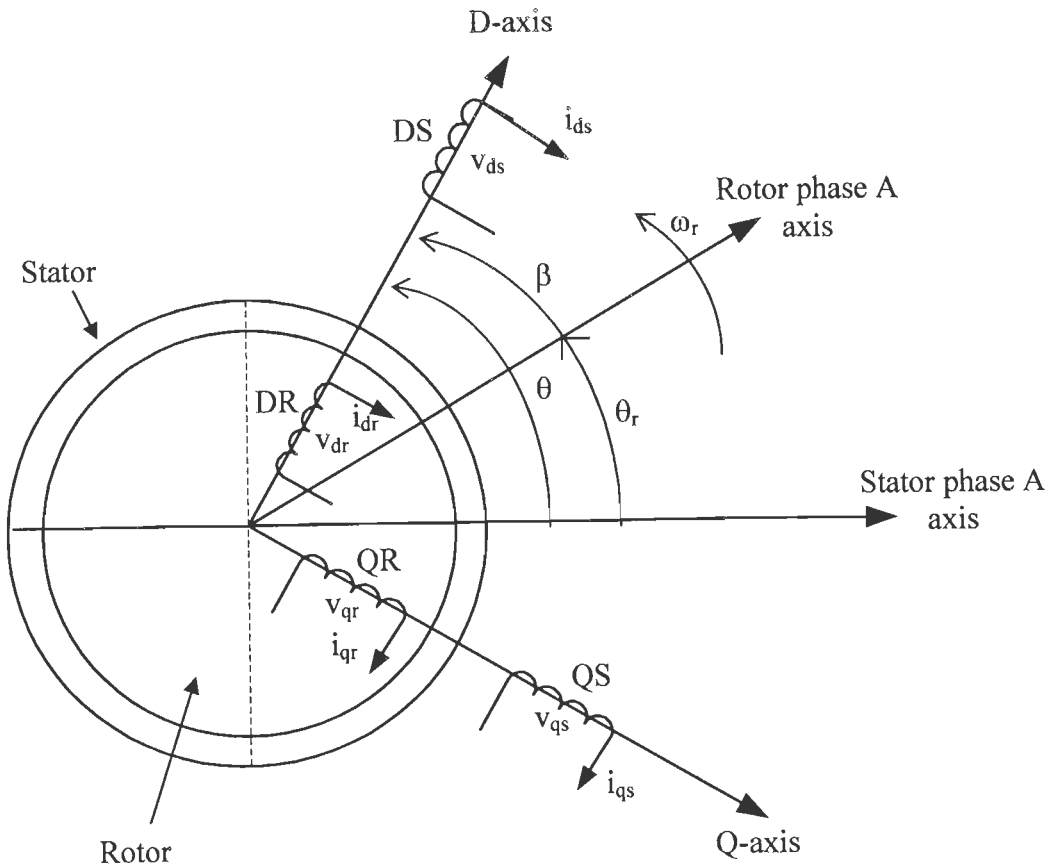


**Figure C.1: D-Q axes superimposed onto a three-phase induction machine and Q-axis lags D-axis by $90^0$**

Since, the magnetizing and mutual inductances are associated with same magnetic flux path, it can be shown that [93]

$$L_{mr} = \left(\frac{N_r}{N_s}\right)^2 L_{ms} \qquad \text{and} \qquad L_{sr} = \left(\frac{N_s N_r}{N_s^{\,2}}\right) L_{ms}$$

If $N_s = N_r$, then

$$L_{mr} = L_{ms} \qquad \text{and} \qquad L_{sr} = L_{ms}$$

In the d-q model, coils DS and QS replace the stator phase coils AS, BS and CS, while coils DR and QR replace the rotor phase coils AR, BR and CR. Although the d,q

axes can rotate at an arbitrary speed, there is no relative speed between the four coils DS, QS, DR and QR.

The transformation of ABC phase variables $[F_{abc}]$ to d-q variables $[F_{dq0}]$ may be expressed as:

$$[F_{dq0s}] = [K_s][F_{abcs}] \quad \text{for stator circuit} \tag{C.3a}$$

$$[F_{dq0r}] = [K_r][F_{abcr}] \quad \text{for rotor circuit} \tag{C.3b}$$

where, $[F_{dq0s}]^T = [f_{ds}\ \ f_{qs}\ \ f_{0s}]^T$ and $[F_{abcs}]^T = [f_{sa}\ \ f_{sb}\ \ f_{sc}]^T$

$[F_{dq0r}]^T = [f_{dr}\ \ f_{qr}\ \ f_{0r}]^T$ and $[F_{abcr}]^T = [f_{ra}\ \ f_{rb}\ \ f_{rc}]^T$

In the above equations 'f' can represent either voltage, current, flux linkage or electric charge. The superscript 'T' represents the transpose of a matrix.

$$[K_S] = \frac{2}{3}\begin{bmatrix} \cos\theta & \cos(\theta-120^0) & \cos(\theta+120^0) \\ \sin\theta & \sin(\theta-120^0) & \sin(\theta+120^0) \\ \frac{1}{2} & \frac{1}{2} & \frac{1}{2} \end{bmatrix}$$

$$[K_S]^{-1} = \begin{bmatrix} \cos\theta & \sin\theta & 1 \\ \cos(\theta-120^0) & \sin(\theta-120^0) & 1 \\ \cos(\theta+120^0) & \sin(\theta+120^0) & 1 \end{bmatrix}$$

$$[K_r] = \frac{2}{3}\begin{bmatrix} \cos\beta & \cos(\beta-120^0) & \cos(\beta+120^0) \\ \sin\beta & \sin(\beta-120^0) & \sin(\beta+120^0) \\ \frac{1}{2} & \frac{1}{2} & \frac{1}{2} \end{bmatrix}$$

Changing the phase variables in the equation (C.1) to d,q variables by applications of the transformation equation (C.3), we get

$$[v_{dq0s}] = [R_s][i_{dq0s}] + [K_s]p[K_s]^{-1}[\lambda_{dq0s}] + [[K_s][K_s]^{-1}p[\lambda_{dq0s}] \tag{C.4a}$$

$$[v_{dq0r}] = [R_r][i_{dq0r}] + [K_r]p[K_r]^{-1}[\lambda_{dq0r}] + [[K_r][K_r]^{-1}p[\lambda_{dq0r}] \tag{C.4b}$$

Hence,

$$[v_{dq0s}] = [R_s][i_{dq0s}] + \begin{bmatrix} 0 & 0 & p\theta \\ 0 & -p\theta & 0 \\ 0 & 0 & 0 \end{bmatrix}[\lambda_{dq0s}] + p[\lambda_{dq0s}] \tag{C.5a}$$

$$[v_{dq0r}] = [R_r][i_{dq0r}] + \begin{bmatrix} 0 & 0 & p\beta \\ 0 & -p\beta & 0 \\ 0 & 0 & 0 \end{bmatrix}[\lambda_{dq0r}] + p[\lambda_{dq0r}] \tag{C.5b}$$

In stationary reference frame

$$\omega = p\theta = 0 \quad \text{and} \quad \beta = \theta - \theta_r.$$

So, $p\beta = -p\theta_r = -\omega_r.$

Changing the phase variables in the equation (C.2) to d-q variables by application of the transformation equation (C.3) gives

$$[\lambda_{dq0s}] = [K_s][L_s][K_s]^{-1}[i_{dq0s}] + [K_s][L_{sr}][K_r]^{-1}[i_{dq0r}] \tag{C.6a}$$

$$[\lambda_{dq0r}] = [K_r][L_{sr}]^T[K_s]^{-1}[i_{dq0s}] + [K_r][L_r][K_r]^{-1}[i_{dq0r}] \tag{C.6b}$$

It can be shown by a simple matrix exercise that

$$[K_s][L_s][K_s]^{-1} = \begin{bmatrix} L_{ls}+L_m & 0 & 0 \\ 0 & L_{ls}+L_m & 0 \\ 0 & 0 & L_{ls} \end{bmatrix},$$

$$[K_r][L_r][K_r]^{-1} = \begin{bmatrix} L_{lr}+L_m & 0 & 0 \\ 0 & L_{lr}+L_m & 0 \\ 0 & 0 & L_{lr} \end{bmatrix}$$

$$[K_s][L_{sr}][K_r]^{-1} = \begin{bmatrix} L_m & 0 & 0 \\ 0 & L_m & 0 \\ 0 & 0 & 0 \end{bmatrix}, \qquad [K_r][L_{sr}][K_s]^{-1} = \begin{bmatrix} L_m & 0 & 0 \\ 0 & L_m & 0 \\ 0 & 0 & 0 \end{bmatrix}$$

where, $L_m = \frac{3}{2}L_{ms}$.

Since, 0's variables are related arithmetically to the abc variables, but not associated with the arbitrary reference frame, the equations of 0's variables are not shown in the d,q equations in what follows.

Substituting the flux linkage equations (C.6) in voltage equations (C.5) and after simplification, we have

$$[v] = [R][i] + [L]\,p[i] + \omega_r[G][i] \tag{C.7}$$

where, $[v] = [v_{ds} \quad v_{qs} \quad v_{dr} \quad v_{qr}]^T$, $\qquad [i] = [i_{ds} \quad i_{qs} \quad i_{dr} \quad i_{qr}]^T$

$$[R] = \begin{bmatrix} R_S & 0 & 0 & 0 \\ 0 & R_S & 0 & 0 \\ 0 & 0 & R_r & 0 \\ 0 & 0 & 0 & R_r \end{bmatrix}, \qquad [L] = \begin{bmatrix} L_{ls}+L_m & 0 & L_m & 0 \\ 0 & L_{ls}+L_m & 0 & L_m \\ L_m & 0 & L_{lr}+L_m & 0 \\ 0 & L_m & 0 & L_{lr}+L_m \end{bmatrix}$$

$$[G]=\begin{bmatrix} 0 & 0 & 0 & 0 \\ 0 & 0 & 0 & 0 \\ 0 & -L_m & 0 & -(L_{lr}+L_m) \\ L_m & 0 & L_{lr}+L_m & 0 \end{bmatrix}$$

The equation (C.7) needs some modification so as to make it suitable for the analysis of saturated induction machine incorporating cross-saturation effect. Since, the saturation affects the magnetizing characteristics, the d,q components of magnetizing voltage described by second term of the equation (C.7) are modified as follows [79]:

$$v_{md}=\frac{d\lambda_{md}}{dt}=\frac{d(L_m i_{md})}{dt}=\frac{dL_m}{dt}i_{md}+\frac{di_{md}}{dt}L_m \tag{C.8a}$$

$$v_{mq}=\frac{d\lambda_{mq}}{dt}=\frac{d(L_m i_{mq})}{dt}=\frac{dL_m}{dt}i_{mq}+\frac{di_{mq}}{dt}L_m \tag{C.8b}$$

where $\lambda_{md}$ and $\lambda_{mq}$ are the magnetizing flux linkages in the d and q axes respectively and $i_{md} = i_{ds} + i_{dr}$, and $i_{mq} = i_{qs} + i_{qr}$ are direct and quadrature axes components of magnetizing current space vector. The magnetizing current $I_m$ is evaluated as:

$$I_m=\sqrt{i_{mq}^2+i_{md}^2}\Big/\sqrt{2} \tag{C.9}$$

Since, $L_m$ is dependent on the magnetizing current, the time derivative of $L_m$ can be expanded as follows:

$$\frac{dL_m}{dt}=\frac{dL_m}{d|I_m|}\frac{d\sqrt{i_{md}^2+i_{mq}^2}}{d(i_{md}^2+i_{mq}^2)}=\frac{dL_m}{d|I_m|}\frac{1}{|I_m|}\left[i_{md}\frac{di_{md}}{dt}+i_{mq}\frac{di_{mq}}{dt}\right] \tag{C.10}$$

Substituting the expression of (C.10) in (C.8) and after simplification, we have

$$v_{md}=L_{md}\frac{di_{md}}{dt}+L_{dq}\frac{di_{mq}}{dt} \tag{C.11a}$$

$$v_{mq}=L_{dq}\frac{di_{md}}{dt}+L_{mq}\frac{di_{mq}}{dt} \tag{C.11a}$$

where,

$$L_{dq}=\frac{dL_m}{d|I_m|}\frac{i_{md}i_{mq}}{|I_m|} \tag{C.12}$$

$$L_{mD}=L_m+L_{dq}\frac{i_{md}}{i_{mq}} \tag{C.13}$$

$$L_{mQ}=L_m+L_{dq}\frac{i_{mq}}{i_{md}} \tag{C.14}$$

Here, $L_{dq}$ represents the cross-coupling between the axes in space quadrature due to saturation, $L_{md}$ and $L_{mq}$ are direct and quadrature axes magnetizing inductances. Hence, the inductance matrix [L] of equation (C.7) is modified to include the effect of saturation as follows:

$$[L]=\begin{bmatrix} L_{ls}+L_{mD} & L_{dq} & L_{mD} & L_{dq} \\ L_{dq} & L_{ls}+L_{mQ} & L_{dq} & L_{mQ} \\ L_{mD} & L_{dq} & L_{lr}+L_{mD} & L_{dq} \\ L_{dq} & L_{mQ} & L_{dq} & L_{lr}+L_{mQ} \end{bmatrix}$$

The self-inductance of the stator and rotor in d,q axes are thus expressed as:

$$L_{sd} = L_{ls} + L_{mD} \tag{C.15a}$$

$$L_{sq} = L_{ls} + L_{mQ} \tag{C.15b}$$

and

$$L_{rd} = L_{lr} + L_{mD} \tag{C.16a}$$

$$L_{rq} = L_{lr} + L_{mQ} \tag{C.16b}$$

It follows from the above equations that due to saturation, $L_{sd} \neq L_{sq}$ and $L_{rd} \neq L_{rq}$. Under linear magnetic conditions, the equations (C.12) – (C.14) reduces to

$$L_{dq} = 0$$

$$L_{md} = L_{mq} = L_m.$$

Hence, $L_{sd} = L_{sq}$ and $L_{rd} = L_{rq}$.

The electromagnetic torque in Newton-meters (N-m) is given by [93]

$$T_e = \left(\frac{P}{2}\right)[i_{abcs}]^T \frac{\partial}{\partial\theta_r}[L_{sr}][i_{abcr}] \tag{C.17}$$

Using the transformation equations (C.3), we have

$$T_e = \left(\frac{P}{2}\right)[[K_s]^{-1}[i_{dq0s}]]^T \frac{\partial}{\partial\theta_r}[L_{sr}][K_r]^{-1}[i_{dq0r}]$$

In terms of currents, this can be written as:

$$T_e = \left(\frac{3}{2}\right)\left(\frac{P}{2}\right)L_m(i_{dr}i_{qs} - i_{qr}i_{ds}) \tag{C.18}$$

Similarly, if the d-axis lags the q-axis by $90^0$ as shown in Figure C.2, the equation (C.7) is modified as:

$$[v] = [R][i] + [L]\,p[i] + \omega_r[G][i] \tag{C.19}$$

where, $[v] = [v_{qs} \quad v_{ds} \quad v_{qr} \quad v_{dr}]^T$, $[i] = [i_{qs} \quad i_{ds} \quad i_{qr} \quad i_{dr}]^T$

$$[R]=\begin{bmatrix} R_s & 0 & 0 & 0 \\ 0 & R_s & 0 & 0 \\ 0 & 0 & R_r & 0 \\ 0 & 0 & 0 & R_r \end{bmatrix},\quad [L]=\begin{bmatrix} L_{ls}+L_m & 0 & L_m & 0 \\ 0 & L_{ls}+L_m & 0 & L_m \\ L_m & 0 & L_{lr}+L_m & 0 \\ 0 & L_m & 0 & L_{lr}+L_m \end{bmatrix}$$

$$[G]=\begin{bmatrix} 0 & 0 & 0 & 0 \\ 0 & 0 & 0 & 0 \\ 0 & -L_m & 0 & -(L_{lr}+L_m) \\ L_m & 0 & L_{lr}+L_m & 0 \end{bmatrix}$$

Considering cross-saturation, the inductance matrix [L] will be modified as:

$$[L]=\begin{bmatrix} L_{ls}+L_{mQ} & L_{dq} & L_{mQ} & L_{dq} \\ L_{dq} & L_{ls}+L_{mD} & L_{dq} & L_{mD} \\ L_{mQ} & L_{dq} & L_{lr}+L_{mQ} & L_{dq} \\ L_{dq} & L_{mD} & L_{dq} & L_{lr}+L_{mD} \end{bmatrix}$$

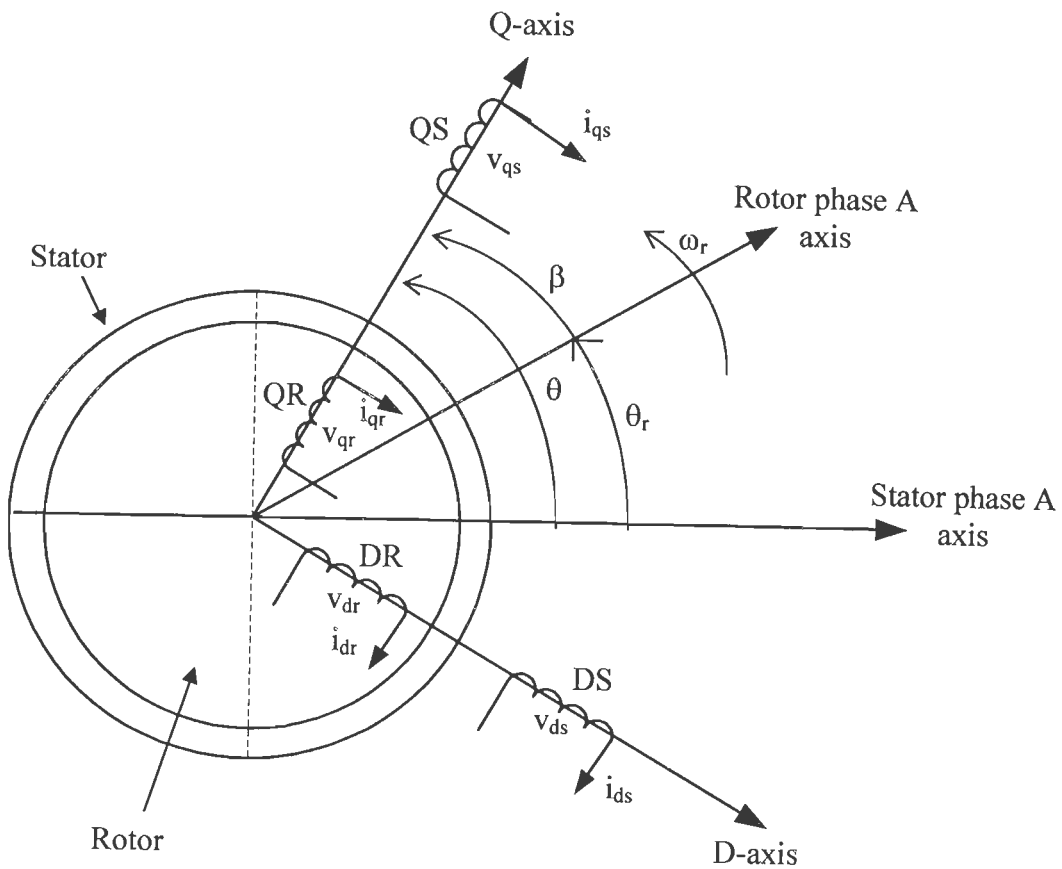


**Figure C.2: D-Q axes superimposed onto a three-phase induction machine and D-axis lags Q-axis by $90^0$**

### C.1.2 Hybrid Variable Model

The time varying inductances of the phase variable model can be eliminated by referring the rotor variables into the variables associated with stationary reference frame using $[K_r]^{-1}$ while $\theta$ as zero. It is assumed that the d-axis lags the q-axis by $90^0$, as shown in Figure C.2. Applying the transformation of rotor variables, and neglecting zero quantities associated with the rotor, the equation (C.1) can be expressed as:

$$[v_h] = [R_h][i_h] + [L_h]p[i_h] + \omega_r[G_h][i_h] \tag{C.20}$$

where $[v_h]$, $[i_h]$, $[R_h]$, $[L_h]$ and $[G_h]$ are the voltage vector, current, resistance matrix, transformer inductance matrix and speed inductance matrix respectively associated with the hybrid model and are defined as:

$$[v_h] = [v_{sa} \quad v_{sb} \quad v_{sc} \quad v_{qr} \quad v_{dr}]^T, \qquad [i_h] = [i_{sa} \quad i_{sb} \quad i_{sc} \quad i_{qr} \quad i_{dr}]^T$$

$$[R_h] = \begin{bmatrix} R_s & 0 & 0 & 0 & 0 \\ 0 & R_s & 0 & 0 & 0 \\ 0 & 0 & R_s & 0 & 0 \\ 0 & 0 & 0 & R_r & 0 \\ 0 & 0 & 0 & 0 & R_r \end{bmatrix}$$

$$[L_h] = \begin{bmatrix} L_{ls}+L_{ms} & -\frac{1}{2}L_{ms} & -\frac{1}{2}L_{ms} & \frac{3}{2}L_{ms} & 0 \\ -\frac{1}{2}L_{ms} & L_{ls}+L_{ms} & -\frac{1}{2}L_{ms} & -\frac{3}{4}L_{ms} & -\frac{3\sqrt{3}}{4}L_{ms} \\ -\frac{1}{2}L_{ms} & -\frac{1}{2}L_{ms} & L_{ls}+L_{ms} & -\frac{3}{4}L_{ms} & \frac{3\sqrt{3}}{4}L_{ms} \\ L_{ms} & -\frac{1}{2}L_{ms} & -\frac{1}{2}L_{ms} & L_{lr}+\frac{3}{2}L_{ms} & 0 \\ 0 & -\frac{\sqrt{3}}{2}L_{ms} & \frac{\sqrt{3}}{2}L_{ms} & 0 & L_{lr}+\frac{3}{2}L_{ms} \end{bmatrix}$$

$$[G_h] = \begin{bmatrix} 0 & 0 & 0 & 0 & 0 \\ 0 & 0 & 0 & 0 & 0 \\ 0 & 0 & 0 & 0 & 0 \\ 0 & \frac{\sqrt{3}}{2}L_{ms} & -\frac{\sqrt{3}}{2}L_{ms} & 0 & -(L_{lr}+\frac{3}{2}L_{ms}) \\ L_{ms} & -\frac{1}{2}L_{ms} & -\frac{1}{2}L_{ms} & L_{lr}+\frac{3}{2}L_{ms} & 0 \end{bmatrix}$$

The electromagnetic torque in hybrid model is evaluated as:

$$T_e = -\frac{3P}{4}L_{ms}\{i_{as}i_{dr} + i_{bs}(-\frac{1}{2}i_{dr} + \frac{\sqrt{3}}{2}i_{qr}) + i_{cs}(-\frac{1}{2}i_{dr} - \frac{\sqrt{3}}{2}i_{qr})\} \tag{C.21}$$

The magnetizing current for hybrid model is obtained from the equation (C.9) after computing d-q components of stator quantities in stationary reference frame using equation (C.3). $L_{ms}$ is related with $L_m$ as:

$$L_{ms} = \frac{2}{3} L_m .$$

## C.2 DYNAMIC MODEL OF TWO PHASE UNSYMMETRICAL INDUCTION MACHINE

Figure C.3 shows a schematic diagram of 2 pole, 2-phase unsymmetrical induction machine with q-d axes superimposed. The d-axis lags the q-axis by $90^0$. The main and auxiliary windings of the machine are represented as phase-A and phase-B respectively. $v_{sa}$, $v_{sb}$ are the voltage across the terminals of stator phase A and B respectively while the current flowing through them are $i_{sa}$, $i_{sb}$.

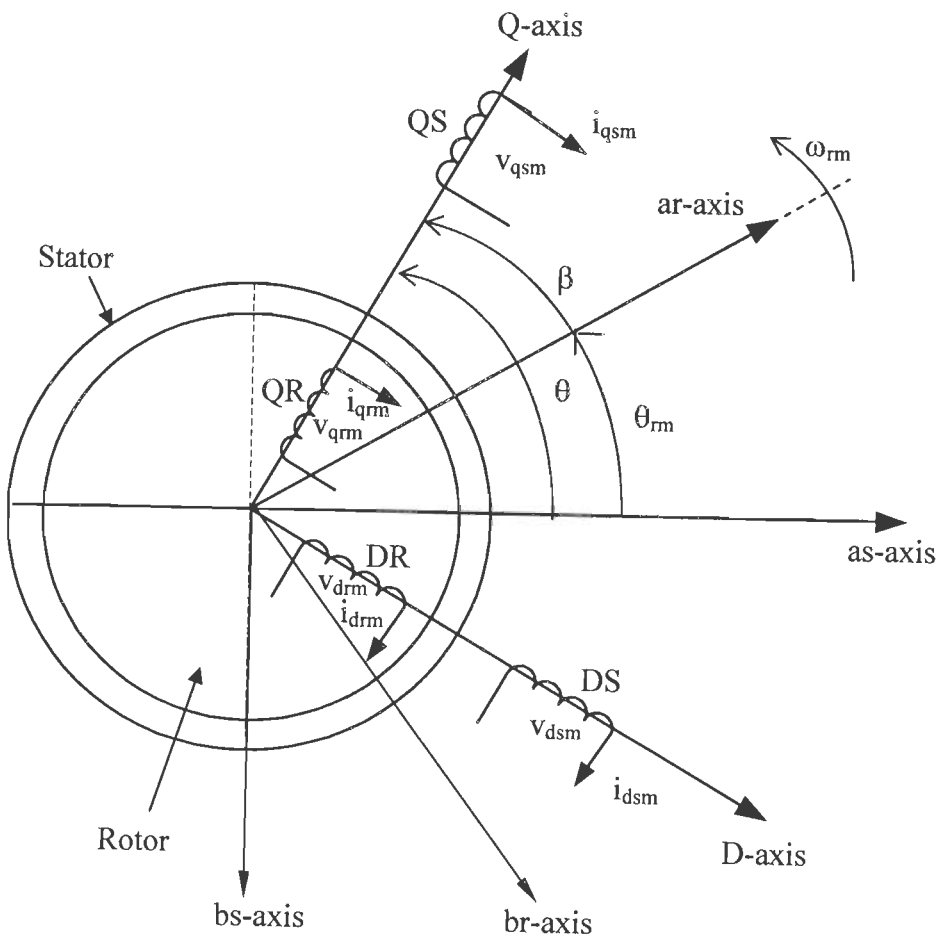


**Figure C.3: Q-D axes superimposed onto a two-phase induction machine**

The voltage and flux linkage equations in phase variables are written as:

$$[v_{abs}] = [R_s][i_{abs}] + p[\lambda_{abs}] \quad \text{(C.22a)}$$

$$[v_{abr}] = [R_r][i_{abr}] + p[\lambda_{abr}] \quad \text{(C.22b)}$$

$$[\lambda_{abs}] = [L_s][i_{abs}] + [L_{sr}][i_{abr}] \quad \text{(C.23a)}$$

$$[\lambda_{abr}] = [L_{sr}]^T[i_{abs}] + [L_r][i_{abr}] \quad \text{(C.23b)}$$

where,

$$[v_{abs}] = [v_{sa}\ \ v_{sb}]^T, \qquad [v_{abr}] = [v_{ra}\ \ v_{rb}]^T$$

$$[i_{abs}] = [i_{sa}\ \ i_{sb}]^T, \qquad [i_{abr}] = [i_{ra}\ \ i_{rb}]^T$$

$$[\lambda_{abs}] = [\lambda_{sa}\ \ \lambda_{sb}]^T, \qquad [\lambda_{abr}] = [\lambda_{ra}\ \ \lambda_{rb}]^T$$

$$[R_s] = \begin{bmatrix} r_{qsm} & 0 \\ 0 & r_{dsm} \end{bmatrix} \qquad [R_r] = \begin{bmatrix} r_{qrm} & 0 \\ 0 & r_{drm} \end{bmatrix}$$

$$[L_{sr}] = \begin{bmatrix} L_{mqm}\cos\theta_{rm} & -L_{mqm}\sin\theta_{rm} \\ L_{mdm}\sin\theta_{rm} & L_{mdm}\cos\theta_{rm} \end{bmatrix}$$

$$[L_s] = \begin{bmatrix} L_{lqsm} + L_{mqm} & 0 \\ 0 & L_{ldsm} + L_{mdm} \end{bmatrix}$$

$$[L_r] = \begin{bmatrix} L_{lqrm} + L_{mqm} & 0 \\ 0 & L_{ldrm} + L_{mdm} \end{bmatrix}$$

In the q-d model, coils QS and DS replace the stator phase coils AS and BS while coils QR and DR replace the rotor phase coils AR and BR. Although the q, d axes can rotate at an arbitrary speed, there is no relative speed between the four coils QS, DS, QR and DR.

The transformation of AB phase variables $[F_{ab}]$ to q-d variables $[F_{qd}]$ may be expressed as:

$$[F_{qds}] = [K_s][F_{abs}] \quad \text{for stator circuit} \quad \text{(C.24a)}$$

$$[F_{qdr}] = [K_r][F_{abr}] \quad \text{for rotor circuit} \quad \text{(C.24b)}$$

where, $[F_{qds}]^T = [f_{qsm}\ \ f_{dsm}]^T$ and $[F_{abs}]^T = [f_{sa}\ \ f_{sb}]^T$

$[F_{qdr}]^T = [f_{qrm}\ \ f_{drm}]^T$ and $[F_{abr}]^T = [f_{ra}\ \ f_{rb}]^T$

In the above equations 'f' can represent either voltage, current, flux linkage or electric charge. The superscript 'T' represents the transpose of a matrix.

$$[K_s] = \begin{bmatrix} \cos\theta & \sin\theta \\ \sin\theta & -\cos\theta \end{bmatrix} = [K_s]^{-1} \qquad [K_r] = \begin{bmatrix} \cos\beta & \sin\beta \\ \sin\beta & -\cos\beta \end{bmatrix} = [K_r]^{-1}$$

Changing the phase variables in the equation (C.22) to q, d variables by applications of the transformation equation (C.24), we get

$$[v_{qds}] = [R_s][i_{qds}] + [K_s]p[K_s]^{-1}[\lambda_{qds}] + [[K_s][K_s]^{-1}p[\lambda_{qds}]] \quad \text{(C.25a)}$$

$$[v_{qdr}] = [R_r][i_{qdr}] + [K_r]p[K_r]^{-1}[\lambda_{qdr}] + [[K_r][K_r]^{-1}p[\lambda_{qdr}]] \quad \text{(C.25b)}$$

or,

$$[v_{qds}] = [R_s][i_{qds}] + \omega[\lambda_{dqs}] + p[\lambda_{qds}] \quad \text{(C.26a)}$$

$$[v_{qdr}] = [R_r][i_{qdr}] + (\omega - \omega_{rm})[\lambda_{dqr}] + p[\lambda_{qdr}] \quad \text{(C.26b)}$$

where, $[\lambda_{dqs}] = [\lambda_{dsm} \quad -\lambda_{qsm}]^T$ and $[\lambda_{dqr}] = [\lambda_{drm} \quad -\lambda_{qrm}]^T$

$p\theta = \omega$ and $p\beta = \omega - \omega_{rm}$

For the stationary reference frame

$$\omega = 0 \quad \text{and} \quad p\beta = -\omega_{rm} \quad \text{(C.27)}$$

Changing the phase variables in the equation (C.23) to q-d variables by application of the transformation equation (C.24) gives

$$[\lambda_{qds}] = [K_s][L_s][K_s]^{-1}[i_{qds}] + [K_s][L_{sr}][K_r]^{-1}[i_{qdr}] \quad \text{(C.28a)}$$

$$[\lambda_{qdr}] = [K_r][L_{sr}]^T[K_s]^{-1}[i_{qds}] + [K_r][L_r][K_r]^{-1}[i_{qdr}] \quad \text{(C.28b)}$$

It can be shown by a simple matrix exercise that

$$[K_s][L_s][K_s]^{-1} = \begin{bmatrix} L_{lqsm} + L_{mqm} & 0 \\ 0 & L_{ldsm} + L_{mdm} \end{bmatrix},$$

$$[K_r][L_r][K_r]^{-1} = \begin{bmatrix} L_{lqrm} + L_{mqm} & 0 \\ 0 & L_{ldrm} + L_{mdm} \end{bmatrix}$$

$$[K_s][L_{sr}][K_r]^{-1} = \begin{bmatrix} L_{mqm} & 0 \\ 0 & L_{mdm} \end{bmatrix},$$

$$[K_r][L_{sr}][K_s]^{-1} = \begin{bmatrix} L_{mqm} & 0 \\ 0 & L_{mdm} \end{bmatrix}$$

where $L_{mqm} = \frac{N_d}{N_q} L_{sr}$.

Using the equations (C.27) and (C.28) in equation (C.26) and referring all q-variables to the 'AS' winding with $N_q$ turns (main winding) and all d-variables to the 'BS' winding with $N_d$ turns (auxiliary winding), the voltage equation of the machine can be written as:

$$v_{qsm} = r_{qsm}i_{qsm} + p\lambda_{qsm} \quad \text{(C.29a)}$$

$$v_{dsm} = r_{dsm} i_{dsm} + p\lambda_{dsm} \tag{C.29b}$$

$$v_{qrm} = r_{qrm} i_{qrm} + p\lambda_{qrm} - \frac{N_q}{N_d}\omega_{rm}\lambda_{drm} \tag{C.29c}$$

$$v_{drm} = r_{drm} i_{drm} + p\lambda_{drm} + \frac{N_d}{N_q}\omega_{rm}\lambda_{qrm} \tag{C.29d}$$

where, $\lambda_{qsm} = (L_{lqsm} + L_{mqm})i_{qsm} + L_{mqm} i_{qrm} = L_{lqsm} i_{qsm} + L_{mqm}(i_{qsm} + i_{qrm})$ (C.30a)

$$\lambda_{dsm} = (L_{ldsm} + L_{mdm})i_{dsm} + L_{mdm} i_{drm} = L_{ldsm} i_{dsm} + L_{mdm}(i_{dsm} + i_{drm}) \tag{C.30b}$$

$$\lambda_{qrm} = (L_{lqrm} + L_{mqm})i_{qrm} + L_{mqm} i_{qsm} = L_{lqrm} i_{qrm} + L_{mqm}(i_{qsm} + i_{qrm}) \tag{C.30c}$$

$$\lambda_{drm} = (L_{ldrm} + L_{mdm})i_{drm} + L_{mdm} i_{dsm} = L_{ldrm} i_{drm} + L_{mdm}(i_{dsm} + i_{drm}) \tag{C.30d}$$

Substituting equation (C.30) in to equation (C.29), the voltage equations can be written as:

$$v_{qsm} = r_{qsm} i_{qsm} + L_{lqsm} p i_{qsm} + p\lambda_{mqm} \tag{C.31a}$$

$$v_{dsm} = r_{dsm} i_{dsm} + L_{ldsm} p i_{dsm} + p\lambda_{mdm} \tag{C.31b}$$

$$v_{qrm} = r_{qrm} i_{qrm} + L_{lqrm} p i_{qrm} + p\lambda_{mqm} - \frac{1}{a}\omega_{rm}(L_{ldrm} i_{drm} + \lambda_{mdm}) \tag{C.31c}$$

$$v_{drm} = r_{drm} i_{drm} + L_{ldrm} p i_{drm} + p\lambda_{mdm} + a\omega_{rm}(L_{lqrm} i_{qrm} + \lambda_{mqm}) \tag{C.31d}$$

where $a = \frac{N_d}{N_q}$ is the turns ratio of auxiliary winding to main winding.

In order to include the effect of cross saturation, the q, d components of air-gap voltage $p\lambda_{mqm}$ and $p\lambda_{mdm}$ given in equation (C.11) are computed as follows:

$$p\lambda_{mqm} = \frac{d(L_{mqm} i_{mqm})}{dt}$$

$$= L_{mqm}\frac{di_{mqm}}{dt} + i_{mqm}\frac{dL_{mqm}}{d|i_m|}\frac{d(\sqrt{(i_{mqm}^2 + i_{mdm}^2)})}{d(i_{mqm}^2 + i_{mdm}^2)}\frac{d(i_{mqm}^2 + i_{mdm}^2)}{dt}$$

$$= \frac{di_{mqm}}{dt}L_{mQm} + L_{qdm}\frac{di_{mdm}}{dt} \tag{C.32a}$$

$$p\lambda_{mdm} = \frac{d(L_{mdm} i_{mdm})}{dt}$$

$$= L_{mdm}\frac{di_{mdm}}{dt} + i_{mdm}\frac{dL_{mdm}}{d|i_m|}\frac{d(\sqrt{(i_{mqm}^2 + i_{mdm}^2)})}{d(i_{mqm}^2 + i_{mdm}^2)}\frac{d(i_{mqm}^2 + i_{mdm}^2)}{dt}$$

$$= \frac{di_{mdm}}{dt}L_{mDm} + L_{dqm}\frac{di_{mqm}}{dt} \tag{C.32b}$$

where,

$$\lambda_{mqm} = L_{mqm}\, i_{mqm} \qquad \lambda_{mdm} = L_{mdm}\, i_{mdm}$$

$$i_{mqm} = i_{qsm} + i_{qrm} \qquad i_{mdm} = i_{dsm} + i_{drm}$$

$$L_{mQm} = L_{mqm} + \frac{i_{mqm}}{i_{mdm}} L_{qdm} \qquad L_{mDm} = L_{mdm} + \frac{i_{mdm}}{i_{mqm}} L_{dqm}$$

$$L_{qdm} = \frac{i_{mqm}\, i_{mdm}}{|i_m|} \frac{dL_{mqm}}{d|i_m|} \qquad L_{dqm} = \frac{i_{mqm}\, i_{mdm}}{|i_m|} \frac{dL_{mdm}}{d|i_m|}$$

From equations (C.11) and (C.12), the voltage equations can be written in matrix form as:

$$[v_{spm}] = [R_{spm}][i_{spm}] + [L_{spm}]\, p[i_{spm}] + \omega_{rm}\, [G_{spm}][i_{spm}] \tag{C.33}$$

where, $[v_{spm}] = [v_{qsm} \quad v_{dsm} \quad v_{qrm} \quad v_{drm}]^T$, $[i_{spm}] = [i_{qsm} \quad i_{dsm} \quad i_{qrm} \quad i_{drm}]^T$

$[R] = \text{diag}[r_{qsm} \quad r_{dsm} \quad r_{qrm} \quad r_{drm}]$,

$$[L_{spm}] = \begin{bmatrix} L_{lqsm} + L_{mQm} & L_{qdm} & L_{mQm} & L_{qdm} \\ L_{dqm} & L_{ldsm} + L_{mDm} & L_{dqm} & L_{mDm} \\ L_{mQm} & L_{qdm} & L_{lqrm} + L_{mQm} & L_{qdm} \\ L_{dqm} & L_{mDm} & L_{dqm} & L_{ldrm} + L_{mDm} \end{bmatrix}$$

$$[G_{spm}] = \begin{bmatrix} 0 & 0 & 0 & 0 \\ 0 & 0 & 0 & 0 \\ 0 & -\frac{L_{mdm}}{a} & 0 & -\frac{(L_{ldrm} + L_{mdm})}{a} \\ aL_{mqm} & 0 & a(L_{lqrm} + L_{mqm}) & 0 \end{bmatrix}$$

The electromagnetic torque in Newton-meters (N-m) is given by

$$T_{em} = \left(\frac{P_m}{2}\right)[i_{abs}]^T \frac{\partial}{\partial \theta_{rm}}[L_{sr}][i_{abr}] \tag{C.34}$$

Using the transformation equations (C.24), we have

$$T_{em} = \left(\frac{P_m}{2}\right)[[K_s]^{-1}[i_{dqs}]]^T \frac{\partial}{\partial \theta_{rm}}[L_{sr}][K_r]^{-1}[i_{dqr}]$$

The instantaneous electromagnetic torque may be expressed as:

$$T_{em} = \left(\frac{P_m}{2}\right)\left(\frac{N_d}{N_q}\right) L_{mQm}\,(i_{qsm}\, i_{drm} - i_{dsm}\, i_{qrm}) \tag{C.35}$$

## TMS320F2812 DSP Overview:

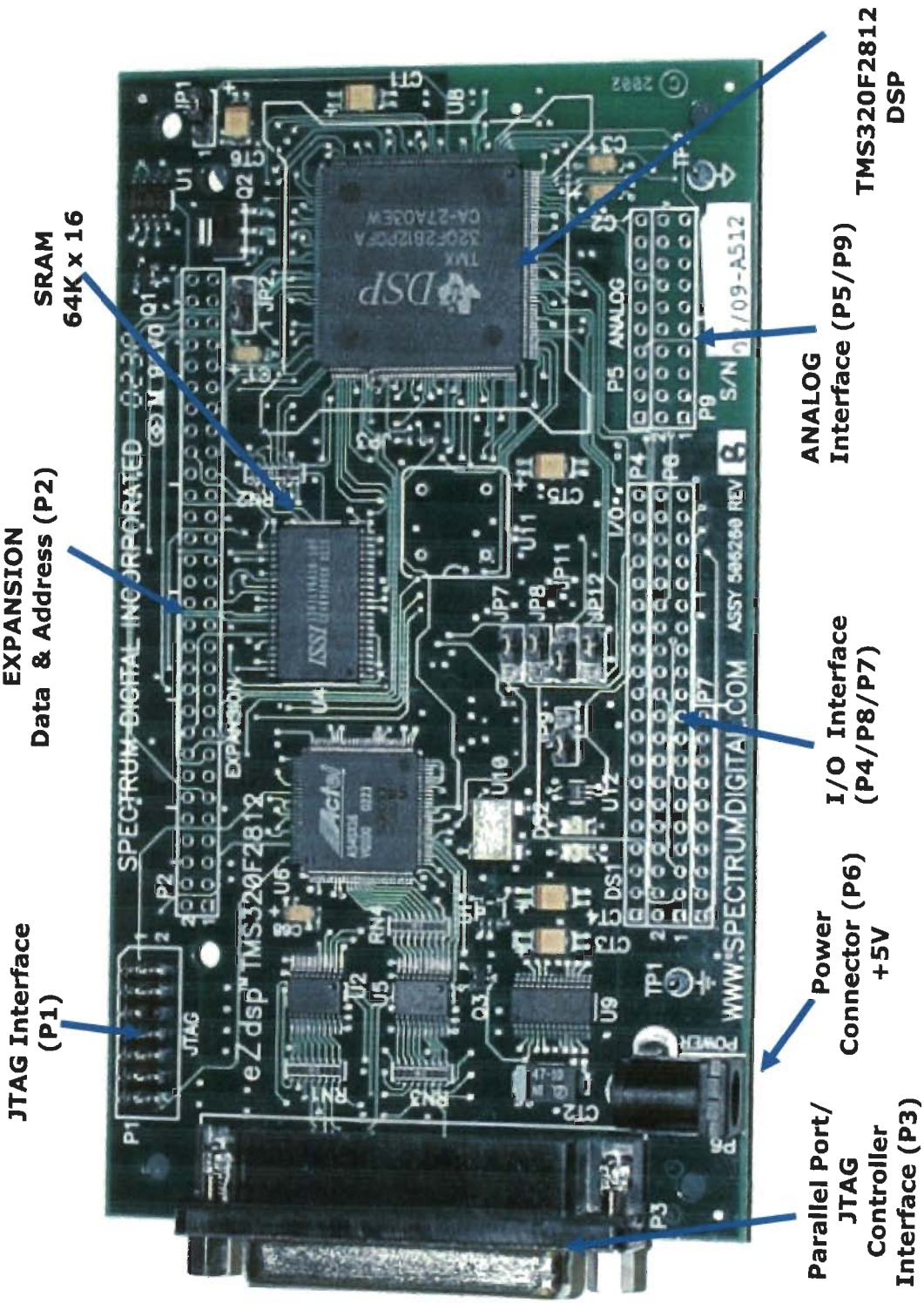


**Figure D.1: eZdsp™ F2812 Hardware**

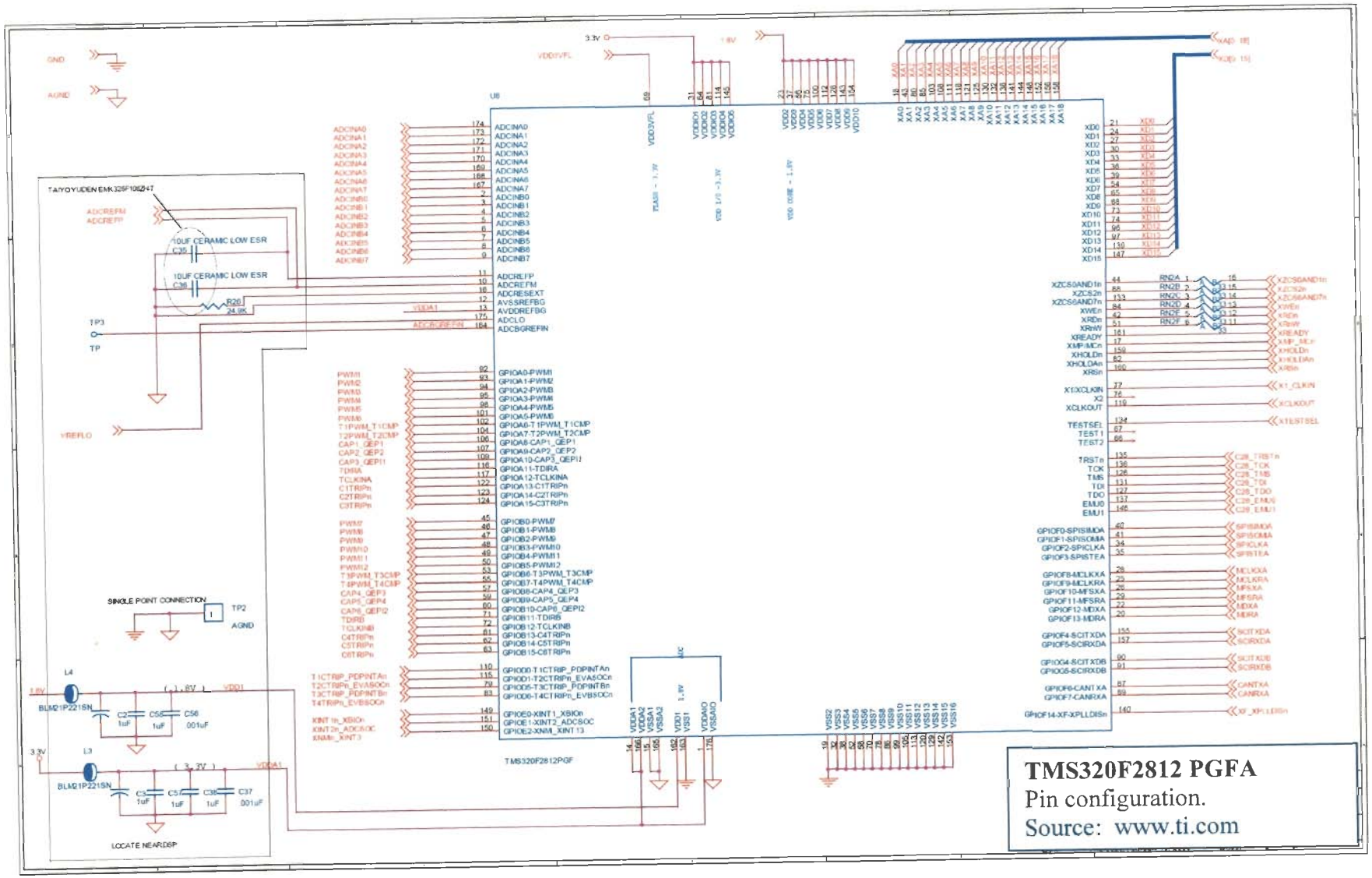


**Figure D.2: Pin configuration of TMS320F2812 DSP**

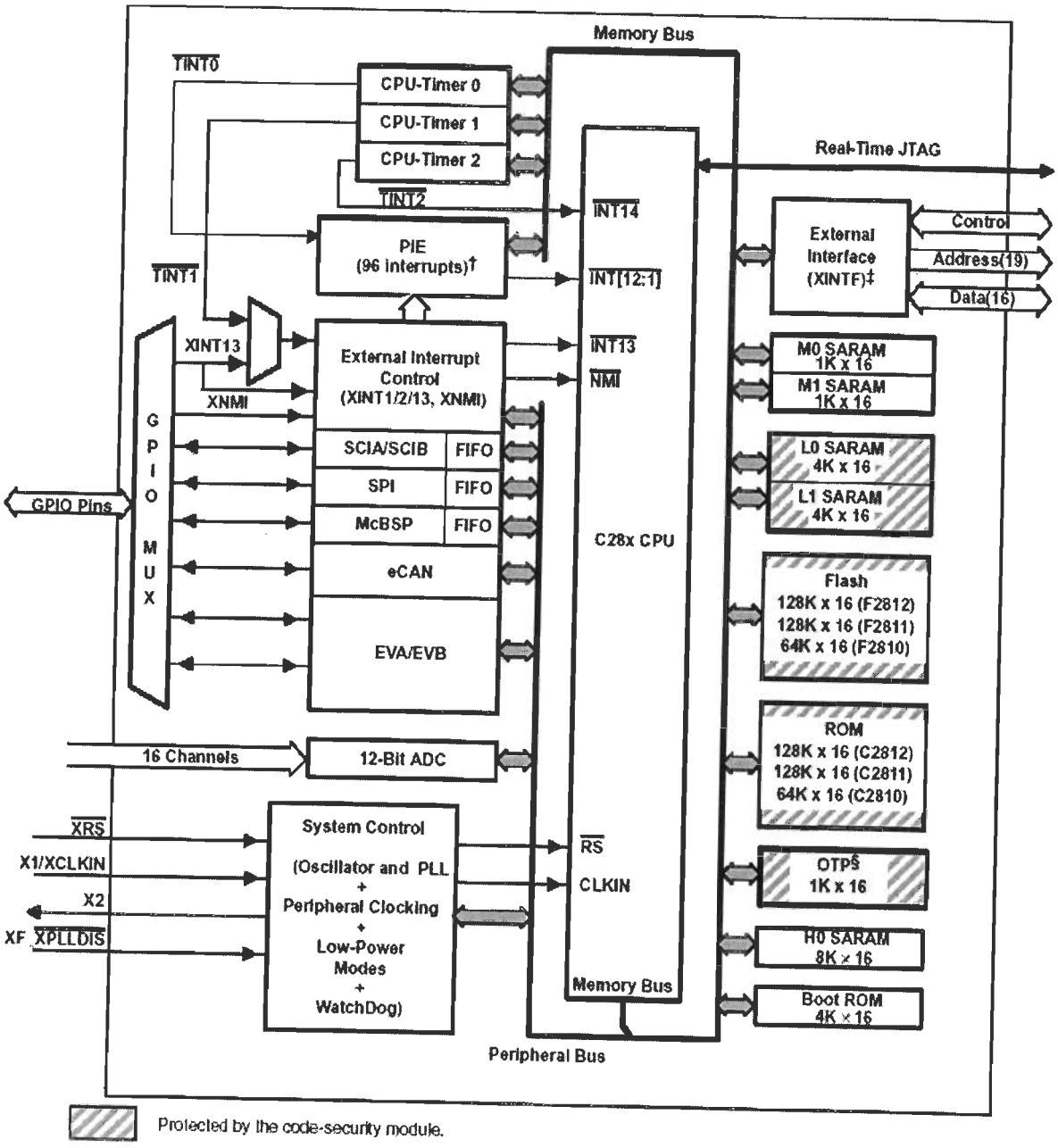


**Figure D.3: Functional block diagram of TMS320 F2812 ( Source: www.ti.com)**

The TMS320F2812 DSP has 12 PWM (6x2) output, 16 general purpose digital input output (GPIO), QEP, Serial port interface, interrupt and CAN services. The 70 pin connector P4, P8 and P7 gives access to these I/O signal from DSP. The layouts of these connectors and pin configurations are as shown:

| | | | | | | | | | | | | | | | | | | | | |
|---|---|---|---|---|---|---|---|---|---|---|---|---|---|---|---|---|---|---|---|---|
| 1 | 2 | 3 | 4 | 5 | 6 | 7 | 8 | 9 | 10 | 11 | 12 | 13 | 14 | 15 | 16 | 17 | 18 | 19 | 20 | **P4** |
| 2 | 4 | 6 | 8 | 10 | 12 | 14 | 16 | 18 | 20 | 22 | 24 | 26 | 28 | 30 | 32 | 34 | 36 | 38 | 40 | **P8** |
| 1 | 3 | 5 | 7 | 9 | 11 | 13 | 15 | 17 | 19 | 21 | 23 | 25 | 27 | 29 | 31 | 33 | 35 | 37 | 39 | |
| 1 | 2 | 3 | 4 | 5 | 6 | 7 | 8 | 9 | 10 | **P7** | | | | | | | | | | |

| **P4 I/O Connector** | | **P8 I/O Connector** | | | | **P7 I/O Connector** | |
|---|---|---|---|---|---|---|---|
| **Pin No.** | **Signal** | **Pin No.** | **Signal** | **Pin No.** | **Signal** | **Pin No** | **Signal** |
| 1 | +3.3 V /+5 V | 1 | +3.3 V /+5 V | 2 | +3.3 V /+5 V | 1 | C1TRIPn/ GPIOA13 |
| 2 | XINT2/ADCSOC | 3 | SCITXDA | 4 | SCIRXDA | 2 | C2TRIPn/GPIOA14 |
| 3 | MCLKXA | 5 | XINT1n/XBIOn | 6 | CAP1/QEP1/ GPIOA8 | 3 | C3TRIPn/ GPIOA15 |
| 4 | MCLKRA | 7 | CAP2/QEP2/ GPIOA9 | 8 | CAP3/QEPI1/ GPIOA10 | 4 | T2CTRIPn/EVASOCn |
| 5 | MFSXA | 9 | PWM1/GPIOA0 | 10 | PWM2/ GPIOA1 | 5 | C4TRIPn/ GPIOB13 |
| 6 | MFSRA | 11 | PWM3/ GPIOA2 | 12 | PWM4/ GPIOA3 | 6 | C5TRIPn/ GPIOB14 |
| 7 | MDXA | 13 | PWM5/ GPIOA4 | 14 | PWM6/ GPIOA5 | 7 | C6TRIPn/ GPIOB15 |
| 8 | MDRA | 15 | T1PWM/T1CMP / GPIOA6 | 16 | T2PWM/T2CMP/ GPIOA7 | 8 | T4CTRIPn/EVABSOCn |
| 9 | N C | 17 | TDIRA/ GPIOA11 | 18 | TCLKINA/ GPIOA12 | 9 | NC |
| 10 | GND | 19 | GND | 20 | GND | 10 | GND |
| 11 | CAP5 / QEP4/ GPIOB9 | 21 | NC | 22 | XINT1N/XBIOn | | |
| 12 | CAP6/QEP12/ GPIOB10 | 23 | SPISIMOA | 24 | SPISOMIA | | |
| 13 | T3PWM/T3CMP/ GPIOB6 | 25 | SPICLKA | 26 | SPISTEA | | |
| 14 | T4PWM/T4CMP/ GPIOB7 | 27 | CANTXA | 28 | CANRXA | | |
| 15 | TDIRB/ GPIOB11 | 29 | XCLKOUT | 30 | PWM7/ GPIOB0 | | |
| 16 | TCLKINB/ GPIOB12 | 31 | PWM8/ GPIOB1 | 32 | PWM9/ GPIOB2 | | |
| 17 | XF/XPLLDISn | 33 | PWM10/ GPIOB3 | 34 | PWM11/ GPIOB4 | | |
| 18 | SCITXDB | 35 | PWM12/ GPIOB5 | 36 | CAP4/QEP3 / GPIOB8 | | |
| 19 | SCIRXDB | 37 | T1CTRIP/PDPINTAn | 38 | T3CTRIP/PDPINTBn | | |
| 20 | GND | 39 | GND | 40 | GND | | |

The F2812 has two groups of 8 analog-to-digital converters, making a total of 16 inputs. The position of 30 pin on the P5/P9 connector and pin configurations are shown as:

| | | | | | | | | | | |
|---|---|---|---|---|---|---|---|---|---|---|
| 1 | 2 | 3 | 4 | 5 | 6 | 7 | 8 | 9 | 10 | **P5** |
| 2 | 4 | 6 | 8 | 10 | 12 | 14 | 16 | 18 | 20 | |
| 1 | 3 | 5 | 7 | 9 | 11 | 13 | 15 | 17 | 19 | **P9** |

| **P5 I/O Connector** | | **P9 I/O Connector** | | | |
|---|---|---|---|---|---|
| **Pin No.** | **Signal** | **Pin No.** | **Signal** | **Pin No.** | **Signal** |
| 1 | ADCB0 | 1 | GND | 2 | ADCA0 |
| 2 | ADCB1 | 3 | GND | 4 | ADCA1 |
| 3 | ADCB2 | 5 | GND | 6 | ADCA2 |
| 4 | ADCB3 | 7 | GND | 8 | ADCA3 |
| 5 | ADCB4 | 9 | GND | 10 | ADCA4 |
| 6 | ADCB5 | 11 | GND | 12 | ADCA5 |
| 7 | ADCB6 | 13 | GND | 14 | ADCA6 |
| 8 | ADCB7 | 15 | GND | 16 | ADCA7 |
| 9 | ADCREFM | 17 | GND | 18 | VREFLO |
| 10 | ADCREFP | 19 | GND | 20 | NC |

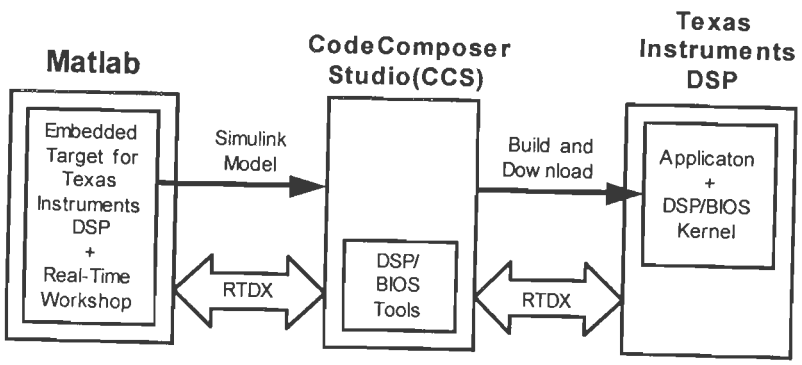


**Figure D.4: The relationship between MATLAB, CCS and a Texas Instruments DSP**

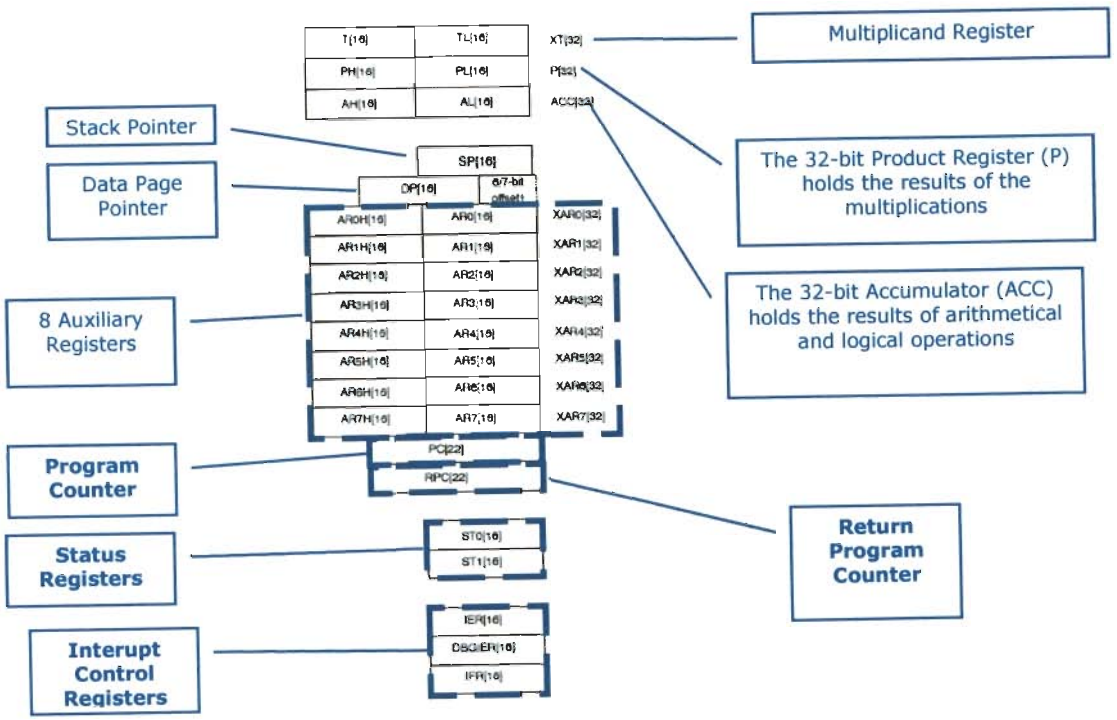


**Figure D.5: The register configuration of TMS320F2812 (Source: www.ti.com)**

## Data Types

- Each of the 32-bit registers have two halves, which means you can also work using 16-bit data.
- Using 16-bit values, you can represent numbers between –32768 and +32767.
- A 16-bit value can comfortably hold the input from an ADC or the output to a DAC.
- A 32-bit register can hold a value between –2 147 483 648 and + 2 147 483 647 as well as fractions in Q1:31 format.

## Decimals using Fixed Point

- Values between –1.000 and +1.000 can be represented in Q1:15 format.
- The left-most bit Q1: is the *sign*:
  - most positive number: 0 111 1111 1111 1111b
  - most negative number:1 000 0000 0000 0000b
- The remaining bits Q :15 are the *fraction*:

  +0.5000 decimal = 0 100 0000 0000 000b

**Multiplication Types**

- For many applications, 16-bit x 16-bit multiplications can be used, producing 32-bit products.
- The largest positive numbers that can be multiplied are 32767 x 32767.
- Where greater resolution is required at the cost of slower execution speed, the F2812 can perform a 32-bit x 32-bit multiplication, generating a 64-bit product.

**Floating-Point Operations**

- The architecture of the F2812 does not directly support floating-point maths.
- However, fixed-point numbers can be converted to floating-point if required.
- It may be useful to implement a Simulink model using floating-point mathematics. This reduces the development, but the application will run slower

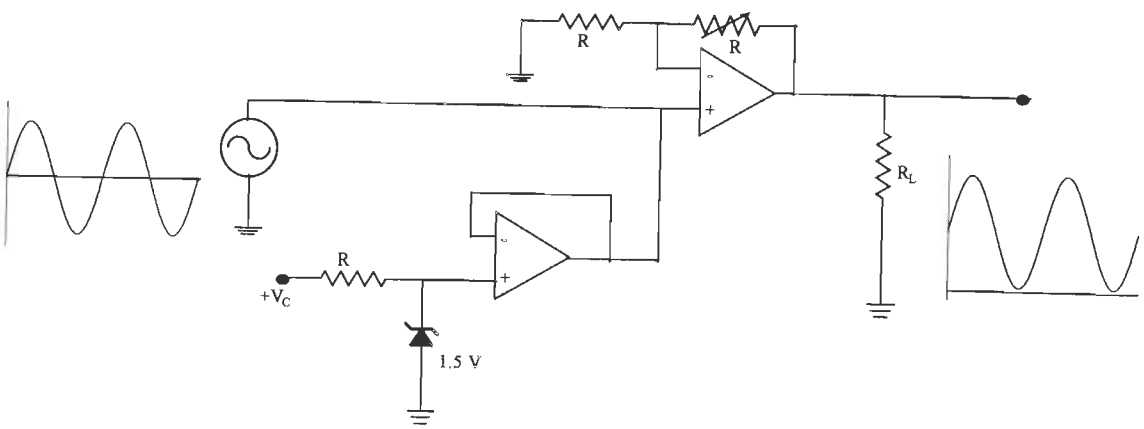


**Figure E.1: Schematic diagram of bipolar to unipolar signal conversion.**

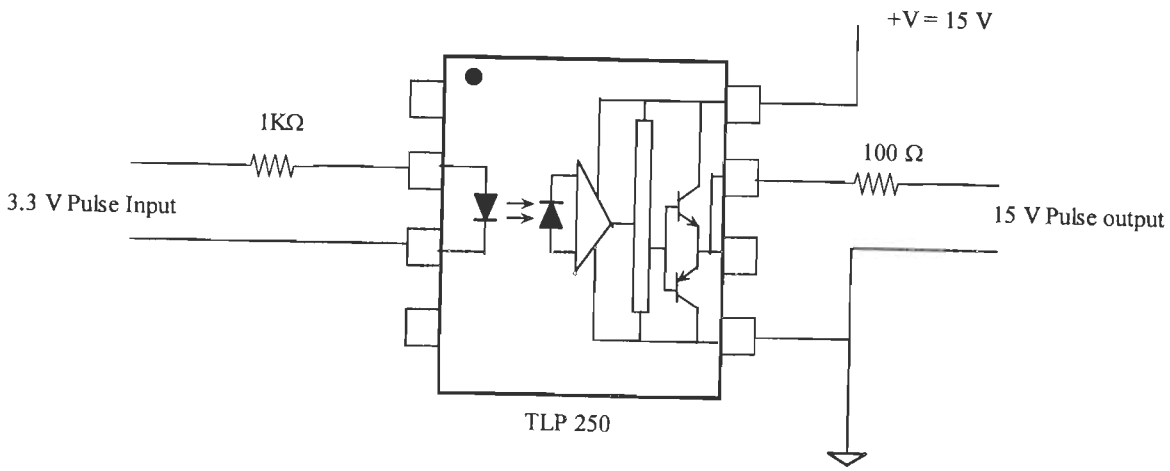


**Figure E.2: Schematic diagram of pulse driver circuit using TLP250.**

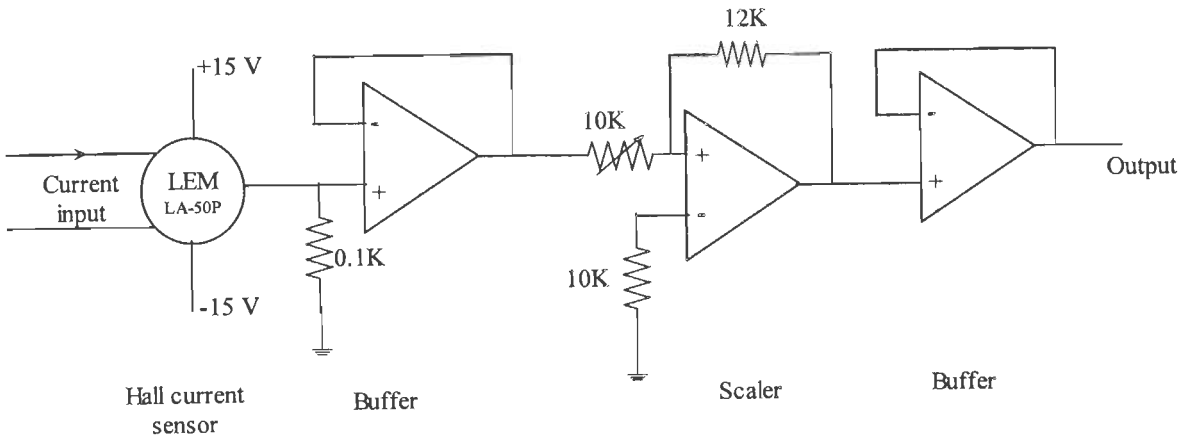


**Figure E.3: Current sensing circuit.**

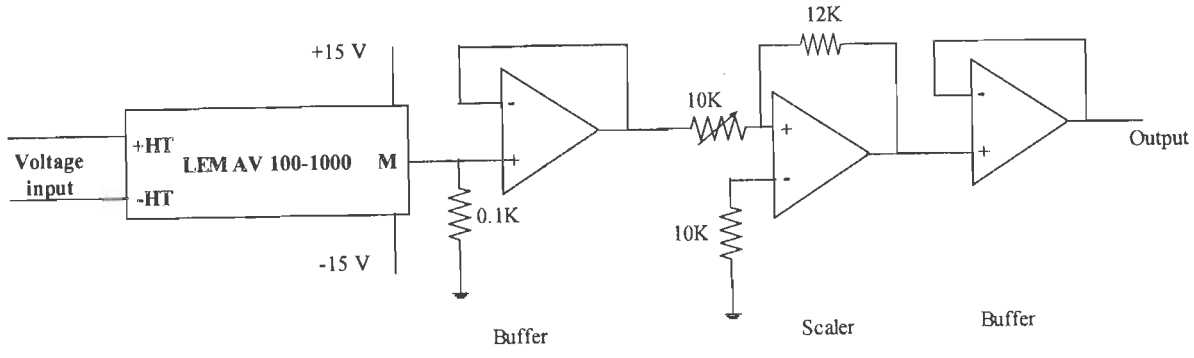


**Figure E.4: Voltage sensing circuit.**

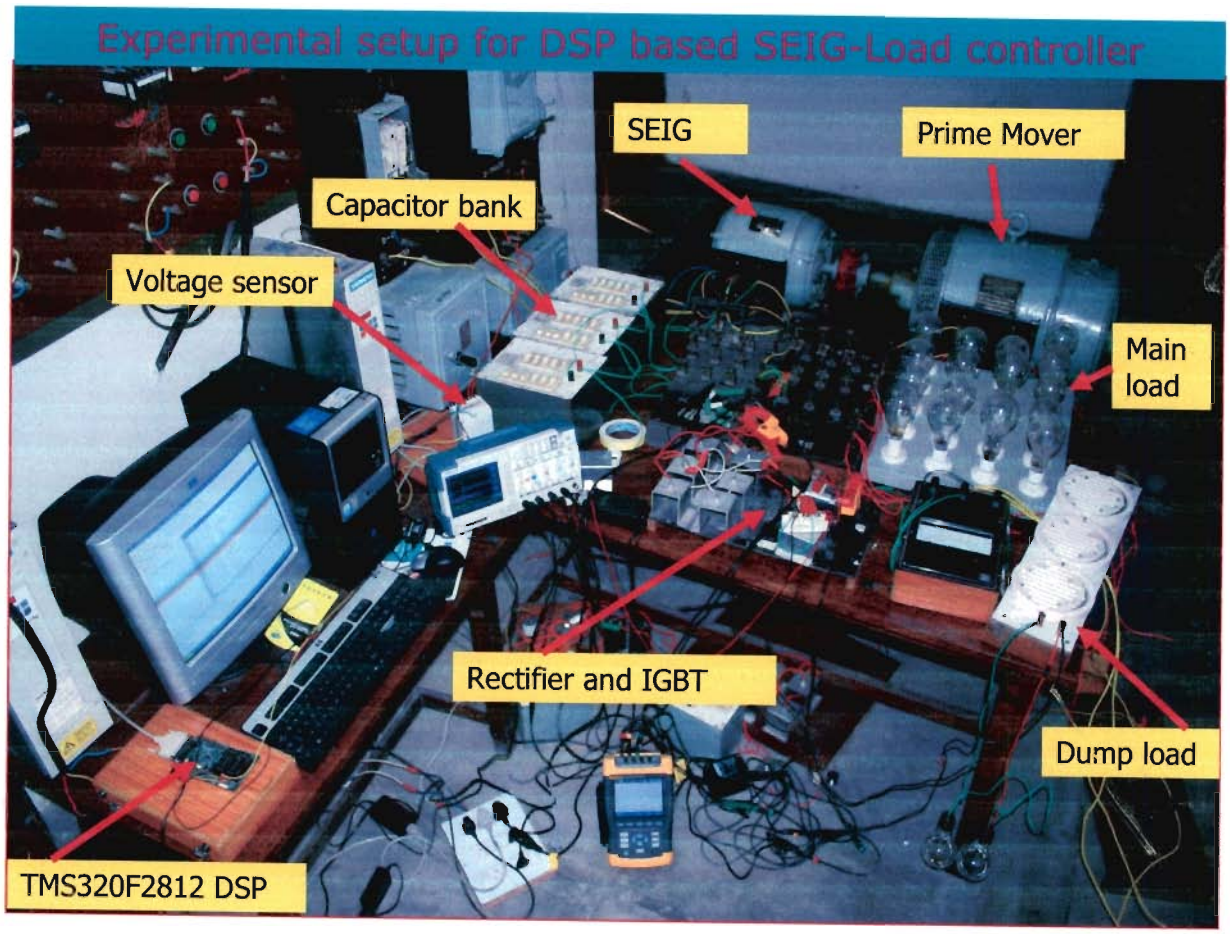


**Figure E.5: Photograph of SEIG-load controller experimental set-up**

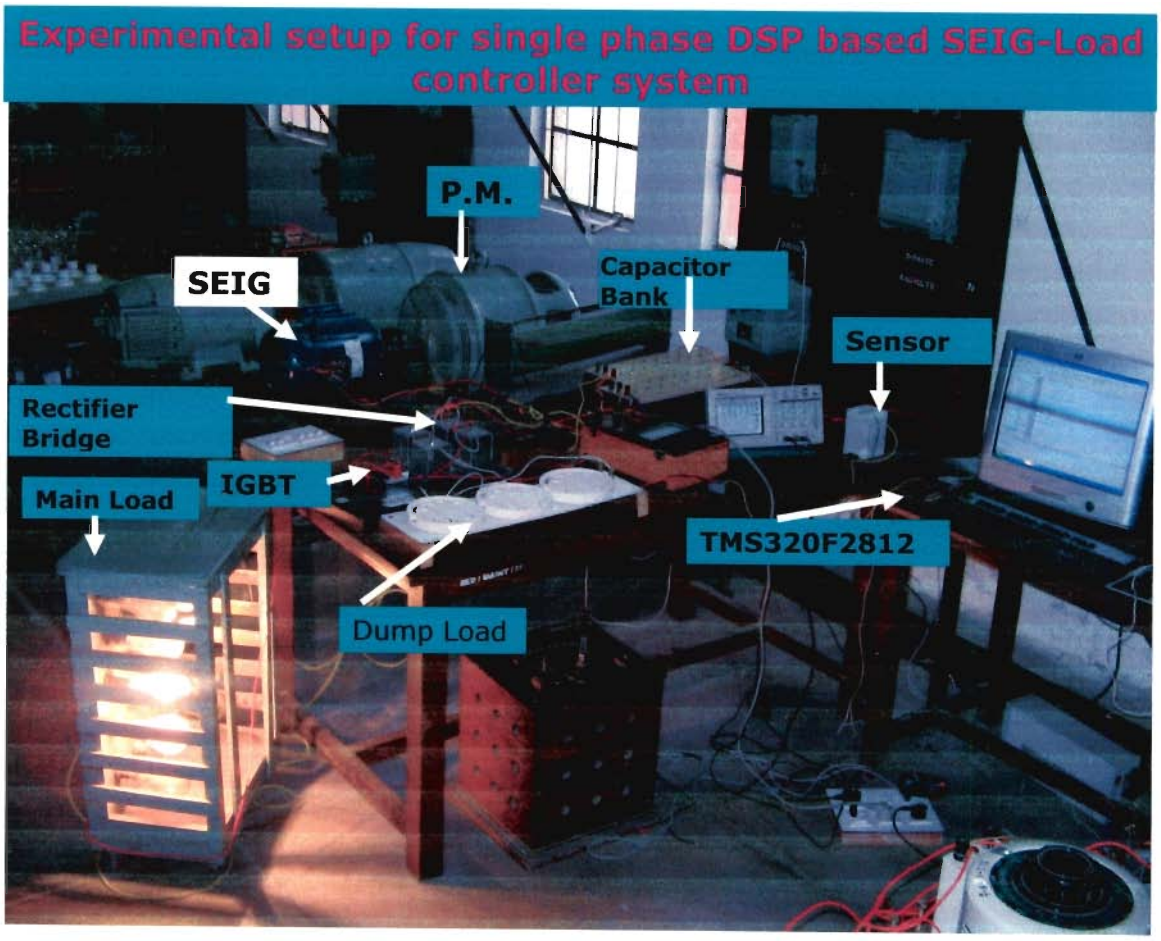


**Figure E.6: Photograph of single phase SEIG-load controller experimental set-up**

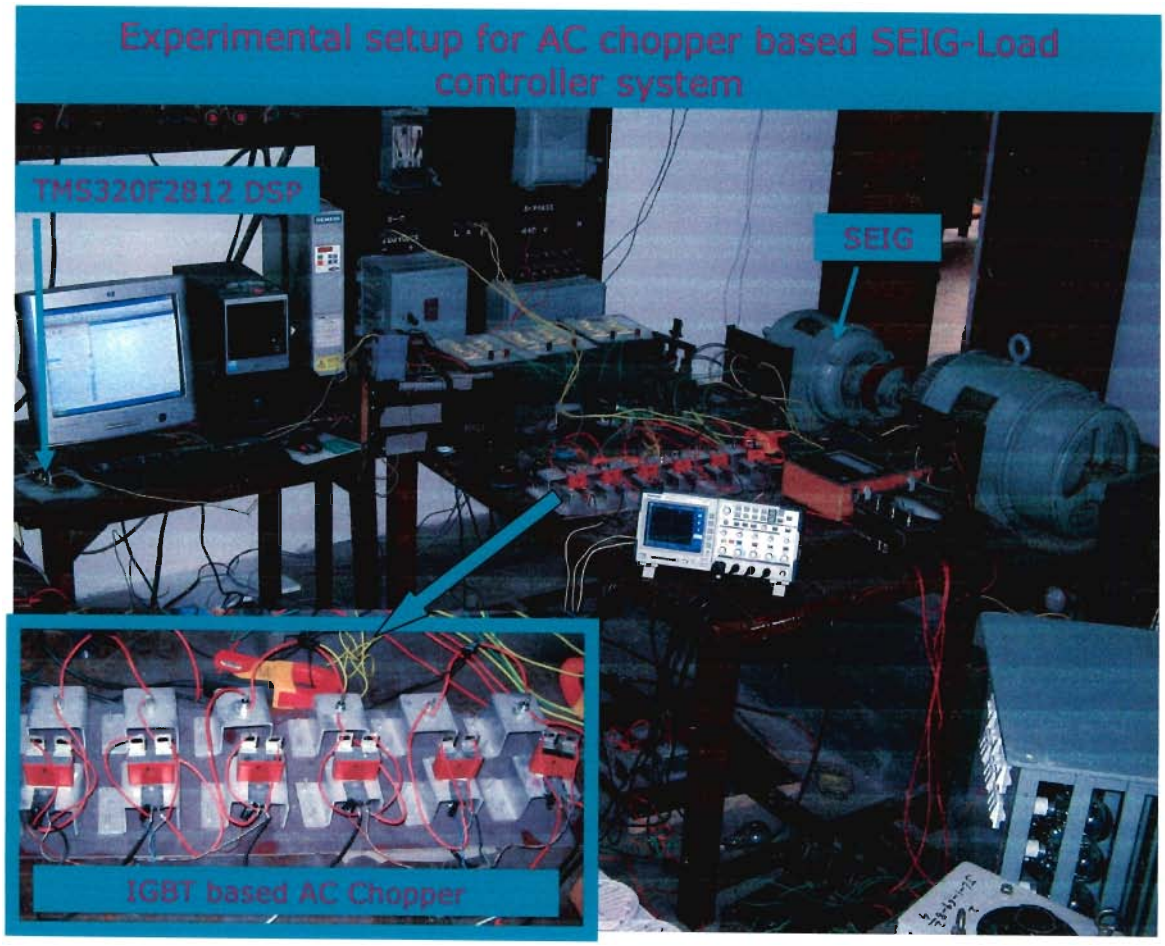


**Figure E.7: Photograph of SEIG-AC chopper control load controller experimental set-up**

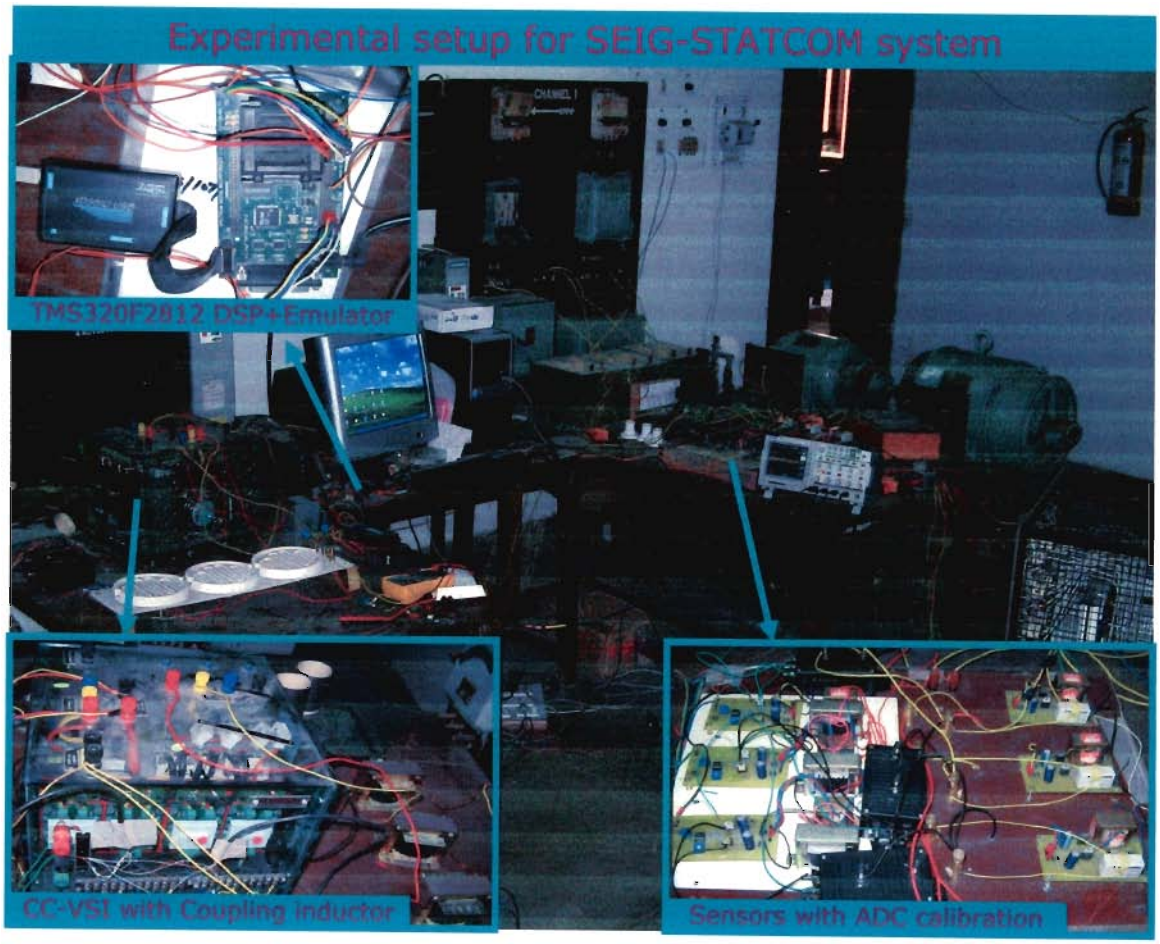


**Figure E.8: Photograph of SEIG-STATCOM experimental set-up**

# List of Publications from the Research Work

**International Journal**

[1] D. K. Palwalia, S. P. Singh, "DSP based induction generator controller for single phase self excited induction generator", *International Journal of Emerging Electric Power Systems*, Vol. 9, Issue 1, Article 2, 2008.

[2] D. K Palwalia, S. P. Singh, "Digital Signal Processor-based Controller Design and Implementation for Self excited Induction Generator", *Electric Power Components and Systems*, Vol. 36, No. 10, pp 1130-1140, Oct-2008.

[3] D. K Palwalia, S. P. Singh, "New load controller for single phase self excited induction generator", *Electric Power Components and Systems*, volume 37, number 6, pp 658-671, June 2009.

[4] D. K. Palwalia, S. P. Singh, "DSP Based Fuzzy Voltage and Frequency Regulator for Self Excited Induction Generator", Electric Power Components and Systems, Publisher: Taylor and Francis, in press.

**Communicated to International Journal**

[5] D. K. Palwalia, S. P. Singh, "Voltage and Frequency Regulator for Self Excited Induction Generator for Nonlinear /Unbalanced Loads", *International Journal of Electric Power and Energy System*, Publisher: Elsevier.

[6] D. K. Palwalia, S. P. Singh, "DSP Based Voltage and Frequency Regulator for Self Excited Induction Generator", *International Journal of Industrial Electronics and Drives*, Publisher: Inderscience.

[7] D. K. Palwalia, S. P. Singh, "STATCOM Based Voltage and Frequency Regulator for Self Excited Induction Generator", *Electric Power Components and Systems*, Publisher: Taylor and Francis.

[8] D. K. Palwalia, S. P. Singh, "DSP Based Voltage and Frequency Regulator for Self Excited Induction Generator", Electrical Engineering, Publisher: Springer.

[9] D. K. Palwalia, S. P. Singh, "DSP based Fuzzy Load Controller for Single Phase Self Excited Induction Generator", *International journal of power electronics*, Special issue. "Power Electronics for Distributed Generation Systems and Micro Grids" Inderscience publisher.

[10] D. K. Palwalia, S. P. Singh, "STATCOM Based Voltage and Frequency Regulator for Self Excited Induction Generator", submitted to *IEEE Tans. on Energy Conversion.*

[11] D. K. Palwalia, S. P. Singh, "Wind Driven SEIG with Voltage and Frequency Regulation and Energy Storage System", submitted to *Electric Power Components and Systems*, Publisher: Taylor and Francis.

**International / National Conference**

[12] D. K Palwalia, S. P. Singh, "Design and implementation of induction generator controller for single phase self excited induction generator", Proceedings of IEEE Conference on Industrial Electronics and Applications, pp 400-404, 3-5 June-2008, Singapore.

[13] D. K Palwalia, S. P. Singh "A New DSP Based Controller for Single Phase Self Excited Induction Generator", Proceedings of IEEE PES–Power India conference, 12-15 Oct.-2008, New Delhi.

[14] D. K Palwalia, S. P. Singh "Voltage and Frequency Regulation of Single Phase Self Excited Induction Generator", Proceedings of National System Conference (NSC-2008), pp. 244-249, Roorkee.

[15] D. K Palwalia, S. P. Singh "Digital Voltage and Frequency Regulator for Self Excited Induction Generator", Proceedings of Cutting Edge Computer and Electronics Technologies (CECET' 09), Pant Nagar, pp. 237-243.

[16] D. K Palwalia, S. P. Singh "Fuzzy Controller for Single Phase Self Excited Induction Generator", Proceedings of Cutting Edge Computer and Electronics Technologies (CECET' 09), Pant Nagar pp. 244-250.

**Communicated to International Conference**

[17] D. K Palwalia, S. P. Singh "STATCOM Based Voltage and Frequency Regulator for Self Excited Induction Generator", 5$^{th}$ IEEE conference on industrial electronics and applications,15 - 17 June 2010, Taiwan.